Customisable Environmental Platforms for the Detection of Nutrients in Natural Waters

Andrew Donohoe (B.Sc.)

Thesis submitted in partial fulfilment of the
requirements for the degree of

Doctor of Philosophy

September 2021

Supervisors: Dr. Margaret McCaul, Prof. Dermot Diamond

Insight Centre for Data Analytics / School of Chemical Sciences

Dublin City University

Declaration

I hereby certify that this material, which I now submit for assessment on the program of study leading to the award of Doctor of Philosophy is entirely my own work, and that I have exercised reasonable care to ensure that the work is original, and does not to the best of my knowledge breach any law of copyright, and has not been taken from the work of others save and to the extent that such work has been cited and acknowledged within the text of my work.

Signed: Name: Andrew Donohoe

Student number: 11503147 Date: 10th September 2021

The specific measurements and devices completed by the candidate include:
Contribution to the development of the benchtop sensing platform and autonomous sensing platform, including testing, fault finding, optimisation, validation and troubleshooting of both the benchtop sensing platform and the autonomous sensing platform. This work included preparation and validation of all associated reagent and calibration standards, validation of the sensing platforms read function through sample calibration, hardware level optimisations and detector performance validation.

Contribution to the fabrication of the PMMA Fluidic chips and responsible for the optimisation of the thermal bonding parameters, and characterisation using optical imaging and profilometry techniques, leak testing, on chip measurement, and interpretation and visualisation of generated data.

Development of a heated fluidic cell, including characterisation of the output from the heater, development, and optimisation of a temperature sensor for feedback and control, and validation of heating on chip-based chemical reactions.

Field work including, site selection, deployment of the autonomous sensing platforms, routine and non-routine sensor servicing and maintenance, environmental sampling and validation, and visualisation of sensor data.

For my Parents

“Equipped with his five senses, man explores the universe around him and calls the adventure Science”

Edwin Powell Hubble, The Nature of Science 1954

Acknowledgements

I would like to thank my supervisors, Prof. Dermot Diamond and Dr. Margaret McCaul, it has been an amazing opportunity to work within the group. Thank you for your support, and contribution during my time in the Adaptive Sensors group. Your support was essential for me in gaining confidence as an early researcher and I am extremely grateful for your input, knowledge, and encouragement. Thank you both for the opportunity to work within the group and introducing me to the field of research.

Thank you to all my colleagues, both past and present that I have worked with over the last number of years. To my colleagues and friends, Ruairi Barrett, Gareth Lacour, Daniel Kerr, Akshay Shinde, and Dr. Peter McCluskey thank you for your positivity, invaluable assistance, and advice over the years. Dr. Brian Kelleher and Dr. Anthony Grey, I am grateful to have had the opportunity to work with both of you during the final months of my PhD, thank you for all your help.

Thank you to all the staff in the NRF and School of Chemical Sciences for all the help, guidance, training, and assistance that has been given during my undergraduate and postgraduate time in DCU.

To all the friends that I have met during my time in DCU Canoe, I am grateful for all the time spent on the water, the club has always allowed me time to de-stress and reflect. I look forward to spending time next season catching up with everyone.

Eolann, thank you for being there both on and off the water, whether it was a rope throw after a missed line or an insight into your own experiences as a PhD candidate. Your advice as both a paddler and a researcher has always been invaluable.

To my family, my parents John and Catherine and my sister Eimear. Thank you for the constant support, advice, and encouragement throughout this entire process, I can't thank you enough for all of the encouragement and support you have given me, this work would not have been possible without all the sacrifices you've made.

List of Publications

Peer Reviewed Articles

1. *Andrew Donohoe*, Gareth Lacour, Peter McCluskey, Dermot Diamond, and Margaret McCaul.
   Development of a Cost-Effective Sensing Platform for Monitoring Phosphate in Natural Waters.
   Published in: *C*hemosensors **2018**, 6 (4), 57–69
   https://doi.org/10.3390/chemosensors6040057

2. *Andrew Donohoe*, Gareth Lacour, D. Jed Harrison, Dermot Diamond, and Margaret McCaul.
   Fabrication of Rugged and Reliable Fluidic Chips for Autonomous Environmental Analysers using combined thermal and pressure bonding of Polymethyl Methacrylate layers.
   Published in: *ACS Omega **2019**, 4 (25), 21131–21140.*
   https://doi.org/10.1021/acsomega.9b01918

3. Paolo Pirovano, Matthew Dorrian, Akshay Shinde, Andrew Donohoe, Aidan J. Brady, Niall M. Moyna, Gordon Wallace, Dermot Diamond, and Margaret McCaul.
   A wearable sensor for the detection of sodium and potassium in human sweat during exercise.
   Published in: *Talanta **2020**, Volume 219, Article 121145*
   https://doi.org/10.1016/j.talanta.2020.121145

   **This work is not presented within the scope of this thesis however represents the range of multidisciplinary projects that I was involved in.*

Book Chapter

1. Andrew Donohoe, Dermot Diamond, and Margaret McCaul.
   Monitoring Environmental Contaminants – A volume in Environmental Contaminants.
   Edited by Steven Johnson

Elsevier 2021

Chapter 2: Emerging Technologies for Autonomous In-Situ Monitoring of Water Quality. Pages 19-55

ISBN: *978-0-444-64335-3*

https://doi.org/10.1016/B978-0-444-64335-3.00001-3

Conference Proceedings

1. Andrew Donohoe, Cameron Hazel, Peter McCluskey, Dermot Diamond, and Margaret McCaul.

   Cost Effective Sensing Platform for the detection of Phosphates in natural waters -

   Sustainable Environmental Solutions – Proceedings CEST 2019

   16th International Conference on Environmental Science and Technology

   *Submitted and under review by Springer to be included in CEST 2019 proceedings

Oral Presentations

1. Andrew Donohoe, Akshay Shinde, Dermot Diamond, and Margaret McCaul.

   Biomarker Analysis in Biofluids.

   Insight Internal Seminar Series - 11th March 2021.

   Virtual Presentation – Insight Centre for Data Analytics, Dublin City University, Dublin, Ireland.

2. Andrew Donohoe, Akshay Shinde, Dermot Diamond, and Margaret McCaul.

   Development of a Customisable Benchtop Platform for the detection of Nitrite and Nitrate utilising Colorimetric Chemistries.

   Environmental Sciences Association of Ireland Environ 2020, 30th Irish Environmental Researchers Colloquium – Ireland Water, Energy and Environment in a Climate and Biodiversity Emergency - 27th to 29th April 2020.

   Virtual Presentation – Water Institute, Dublin City University, Dublin, Ireland.

3. *Andrew Donohoe*, Ruairi Barrett, Akshay Shinde, Komala Pandurangan, Dermot Diamond, and Margaret McCaul.
   HoliFab: Precise Flow Control using Photo Actuated Hydrogel Valves and PI Controlled LED Actuation for Microfluidic MEMS.
   6th Insight Student Conference 2020 – 12th February 2020.
   Insight Centre for Data Analytics, National University of Ireland Galway, Galway, Ireland.

4. *Andrew Donohoe*, Cameron Hazel, Akshay Shinde, Peter McCluskey, Dermot Diamond, and Margaret McCaul.
   Customisable Environmental Platforms for the detection of Nutrients in Natural Waters.
   4th DCU Chemistry Day – 10th May 2019.
   DCU School of Chemistry, Dublin City University, Dublin, Ireland.

5. *Andrew Donohoe*, Cameron Hazel, Akshay Shinde, Peter McCluskey, Margaret McCaul, and Dermot Diamond.
   Customisable Environmental Platforms for the detection of Nutrients in Natural Waters - Flash Talk.
   Insight Internal Seminar Series - 25th October 2018.
   Insight Centre for Data Analytics, Dublin City University, Dublin, Ireland.

6. *Andrew Donohoe*, Gareth Lacour, Peter McCluskey, Margaret McCaul, and Dermot Diamond.
   Development of a cost-effective sensing platform for the detection of Phosphate in Natural Waters.
   CASi 9th Conference for Analytical Sciences in Ireland 2018 – 16th to 17th May 2018.
   Maynooth University, Kildare, Ireland.

7. *Andrew Donohoe*, Gareth Lacour, Peter McCluskey, Margaret McCaul, and Dermot Diamond.

Development of an autonomous sensing platform for detection of nutrients in natural waters - Flash Talk.
Europtrode XIV 25th – 28th March 2018.
Naples, Italy.

8. *Andrew Donohoe*, Margaret McCaul, Adam Porter, Ruairi Barrett, Gordon Wallace, and Dermot Diamond.
   A wearable platform for harvesting and analysing electrolyte content in sweat.
   Flex 2018 (Semicon Europa) – 13th -16th November 2018.
   Messe München, Munich, Germany.

9. *Andrew Donohoe*, Gareth Lacour, Margaret McCaul, and Dermot Diamond.
   Cost Effective Sensing Platform for the Detection of Phosphate in natural waters.
   AquaEnviro, The Big Phosphorus Conference and Exhibition – Removal and Recovery – 4th -5th July 2017.
   Manchester United Stadium, Manchester, United Kingdom.

Poster Presentations

1. *Andrew Donohoe*, Peter McCluskey, Dermot Diamond, and Margaret McCaul.
   Customisable Environmental Platforms for the Detection of Nutrients in Natural Waters.
   6th Insight Student Conference 2020 – 12th February 2020.
   Insight Centre for Data Analytics, National University of Ireland Galway, Galway, Ireland.

2. *Andrew Donohoe*, Peter McCluskey, Margaret McCaul, and Dermot Diamond.
   Customisable Environmental Platforms for the Detection of Phosphate in Natural Waters.
   Xenowac II 2018 - Challenges and Solutions related to Xenobiotics and Antimicrobial Resistance in the Framework of Urban Wastewater Reuse: Towards a Blue Circle Society – 10th -12th October 2018
   Limassol, Cyprus.

3. *Andrew Donohoe*, Gareth Lacour, Peter McCluskey, Margaret McCaul, and Dermot Diamond.
   Customisable Environmental Platforms for the Detection of Nutrients in Natural Waters.
   5th Insight Student Conference 2018 – 7th September 2018.
   Insight Centre for Data Analytics, University College Dublin, Dublin, Ireland.

4. *Andrew Donohoe*, Gareth Lacour, Peter McCluskey, Margaret McCaul, and Dermot Diamond.
   Development of an autonomous sensing platform for detection of nutrients in natural waters.
   Europtrode XIV 25th – 28th March 2018,
   Naples, Italy.

5. *Andrew Donohoe*, Gareth Lacour, Peter McCluskey, Margaret McCaul, and Dermot Diamond.
   Development of an autonomous sensing platform for detection of nutrients in natural waters.
   4th Insight Student Conference 2017 – 8th September 2017
   Insight Centre for Data Analytics, University College Cork, Cork, Ireland.

6. *Andrew Donohoe*, Gareth Lacour, Eoin McNamara, Margaret McCaul, and Dermot Diamond.
   Poster and Sensor Demonstration on the Development of an Autonomous Sensing Platform.
   ACEs 12th International Electromaterials Science Symposium, Dublin Workshop - 7th February 2017.
   The Helix, Dublin City University, Dublin, Ireland.

7. *Andrew Donohoe*, Gareth Lacour, Eoin McNamara, Margaret McCaul, and Dermot Diamond.
   Poster and Sensor Demonstration on the Development of a cost-effective sensor for the in-situ monitoring of Phosphate.

NAPES (Next Generation Analytical Platforms for Environmental Sensing)
Workshop 2 Sensing our Environment: From Innovative Materials to Autonomous Sensors and Earth Observation – 27th -28th March 2017
Crokepark Stadium, Dublin, Ireland.

8. *Andrew Donohoe*, Gareth Lacour, Margaret McCaul, Carla Navarro-Hérnandez, Pablo Fanjul, and Dermot Diamond.
   Development of a cost-effective sensor for the in-situ monitoring of Heavy Metals.
   Royal Society of Chemistry, Analytical Research Forum 7th July 2017.
   Royal Society of Chemistry, London, United Kingdom.

Workshops and Demonstrations

1. IOT Agriculture Water and Technology Workshop 2018 – 16th July 2018
   Dingle Hub, Kerry, Ireland.
   Workshop on the possibilities for supporting agriculture in raising efficiency and protecting the environment in Dingle.

2. NAPES (Next Generation Analytical Platforms for Environmental Sensing)
   Workshop 2 Sensing our Environment: From Innovative Materials to Autonomous Sensors and Earth Observation – 27th -28th March 2017.
   Crokepark Stadium, Dublin, Ireland.
   Demonstration of Prototype nutrient sensing technology for Phosphate detection.

Awards

1. Dr Colin Barnes commemorative award for Postgraduate Excellence 2019.
   4th DCU Chemistry Day – Awarded 10th May 2019
   DCU School of Chemistry, Dublin City University, Dublin, Ireland.
   Awarded best Postgraduate talk, entitled, Customisable Environmental Platforms for the detection of Nutrients in Natural Waters.

2. Postgraduate Speaker Prize.
   CASi 9th Conference for Analytical Sciences in Ireland 2018 – Awarded 17th May 2018.
   Maynooth University, Kildare, Ireland.
   Awarded runner up best Postgraduate speaker prize at CASi 2018, entitled, the Development of a Cost-Effective Sensing Platform for the Detection of Phosphate in Natural Waters.

3. Andrew Donohoe, Gareth Lacour, Margaret McCaul, and Dermot Diamond.
   INVENT 2017 Commercialisation Award for Engagement with Business and Industry – Awarded 11th April 2018
   INVENT innovation centre, Dublin City University, Dublin, Ireland.
   DCU Invent Commercialisation Award 2017 for Innovation Partnership with TE Laboratories on the Development of Customisable Environmental Monitoring Platforms based on 3D Printed Microfluidics.
   Enterprise Ireland Innovation Partnership Programme.
   Project number IP/2016/0502.

4. Lab on a Chip Poster Prize
   Royal Society of Chemistry, Analytical Research Forum - Awarded 7th July 2017, Royal Society of Chemistry, London, United Kingdom.
   Awarded Lab on a Chip best poster titled Development of Cost-Effective Sensors for the In-Situ Monitoring of Heavy Metals.

Author Contribution

This thesis includes 2 original manuscripts that have been published in peer reviewed journals and one book chapter that has been published. The writing up of all the manuscripts in the thesis were the principal responsibility of myself, the candidate, working within Insight Centre for Data Analytics / the School of Chemical Sciences under the supervision of Prof. Dermot Diamond and Dr Margaret McCaul. The inclusion of co-authors reflects the contribution of work by the multidisciplinary team within the Adaptive Sensors Group and collaborators. In the case of the published chapters my contribution to the work involved:

Thesis Chapter	Publication	Candidate Contribution
1	Andrew Donohoe, Dermot Diamond, and Margaret McCaul. Monitoring Environmental Contaminants – A volume in Environmental Contaminants. Edited by Steven Johnson Elsevier 2021 Chapter 2: Emerging Technologies for Autonomous In-Situ Monitoring of Water Quality. Pages 19-55 ***ISBN:*** *978-0-444-64335-3* https://doi.org/10.1016/B978-0-444-64335-3.00001-3	First author, manuscript development and writing up.

4	*Andrew Donohoe*, Gareth Lacour, Peter McCluskey, Dermot Diamond, and Margaret McCaul. Development of a Cost-Effective Sensing Platform for Monitoring Phosphate in Natural Waters. ***Published in:*** *Chemosensors* **2018**, *6* (4), 57–69 https://doi.org/10.3390/chemosensors6040057	First author, manuscript development and writing up, sensor testing and validation, field work, data collection, analysis, and visualisation.
5	*Andrew Donohoe*, Gareth Lacour, D. Jed Harrison, Dermot Diamond, and Margaret McCaul. Fabrication of Rugged and Reliable Fluidic Chips for Autonomous Environmental Analysers using combined thermal and pressure bonding of Polymethyl Methacrylate layers. ***Published in:*** *ACS Omega* **2019**, *4* (25), 21131–21140. https://doi.org/10.1021/acsomega.9b01918	First Author, manuscript development, sensor testing and validation, field work, data collection, analysis, and visualisation.

Signed: **Date:** 10/09/2021

Andrew Donohoe

Signed: **Date:** 10/09/2021

Margaret McCaul

Signed: 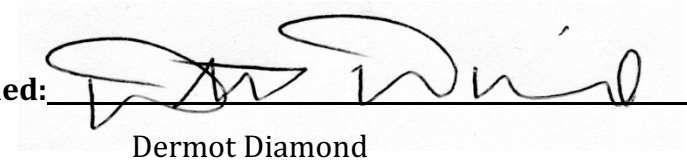 **Date:** 10/09/2021

Dermot Diamond

Outline of Chapters

Chapter 1

Literature Review - Emerging Technologies for Autonomous In-Situ Monitoring of Water Quality.

This chapter gives context to emerging sensor technologies, the current approach to water quality monitoring and analytical methods used for the detection of nutrients. It discusses current state of autonomous sensing and potential advantages of combining real time in situ measurement with remote sensing. This chapter presents the context in which the experimental chapters contribute to the scientific advancement of the research area covering important areas such as water quality analysis, microfluidics, and analytical methods for the determination of nutrients.

Chapter 2:

Development and optimisation of a customisable benchtop sensing platform for the detection of optical colorimetric chemistries.

This chapter presents the initial development of a bench top sensing platform for the detection of colorimetric chemical reactions and its optimisation. A detailed study with both software and hardware level refinement was carried out with the aim of improving the measurement signal as well as the accuracy and precision. The fabrication of this system is discussed and the ability of a cost-effective electrical circuit to detect phosphate and nitrite. The sensing platform is tested using a series of known standards and environmental samples.

Chapter 3:

Development of a regulated heated fluidic system for on chip fluidic detection of nutrients.

This chapter further advances the prototype benchtop sensing platform discussed in chapter 2 with the addition of a regulated heated cell. The addition of a heated fluidic chip allows for the regulation of temperature within the chip as well as the ability to carry out heated colorimetric reactions with improved reaction times. Nitrate detection was carried out using a reducing agent in combination with heat as a catalyst to reduce nitrate to nitrite where it could be detected using the Griess assay outlined in chapter 2. This method was tested against a series of known standards and environmental samples.

Chapter 4:

Development of a Cost-Effective Sensing Platform for Monitoring Phosphate in Natural Waters.

This chapter discusses the development of a prototype autonomous sensing platform. The design, fabrication and internal layout of the sensor are presented. The platforms analytical performance is tested by a series of in lab tests and a preliminary field assessment is carried out by deployment over a five-day period.

Chapter 5:

Fabrication of Rugged and Reliable Fluidic Chips for Autonomous Environmental Analysers using combined thermal and pressure bonding of PMMA layers.

This chapter focuses on fabrication of PMMA fluidic chips in detail. The fluidic chips are developed with a focus on robustness for environmental deployment applications. The fabrication and thermal bonding method are assessed in terms of bond strength,

reproducibility, and failure rate. The fluidic chip is then tested both in lab and in the field with a 28-day deployment in an integrated autonomous sensing platform.

Chapter 6:

Summary and Conclusions.

To conclude the work demonstrated a summary of the work carried out is discussed. This chapter presents the conclusions of the thesis and discusses the impact this work could have on future developments of autonomous sensing platforms.

Table of Contents

Declaration ..... *ii*

Acknowledgements ..... *v*

List of Publications ..... *vi*

Author Contribution ..... *xiii*

Outline of Chapters ..... *xvi*

List of Abbreviations ..... *xxxi*

Thesis Abstract ..... *xxxiii*

Chapter 1 - Emerging Technologies for Autonomous In-Situ Monitoring of Water Quality

Abstract *2*

1.1. Introduction *3*

1.2. Water quality monitoring *5*

1.3. Sensing challenges: Platform and deployment hierarchies *6*

1.4. Stability challenges with chemical sensors *11*

1.5. Influence of microfluidics *13*

1.6. Manual single-use sensing *15*

1.7. Autonomous in-situ sensing for nutrients *17*

1.7.1. Phosphorus **18**

1.7.2. Phosphate-sensing methods **19**

1.7.3. Nitrogen **22**

1.7.4. Nitrite and nitrate colorimetry **22**

1.7.5. Ammonia colorimetry **24**

1.8. Current and emerging nutrient sensing systems *25*

1.8.1. Examples of current sensing systems **25**

1.8.2. Emerging sensing systems **28**

1.9. Challenges for autonomous in-situ sensing systems ***31***

1.9.1. Sensing platform fouling **32**

1.10. Remote sensing ***35***

1.11. Conclusion ***38***

1.12. References ***39***

Chapter 2 - Development and optimisation of a customisable benchtop sensing platform for the detection of optical colorimetric chemistries

Abstract ***56***

2.1. Introduction ***57***

2.2. Materials and Methods ***58***

2.2.1. Reagent and Standard Preparation **58**

2.2.2. Instrumentation **59**

2.2.3. Benchtop sensing platform design **60**

2.2.3.1. Measurement control of the benchtop sensing platform 62

2.2.3.2. Optical Cell Setup 62

2.3. Results and Discussion ***64***

2.3.1. Characterisation of the colorimetric methods. **64**

2.3.1.1. Wavelength selection – Spectrum Scan 64

2.3.1.2. Reaction rates – Kinetics 67

2.3.1.3. Working Range – Linear Calibration 70

2.3.1.4. Interference study – Salinity Effects 71

2.3.2. Detection using the Benchtop sensing platform **73**

2.3.2.1. PWM Control – LED Characterisation 73

2.3.2.2. Optimization of measurement signal and LED output. 76

2.3.2.3. Optimization of PWM signal 81

2.3.3. Benchtop sensing platform performance vs UV-Vis spectrometer 85
2.3.3.1. Calibration Curve on benchtop sensing platform versus UV-Vis spectrometer. 85
2.3.3.2. Environmental Sampling 88
2.4. Conclusion 94
2.5. References 96

Chapter 3- Development of a regulated heated fluidic system for on chip detection of nutrients

Abstract 103
3.1. Introduction 104
3.2. Materials and Methods 105
3.2.1. Reagent and Standard Preparation 105
3.2.2. Instrumentation / Electronics Design 106
3.2.3. Temperature Sensor Development 107
3.2.4. Integrated Fluidic heater 108
3.3. Results and Discussion 109
3.3.1. Characterisation of the colorimetric methods. 109
3.3.1.1. Wavelength selection – Spectrum Scan 109
3.3.1.2. Reaction rates – Kinetics 110
3.3.1.3. Working Range – Linear Calibration 112
3.3.1.4. Interference Study – Salinity Effects 113
3.3.1.5. Interference Study – Nitrite interference 116
3.3.2. Heater Selection and Characterisation 119
3.3.2.1. Heater Characterisation – Voltage Control 119
3.3.2.2. Temperature Regulation and Validation (feedback thermostat loop) 120
3.3.2.3. Integration of PID refinement 122
3.3.3. Heated Platform Performance vs UV-Vis Spectrometer 124
3.3.3.1. Calibration curve on benchtop sensing platform versus UV-Vis spectrometer. 124
3.3.3.2. Environmental Sampling 126
3.4. Conclusion 130

3.8. References *132*

Chapter 4 - Development of a Cost-Effective Sensing Platform for Monitoring Phosphate in Natural Waters

Abstract *137*

4.1. Introduction *138*

4.2. Materials and methods *139*

4.2.1. Reagents and standard preparation **139**

4.2.2. Fluidic handling **140**

4.2.3. Fluidic chip and optical detection **142**

4.2.4. Chassis, housing, and tubing **143**

4.2.5. Electrical control and transmittance **143**

4.2.6. Analytical performance **144**

4.2.7. Long-term laboratory assessment of the sensing platform in fully autonomous mode **144**

4.2.8. Field deployment **145**

4.3. Results and discussion *147*

4.3.1. Validation of sampling and optical detection (methods 1 and 2) **147**

4.3.2. Long-term laboratory assessment of the sensing platform in fully autonomous mode **149**

4.3.3. Preliminary Field Assessment of the Sensing Platform **152**

4.4. Discussion *153*

4.5. Conclusions *155*

4.6. References *155*

Chapter 5 - Fabrication of Rugged and Reilable Fluidic Chis for Autonomous Environmental Analysers using combined thermal and pressure bonding of Polymethly Methacrylate layers

Abstract *158*

5.1. Introduction *159*

5.2. Materials and Methods *161*

5.2.1. Analytical Method **161**

5.2.2. Bonding Procedure **164**

5.2.3. PMMA Fluidic Chip Characterisation **164**

5.2.4. Chip Leak Testing **165**

5.2.5. Inter-Layer Tensile Strength Measurements **166**

5.3. Results and Discussion *167*

5.3.1. Chip Inter-Layer Bond Strength Analysis **167**

5.3.2. Post-Bonding Fluidic Chip Channel Characterisation **169**

5.3.3. Fluidic Chip Characterisation - Leak testing **174**

5.3.4. Performance of Fluidic Chip in prototype Nutrient analyser **174**

5.3.4.1. In-lab testing **174**

5.3.4.2. In-Situ Field Testing 176

5.4. Conclusion *181*

5.5. References *182*

Chapter 6 - Summary and Conclusions

6.1. Introduction *186*

6.2. Aims and achievements *186*

6.3. Limitations to in-situ remote sensing *187*

6.4. Research drivers 188

6.5. Future progress of the autonomous sensing platform 189

6.6. Challenges to further development and progress 190

6.7. Strategies for achieving further progress 191

6.8. Advancing Sensor Networks 192

6.9. References 192

Supplementary Information

Chapter 2 197

Chapter 3 209

Chapter 5 226

List of Figures

Chapter 1 - Emerging Technologies for Autonomous In-Situ Monitoring of Water Quality

Figure 1.1. *Remote continuous sensing challenges, platform, and deployment hierarchies.....8*
Figure 1.2. *Map of distributed total operational sensing floats (3852 top) under the ARGO project versus operational biogeochemical floats (372 bottom). [35] accessed September 2019 – credit http://argo.jcommops.org.....10*
Figure 1.3. *Calibration data for the mean responses of disposable solid-contact-ion selective electrodes for environmental monitoring of lead stored in (A) 10^{-9} M Pb^{2+}, pH = 4 in lab and, (B) continuous contact with river water [44].....12*
Figure 1.4. *Examples of microfluidic prototype technology used in sensing platforms. (1) PMMA layer of lab on chip for phosphate detection [48], (2) microfluidic chip for the direct determination of nitrate [49], (3) opaque fluidic chip with optically clear windows for nutrient analysis [50] (4) z shaped optical microfluidic detector, render adapted from Murray et al. [51], (5) PhosphaSense lab on disk for phosphate analysis [52], (6) flow control microfluidic chip containing in-situ photo responsive hydrogel valves [45,53].....14*
Figure 1.5. *Freshwater watch interface showing sample data input by a volunteer citizen scientist including location, site image, Hydrological, chemical and optical results.[56] Credit EarthWatch, Citizen Scientist: Kevine – Friday August 23 2019.....16*
Figure 1.6. *Conceptual reaction schematic of standard colorimetric methods for phosphate detection (Top) Vanadomolybdophosphoric Acid method (yellow) (ε = 8.38 x 10^3 mol L^{-1} cm^{-1} at λ_{max} 380 nm [83]) and (Bottom) molybdenum blue ascorbic acid method (blue method) (ε = 2.61 x 10^4 mol L^{-1} cm^{-1} at λ_{max} 820 nm [84]).....21*
Figure 1.7. *Conceptual reaction schematic of the Griess assay for colorimetric detection of nitrite (ε = 3.56 x 10^3 mol L^{-1} cm^{-1} at λ_{max} 520 nm [98]).....23*
Figure 1.8. *Conceptual reaction schematic of the Berthelot assay for colorimetric detection of ammonia (ε = 6.07 x 10^{-2} mol L^{-1} cm^{-1} at λ_{max} 660 nm [91]).....25*
Figure 1.9. *Commercial water sensing platforms(1) TresCon UNO [102] credit Xylem Analytics Germany, (2) Hach 5500 SC [103] , (3) ChemScan Mini oP [104] and, (4)Alyza IQ [105] credit Xylem Analytics Germany.....26*
Figure 1.10. *Prototype sensing platforms for nutrient monitoring (1) Ecosens Aquamonitrix portable IC system for determination of nitrite and nitrate [51,107], (2) National Oceanography Centre Southhampton phosphate analyser [38], (3) Sea-Bird Scientific Hydrocycle PO_4 sensor [40,108] (4) Phosphate sensing platform developed by the Adaptive Sensor Group at DCU Insight Centre[50], (5) Systea WIZ Probe [109], (6) Systea NPA Pro [110].....29*
Figure 1.11. *Biofouling accumulation on deployed water sensing platforms (1) Sea-bird Scientific Hydrocycle -PO_4 prior to and following a 32 day field test in the Maumee river [40], (2) Prototype nutrient analyser removed after 3 week deployment, (3) Prefilter on an inlet of nutrient sensing platform deployed in the marine environment after 1 week, (4) Fouled YSI Sonde after deployment with clean sensing surfaces [128] Image Courtesy: YSI, a Xylem brand,(5) Fluorometer after 30 days in Helgoland (Germany) [120] ,(6) NOC sensing platform prior to and following a 32 day field test in the Maumee River [38].....34*
Figure 1.12. *Correlation between temperature, salinity and phosphate measurements taken using combination remote and in-situ sensing at Kinvara Bay, Galway, Ireland. Figure adapted from McCaul et al. [129].....37*

Chapter 2 - Development and optimisation of a customisable benchtop sensing platform for the detection of optical colorimetric chemistries

Figure 2.1. *(A) Schematic showing experimental setup of benchtop sensing platform. (B, C) images of the manufactured benchtop sensing platform and (D) optical cell consisting of a PMMA fluidic chip aligned between the LED - photodiode detector.* *61*
Figure 2.2. *Schematic showing experimental setup of benchtop sensing platform. Method 1 Complete benchtop sensing platform with controlled output from LED measured and converted to a signal by on board photodiode and Method 2 Output from LED controlled by benchtop sensing platform and its output measured externally using an ocean optics fibre optic detector.* *63*
Figure 2.3. *Spectrum scan of (A) vanadomolybdophosphoric acid method of phosphate detection and (B) spectrum scan of Griess assay for nitrite detection on UV-Vis spectrometer.* *65*
Figure 2.4. *Spectrum scan of the fluidic chip optical window (black line) and alternative variations of "clear" Polymethyl methacrylate.* *66*
Figure 2.5. *Kinetic study of yellow reagent complex (A) varying reaction temperature and (B) varying standard concentration.* *68*
Figure 2.6. *Kinetic study of Griess reagent complex (A) varying reaction temperature and (B) varying standard concentration.* *69*
Figure 2.7. *Calibration curve of (A) phosphate standards and (B) nitrite standards tested at 0, 20 and 40 g/L Artificial Seawater matrix. The error bars represent the standard deviations for n=3.* *72*
Figure 2.8. *Method 1 Digital output from the photodiode measuring PWM controlled LED intensity at a range of 1000 – 3000 PWM.* *74*
Figure 2.9. *Method 2 Measured LED output under PWM control (200-3800) using fibre optic detector with (A) showing chosen LED for phosphate detection and (B) showing chosen LED for nitrite detection.* *75*
Figure 2.10. *Measured LED output at PWM 500 of a blank solution showing LED overshoot prior to stabilisation of measurement.* *77*
Figure 2.11. *Calibration curve for phosphate (PO_4^{3-}) presenting (A) in bits (raw data) and (B) converted absorbance using benchtop sensing platform averaging the initial 100 measurements from the unstable portion of the LED (375 nm) output.* *79*
Figure 2.12. *Calibration curve for phosphate (PO_4^{3-}) (A) in bits (raw data) and (B) converted absorbance using benchtop sensing platform averaging the final 100 measurements from the stable portion of the LED (375 nm) output.* *80*
Figure 2.13. *Calibration curve for phosphate (PO_4^{3-}) presenting (A) in bits (raw data) and (B) converted absorbance using benchtop sensing platform at 47 Ω resistance.* *82*
Figure 2.14. *Calibration curve for phosphate (PO_4^{3-}) presenting (A) in bits (raw data) and (B) converted absorbance using benchtop sensing platform at 100 Ω resistance.* *83*
Figure 2.15. *Linear calibration curves for the detection of (A) phosphate 0-50 µM and (B) nitrite 0-10 µM on the benchtop sensing platform versus UV-Vis spectrometer.* *86*
Figure 2.16. *Environmental sampling map showing ten sampling points along the river Liffey.* *89*
Figure 2.17. *Nutrient concentrations measured across the ten sampling points along the river Liffey for (A) phosphate and (B) nitrite.* *92*

Chapter 3- Development of a regulated heated fluidic system for on chip detection of nutrients

Figure 3.1. *Thermistor based temperature sensor circuit layout using an Arduino based microcontroller and a voltage divider using a thermistor and a fixed resistor in series.* *108*
Figure 3.2. *Schematic diagram of PMMA fluidic chip with integrated heater and temperature sensor.*. *109*
Figure 3.3. *Spectrum scan of nitrate detection using the Griess method with vanadium chloride (III) reduction step.* *110*
Figure 3.4. *Kinetic study of heated nitrate detection with (A) varying reaction temperature and (B) varying standard concentration.* *111*
Figure 3.5. *Calibration curve of nitrate standards tested at 0, 20 and 40 g/L artificial seawater matrix. The error bars represent the standard deviations for n=3.* *114*
Figure 3.6. *Spectrum scan of nitrate standards tested at 0, 20 and 40 g/L artificial seawater matrix.*... *115*
Figure 3.7. *Calibration curve of nitrite, nitrate and mixed standards, showing (A) nitrite detection and (B) combined nitrite and nitrate detection. The error bars represent the standard deviations for n=3.*.. *117*
Figure 3.8. *Determination of individual species in mixed samples containing nitrite and nitrate.* *118*
Figure 3.9. *Measured output of silicone heater attached to PMMA fluidic chip at 3.3 V, 6 V, 9 V, 12 V and 14.4 V over a period of one hour.* *119*
Figure 3.10. *Schematic for feedback loop for temperature regulation using a microcontroller and temperature sensor to trigger the heater on or off* *121*
Figure 3.11. *Measured heat of the PMMA fluidic device versus the heaters state (on or off) using the feedback loop.* *122*
Figure 3.12. *Measured heat of the PMMA fluidic device versus the heaters output using PID control.*.... *123*
Figure 3.13. *Comparison of the two tested methods of heater regulation, thermistor feedback versus PID control.* *124*
Figure 3.14. *Linear calibration curves for the detection of nitrate 0-10 μM using VCl_3 and Griess reagent on the heated benchtop sensing platform vs UV-Vis spectrometer at 545 nm.* *125*
Figure 3.15. *Environmental Sampling map showing ten sampling points along the river Boyne.* *127*
Figure 3.16. *Nutrient concentrations measured across the six sampling points along the river Boyne for (A) nitrite and (B) nitrate.* *129*

Chapter 4 - Development of a Cost-Effective Sensing Platform for Monitoring Phosphate in Natural Waters

Figure 4.1. *Picture of the autonomous sensing platform. (A) inlet system, (B) bags holding sample, high calibration standard, and low calibration standard, (C) detection chamber housing the microfluidic chip, LED (375 nm), and photodiode, (D) poly (methyl methacrylate) (PMMA) fluidic board, (E) battery, (F) reagent bag, (G) waste bag and (H) electronics.* *140*
Figure 4.2. *Schematic diagram illustrating the sensing platform fluidic system. The portion including the fluidic chip is within the area bounded by the dashed line.* *141*
Figure 4.3. *(A) Exploded render of the microfluidic chip showing 1) the top PMMA layer with the milled reagent/sample inlet and waste outlet, 2) the clear PMMA optical windows at each side of the optical channel and 3) the capping layer of the PMMA chip. (B) Render of the microfluidic chip custom 3D printed alignment rail and sliders with detector components: 1) 375 nm UV LED; 2) photodiode; 3) LED slider; 4) photodiode slider; 5) microfluidic chip mount and alignment rail; and 6) microfluidic chip. (C) Image of the fluidic chip integrated into the alignment rail.* *143*
Figure 4.4. *(A) Satellite image of the sampling location at Loughrea Co. Galway, Ireland. (53°11′47.5″ N: 8°34′6.8″ W) [13]. (B) Picture of the prototype sensing platform deployment at Lough Rea angler's fish hatchery, Loughrea Co. Galway, Ireland.* *146*

Figure 4.5. *(A) Comparison of phosphate linear calibrations (0–50 µM) obtained using the UV-Vis spectrophotometer and the fluidic chip detector with off-chip pre-mixed solutions (Method 1); (B) comparison of phosphate linear calibrations obtained using the UV-Vis spectrophotometer and the fluidic chip detector with automated sampling and on-chip mixing (Method 2). Method 1 (off-chip solution mixing) was also repeated with the same solutions for comparison. The excellent precision is evidenced by masking of error bars (standard deviations for n = 10 replicate measurements) by the point symbols.. 148*
Figure 4.6. *Laboratory analysis of phosphate standards (PO_4^{3-}) with the autonomous sensing platform (grey dots) and the UV-Vis spectrophotometer reference method (red dots). Performance issues Sections 1 and 2 (blue line)..... 150*
Figure 4.7. *Variation in phosphate concentration (PO_4^{3-}) measurements in Lough Rea over the 5-day deployment. The red dots represent concentrations of PO_4^{3-} in grab samples collected at the site during the deployment and measured with the lab-based UV-Vis reference method..... 152*

Chapter 5 - Fabrication of Rugged and Reilable Fluidic Chis for Autonomous Environmental Analysers using combined thermal and pressure bonding of Polymethly Methacrylate layers

Figure 5.1. *The two-layer design showing; (A) bottom channel layer containing milled fluidic channels incorporating a merging point (1) for sample and reagent inputs, a serpentine mixing region (2) for mixing of sample and reagent, an outlet line (3) for flushing of waste after analysis, and optical channel (4) for detection on chip, and two optically clear windows (5) for coupling light into and out of the detection channel. (B) Upper capping layer incorporating two holes (6) to house alignment pins for the two layers during bonding, and three 6.5 mm circular through holes, two inlets for sample and reagent intake (7) and one outlet (8) for waste..... 162*
Figure 5.2. *Manufacturing scheme for prototyping of two-layer PMMA fluidic chips. (1) micro-milling is used to produce a batch of two layer fluidic chips (x3) from a 145 x 145 mm laser cut PMMA milled plate, (2) the cleaned capping, channel layer and optically clear windows are aligned to fluidic chip design, (3) bonding is carried out using heat and pressure with the aligned fluidic chip positioned between two glass compression plates and a brass weight on top and (4) barbed liquid connectors are integrated and the fluidic chips are leak tested prior to use..... 163*
Figure 5.3. *Channel layout and the target areas used for characterisation of the channels in the channel layer of the Fluidic chip. 1) sample and reagent inlet where sample and reagent merge after intake onto the chip, 2) initial portion of the serpentine mixing region where the sample and reagent mix on chip prior to measurement, 3) waste outlet channel through which sample and reagent are flushed after analysis and 4) optical channel for colorimetric detection of the sample/reagent mixture. These regions are discussed further (see Figure 5.8.). The blue line in the waste outlet channel (3) is the location used to obtain the section shown in figure 5.7..... 165*
Figure 5.4. *Experimental setup for bond strength testing with two-layer chip fixed between two clamps used to apply tension; Left: rendering of the test rig with the upper (A) and lower (B) clamps; Middle: photo of the test rig in position prior to pull-apart testing; Right: chip after pull-apart test showing channel layer (A) and capping layer (B)..... 166*
Figure 5.5. *Bond strength analysis carried for methods (1) fluidic chip adhered directly to metal plates using epoxy, failure was seen at the epoxy interface, (2) fluidic chip with roughened surface adhered to metal plates using epoxy, failure was seen at the epoxy interface and (3) fluidic chip with roughened surface adhered to metal plate with roughened and scored surface using epoxy, failure occurred at the bond between the fluidic chip layers..... 168*
Figure 5.6. *Images of chips after layer separation; (A) photo of the bottom fluidic layer showing channels; close up photos of the bottom layer (B) and top layer (C) showing the channel layout imprinted on the top layer; Keyence microscope images the lower layer showing a section of the serpentine mixing channel (D) and its imprint (E) on the same region of the top layer..... 169*

Figure 5.7. *Section across the lower layer channel (blue) and the equivalent section of the upper layer imprint (teal) at the location marked in teal in figure 5.3. Data obtained using the Bruker ContourGT Optical Profilometer.* *170*
Figure 5.8. *Optical profile and microscope images of channel layer before and after bonding of the (1) merging point, (2) mixing channel, (3) waste outlet, (4) optical channel (see Figure 5.3.).* *171*
Figure 5.9. *Optical detection for phosphate (PO_4^{3-}) using the yellow method comparing the Prototype Analyser incorporating the fluidic chip and the UV-Vis spectrometer (375nm)*..... *176*
Figure 5.10. *(A) Picture of the prototype sensing platform deployment at Liffey deployment location, Co. Dublin, Ireland (B) Satellite image of the sampling location at Palmerstown, Co. Dublin, Ireland. (Coordinates 53.356246, -6.360325999999986)*..... *177*
Figure 5.11. *In-Situ environmental monitoring. (A) water level (cm) from 21/02/2018 to 20/03/2018, (B) external and internal temperature (°C) from 21/02/2018 to 11/03/2018.* *178*
Figure 5.12. *Prototype analyser with integrated fluidic chip, phosphate (PO_4^{3-}) detection at the deployment site over a 28-day period.*..... *180*

Supplementary Information

Figure SI.2.1. *Initial setup code for microcontroller function with modifiable system variables.*..... *197*
Figure SI.2.2. *Spectrum scan of fluidic chip optical window (Black Line) and alternative variations of "clear" Polymethyl methacrylate.* *198*
Figure SI.2.3. *Calibration curve of (A) phosphate standards ranging from 0-2000 µM and (B) nitrite standards ranging from 0-100 µM carried out on UV-Vis Spectrometer. The error bars represent the standard deviations for n=3.* *199*
Figure SI.2.4. *Roithner LaserTechnik XSL-375-TF-R2 UV LED (A) LED batch to batch intensity variation and (B) corrected LED intensity (N=10)*..... *200*
Figure SI.2.5. *Roithner LaserTechnik LED 545-33 (A) LED batch to batch intensity variation and (B) corrected LED intensity (N=10)*..... *201*
Figure SI.2.6. *TSL257 LF ams Photodiode (A) Photodiode batch to batch intensity measurement variation and (B) corrected Photodiode measurement (N=10)* *202*
Figure SI.2.7. *Calibration curve for nitrite (NO_2^-) presenting (A) in bits (raw data) and (B) converted absorbance using benchtop detection platform at 67 Ω resistance.* *203*
Figure SI.2.8. *Calibration curve for nitrite (NO_2^-) presenting (A) in bits (raw data) and (B) converted absorbance using benchtop detection platform at 390 Ω resistance.*..... *204*
Figure SI.2.9. *Measurement stability accounting for initial LED overshoot prior to data acquisition.*.... *205*
Figure SI.2.10. *Calibration curve of (A) phosphate standards ranging from 0-2000 µM and (B) nitrite standards ranging from 0-50 µM carried out on Benchtop sensing platform. The error bars represent the standard deviations for n=3.* *206*
Figure SI.2.11. *Environmental sampling map showing the start and end point of the samples collected across the 14 km transect of the river Liffey.*..... *207*
Figure SI.2.12. *Component cost breakdown of benchtop platform*..... *208*
Figure SI.3.1. *Code of resistance-based temperature measurement and conversion of ADC value to Celsius using the Steinhart equation.* *210*
Figure SI.3.2. *Circuit diagram of temperature sensor schematic.* *210*
Figure SI.3.3. *Calibration curve for nitrate detection using standards ranging from 0-100 µM carried out on UV-Vis Spectrometer. The error bars represent the standard deviations for n=3.* *211*
Figure SI.3.4. *Comparison of temperature output with and without an integrated boost convertor.*..... *212*
Figure SI.3.5. *Code of temperature regulation using limits and feedback from the integrated temperature sensor.* *215*
Figure SI.3.6. *Code of temperature regulation using PID control.* *220*
Figure SI.3.7. *Introduction of room temperature solution (5 mL) to the heated fluidic cell showing a reduction in temperature upon sample addition before returning to regulated values.*..... *221*

Figure SI.3.8. *Bubble generation within the microfluidic channels when heated reaction is occurring at higher temperatures.* *222*
Figure SI.3.9. *Calibration curve of nitrate standards ranging from 0-50 µM carried out on Benchtop sensing platform. The error bars represent the standard deviations for n=3.* *223*
Figure SI.3.10. *Environmental sampling map showing the start and end point of the samples collected across the 7 km transect of the river Boyne catchment.* *224*
Figure SI.3.11. *Combined nitrite and nitrate concentrations measured across the six sampling points along the river Boyne.* *225*
Figure SI.5.1. *Experimental setup for thermal bonding of two-layer PMMA fluidic chip. (A) brass weight (220 g), (B) glass compression plates (200 x 100 mm) with (C) Aligned two-layer fluidic chip.* *226*
Figure SI.5.2. *Channel layout and the target areas used for characterisation of the channels in the channel layer of the Fluidic chip. 1) Sample and reagent inlet where sample and reagent merge after intake onto the chip, 2) initial portion of the serpentine mixing region where the sample and reagent mix on chip prior to measurement, 3) waste outlet channel through which sample and reagent are flushed after analysis and 4) optical channel for colorimetric detection of the sample/reagent mixture. These regions are imaged in figure S3 and transects shown in red are graphed alongside.* *228*
Figure SI.5.3. *Optical Profile images of channel layer target areas (see figure SI.5.2.) before bonding with transects showing channel width and depth of the (1) Merging Point, (2) Mixing Channel, (3) Waste Outlet, (4) Optical Channel.* *229*

List of Abbreviations

abs	*Absorbance*
ACT	*Alliance Coastal Technologies*
ADC	*Analogue to Digital Convertor*
DO	*Dissolved Oxygen*
EPA	*Environmental Protection Agency*
FIA	*Flow Injection Analysis*
GPRS	*General Packet Radio Service*
GSM	*Global System for Mobile (communication)*
IIWQ	*International Initiative on Water Quality*
IDE	*Integrated Development Environment*
IoT	*Internet of Things*
ISE	*Ion Selective Electrode*
LED	*Light Emitting Diode*
LOD	*Limit of Detection*
LOQ	*Limit of Quantification*
MODIS	*Moderate Resolution Imaging Spectroradiometer*
NEDD	N-1-naphthylethylenediamine dichloride
nm	*Nano Metre*
NSA	*Nutrient Sensitive Area*
NTL	*Nominal Tidal Limit*
NOC	*National Oceanography Centre*
PCB	*Printed Circuit Board*
PD	*Photo Diode*
PID	*Proportional Integral Derivative*
PLA	*polylactic acid*
PMMA	*polymethyl methacrylate*
PVDF	*polyvinylidene fluoride*
PWM	*Pulse Width Modulation*
RE	*Relative Error*
RMS	*Route Mean Square*
RSD	*Relative Standard Deviation*
SPM	*Suspended Particulate Matter*

UHP	*Ultra-High Purity*
UNESCO	*United Nations, Educational, Scientific and Cultural Organisation*
USB	*Universal Serial Bus*
UV	*Ultraviolet*
UV-Vis	*Ultraviolet Visible*
WFD	*Water Framework Directive*

Customisable Environmental Platforms for the Detection of Nutrients in Natural Waters

Andrew Donohoe

Thesis Abstract

Water ways and aquatic ecosystems are increasingly under threat from contamination world-wide due to influence from both anthropogenic and naturogenic sources. The ability to monitor and sense levels of key contaminants within environmental waters is a critical step towards reversing this trend and improving water quality. This necessitates the need for reliable methods of monitoring water quality on a global scale with the potential for high spatial and temporal resolution.

This research described in this thesis is focused on the development of autonomous analytical devices for monitoring of environmental water quality with the ability to contribute and scale into future sensing networks. The goal of this work has been to develop and validate chemical sensors which are capable of sensing reliably and robustly.

By integrating optimised reagent-based detection methods into simple and reliable optical detection systems this goal can be achieved. Through this strategy an adaptable benchtop sensing platform has been developed and optimised which can detect several colorimetric chemical methods using a modular LED and photodiode detector integrated with a fluidic chip. This work was further developed into an autonomous based platform capable of delivering environmental samples as well as calibration standards to the detector for reliable autonomous environmental sensing. This system has been shown to provide a base platform that can be used for the detection of several key analytes remotely and autonomously. The platform's analytical performance was successfully tested both in the Lab and in field deployments.

Chapter 1

Emerging Technologies for Autonomous In-Situ Monitoring of Water Quality

---

Andrew Donohoe [a], Dermot Diamond [a] and Margaret McCaul [a].

[a.] Insight Centre for Data Analytics National Centre for Sensor Research, Dublin City University, Glasnevin, Dublin 9, Ireland

This chapter has been published in "Monitoring Environmental Contaminants – A volume in Environmental Contaminants", edited by Steven Johnson, Elsevier 2021 Chapter 2: Emerging Technologies for Autonomous In-Situ Monitoring of Water Quality. Pages 19-55

ISBN: *978-0-444-64335-3*

https://doi.org/10.1016/B978-0-444-64335-3.00001-3

Abstract

Contamination of water sources world-wide is increasing due to both anthropogenic and naturogenic causes. The ability to correctly monitor and sense levels of key contaminants is a critical step towards the implementation of water quality management strategies designed to reverse this trend and improve water status. Stricter regulatory frameworks and public concern are driving increasing demand for more effective ways to detect pollutants and contaminants within water bodies. This in turn is driving the development of reliable autonomous remote sensing platforms that can provide continuous data on key analytes. The availability of such instruments at an affordable cost will facilitate monitoring at multiple locations, which will enable breaches of regulatory thresholds to be detected much more quickly than conventional approaches based on occasional sampling followed by analysis at centralised laboratory facilities. As a result, the potential damage caused by contamination can be significantly reduced due to much more rapid and effective responses. In this review the developments in these sensing technologies are discussed with a particular focus on nutrient sensing technologies. A comparison of current and emerging technologies will be presented, along with some thoughts on how to move towards much larger-scale, highly distributed monitoring of water quality.

1.1. Introduction

Reliable high-frequency and widely distributed data relating to the water quality of lakes, rivers, and oceans are essential for effective water management and for implementing strategies designed to improve the overall quality of water resources [1]. Monitoring the concentration and composition of potential contaminants in natural waters over time in multiple locations is also necessary to characterize and understand the aquatic environment [2,3]. Imbalances of nutrients or other potential contaminants such as heavy metals can cause major damage to aquatic ecosystems and water bodies [4,5].

Current approaches to water quality monitoring typically involve grab sampling at a restricted number of target locations and times. These samples are then stored and transported to a centralized analytical laboratory where they are subsequently analysed using traditional methods such as colorimetry, ion chromatography, atomic absorption spectroscopy, and mass spectrometry [6]. This analytical approach has several drawbacks. For example, while centralized instrumentation may be highly automated, sampling is highly labour-intensive, and there is considerable potential for sample degradation and contamination during collection, transport, or storage prior to analysis. Furthermore, this approach is time-consuming, leading to significant delays between sampling and reporting, and costly (i.e., it is non-scalable in terms of the number of locations sampled and frequency of sampling) [7–9]. This results in data with poor temporal and spatial resolution, providing at best only a superficial picture of the status of a water body. Sensors are devices capable of quantifying physical properties, chemical potential, or biological pathogens within a water body by means of an electrical response [10]. In comparison to the abovementioned traditional grab sampling methods, autonomous sensing platforms can generate higher-frequency in-situ measurements, with minimal risk of degradation of the target analytes or contamination of the sample, as the sample is measured directly on-site in real time.

The higher frequency of measurement coupled with reduced costs means that more devices can be deployed in situ, improving the temporal and spatial resolution of the data generated, which is especially important in areas where access is difficult for grab sampling [11,12]. Scaled deployments provide a much more detailed picture of

waterbody status dynamics, enabling rapid identification of a contamination event and source, and more effective implementation of control/remediation strategies [2]. For in-situ autonomous sensing, reliability, and cost are the key factors determining scalability [13]. Recent improvements in autonomous sensor capabilities have the potential to provide a scalable model for high-frequency sampling strategies on a much larger scale. A number of autonomous water quality sensing platforms are currently commercially available, while others are still in early research and developmental stages. The most widely available and robust sensors for water quality monitoring are physical sensors followed by chemical and finally biological sensors [14]. As discussed later, this reflects the increasing challenges associated with the creation of autonomous sensing platforms along with the trend from physical to chemical to biological sensing.

Currently, a number of parameters such as pH, conductivity, and dissolved oxygen (DO) can be tracked using well-established sensors that provide real-time in-situ data [15]. However, monitoring of chemical contaminants such as nutrients requires more complex analytical methods and is still overwhelmingly based on manual sampling followed by laboratory analysis. Lab-on-a-chip technology has the potential to dramatically improve instrumentation for such environmental measurements [16]. These are typically developed and tested in research laboratories but are rarely rigorously assessed within the real environment, due to the barriers that inhibit effective transfer of emerging technologies toward higher technology readiness levels. Improved robustness and reliability are essential for these methods, so that they can withstand harsh conditions that can often occur during real-world extended deployments [17]. If these improvements can be delivered, cost-effective widely distributed sensing networks present enormous opportunities for the collection of rich data sets that, together with data from other sources such as satellite remote sensing, will provide us with a much clearer picture of the chemical processes that occur within water bodies [14,18,19].

1.2. Water quality monitoring

To correctly manage water resources, it is essential to monitor water quality status with appropriate temporal and spatial resolutions for accurate modelling. Typically, this requires a multiparametric approach encompassing pH, temperature, conductivity, dissolved oxygen, alkalinity, nitrogen, phosphorus, organic compounds (organic carbon, humic substances), microorganism profiling, and biologically active compounds (algae, phytoplankton). To cover all of these is beyond the scope of this chapter, focus will be on nutrient monitoring as an exemplar, as this will encompass issues and potential solutions that apply to many other analytes.

Several EU and global policies and directives are driving increased demand for autonomous sensing platforms, as current approaches cannot provide the means to scale up deployments toward the required temporal and spatial resolution. The EU Water Framework Directive (WFD) aims to prevent further deterioration in the status of surface waters, groundwater, and water-dependent ecosystems and aims to restore noncompliant water bodies to at least "good status" [20]. The five water categories under the water framework directive are river, lakes, groundwater, transitional, and coastal [21]. This directive is further supported by the Nitrates Directive, the Urban Wastewater Directive, the Drinking Water Directive, and the Groundwater Directive. The Water Framework monitoring programs are integral parts of the new management strategy for water to meet the "good status" aim. This can be achieved through the establishment of integrated monitoring programs that are capable of collecting physical, chemical, and biological data, in order to provide for the assessment of water quality status of both surface waters and groundwater. Through its International Initiative on Water Quality (IIWQ), the United Nations Educational, Scientific and Cultural Organization (UNESCO) has launched a comprehensive worldwide water quality portal based on remote satellite earth observational data which deal with freshwater systems, lakes, and rivers. The aim is to use the portal to assist in global water quality assessment, while also providing an educational resource for environmental managers, politicians and scientists on water quality from a global perspective [22].

1.3. Sensing challenges: Platform and deployment hierarchies

To be successful, future autonomous environmental sensing platforms must meet a number of critical requirements. For example, they must be relatively inexpensive to buy and maintain so that they provide a route toward larger-scale deployments. This in turn demands that they can function autonomously for longer periods between servicing intervals, ideally up to several months. Throughout the periods between servicing, they must be capable of providing reliable continuous analytical data via wireless communications to cloud databases. Despite the increasing range and diversity of techniques currently available, continuous, online measurement systems remain largely limited by factors such as access to power, short service lifetimes, the need for frequent calibration, interferences, and fouling problems. These challenges must be considered during the development and deployment of more effective autonomous platforms.

In recent years, a number of initiatives have been launched with the specific aim of reducing the cost of in-situ sensing. For example, the Alliance for Coastal Technologies (ACT) "Nutrient Sensor Challenge" [23] provided significant awards and access to potential markets for technologies with a unit cost of $5000 or less, compared to the typical $20,000+ for such devices [24,25]. This nutrient challenge was initially introduced in 2014, with a second stage called in 2018 by the United States Environmental Protection Agency (EPA). The second stage required applicants to demonstrate how the data generated from in-situ sensing instruments could be used to inform decisions and actions, enhance nutrient management strategies, and inform communities of local water status. Such initiatives can drive competition in sensor development and help reduce sensor costs. The aim is that eventually, unit costs reduce to a "tipping point" that leads to larger uptake by state agencies and industry, thus increasing the size of the overall market.

The cost and complexity of a sensing platform (and as a result its scalability) depend both on the type of analyte and on the deployment scenario (see Figure 1.1.). Physical parameters (e.g., temperature, turbidity, conductivity, and colour) are the least complex to track due to the availability of very reliable, low-cost sensors. As a result, these sensors can be deployed within the environment at a large scale. Physical sensors

are typically low power, allowing long-term deployments without the need for servicing or maintenance.

Chemical analytes (e.g., nutrients and heavy metals) often require complex detection methodologies and sophisticated sensing platforms to provide accurate in-situ data. The need for regular calibration is a major issue, as this requires a fluidic system to enable calibration and sampling lines to be switched. Calibration is required because of stability issues arising from changes in the surfaces of fluidic channels, optical detection windows, or functionalized sensors that are in contact with the sample. Introducing calibration also requires the storage of standards and retention of waste within the fluidic-based instrument. Furthermore, in addition to the requirement for reliable power and electronics common to all environmental sensing systems, reagents, and standards used in fluidic chemical analysers must be stable for the duration of the servicing interval.

Biological analytes remain the most challenging sensing methods due lifetime and ruggedness issues associated with biosensors and biomaterials used in bioassays. Antibody-based measurements, while highly selective, are typically single use, due to the irreversible nature of the binding, making the provision of multiple time-series measurements extremely challenging. In general, enzymes degrade quickly and are incapable of working reliably over long periods of time in environmental deployments. Furthermore, complex environmental matrices can produce interferences that inhibit the detection of the target analyte [26].

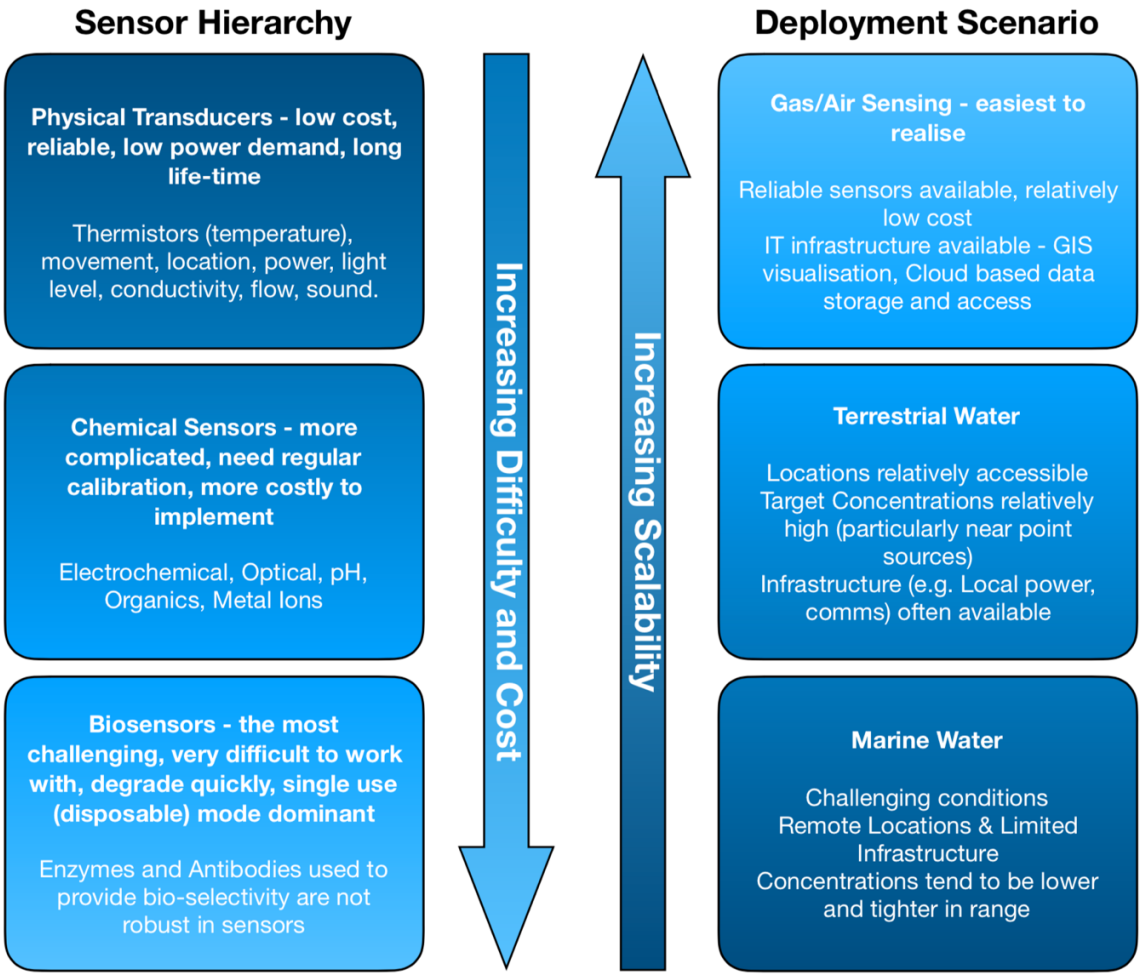

Figure 1.1. *Remote continuous sensing challenges, platform, and deployment hierarchies.*

In addition to the position of the sensing technology in the hierarchy, the deployment scenario must also be accounted for. Generally speaking, gas/air sensing is the most accessible deployment scenario, and the marine environment the most challenging, particularly far offshore ocean deployments (see ARGO, Figure 1.2.). Between these lies on-land freshwater monitoring.

The matrix presented in Figure 1.1. is a useful guide for assessing the risk associated with a sensing deployment scenario. For example, deploying physical sensors to track air quality is the least risky combination, and this is reflected in the examples of such deployments worldwide [27–31] that are already providing data with high spatial and temporal resolutions [32]. Increasing effort from scientists and instrument manufacturers as well as improvements in wireless technology has made it possible to reduce the cost of these sensors by up to three orders of magnitude, and as a result,

broader utilization of information on air pollution and weather data has become possible [33]. For example, Popoola et al. [34] presented the use of low-cost air monitoring networks to quantify air quality in urban settings at London Heathrow Airport using low-cost sensing, but the approach could be applied to a wide range of environmental deployment scenarios.

In contrast, the deployment of biosensors in the marine environment is very high risk, with virtually no chance of success. Therefore, it is no surprise that marine deployments are focused overwhelmingly on monitoring physical parameters such as temperature, depth, flow, colour, and turbidity, with chemical-sensing activity happening to a much lesser extent. This is exemplified in the ARGO project, which is a global network of almost 4000 profiling floats that provide continuous measurement of multiple parameters in the ocean [35,36]. These floats are sited at fixed depths (typically 1000–2000 m) and are designed to surface at 9-day intervals. While surfacing, they autonomously measure temperature and salinity. Upon reaching the surface, they transmit their accumulated data via satellite.

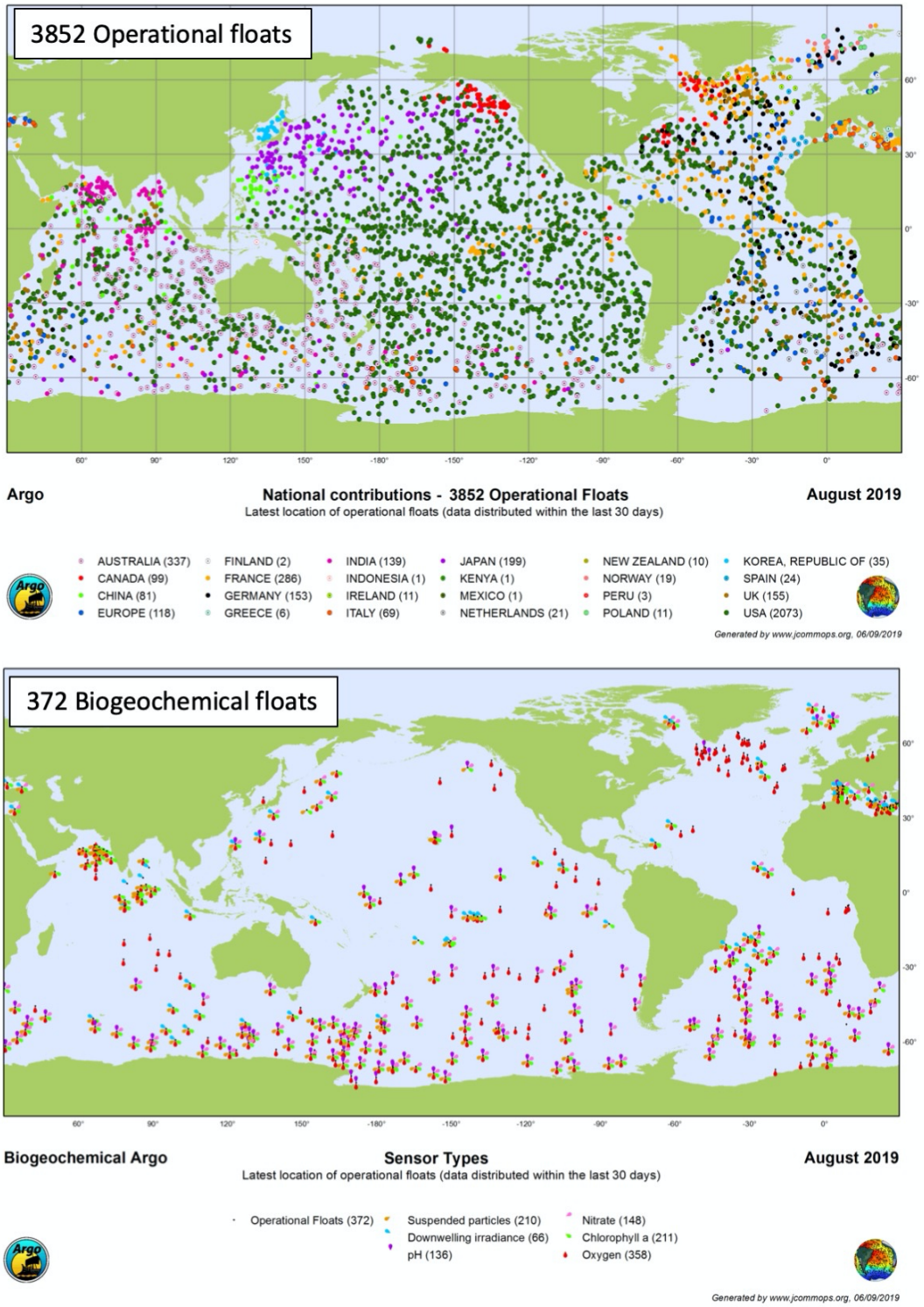

Figure 1.2. *Map of distributed total operational sensing floats (3852 top) under the ARGO project versus operational biogeochemical floats (372 bottom). [35] accessed September 2019 – credit http://argo.jcommops.org.*

Figure 1.2. shows the number of currently deployed floats (3852) within the ARGO project. Of these, only 372 (9.7%) floats produce data on what are referred to as

"biogeochemical parameters," with 148 (3.8%) of these providing nitrate data (by direct ultraviolet (UV) absorbance (abs) at 220 nano metre (nm)), 211 detecting chlorophyll (by colour measurements), 136 providing pH data (3.5%, reagent-based measurements), and 358 measuring DO (9.3%, Clark-type cells) [35] (monthly data, accessed in September 2019). It should be appreciated that the nitrate and chlorophyll measurements, while they report important chemical and biological information, do not employ chemical sensing/biosensing methods. This is clear evidence of the complexity and unreliability of chemical sensing and biosensing methods inhibiting their use in challenging deployment scenarios. Furthermore, the marinized Clark-type cells used for the DO measurements must withstand high pressures and very hostile external ocean environment, and consequently cost ca. $60,000 each. Even with complex corrections for effects arising from variable temperature, pressure, and salinity on the signal, "calibration of the DO measurements by the SBE-IDO sensor remains an important issue for the future."[37]

In Figure 1.1., chemical-sensing and freshwater deployment scenarios fall between these extremes in terms of the complexity of the measurement technology and challenging deployment scenarios. It is understandable, therefore, that this combination is the focus of considerable research activity, as it provides an intermediate balance between risk and potential reward, and consequently this is where new technologies are most likely to emerge and be adopted. The emergence of a number of these new chemical sensors for freshwater and marine sensing has been highlighted by stage two of the Alliance for Coastal Technologies "Nutrient Sensor Challenge." The National Oceanography Centre (NOC), Southampton [38,39], Sea-Bird Scientific [40], and Systea [41,42] all partook in performance verification during stage two where a series of protocols were assessed using both reference samples and environmental deployments.

1.4. Stability challenges with chemical sensors

Most chemical sensors reported in the literature arise from research performed by academic groups, with little attention given to their performance under real-use scenarios. A sensor that has been tested only within a laboratory requires a significant amount of in-situ testing to determine its operational limits, how long it can function

acceptably in the field, and the appropriate deployment strategy for the sensor. This extends to commercial chemical sensors designed for laboratory use [43]. For example, ion-selective electrodes (ISEs) under laboratory conditions can provide rapid analysis of pH and a large number of cationic and anionic species. The ISEs are generally considered less applicable platforms for in-situ environmental monitoring because they require frequent calibration due to signal drift, degradation of the electrode membrane, and reduction of their effectiveness due to biofouling of the active sensing surface.

Anastasova et al. [44] presented a solid-contact ion selective electrode (ISE) for environmental monitoring of lead in water. The limit of detection (LOD) in the nanomolar range made the electrodes favourable for the detection of low-level Pb^{2+} in environmental waters. Low-cost ISEs are applicable for single use or short use for on-the-spot testing of Pb^{2+}. However, continuous exposure to contaminated river water caused rapid changes in the sensor research characteristics, with the entire response function shifting by ca. +30 mV after one day (i.e., approximately an order of magnitude error; see Figure 1.3.). This type of instability means that these simple devices must be incorporated into a sophisticated fluid-handling system to enable regular calibration and fault checking, if they are to have any chance of success in a remote deployment.

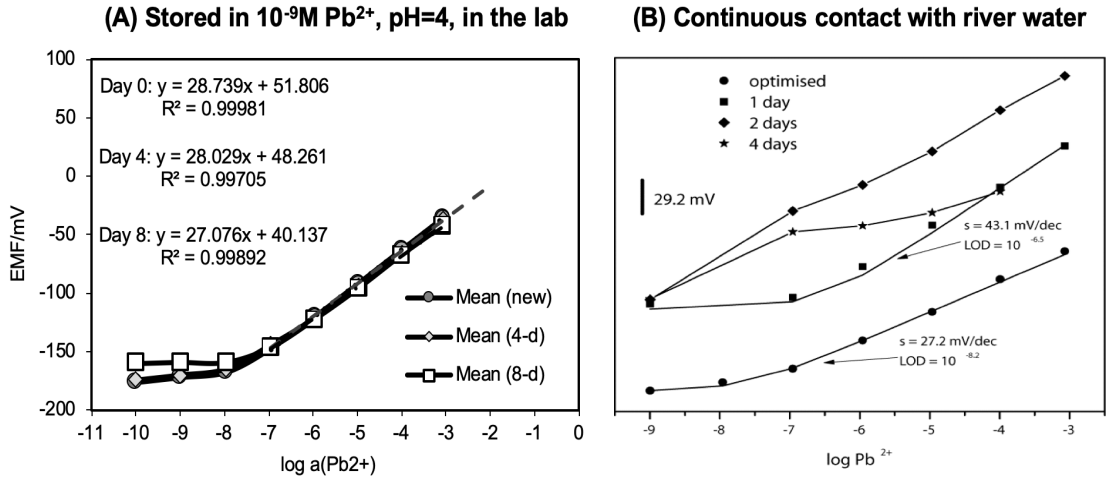

Figure 1.3. *Calibration data for the mean responses of disposable solid-contact-ion selective electrodes for environmental monitoring of lead stored in (A) 10^{-9} M Pb^{2+}, pH = 4 in lab and, (B) continuous contact with river water [44].*

In this paper, the possibility of including arrays of sensors was highlighted as a possible route to achieve long-term deployments, by using each for a short period of time, within which they hopefully remain within calibration, and then switching in successive electrodes sequentially. The suggested arrays would have the sensors incorporated into microfluidic platforms that would control the sensor conditioning, perform sample calibration or standard additions, and restrict the sensor period of exposure to real samples. Similar to biosensing (which also suffers from short-period or single-use and shot-use models), this method would have significant restrictions due to the required complexity of the fluidic system and associated cost. For instance, to use an array, the sensor would have to incorporate a series of valves into the sensing platform to allow sequential selection of each sensor. Therefore, in order to make this a feasible strategy, new approaches for creating fully integrated, low-cost, reliable valve structures within fluidic systems are needed [45].

1.5. Influence of microfluidics

As mentioned earlier, microfluidic technology has tremendous potential to enable the integration of increasingly complex analytical procedures into autonomous instruments that are capable of mimicking laboratory-based methodologies with increased sensitivity and reduced analyte consumption. The concepts underlying microfluidics took inspiration from the tremendous success of integration and miniaturization in electronics in the 1960s and 1970s [46]. Microfluidics typically utilizes microchannels with diameters in the range of 10 to 500 μm created in polymer, glass, or silicon substrates, to carry out reactions on a microscale by the manipulation of liquid samples and reagents [47]. Low dead volume is advantageous as it minimizes reagent consumption and waste generation. This minimization of fluid volumes used per assay dramatically reduces power requirements. As a result of the reduced reagent/sample volumes and power consumption, microfluidics provides a route toward the realization of platforms capable of longer deployment times in comparison to macroscale devices. The use of microfluidic technologies, therefore, is a key element in the development of compact low-cost sensing platforms, particularly when paired with low-cost detectors. Some examples are presented in Figure 1.4.

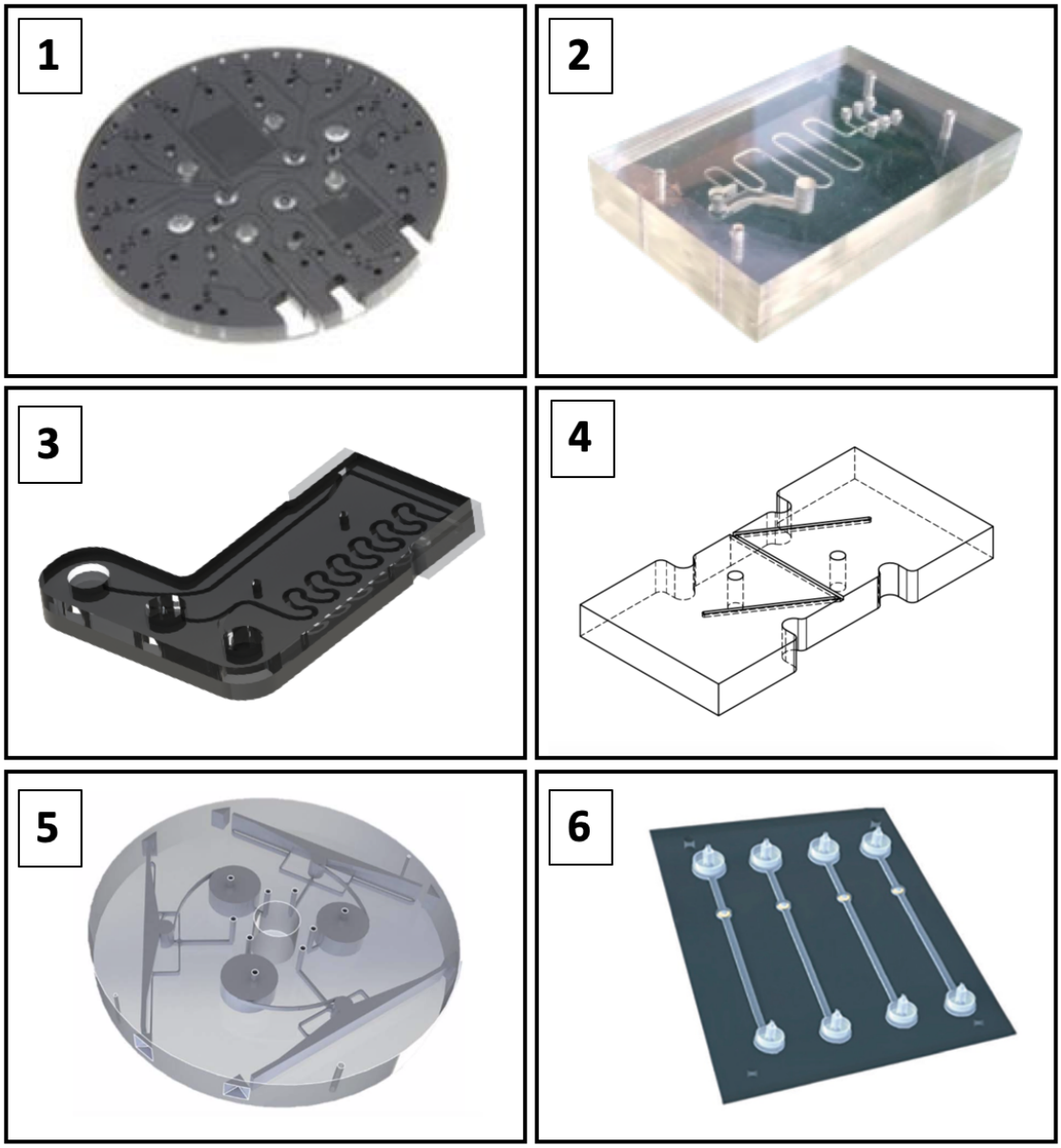

Figure 1.4. *Examples of microfluidic prototype technology used in sensing platforms. (1) PMMA layer of lab on chip for phosphate detection [48], (2) microfluidic chip for the direct determination of nitrate [49], (3) opaque fluidic chip with optically clear windows for nutrient analysis [50] (4) z shaped optical microfluidic detector, render adapted from Murray et al. [51], (5) PhosphaSense lab on disk for phosphate analysis [52], (6) flow control microfluidic chip containing in-situ photo responsive hydrogel valves [45,53].*

However, there are also a number of challenges or disadvantages associated with the use of microfluidics. For example, due to the microscale channels, they are susceptible to blockages or interference caused by suspended solids during measurements. This can be mitigated by using wider channels (but this also increases dead volume) and implementing prefiltration of the sample prior to analysis (but this limits the target analytes detectable to only the dissolved fraction of the sample).

Measuring only using microlitres of the sample also has implications in terms of representative sampling, as small volumes of sample are often assumed to correlate with large water bodies, which may be highly heterogeneous in nature. However, this is more than compensated by the ability to take higher-frequency in-situ measurements at multiple locations (due to lower unit cost and increased scale), which will provide a much-improved description of the waterbody heterogeneity and dynamics.

1.6. Manual single-use sensing

Manual grab sampling remains a standard methodology for water sensing where samples are obtained and brought back to the laboratory for subsequent analysis. Once sample collection, transport, storage, and analysis are carried out correctly, this method generates high-quality, highly reliable data. However, the cost per sample is high due to the highly manual nature of this approach and the time required to harvest and transport samples to the centralized facility. As a result, a number of on the spot tests for in-situ sensing have been developed to remove the need for storage and transport back to the laboratory [7]. These single-use tests are usually cost effective per sample but still require manual user input and potentially require pre-treatment stages before results can be generated in the field.

In an attempt to increase the spatial and temporal resolution of single-use measurements, initiatives like the EarthWatch Institute Water Blitz [54] and FreshWater Watch [55] have been initiated. These initiatives encourage volunteers to carry out local sampling and analysis for key parameters such as phosphate and nitrite. The strategy of using trained volunteers provides a way to generate a widely distributed data set that complements data acquired by more conventional means. Freshwater Watch is a global program developed by EarthWatch, which has gained over 100,000 volunteers worldwide, contributing to 10,000,000 hours of data collection. Results can be logged on-site using a mobile phone app and can be visualized using its website (see Figure 1.5.). Similarly, the EarthWatch Institute carries out Water Blitz's through which a drive for sampling is carried out on specific dates so that water quality can be directly correlated across Europe at the same time. The most recent

Water Blitz aimed to sample in Dublin, Paris, and Luxembourg with volunteers sampling over a 3-day period (September 20–23, 2019). During this Blitz, volunteers sampled water for nutrients (nitrate and phosphate) using simple colorimetric kits and a visual colour chart, turbidity, and colour. A visual inspection of the sampling site is also logged to assess the surroundings, bank vegetation, and any potential sources of pollution in the immediate area.

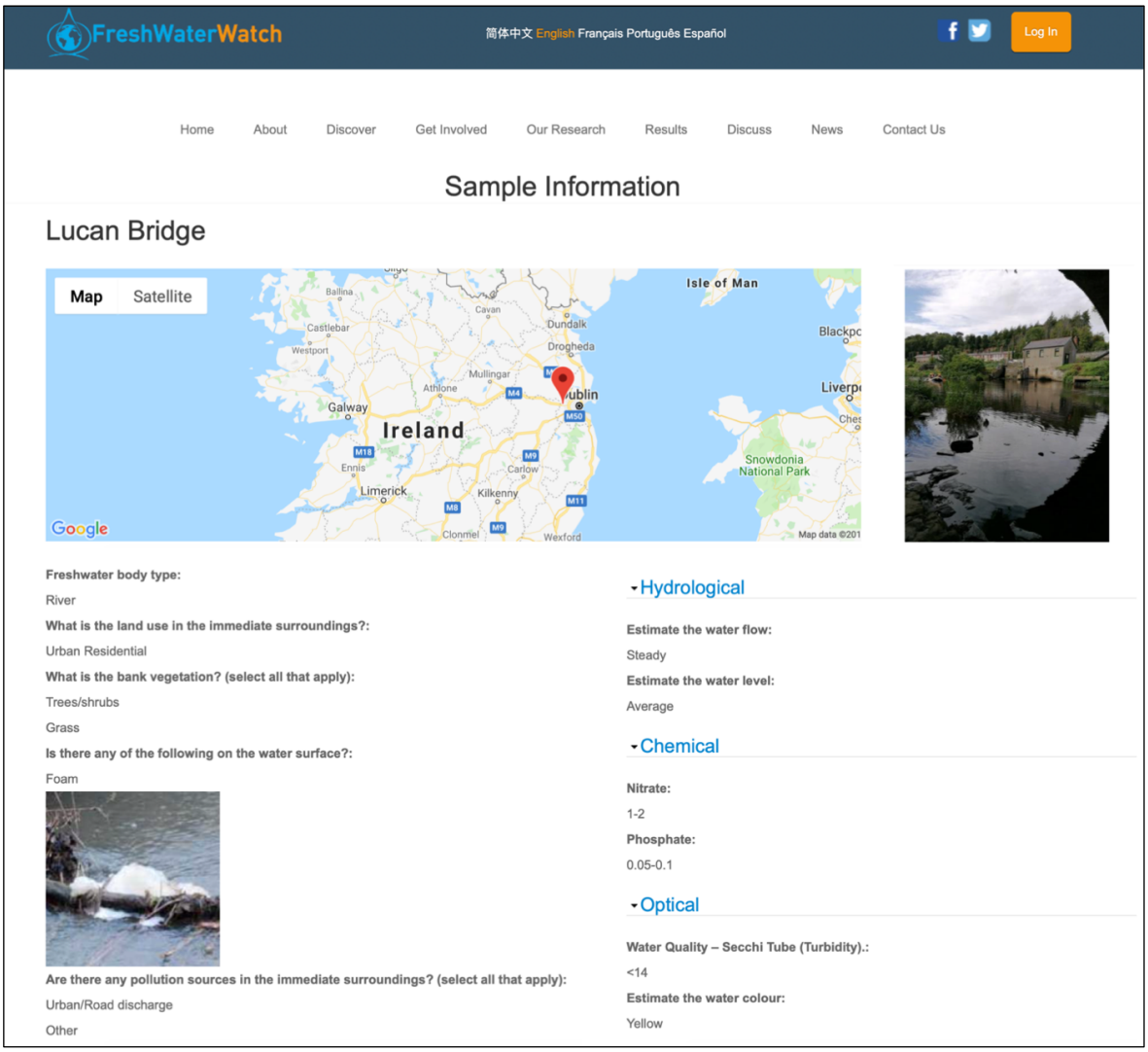

Figure 1.5. *Freshwater watch interface showing sample data input by a volunteer citizen scientist including location, site image, Hydrological, chemical and optical results.[56] Credit EarthWatch, Citizen Scientist: Kevine – Friday August 23 2019.*

Handheld colorimeters [57] provide a quick and simple way to perform environmental water quality measurements in the field. Other methods include novel portable microfluidic technology such as that developed by Duffy et al. [52] (see Figure 1.4.

image 5). This novel microfluidic disk is capable of in-situ quantitation of phosphate in natural waters using the molybdenum blue ascorbic acid colorimetric method.

1.7. Autonomous in-situ sensing for nutrients

Nutrients such as phosphorus and nitrogen are essential for plant growth and therefore for human life. However, the effect of population growth, agricultural practices, industrial processes, and pollution events has led to an excess of these nutrients in natural waters. Excessive nutrient concentrations in water bodies can lead to eutrophication, which can cause release of algal toxins, formation of dead zones, and contamination of drinking water [58–61]. Nutrients causing eutrophication can arise from anthropogenic and naturogenic effects [62] and can enter water bodies via point and diffuse sources [63]. Point sources include direct releases from industry sites, wastewater treatment plant effluent pipes, and agricultural waste streams, whereas diffuse contamination of a water system occurs at multiple locations along its boundaries due to, for example, runoff from fields [64]. The diversity of these sources can make accurate profiling a challenging task. As a result, nutrient pollution remains one of the most problematic environmental issues.

Eutrophication can drastically affect humans, animals, and plant life, and remediation is expensive, encompassing treatment costs for the removal of nitrogen, algal toxins, and decomposition products. They also impact communities through reduced value for waterfront dwellings, reduced recreational and amenity value of water bodies, and economic losses for the tourism industry [65]. The economic cost of these events is estimated to be over $2.2 billion annually [66] in the USA and £160 million annually in England and Wales [65]. Mitigation measures are difficult to implement without an accurately informed temporal and spatial model of the concentration profiles for nutrients within the water body [67]. Therefore, higher-frequency nutrient measurements taken at a larger number of locations are essential to effectively combat this truly global problem.

One way to achieve this is using autonomous in-situ sensing platforms to continually monitor the concentration of nutrients at varying locations within a water body. Autonomous sensing platforms are typically deployed in a fixed position during the

sampling lifetime and aim to measure nutrient concentrations for extended periods ranging from months to years, with planned servicing intervals during their lifetime. This deployment methodology allows for high-frequency data at a single-point source at various locations. For long-term monitoring using autonomous in-situ sensing it is favourable for a platform to have the following characteristics:

1. Highly precise data with low detection limits.
2. Fast measurement response time with good reproducibility.
3. Stable long-term operation.
4. Antifouling resistance.

Sensor costs often limit the number of platforms available to deploy at a specific site. As a result, a compromise must be made for high-frequency data with good temporal resolution but with low spatial resolution per sensor deployed. The following section reviews the autonomous sensing platforms for the detection of target nutrients contributing to eutrophication that are either commercially available or currently under development.

1.7.1. Phosphorus

Phosphorus is an essential element for all life. It occurs in plants, microorganisms, and animal waste; it is also widely used in agricultural fertilizer and detergents [68]. Phosphorus is one of the limiting nutrients in eutrophication [69]. In water, phosphorus is present in several chemical forms with the most common being phosphates of which the inorganic orthophosphate form is of the most stable. Phosphates occur in a number of forms, orthophosphates, pyrophosphates, metaphosphates, polyphosphates, and organic and inorganic phosphates [70]. Phosphate is mainly produced by anthropogenic processes and enters water bodies in several ways. Orthophosphates enter mainly through agricultural runoff of soluble fertilizers from fields [71]. Organic phosphates enter water through biological processes associated with food and wastewater treatment. Condensed phosphates enter water through water treatment and through laundering and cleaning processes, although the latter is decreasing in importance due to the phasing out of phosphorus containing detergents and cleaning products [69].

1.7.2. Phosphate-sensing methods

Electrochemical methods are generally inexpensive, but phosphate electrochemical sensors have limited selectivity (due to chloride, bromide, iodide, and sulphide cross-sensitivity) and are prone to signal drift and long-term stability issues [72,73]. Phosphate can be detected electrochemically using potentiometry and indirect voltametric detection based on the reaction of phosphate with a number of metals and associated complexes [74].

Fluorescence based detection typically has higher sensitivity and lower limit of detection than absorbance based colorimetric methodologies. Fluorescent detection of phosphate can be achieved by the replacement of a competing florescent ion within a complex with phosphate, which can then be detected optically. To date, this technique has been applied to flow through systems but while it has the potential to be integrated into an autonomous system in a similar way to colorimetric-based systems, this has not been reported to our knowledge. Frank et al. [75] proposed a method for the determination of dissolved reactive phosphorus using sequential injection analysis with the fluorescence quenching of rhodamine 6G-molybdate. This detection method had a limit of detection of 0.05 µM [75]. This sequential injection system was used for the analysis of surface water in the North Sea, Wadden Sea, and Elbe Estuary. A reverse flow injection method using the same chemistry achieved a limit of detection of 7 nM for phosphate in seawater [76]. Similarly, a flow injection method with chemiluminescence detection based on luminol oxidation by 12-MPA has also been used to determine phosphate in freshwater [77].

The most common method for the determination of phosphate in water is the use of colorimetric chemistries coupled with a light source and photodetector to measure the absorbance of a distinct colour that results from a reaction between phosphate in the sample and a selective colorimetric reagent. The use of colorimetric chemistries has been optimized for use in flow-through systems and is favourable due to their selectivity, sensitivity, and reagent lifetime for some methods. The density of the colour produced is related to the concentration of the target analyte using the Beer-Lambert law ($(A = log^{10}\left(\frac{I_o}{I}\right) = Lc)$) [78]. When implementing these methods in autonomous

instruments, reagent storage, stability, and waste containment must be considered, along with high method sensitivity to orthophosphate (large molar extinction coefficient, ε), broad linear calibration range, and reagent stability [79,80].

Figure 1.6. shows a conceptual schematic for two common colorimetric reactions for phosphate detection, vanadomolybdophosphoric acid method, and the ascorbic acid method. The vanadomolybdophosphoric acid method (yellow method) for the detection of phosphorus is based on the colorimetric reaction of PO_4^{3-} with acidified vanadomolybdophosphoric that produces a yellow-coloured solution detectable in the UV range below 400 nm. It is a simple colorimetric technique where under acidic conditions orthophosphate reacts with molybdate ions to form molybdophosphoric acid. In the presence of vanadate ions, this complex will form the strongly yellow-coloured vanadomolybdophosphoric acid. This method is widely used due to the long-term stability of the reagent (at least 12 months) and its ease of integration into microfluidic technology [81].

The molybdenum blue/ascorbic acid method has been widely used for the determination of orthophosphate in environmental waters due to its high sensitivity and selectivity for orthophosphate. However, the method has a tendency to form precipitates in the final stage [82] that can cause issues in microfluidic systems such as clogging or changing flow characteristics within the chip itself as reported by Sequeira et al. [2]. The reaction takes place in two stages, with the first stage involving the formation of a heteropoly acid Keggin ion around the analyte anion. The second stage involves the reduction of this heteropoly acid to form a deeply blue-coloured product. The resulting, blue-coloured complex can be detected spectroscopically between 660 and 880 nm. Although the vanadomolybdophosphoric acid method has a lower sensitivity with a low molar extinction coefficient (ε = 8.38 x 10^3 mol L^{-1} cm^{-1} at λ_{max} 380 nm) [83] in comparison to the blue method (ε = 2.61 x 10^4 mol L^{-1} cm^{-1} at λ_{max} 820 nm) [84], this is counterbalanced by its excellent reagent stability (up to 1 year) [85]. In contrast, the molybdenum blue ascorbic acid method is more suited for use on in-line sensors, as it has a high sensitivity but suffers from poor reagent stability [2,86].

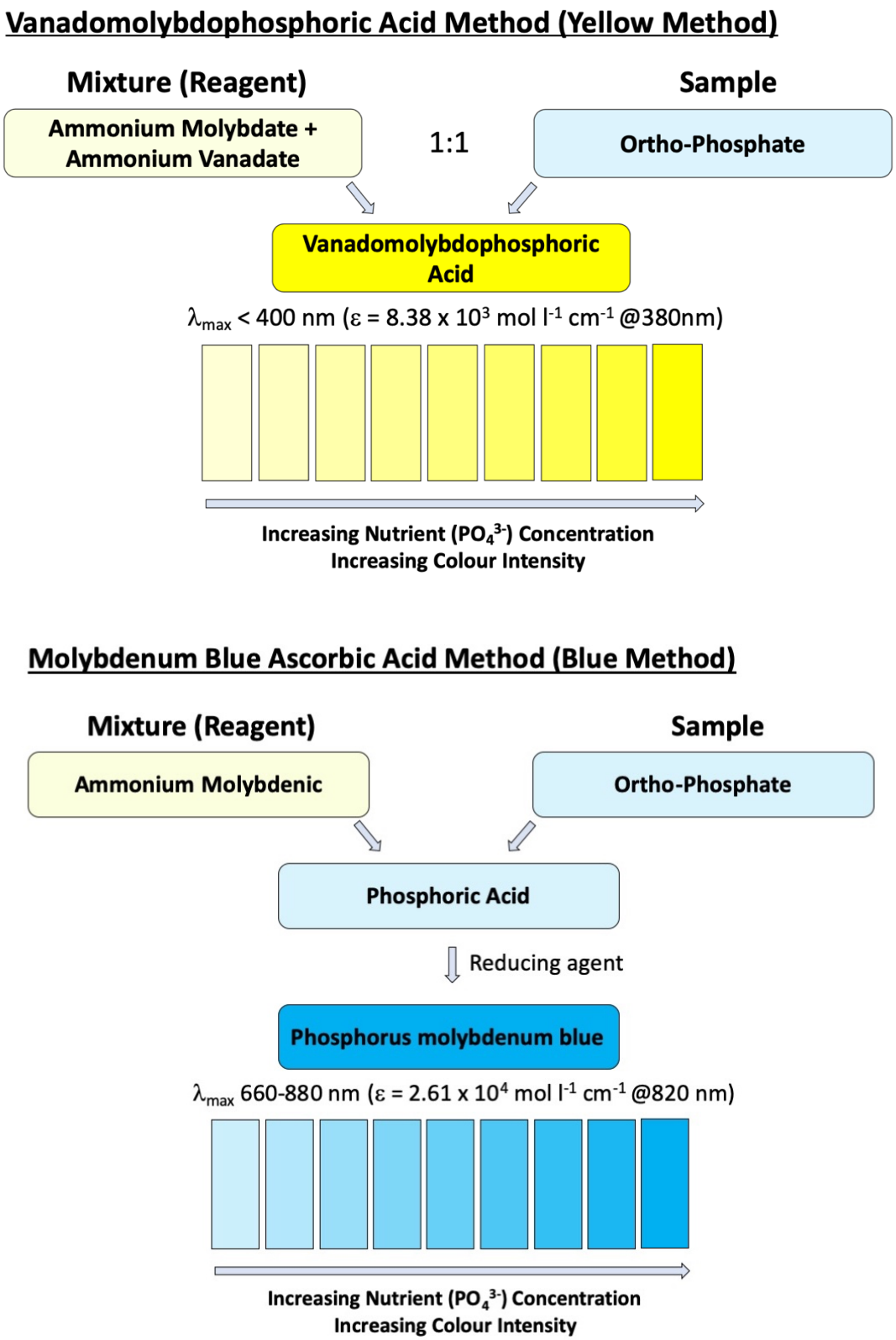

Figure 1.6. *Conceptual reaction schematic of standard colorimetric methods for phosphate detection (Top) Vanadomolybdophosphoric Acid method (yellow) (ε = 8.38 x 10^3 mol L^{-1} cm^{-1} at λ_{max} 380 nm [83]) and (Bottom) molybdenum blue ascorbic acid method (blue method) (ε = 2.61 x 10^4 mol L^{-1} cm^{-1} at λ_{max} 820 nm [84]).*

1.7.3. Nitrogen

Nitrogen is present in water in several chemical forms, the most common being nitrate (NO_3^-), nitrite (NO_2^-), organic nitrogen, and ammonia (NH_3)[87]. Nitrite and nitrate concentrations within natural and wastewaters vary widely. Nitrate is found in a number of natural processes such as during nitrogen fixation by cyano and azotobacteria and during soil degradation [88] The most common form of entry of nitrate into natural waters in excess is through anthropogenic processes. Anthropogenic sources of nitrate include agricultural fertilizers, plant and animal waste and wastewater discharges [89]. Elevated levels of nitrates in natural water systems pose a risk to both the environment and human health [90].

Ammonia is a naturally occurring form of nitrogen in the nitrogen cycle. Dissolved ammonia gas is toxic to aquatic life in concentrations as low as 25 μg/L ranges in concentration from as low as 10 μg/L in surface and groundwaters and up to 30 mg/L in wastewaters [91]. Ammonia enters the aquatic environment in excess through anthropogenic sources such as agricultural runoff and wastewater discharged and is also released during nitrogen fixation and the breakdown of animal and plant waste [91,92]

1.7.4. Nitrite and nitrate colorimetry

The colorimetric Griess assay is the most used method for the detection of nitrite. Figure 1.7. shows a conceptual schematic for colorimetric reactions for nitrite detection. The reaction is based on the diazotization reaction of nitrite with sulphanilamide and N-1-naphthylethylenediamine dichloride (NEDD) under acidic conditions, which results in the formation of a very intense pink azo dye that can be detected spectroscopically at 540 nm [93]. Nitrite is usually present in water at a concentration lower than 0.01 mg/L.

The method has been extended to include nitrate by incorporation of a reduction step that converts the nitrate quantitatively to nitrite. The nitrate concentration is found by subtracting the background nitrite from the total nitrate and nitrite obtained after the reduction step. A number of versions of the method have been reported, including the use of vanadium chloride [94] or cadmium columns [95–97] for the nitrate reduction

step. The addition of this step makes nitrate detection more complex as a more sophisticated fluidic system is required, further increasing the cost of implementation in an autonomous platform. However, work has recently been carried out to reduce the complexity of these methods. For example, Wang et al. [94] presented the use of vanadium chloride (VCl_3) as the reductant instead of the well-known cadmium column for reducing nitrate to nitrite. The work employed an automated flow injection analysis system using a single analytical solution comprising VCl_3 mixed with the Griess reagent. This method was favoured as it removed the need for the use of the toxic cadmium column, and this mixed reagent aimed to simplify the fluidic system by combining both the reducing VCl_3 and the reactive Griess reagent into one solution.

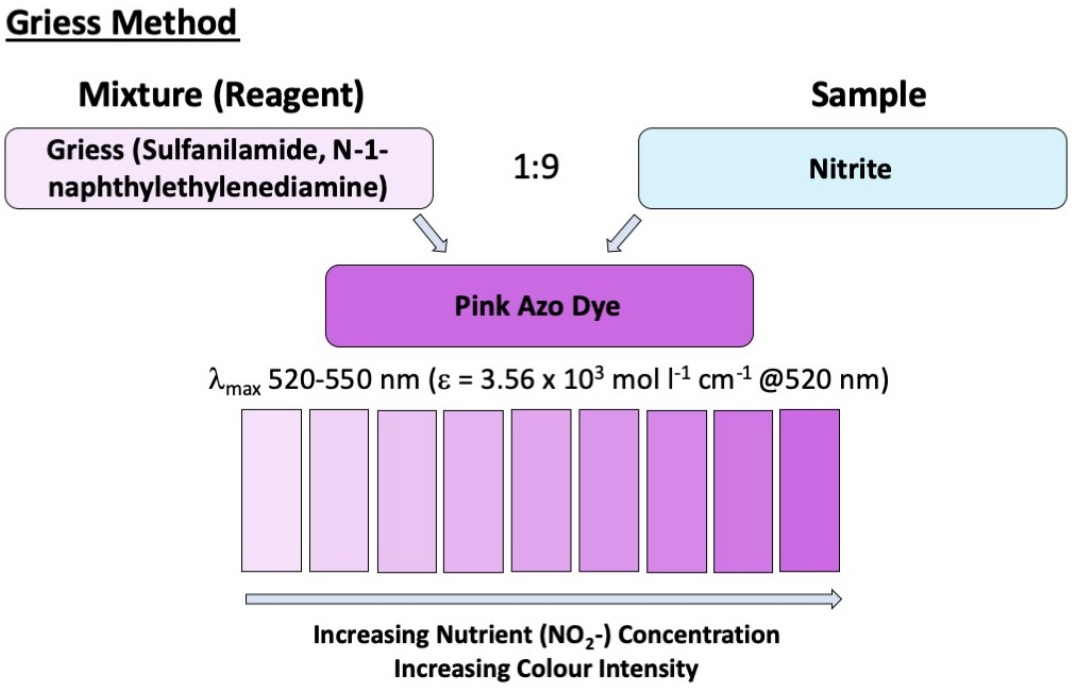

Figure 1.7. *Conceptual reaction schematic of the Griess assay for colorimetric detection of nitrite (ε = 3.56 x 10^3 mol L^{-1} cm^{-1} at λ_{max} 520 nm [98]).*

1.7.5. Ammonia colorimetry

The most widely used colorimetric method for the direct determination of ammonia is the Berthelot method. This method has a high sensitivity (LOD at μg/l levels) and an intense colour production at 630 nm [99]. The original Berthelot method was based on the formation of a green colour when ammonia, phenol, and hypochlorite react [100]. In recent years, sodium salicylate has been used in place of the highly toxic phenol. The salicylate version of the method has been applied to environmental sensing using both fresh and marine water samples [92].

In the presence of sodium hydroxide, the Berthelot reagent reacts with ammonia to produce a green colour at 660 nm (salicylate). When ammonia forms a monochloramine in the presence of hypochlorite, it is then converted to 5-aminosalicylate by the salicylate, which is then oxidized to produce the blue indophenol complex [91,99].

The Berthelot method traditionally utilized a three-step process in which three reagents were added sequentially with specific wait times between each step to allow the reaction to take place. To improve the sensitivity of the colour development, the solutions were also heated up to 45 °C [101]. Daridon et al. [101] successfully implemented the method in a microfluidic system, which compared well to standard spectroscopic detection. However, the sequential multistep approach along with the addition of heat made this application difficult to automate and apply to autonomous sensing. Cogan et al. [91] simplified the traditional method by utilizing a premixed reagent that could be added directly to the sample in a 1:1 v/v ratio. This less complex method was much simpler to implement in a microfluidic system (Figure 1.8.).

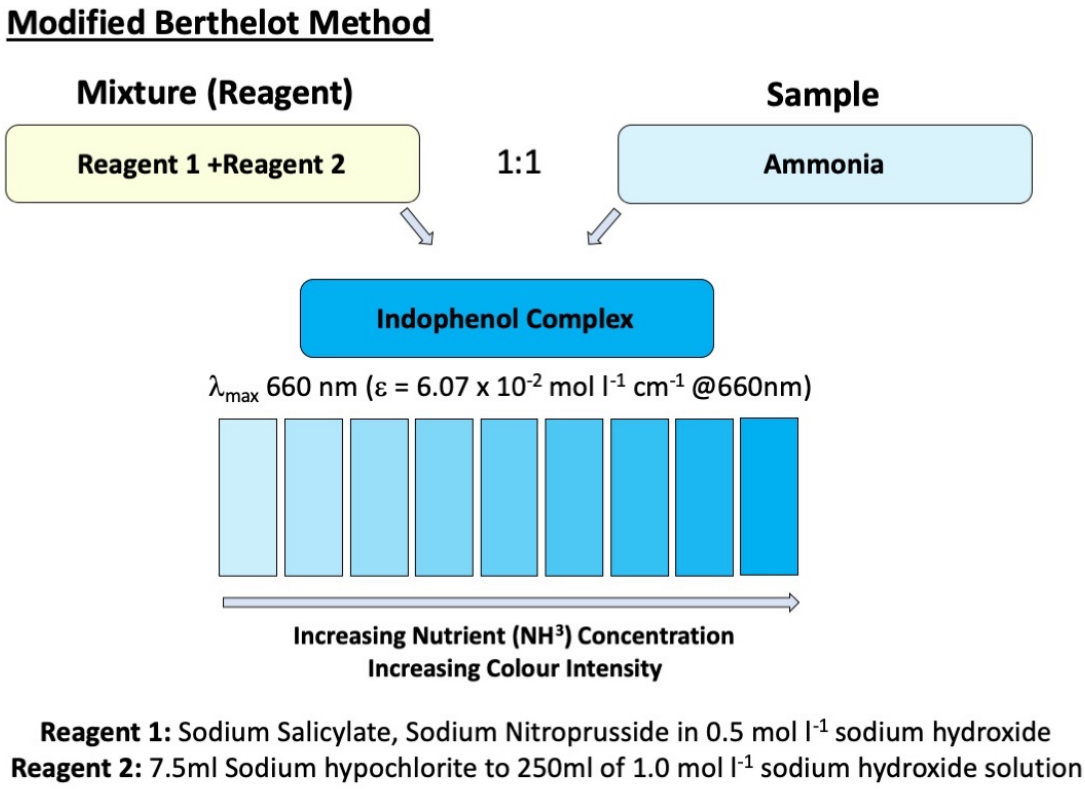

Figure 1.8. *Conceptual reaction schematic of the Berthelot assay for colorimetric detection of ammonia (ε = 6.07 x 10^{-2} mol L^{-1} cm^{-1} at λ_{max} 660 nm [91]).*

1.8. Current and emerging nutrient sensing systems

1.8.1. Examples of current sensing systems

Several commercially available water quality sensors of various configurations are available. Traditionally, these sensors are typically online analysers requiring mains power and permanent deployment locations where maintenance and calibration can be carried out and have been more suited to industrial applications than remote deployments. Recently, several companies have released in-situ-based nutrient analysers, some examples of which are presented in Figure 1.9.

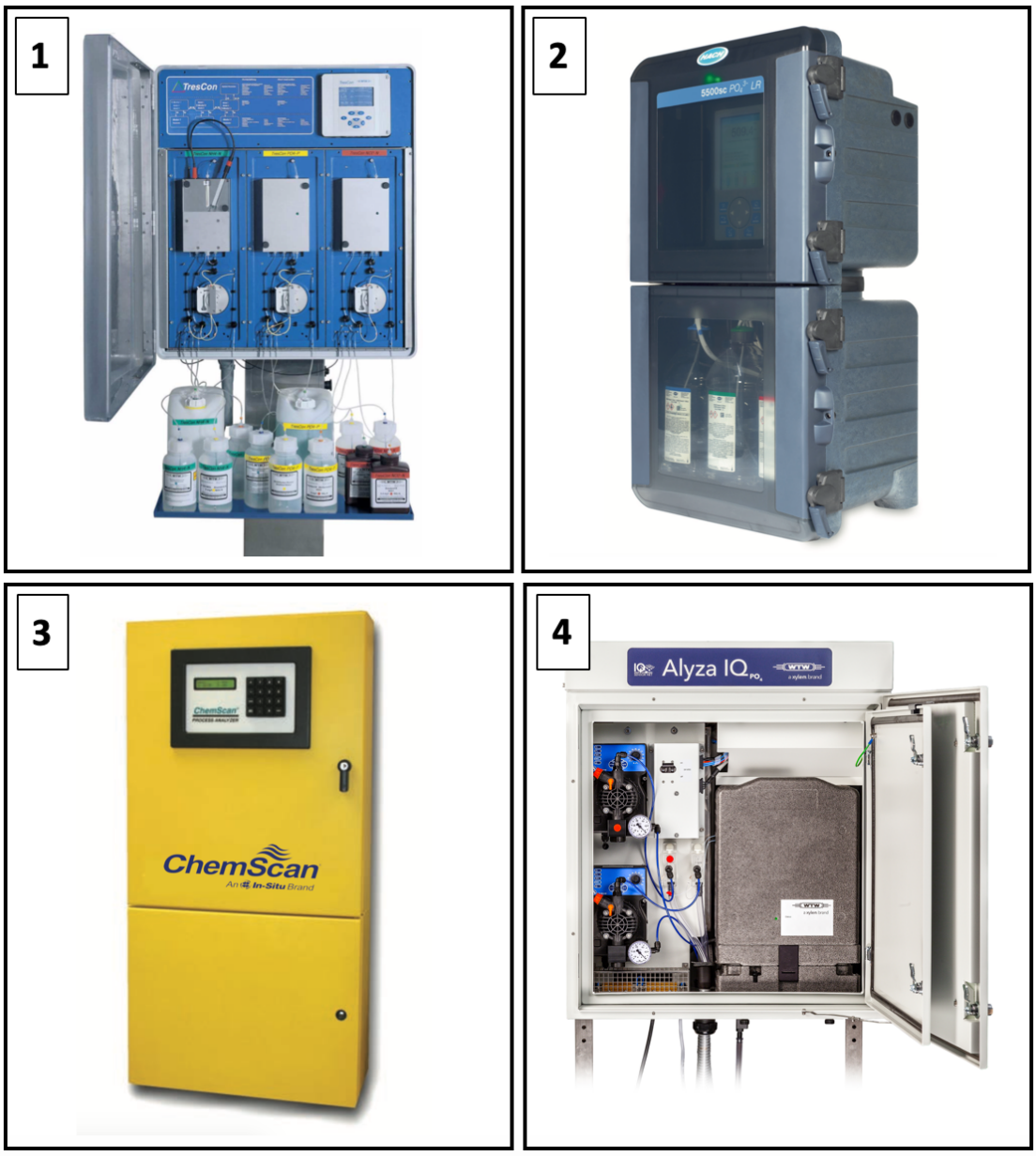

Figure 1.9. *Commercial water sensing platforms(1) TresCon UNO [102] credit Xylem Analytics Germany, (2) Hach 5500 SC [103] , (3) ChemScan Mini oP [104] and, (4)Alyza IQ [105] credit Xylem Analytics Germany.*

TresCon UNO (see Figure 1.9. image 1) is an online water analysis sensor developed by WTW analysers. It is capable of continuous measurement of ammonia, phosphate, and nitrite or nitrate. It is developed as a modular system that can be set up to measure single or multiple parameters. The TresCon system relies on a continuous supply of water to operate, which is subsampled to supply the sample modules at a typical flow rate of 2–3 litres per hour. The phosphate module measures phosphate photometrically using the vanadomolybdophosphoric acid method (yellow method).

The nitrate module measures UV absorbance at two wavelengths to ratiometrically obtain an estimate of nitrate concentration by direct absorbance. The ammonia module uses an ammonia sensitive electrode to measure gaseous ammonia released when the sample is mixed with a basic reagent [102].

Hach 5500 SC phosphate analyser (see Figure 1.9. image 2) is an online water analysis sensor with a 15-min measurement cycle, capable of a 90-day runtime and consuming two litres of reagent during this period. The sensor is based on colorimetric chemistries utilizing two different methods depending on the concentration range of phosphate to be detected. The low-range measurement uses the ascorbic acid method, which is measured at 880 nm and has a range of 0.0004 to 5 mg/L PO_4. The high-range measurement uses the molybdovanadate method (yellow method) measured at 480nm and has a range of 0.02 to 50 mg/L PO_4 [103].

ChemScan mini oP XR (see Figure 1.9. image 3) is a water analysis sensor for the measurement of phosphate using a combination of wet chemistry and spectrophotometry. The sensor comes with low and extended working ranges. The low range measures between 0.003 and 1 mg/L PO_4-P, and the extended working range measures between 0.3 and 60 mg/L PO_4-P. The sensor utilizes large sample tubing to minimize block- ages and ensures that any suspended solids less than 150 mg/L can be flushed through the sensor [104].

Alyza IQ (see Figure 1.9. image 4) is an online water analysis sensor capable of measuring ammonia and phosphate. The sensing platform utilizes colorimetric chemistries and automatically calibrates using one and two-point calibrations. Ammonia is detected using the Berthelot method. A catalyst along with heat is used to accelerate this reaction. Phosphate is detected using the molybdovanadate method (yellow method). The Alyza IQ Ammonia is equipped with two working ranges, 0.02 to 4 mg/L NH_4-N with a resolution of 0.01 mg/L NH_4-N and 0.1 to 20 mg/L NH_4-N with a resolution of 0.05 mg/L NH_4-N. The Alyza Phosphate can have either a low working range of 0.02 to 15 mg/L PO_4-P with a resolution of 0.01 mg/L PO_4-P or 0.2 to 50 mg/L PO_4-P with a resolution of 0.05 mg/L PO_4-P [105].

1.8.2. Emerging sensing systems

Currently, the most readily available commercial nutrient sensors are based on online platforms powered by mains. These typically favour industrial settings where they can regularly be maintained and calibrated.

In-situ deployments are much more challenging, in terms of system maintenance, power management, and unpredictable factors (e.g., weather, deliberate interference, and accidental damage). Most of these novel in-situ analysers are based around flow systems that intake sample from the water source [106], mixing with a reagent that produces an optical response proportional to the concentration of the target analyte, measuring the absorbance in the spectral region coinciding with strong absorbance, communicating the resulting data, and storing the waste. Figure 1.10. presents a number of sensing platforms that have been developed or are currently being developed around these principles.

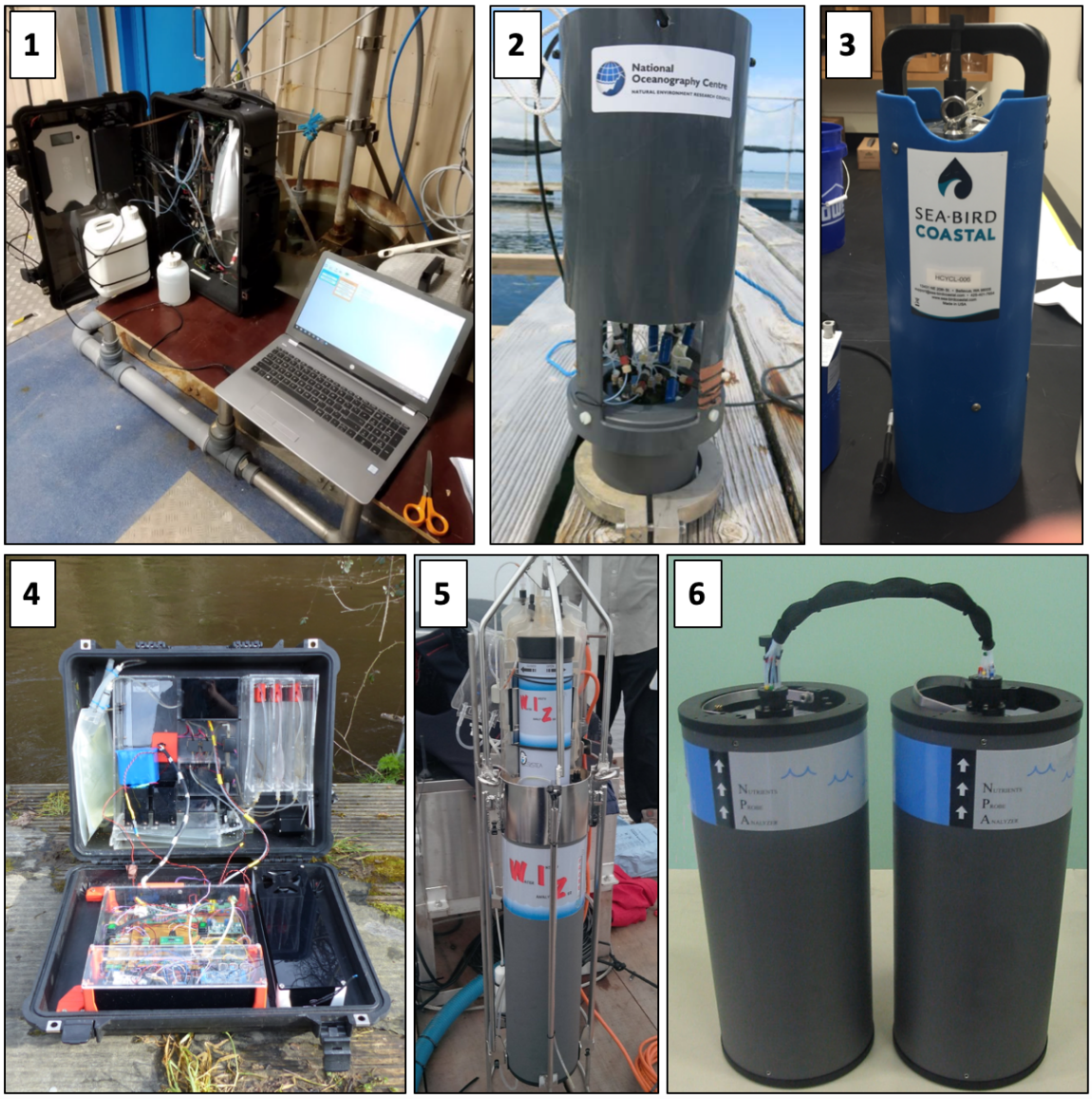

Figure 1.10. *Prototype sensing platforms for nutrient monitoring (1) Ecosens Aquamonitrix portable IC system for determination of nitrite and nitrate [51,107], (2) National Oceanography Centre Southhampton phosphate analyser [38], (3) Sea-Bird Scientific Hydrocycle PO_4 sensor [40,108] (4) Phosphate sensing platform developed by the Adaptive Sensor Group at DCU Insight Centre[50], (5) Systea WIZ Probe [109], (6) Systea NPA Pro [110].*

The Ecosens Aquamonitrix (see Figure 1.10. image 1) is a portable water monitoring platform utilizing ion chromatography. The device is capable of carrying out near-continuous analysis (15min) of water for nitrate and nitrite as well as using reagent-less detection to monitor other parameters, reducing reagent consumption [107]. This portable instrument utilizes a low-cost, UV absorbent microfluidic detector that incorporates a 235-nm Light Emitting Diode (LED) [51].

The National Oceanography Centre (NOC), Southampton (see Figure 1.10. image 2), phosphate analyser is an autonomous platform based on the vanadomolybdate method and has been applied for the determination of soluble reactive phosphate in seawater. The platform is based on a tinted polymethyl methacrylate (PMMA) microfluidic chip in which liquid flow is delivered via syringe pumps. The linear response has been reported up to 60 μM with a limit of detection of 52 nM [38]

The Sea-Bird Scientific Hydrocycle PO_4 (see Figure 1.10. image 3) is a wet chemical sensor for the in-situ detection of dissolved phosphate. The sensor has a detection limit of 0.0023 mg/L PO_4-P and a nominal range of 0 to 0.3 mg/L PO_4- P. The sensing platform uses optical detection with a wavelength of 870 nm and a path length of 5 cm. The Hydrocycle has a reagent lifetime of 5 months and is capable of taking 1500 measurements between servicing, being capable of measuring up to 4 samples per hour [40]

At the Insight Centre, Dublin City University, (see Figure 1.10. image 4), we have developed a phosphate-sensing platform using a combination of microfluidics, colorimetric reagent chemistries (vanadomolybdate method) and low-cost LED-based optical detection. The platform has been tested both in laboratory and in field deployments. The linear response was measured up to 50 μM with a limit of detection of 0.09 μM PO_4^{3-} [50].

The Systea WIZ Probe (see Figure 1.10. image 5) is an in-situ probe that can be used to measure up to four nutrients in surface or seawater. It is capable of measuring ammonia (N-NH_3), orthophosphate (P-PO_4), nitrate + nitrite (N-(NO_3 + NO_2)), and nitrite (N-NO_2). The process is carried out using spectrophotometric wet chemistries for phosphate, nitrite, and nitrate and using a fluorometric method for ammonia [111].

The Systea NPA Pro (see Figure 1.10. image 6) is an in-situ sensor suited for deployment on remote buoys. The design consists of two separate cylinders, the first containing hydraulic and electrical components and the second containing reagents, calibration standards, DI water, and waste bags. The design is split so that it can be balanced with each cylinder placed into the body holes of the buoy. Similar to the WIZ

Probe, the NPA Pro can measure up to four nutrients. Ammonia is measured using the Berthelot method, phosphate using the molybdenum blue ascorbic acid method, and nitrate/nitrite using cadmium column and Griess method as described earlier [111].

1.9. Challenges for autonomous in-situ sensing systems

There are several limitations to the current real-time autonomous sensing systems, which adds complexity to design and prevent wide-scale adoption of these platforms. To function and have wide-scale adoption, issues with robustness, power, detection methods, and fouling must first be addressed. As mentioned previously in Section 3, as the complexity of a sensor increases, the cost of the sensor will also increase and the scalability in terms of deployments will decrease. The cost of the sensing platform relates to not only the initial purchase cost but also its running costs. It is important for sensors to be easy to install, maintain, and use. Software and firmware must be intuitive to use, enabling operators to access, visualize, and analyse data remotely in real time [112]. The deployment of sensors into the environment exposes them to harsh conditions. The sensor must therefore be capable of withstanding exposure to rain, ice, dust, and variations in temperature and internal humidity. Power consumption remains a major limitation for in-situ sensing if sensing platforms are to be deployed in areas without a local power source. Energy harvesting options such as solar panels are available, but they can be expensive and as a result can add significantly to the unit cost of the sensor [113]. The return of investment for solar panels may be in the order of years, which may be longer than the planned lifetime of the deployment. Battery sources remain the most common method of power for autonomous sensors. Major international research efforts driven by the e-car industry will advance this technology rapidly in the future [114].

Platform chemistries can also be a considerable limitation for in-situ sensing. Reagent stability is critically important for environmental monitoring due to the need for platforms to be successfully deployed for extended periods of time [12] (at least several months). Reagent-based methods are dependent on the time for the development of a coloured product before a measurement can be recorded, and this is highly temperature dependent [115–118]. The time for the coloured product to be developed determines the sampling frequency for the sensing platform. The reaction

time can be reduced through the use of heat, but the integration of in-line sample heaters affects power draw and lifetime of the battery [119]. This along with other factors such as reagent lifetime and reagent consumption rate limit the servicing interval. Careful choice of reagent and calibration standards or extending their lifetime is key to maximizing service intervals and extending deployment periods, which in turn can dramatically reduce the cost of ownership and enhance scalability.

1.9.1. Sensing platform fouling

Fouling remains one of the largest and almost universal challenges to in-situ sensing within the environment. From the moment a sensing platform is immersed in water, it will begin to be affected by fouling, which disrupts the performance of a sensing platform [120]. Fouling can be classified into several different types (e.g., colloidal, organic, and biofouling) based on the nature of the effect. Each classification of fouling has its own implications and can have unique remediation or preventative measures when it comes to maintaining sensor performance. Colloidal foulants range in size from 1 nm to 1 μm [121]. Colloidal fouling occurs when a cake layer is accumulated on the surface or within the pores of a membrane (e.g., prefiltration unit). Clay minerals, colloidal silica, organic colloids, and suspended matter all contribute to colloidal fouling. Organic foulants are caused by substances that are dissolved within the water column and tend to stick to the surface. Common organic foulants include macromolecules, proteins, and oils [122].

Biofouling is the formation of living microorganisms or plant life on a surface in contact with water. Biofouling affects the hydraulic performance of sensor inlets making it hard to intake environmental samples through prefilters [123]. It is caused by aquatic organisms that can form colonies that cause biofouling due to the interactions of microorganisms with the membrane and dissolved substances within the water column. Biofilms form when free-floating organisms interact and attach with a surface. Initial interactions are usually through reversible, weak van der Walls forces that over time become more permanent due to cell adhesion [124]. The initial attachment of the microbial cells to the surface is known as the conditioning step. A conditioning layer is formed soon after submersion in the water (hours) and leads to the gradual build-up of a thicker biofilm layer over time.

Many approaches have been suggested to combat fouling, but none seem to be universally effective [125]. Some have been investigated as a means to extend sensor deployment lifetimes, including physical brushes or wipers (shown in Figure 1.11. image 4), UV irradiation [126], or copper/antifouling coatings [38]. Biofouling accumulation drastically affects sensor surfaces, leading to device failure, requiring regular cleaning and replacement of prefilters and other system components. Biofouling does not occur so readily internally within fluidic systems implementing the reagent-based methods described earlier, due to the relatively harsh chemical conditions required to drive the reagent/sample reaction (e.g., extremely acidic, or alkaline conditions and redox chemistries). Walker et al. [127] carried out an investigation of the effects of common reagents used in microfluidic devices including the Griess assay for nitrite on the formation of biofilms by mixed marine communities. It was shown that Griess and other chemical reagents can stop biofilm formation before they can attach to internal surfaces.

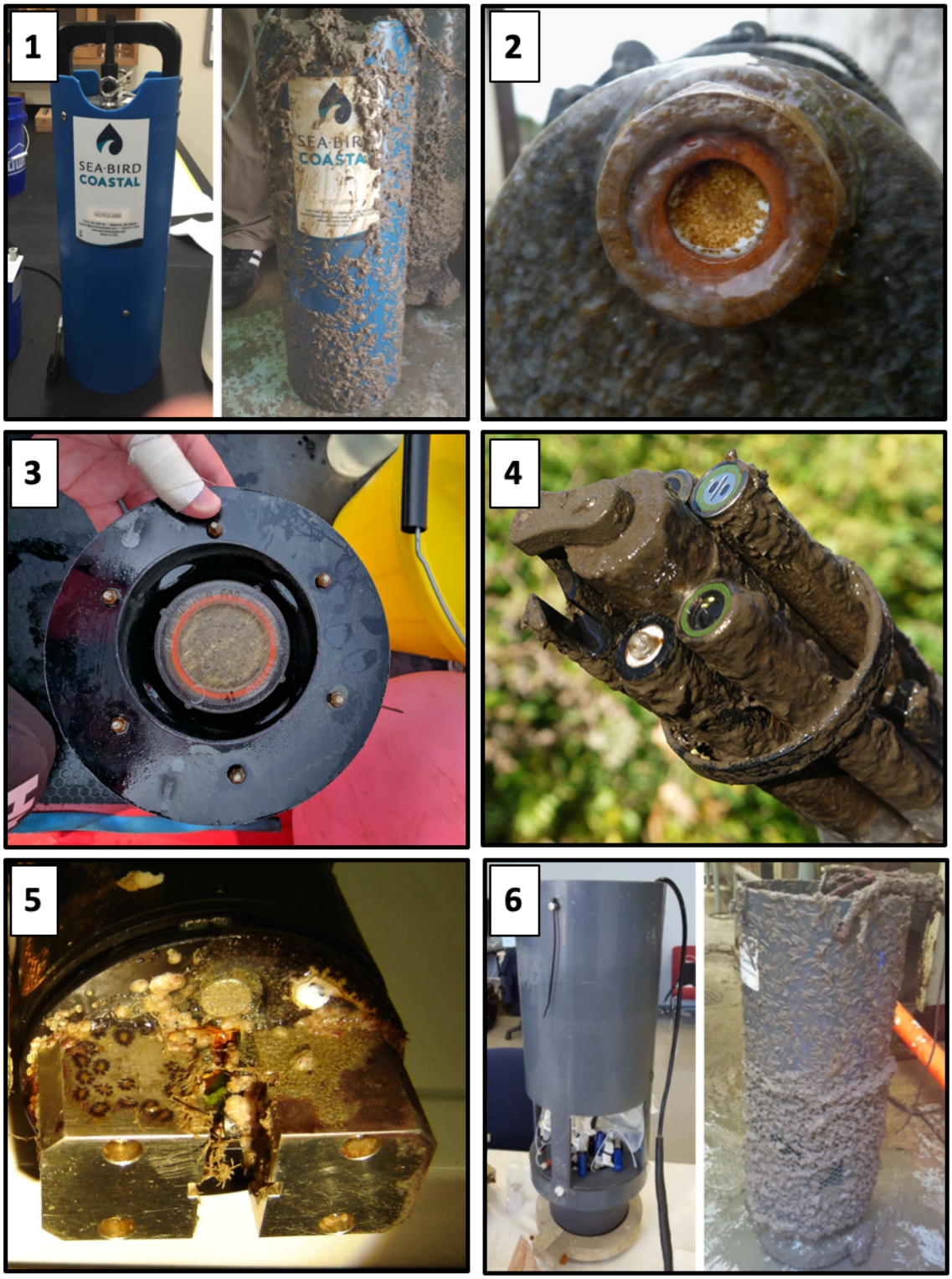

Figure 1.11. *Biofouling accumulation on deployed water sensing platforms (1) Sea-bird Scientific Hydrocycle -PO_4 prior to and following a 32 day field test in the Maumee river [40], (2) Prototype nutrient analyser removed after 3 week deployment, (3) Prefilter on an inlet of nutrient sensing platform deployed in the marine environment after 1 week, (4) Fouled YSI Sonde after deployment with clean sensing surfaces [128] Image Courtesy: YSI, a Xylem brand,(5) Fluorometer after 30 days in Helgoland (Germany) [120] ,(6) NOC sensing platform prior to and following a 32 day field test in the Maumee River [38].*

1.10. Remote sensing

Remote sensing involves the use of satellites or aerial flyovers by aircraft or drones to obtain information about areas from a distance using attenuation or reflection to carry out surface measurements [129]. Remote sensing is capable of giving high spatial information about a water body such as sea surface temperatures or colour [130]. Satellite remote sensing in environmental monitoring can provide multispectral and hyperspectral images of continuously increasing spatial accuracy. Satellite remote sensing/earth observation is a growing area with ever-increasing resolution and frequency. The use of this technology allows for the observation of environmental changes at inaccessible locations remotely. Using the information provided by remote sensors such as the EU Copernicus program, Sentinel programs, Landsat 8, and SERVIR allows for changes in the environment to be mapped. Due to its speed and efficiency in information gathering, the applications of satellite remote sensing are continually increasing and it is rapidly becoming a vital part of environmental resource management [131–133].

Chen et al. [134] presented the use of remote sensing in support of the European Union's Water Framework Directive using the Gulf of Finland as a case study. The study focused on using remote sensing to measure the spatial distribution of nitrate concentrations in surface waters. The spatial distribution of this water quality information was produced using empirical algorithms from satellite-based observations, which were verified using in-situ measurements. Satellite remote sensing is capable of providing globally scaled data at an impressive spatial resolution (30 m for Landsat to 1 km for MODIS) [135]. As the technology relies on satellite or aerial earth imaging, it functions best on clear days where cloud cover is not an issue [136,137]. In the case of the above-mentioned study by Chen et al., the majority of their data set from April to May was cloudy or partly cloudy. For water quality measurements, optical-based observations can be affected by the radiation from direct reflectance from the water surface, but this can be compensated for during data processing [113]. Remote sensing is limited only to surface layers and requires ground truthing to validate the model used for data processing [138].

The combination of in-situ and remote sensing is a powerful tool for water quality monitoring [135]. In-situ and remote sensing are complementary approaches, as in-situ measurements are capable of providing validated high- frequency measurements of the local concentration of specific analytes, while remote sensing is capable of providing more generalized data at the global scale [139,140]. This complementary approach can provide the ability to actively monitor water processes at a global scale and at a resolution that enables highly localized behaviour to be visualized and extended to much larger area [110]. This allows for modelling and understanding of how local events are contributing to the global environment. Tintore et al. [141] highlight the need for further cooperation between in-situ and remote sensing as there is little connection at present between the research communities working on satellite remote sensing and in-situ sensing. This lack of a connection is hindering the quality of the data that can be produced from remote sensing. Currently, satellite observations are capable of covering the entire Mediterranean but not at a high enough resolution to capture fine-scale processes that characterize the high temporal and spatial variability of the basin. Further cooperation between the two sensing types would improve the range of parameters that can be observed and carried out remotely, with in-situ ground-truthing improving modelling for satellite sensing.

Albeit at a small scale, the benefits of combining in-situ and remote sensing were illustrated in an investigation to track Marine/Freshwater Mixing Dynamics within Kinvara Bay, Galway, Ireland. McCaul et al. [129] highlighted the advantages of combined sensing where dynamic processes could be directly visualized at a large scale with a resolution that allowed highly localized behaviour to be tracked. This work generated large and varied forms of data encompassing in-situ temperature, salinity, and phosphate measurements, together with flyover IR thermal imaging, coordinated for temporal and spatial coverage and satellite sea surface temperature measurements. The correlation of this data suggested that it may be possible to track the dynamics of nutrient freshwater/marine mixing in bays using temperature and in-situ ground truthing. In this study, the nutrients entered the bay primarily through freshwater springs, which were sufficiently colder than the warmer sea water to enable tracking of the freshwater movement in the bay by satellite sea surface temperature measurements. As the waterbody (fresh/sea) composition was largely conserved, at

least at the surface, the suggestion was the nutrient movements would be highly correlated with sea-surface temperature (see Figure 1.12), reducing the need for dense deployments of autonomous nutrient sensors to track this movement.

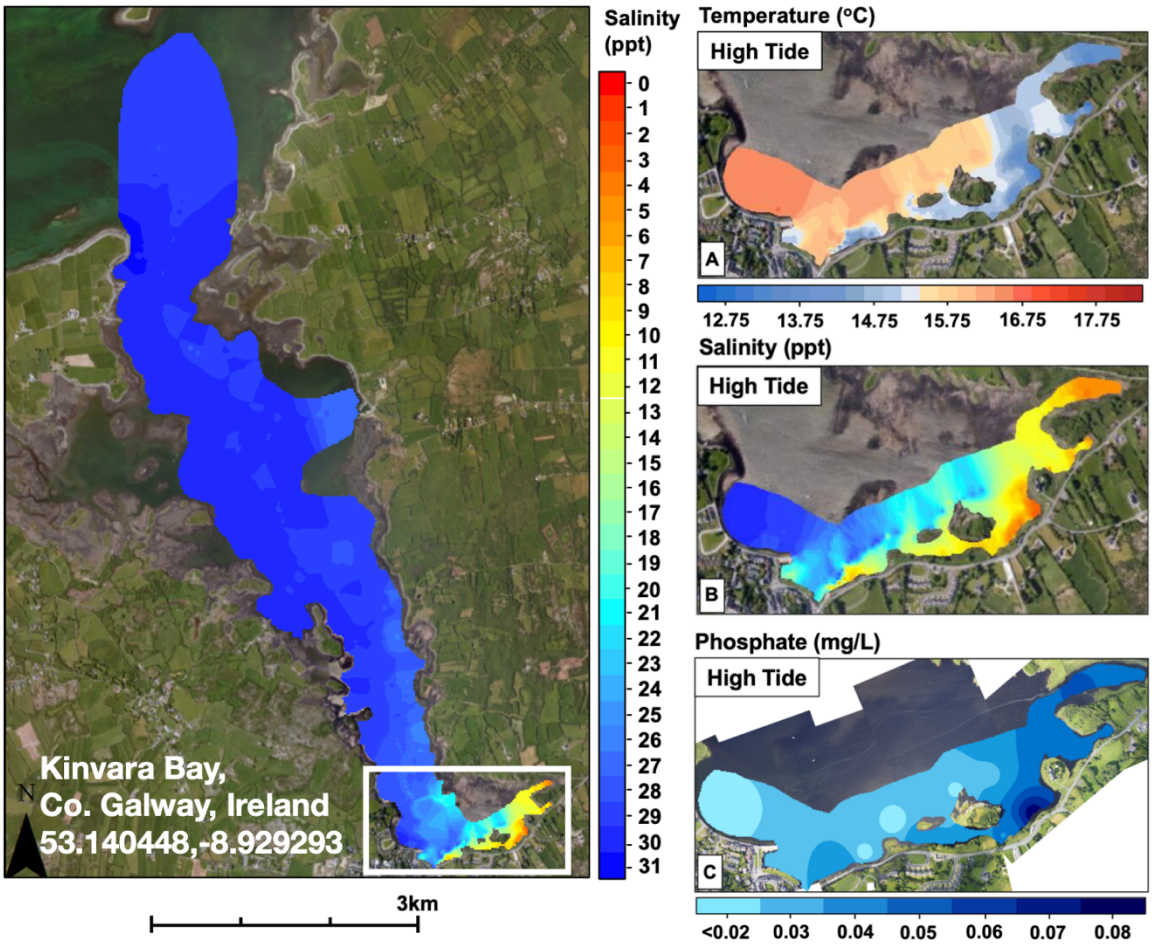

Figure 1.12. *Correlation between temperature, salinity and phosphate measurements taken using combination remote and in-situ sensing at Kinvara Bay, Galway, Ireland. Figure adapted from McCaul et al. [129].*

This combined sensing strategy will prove to be a powerful tool in the future where complementary methods improve the overall resolution and reliability of a measurement. A combination sensing network where in-situ sensors are taking highly localized data in combination with large area measurement from a remote sensor (satellite, aircraft, and drone) has the potential to drastically change how water monitoring is carried out.

1.11. Conclusion

Like many other ecosystems, global freshwater, transitional, and marine waters are threatened by the effects of multiple, co-occurring environmental pressures, notably nutrient enrichment and other organic and inorganic pollutants, climate change, and acidification. Real-time monitoring provides reliable in-situ data that will enhance understanding of the processes that drive these changes in water chemistry and therefore strengthen the development of projection models for mitigation measures to reduce impacts seen by contamination such as eutrophication. This chapter highlights the cost and complexity of sensing technology development (and as a result its scalability) depending both on the type of analyte and on the deployment scenario. Physical parameters (e.g., temperature, turbidity, conductivity, and colour) are the least complex to track due to the availability of very reliable, low-cost sensors. Physical sensors are typically low power, allowing long-term deployments without the need for servicing or maintenance. However, chemical analytes such as nutrients often require complex detection methodologies and sophisticated sensing platforms to provide accurate in-situ data. Although analytical chemistry techniques have rapidly improved, the cost of in-situ sensors for nutrient detection remains the prohibiting factor in widescale deployments necessary to generate a significant amount of data to respond to policies and implement change. Notable advances in electronics, rapid prototyping, microfluidics, and fabrication technologies such as 3D printing have led to the development of new and emerging sensing technologies for the detection of nutrients. However, the global challenge still remains, to develop nutrient sensors at a low cost with specific analytical requirements, coupled with internal calibration, long maintenance intervals, and validation with other analytical techniques. Furthermore, intensive field trials are necessary to make the adoption of these new and emerging technologies feasible for integration into large-scale distributed in-situ sensing networks. Major opportunities still exist for the fusion of in-situ and remote sensing data that is augmented by a comprehensive ground-truthing survey using in-situ sensor networks. Combining the powerful spatial density and wide geographical reach of remote sensing (using drones, flyovers, and satellites) with ground truthing via appropriately located physical and chemical (new and existing) in-situ sensors will generate new data streams that have not been previously accessible. These datasets

have the potential to produce a more complete and accurate picture of processes that influence water quality within marine and freshwater bodies.

1.12. References

(1) Water Quality Monitoring: A Practical Guide to the Design and Implementation of Freshwater Quality Studies and Monitoring Programmes; Ballance, R., Bartram, J., Eds.; Spon Press, 1998. https://doi.org/10.4324/9780203476796.

(2) Sequeira, M.; Bowden, M.; Minogue, E.; Diamond, D. Towards Autonomous Environmental Monitoring Systems. Talanta **2002**, 56 (2), 355–363. https://doi.org/10.1016/S0039-9140(01)00601-4.

(3) Hou, D.; He, J.; Lü, C.; Sun, Y.; Zhang, F.; Otgonbayar, K. Effects of Environmental Factors on Nutrients Release at Sediment-Water Interface and Assessment of Trophic Status for a Typical Shallow Lake, Northwest China. The Scientific World Journal **2013**, 2013, 1–16. https://doi.org/10.1155/2013/716342.

(4) Jaishankar, M.; Tseten, T.; Anbalagan, N.; Mathew, B. B.; Beeregowda, K. N. Toxicity, Mechanism and Health Effects of Some Heavy Metals. Interdiscip Toxicol **2014**, 7 (2), 60–72. https://doi.org/10.2478/intox-2014-0009.

(5) Chapra, S. C.; Boehlert, B.; Fant, C.; Bierman, V. J.; Henderson, J.; Mills, D.; Mas, D. M. L.; Rennels, L.; Jantarasami, L.; Martinich, J.; Strzepek, K. M.; Paerl, H. W. Climate Change Impacts on Harmful Algal Blooms in U.S. Freshwaters: A Screening-Level Assessment. Environ. Sci. Technol. **2017**, 51 (16), 8933–8943. https://doi.org/10.1021/acs.est.7b01498.

(6) Williams, R. J.; Johnson, A. C.; Smith, J. J. L.; Kanda, R. Steroid Estrogens Profiles along River Stretches Arising from Sewage Treatment Works Discharges. Environ. Sci. Technol. **2003**, 37 (9), 1744–1750.

(7) Prien, R. D. The Future of Chemical in Situ Sensors. Marine Chemistry **2007**, 107 (3), 422–432. https://doi.org/10.1016/j.marchem.2007.01.014.

(8) Duan, W.; He, B.; Takara, K.; Luo, P.; Nover, D.; Sahu, N.; Yamashiki, Y. Spatiotemporal Evaluation of Water Quality Incidents in Japan between 1996 and 2007. Chemosphere **2013**, 93 (6), 946–953. https://doi.org/10.1016/j.chemosphere.2013.05.060.

(9) Duan, W.; Takara, K.; He, B.; Luo, P.; Nover, D.; Yamashiki, Y. Spatial and Temporal Trends in Estimates of Nutrient and Suspended Sediment Loads in the

Ishikari River, Japan, 1985 to 2010. Science of The Total Environment **2013**, 461–462, 499–508. https://doi.org/10.1016/j.scitotenv.2013.05.022.

(10) Mehrotra, P. Biosensors and Their Applications – A Review. Journal of Oral Biology and Craniofacial Research **2016**, 6 (2), 153–159. https://doi.org/10.1016/j.jobcr.2015.12.002.

(11) Herfort, L.; Seaton, C.; Wilkin, M.; Roman, B.; Preston, C. M.; Marin, R.; Seitz, K.; Smith, M. W.; Haynes, V.; Scholin, C. A.; Baptista, A. M.; Simon, H. M. Use of Continuous, Real-Time Observations and Model Simulations to Achieve Autonomous, Adaptive Sampling of Microbial Processes with a Robotic Sampler: Adaptive Sampling in an Estuary. Limnol. Oceanogr. Methods **2016**, 14 (1), 50–67. https://doi.org/10.1002/lom3.10069.

(12) Diamond, D.; Collins, F.; Cleary, J.; Zuliani, C.; Fay, C. Distributed Environmental Monitoring. In Autonomous Sensor Networks; Filippini, D., Ed.; Springer Series on Chemical Sensors and Biosensors; Springer Berlin Heidelberg: Berlin, Heidelberg, 2012; Vol. 13, pp 321–363. https://doi.org/10.1007/5346_2012_33.

(13) Albaladejo, C.; Soto, F.; Torres, R.; Sánchez, P.; López, J. A. A Low-Cost Sensor Buoy System for Monitoring Shallow Marine Environments. Sensors **2012**, 12 (7), 9613–9634. https://doi.org/10.3390/s120709613.

(14) Goldman, J.; Ramanathan, N.; Ambrose, R. F.; Caron, D.; Estrin, D.; Fisher, J.; Gilbert, R.; Hansen, M.; Harmon, T. C.; Jay, J. A.; Kaiser, W. J.; Sukhatme, G.; Tai, Y.-C. Distrbuted Sensing Systems for Water Quality Assesment and Management. **2007**.

(15) Kruse, P. Review on Water Quality Sensors. J. Phys. D: Appl. Phys. **2018**, 51 (20), 203002. https://doi.org/10.1088/1361-6463/aabb93.

(16) Jang, A.; Zou, Z.; Lee, K. K.; Ahn, C. H.; Bishop, P. L. State-of-the-Art Lab Chip Sensors for Environmental Water Monitoring. Measurement Science and Technology **2011**, 22 (3), 032001. https://doi.org/10.1088/0957-0233/22/3/032001.

(17) Jokerst, J. C.; Emory, J. M.; Henry, C. S. Advances in Microfluidics for Environmental Analysis. Analyst **2012**, 137 (1), 24–34. https://doi.org/10.1039/C1AN15368D.

(18) Clements, A. L.; Griswold, W. G.; Rs, A.; Johnston, J. E.; Herting, M. M.; Thorson, J.; Collier-Oxandale, A.; Hannigan, M. Low-Cost Air Quality Monitoring Tools: From

Research to Practice (A Workshop Summary). Sensors **2017**, 17 (11), 2478. https://doi.org/10.3390/s17112478.

(19) Jones, D. O. B.; Gates, A. R.; Huvenne, V. A. I.; Phillips, A. B.; Bett, B. J. Autonomous Marine Environmental Monitoring: Application in Decommissioned Oil Fields. Science of The Total Environment **2019**, 668, 835–853. https://doi.org/10.1016/j.scitotenv.2019.02.310.

(20) Gordon, K. How Chemical Monitoring of Our Rivers Can Help Us Understand Their Story – Why, What, Where and When. Catchments.ie, 2016.

(21) Agency (EPA), E. P. Water Monitoring and Assessment - Environmental Protection Agency (EPA https://www.epa.ie/water/wm/ (accessed 2019 -05 -30).

(22) International Initiative on Water Quality: Promoting Scientific Research, Knowledge Sharing, Effective Technology and Policy Approaches to Improve Water Quality for Sustainable Development; 2015. 26.

(23) Bourgeois, W.; Romain, A.-C.; Nicolas, J.; Stuetz, R. M. The Use of Sensor Arrays for Environmental Monitoring: Interests and Limitations. Journal of environmental monitoring : JEM **2003**, 5 (6), 852–860. https://doi.org/10.1039/b307905h.

(24) Alliance for Coastal Technologies - Nutrient Sensor Challenge http://www.act-us.info/nutrients-challenge/partcomps/Real_Tech.php (accessed 2019 -03 -26).

(25) Pellerin, B. A.; Stauffer, B. A.; Young, D. A.; Sullivan, D. J.; Bricker, S. B.; Walbridge, M. R.; Clyde, G. A.; Shaw, D. M. Emerging Tools for Continuous Nutrient Monitoring Networks: Sensors Advancing Science and Water Resources Protection. JAWRA Journal of the American Water Resources Association **2016**, 52 (4), 993–1008. https://doi.org/10.1111/1752-1688.12386.

(26) Nigam, V. K.; Shukla, P. Enzyme Based Biosensors for Detection of Environmental Pollutants-A Review. Journal of Microbiology and Biotechnology **2015**, 25 (11), 1773–1781. https://doi.org/10.4014/jmb.1504.04010.

(27) Bouabana, A.; Şanal, E.; Sourkounis, C. Development of a Low Cost Universal Sensor for an Accurate Measurement of Current, Voltage and Temperature. In 2016 IEEE International Conference on Renewable Energy Research and Applications (ICRERA); 2016; pp 391–395. https://doi.org/10.1109/ICRERA.2016.7884367.

(28) Singh, R.; Singh, S. P. Development of a Low Cost Wireless Temperature Monitoring System for Industrial & Research Application. 7.

(29) Young, D. T.; Chapman, L.; Muller, C. L.; Cai, X.-M.; Grimmond, C. S. B. A Low-Cost Wireless Temperature Sensor: Evaluation for Use in Environmental Monitoring Applications. J. Atmos. Oceanic Technol. **2014**, 31 (4), 938–944. https://doi.org/10.1175/JTECH-D-13-00217.1.

(30) Mota, L.; Mota, A.; Pezzuto, C.; Carvalho, M.; Lavorato, M.; Coiado, L.; Oliveira, E. Development of a Surface Temperature Sensor to Enhance Energy Efficiency Actions in Buildings. Sensors (Basel) **2018**, 18 (9). https://doi.org/10.3390/s18093046.

(31) Lazarescu, M. T. Design and Field Test of a WSN Platform Prototype for Long-Term Environmental Monitoring. Sensors (Basel) **2015**, 15 (4), 9481–9518. https://doi.org/10.3390/s150409481.

(32) Morawska, L.; Thai, P. K.; Liu, X.; Asumadu-Sakyi, A.; Ayoko, G.; Bartonova, A.; Bedini, A.; Chai, F.; Christensen, B.; Dunbabin, M.; Gao, J.; Hagler, G. S. W.; Jayaratne, R.; Kumar, P.; Lau, A. K. H.; Louie, P. K. K.; Mazaheri, M.; Ning, Z.; Motta, N.; Mullins, B.; Rahman, M. M.; Ristovski, Z.; Shafiei, M.; Tjondronegoro, D.; Westerdahl, D.; Williams, R. Applications of Low-Cost Sensing Technologies for Air Quality Monitoring and Exposure Assessment: How Far Have They Gone? Environ Int **2018**, 116, 286–299. https://doi.org/10.1016/j.envint.2018.04.018.

(33) Kumar, P.; Morawska, L.; Martani, C.; Biskos, G.; Neophytou, M.; Di Sabatino, S.; Bell, M.; Norford, L.; Britter, R. The Rise of Low-Cost Sensing for Managing Air Pollution in Cities. Environment International **2015**, 75, 199–205. https://doi.org/10.1016/j.envint.2014.11.019.

(34) Popoola, O. A. M.; Carruthers, D.; Lad, C.; Bright, V. B.; Mead, M. I.; Stettler, M. E. J.; Saffell, J. R.; Jones, R. L. Use of Networks of Low Cost Air Quality Sensors to Quantify Air Quality in Urban Settings. Atmospheric Environment **2018**, 194, 58–70. https://doi.org/10.1016/j.atmosenv.2018.09.030.

(35) Argo. Argo Float Data and Metadata from Global Data Assembly Centre (Argo GDAC), 2019. https://doi.org/10.17882/42182.

(36) (4) (PDF) The Argo Program Observing the Global Ocean with Profiling Floats https://www.researchgate.net/publication/33549908_The_Argo_Program_Observing_the_Global_Ocean_with_Profiling_Floats (accessed 2019 -05 -30).

(37) Thierry, V.; Bittig, H.; Gilbert, D.; Kobayashi, T.; Kanako, S.; Schmid, C. Processing Argo Oxygen Data at the DAC Level; Ifremer, 2018. https://doi.org/10.13155/39795.

(38) Performance Verification Statement for the NOC Phospate Analyzer http://www.act-us.info/Download/Evaluations/NextGenNutrient/NOCPO4/#16 (accessed 2019 -06 -04).

(39) Performance Verification Statement for the NOC Nitrate Analyzer http://www.act-us.info/Download/Evaluations/NextGenNutrient/NOCNitrate/#1 (accessed 2019 -09 -15).

(40) Performance Verification Statement for Sea-Bird Scientific HydroCycle-Phosphate Analyzer http://www.act-us.info/Download/Evaluations/NextGenNutrient/SeaBird/ (accessed 2019 -09 -15).

(41) Performance Verification Statement for the Systea WIZ Probe Nitrate Analyzer http://www.act-us.info/Download/Evaluations/NextGenNutrient/SysteaNitrate/ (accessed 2019 -09 -21).

(42) Performance Verification Statement for the Systea WIZ Probe Phospate Analyzer http://www.act-us.info/Download/Evaluations/NextGenNutrient/SysteaP04/ (accessed 2019 -09 -21).

(43) Ho, C. K.; Robinson, A.; Miller, D. R.; Davis, M. J. Overview of Sensors and Needs for Environmental Monitoring. Sensors (Basel) **2005**, 5 (2), 4–37.

(44) Anastasova, S.; Radu, A.; Matzeu, G.; Zuliani, C.; Mattinen, U.; Bobacka, J.; Diamond, D. Disposable Solid-Contact Ion-Selective Electrodes for Environmental Monitoring of Lead with Ppb Limit-of-Detection. Electrochimica Acta **2012**, 73, 93–97. https://doi.org/10.1016/j.electacta.2011.10.089.

(45) Delaney, C.; McCluskey, P.; Coleman, S.; Whyte, J.; Kent, N.; Diamond, D. Precision Control of Flow Rate in Microfluidic Channels Using Photoresponsive Soft Polymer Actuators. Lab Chip **2017**, 17 (11), 2013–2021. https://doi.org/10.1039/C7LC00368D.

(46) Manz, A.; Graber, N.; Widmer, H. M. Miniaturized Total Chemical Analysis Systems: A Novel Concept for Chemical Sensing. Sensors and Actuators B: Chemical **1990**, 1 (1), 244–248. https://doi.org/10.1016/0925-4005(90)80209-I.

(47) Czugala, M.; Ziolkowski, B.; Byrne, R.; Diamond, D.; Benito-Lopez, F. Materials Science: The Key to Revolutionary Breakthroughs in Micro-Fluidic Devices. In Nano-Opto-Mechanical Systems (NOMS); International Society for Optics and Photonics, 2011; Vol. 8107, p 81070C. https://doi.org/10.1117/12.895330.

(48) Grand, M. M.; Clinton-Bailey, G. S.; Beaton, A. D.; Schaap, A. M.; Johengen, T. H.; Tamburri, M. N.; Connelly, D. P.; Mowlem, M. C.; Achterberg, E. P. A Lab-On-Chip Phosphate Analyzer for Long-Term In Situ Monitoring at Fixed Observatories: Optimization and Performance Evaluation in Estuarine and Oligotrophic Coastal Waters. Frontiers in Marine Science **2017**, 4. https://doi.org/10.3389/fmars.2017.00255.

(49) Cogan, D.; Fay, C.; Boyle, D.; Osborne, C.; Kent, N.; Cleary, J.; Diamond, D. Development of a Low Cost Microfluidic Sensor for the Direct Determination of Nitrate Using Chromotropic Acid in Natural Waters. Anal. Methods **2015**, 7 (13), 5396–5405. https://doi.org/10.1039/C5AY01357G.

(50) Donohoe, A.; Lacour, G.; McCluskey, P.; Diamond, D.; McCaul, M. Development of a Cost-Effective Sensing Platform for Monitoring Phosphate in Natural Waters. Chemosensors **2018**, 6 (4), 57. https://doi.org/10.3390/chemosensors6040057.

(51) Murray, E.; Roche, P.; Harrington, K.; McCaul, M.; Moore, B.; Morrin, A.; Diamond, D.; Paull, B. Low Cost 235 Nm Ultra-Violet Light-Emitting Diode-Based Absorbance Detector for Application in a Portable Ion Chromatography System for Nitrite and Nitrate Monitoring. Journal of Chromatography A **2019**, S0021967319305424. https://doi.org/10.1016/j.chroma.2019.05.036.

(52) Duffy, G.; Maguire, I.; Heery, B.; Nwankire, C.; Ducrée, J.; Regan, F. PhosphaSense: A Fully Integrated, Portable Lab-on-a-Disc Device for Phosphate Determination in Water. Sensors and Actuators B: Chemical **2017**, 246, 1085–1091. https://doi.org/10.1016/j.snb.2016.12.040.

(53) Coleman, S.; ter Schiphorst, J.; Ben Azouz, A.; Bakker, S.; Schenning, A. P. H. J.; Diamond, D. Tuning Microfluidic Flow by Pulsed Light Oscillating Spiropyran-

Based Polymer Hydrogel Valves. Sensors and Actuators B: Chemical **2017**, 245, 81–86. https://doi.org/10.1016/j.snb.2017.01.112.

(54) Hunston, E. WaterBlitz Registration Page https://earthwatch.org.uk/get-involved/waterblitz (accessed 2019 -09 -03).

(55) Earthwatch FreshWater Watch https://freshwaterwatch.thewaterhub.org/ (accessed 2019 -09 -03).

(56) Lucan Bridge-23-08-2019-0 https://freshwaterwatch.thewaterhub.org/sample/lucan-bridge-23-08-2019-0 (accessed 2019 -09 -19).

(57) DR900 Multiparameter Portable Colorimeter | Hach USA - Overview https://www.hach.com/dr900-multiparameter-portable-colorimeter/product?id=15684103251 (accessed 2019 -06 -04).

(58) Tchounwou, P. B.; Yedjou, C. G.; Patlolla, A. K.; Sutton, D. J. Heavy Metal Toxicity and the Environment. In Molecular, Clinical and Environmental Toxicology; Luch, A., Ed.; Springer Basel: Basel, 2012; Vol. 101, pp 133–164. https://doi.org/10.1007/978-3-7643-8340-4_6.

(59) Yool, A.; Popova, E. E.; Anderson, T. R. MEDUSA-2.0: An Intermediate Complexity Biogeochemical Model of the Marine Carbon Cycle for Climate Change and Ocean Acidification Studies. Geoscientific Model Development **2013**, 6 (5), 1767–1811. https://doi.org/10.5194/gmd-6-1767-2013.

(60) Heisler, J.; Glibert, P.; Burkholder, J.; Anderson, D.; Cochlan, W.; Dennison, W.; Gobler, C.; Dortch, Q.; Heil, C.; Humphries, E.; Lewitus, A.; Magnien, R.; Marshall, H.; Sellner, K.; Stockwell, D.; Stoecker, D.; Suddleson, M. Eutrophication and Harmful Algal Blooms: A Scientific Consensus. Harmful Algae **2008**, 8 (1), 3–13. https://doi.org/10.1016/j.hal.2008.08.006.

(61) Smith, V. H. Eutrophication of Freshwater and Coastal Marine Ecosystems a Global Problem. Environ Sci & Pollut Res **2003**, 10 (2), 126–139. https://doi.org/10.1065/espr2002.12.142.

(62) Yang, X.; Wu, X.; Hao, H.; He, Z. Mechanisms and Assessment of Water Eutrophication. J Zhejiang Univ Sci B **2008**, 9 (3), 197–209. https://doi.org/10.1631/jzus.B0710626.

(63) Bol, R.; Gruau, G.; Mellander, P.-E.; Dupas, R.; Bechmann, M.; Skarbøvik, E.; Bieroza, M.; Djodjic, F.; Glendell, M.; Jordan, P.; Van der Grift, B.; Rode, M.;

Smolders, E.; Verbeeck, M.; Gu, S.; Klumpp, E.; Pohle, I.; Fresne, M.; Gascuel-Odoux, C. Challenges of Reducing Phosphorus Based Water Eutrophication in the Agricultural Landscapes of Northwest Europe. Front. Mar. Sci. **2018**, 5, 276. https://doi.org/10.3389/fmars.2018.00276.

(64) Davidson, K.; Gowen, R. J.; Harrison, P. J.; Fleming, L. E.; Hoagland, P.; Moschonas, G. Anthropogenic Nutrients and Harmful Algae in Coastal Waters. Journal of Environmental Management **2014**, 146, 206–216. https://doi.org/10.1016/j.jenvman.2014.07.002.

(65) Pretty, J. N.; Mason, C. F.; Nedwell, D. B.; Hine, R. E.; Leaf, S.; Dils, R. Environmental Costs of Freshwater Eutrophication in England and Wales. Environ. Sci. Technol. **2003**, 37 (2), 201–208. https://doi.org/10.1021/es020793k.

(66) Dodds, W. K.; Bouska, W. W.; Eitzmann, J. L.; Pilger, T. J.; Pitts, K. L.; Riley, A. J.; Schloesser, J. T.; Thornbrugh, D. J. Eutrophication of U.S. Freshwaters: Analysis of Potential Economic Damages. Environ. Sci. Technol. **2009**, 43 (1), 12–19. https://doi.org/10.1021/es801217q.

(67) Nutrient Pollution - an overview | ScienceDirect Topics https://www.sciencedirect.com/topics/earth-and-planetary-sciences/nutrient-pollution (accessed 2019 -05 -30).

(68) Khan, F. A.; Ansari, A. A. Eutrophication: An Ecological Vision. The Botanical Review **2005**, 71 (4), 449–482. https://doi.org/10.1663/0006-8101(2005)071[0449:EAEV]2.0.CO;2.

(69) Bowden, M.; Sequiera, M.; Krog, J. P.; Gravesen, P.; Diamond, D. Analysis of River Water Samples Utilising a Prototype Industrial Sensing System for Phosphorus Based on Micro-System Technology. Journal of Environmental Monitoring **2002**, 4 (5), 767–771. https://doi.org/10.1039/b200330a.

(70) Phosphate - an overview | ScienceDirect Topics https://www.sciencedirect.com/topics/medicine-and-dentistry/phosphate (accessed 2019 -05 -30).

(71) Brogan, J.; Crowe, M.; Carty, G.; Ireland; Environmental Protection Agency. Developing a National Phosphorus Balance for Agriculture in Ireland: A Discussion Document; Environmental Protection Agency: Johnstown Castle, Co. Wexford, 2001.

(72) Bresnahan, P. J.; Martz, T. R.; Takeshita, Y.; Johnson, K. S.; LaShomb, M. Best Practices for Autonomous Measurement of Seawater PH with the Honeywell Durafet. Methods in Oceanography **2014**, 9, 44–60. https://doi.org/10.1016/j.mio.2014.08.003.

(73) Fay, C.; Anastasova, S.; Slater, C.; Buda, S. T.; Shepherd, R.; Corcoran, B.; O'Connor, N. E.; Wallace, G. G.; Radu, A.; Diamond, D. Wireless Ion-Selective Electrode Autonomous Sensing System. IEEE Sensors Journal **2011**, 11 (10), 2374–2382. https://doi.org/10.1109/JSEN.2011.2122331.

(74) Chen, X.; Zhou, G.; Mao, S.; Chen, J. Rapid Detection of Nutrients with Electronic Sensors: A Review. Environ. Sci.: Nano **2018**, 5 (4), 837–862. https://doi.org/10.1039/C7EN01160A.

(75) Frank, C.; Schroeder, F.; Ebinghaus, R.; Ruck, W. Using Sequential Injection Analysis for Fast Determination of Phosphate in Coastal Waters. Talanta **2006**, 70 (3), 513–517. https://doi.org/10.1016/j.talanta.2005.12.055.

(76) Kröckel, L.; Lehmann, H.; Wieduwilt, T.; Schmidt, M. A. Fluorescence Detection for Phosphate Monitoring Using Reverse Injection Analysis. Talanta **2014**, 125, 107–113. https://doi.org/10.1016/j.talanta.2014.02.072.

(77) Gimbert, L. J.; Haygarth, P. M.; Worsfold, P. J. Determination of Nanomolar Concentrations of Phosphate in Natural Waters Using Flow Injection with a Long Path Length Liquid Waveguide Capillary Cell and Solid-State Spectrophotometric Detection. Talanta **2007**, 71 (4), 1624–1628. https://doi.org/10.1016/j.talanta.2006.07.044.

(78) Swinehart, D. F. The Beer-Lambert Law. J. Chem. Educ. **1962**, 39 (7), 333. https://doi.org/10.1021/ed039p333.

(79) Radu, T.; Ireland; Environmental Protection Agency; EPA STRIVE Programme. Analytical Devices for Autonomous Monitoring of the Environment; Environmental Protection Agency: Johnstown Castle, Co. Wexford, 2009.

(80) Cleary, J.; Slater, C.; McGraw, C.; Diamond, D. An Autonomous Microfluidic Sensor for Phosphate: On-Site Analysis of Treated Wastewater. IEEE Sensors Journal **2008**, 8 (5), 508–515. https://doi.org/10.1109/JSEN.2008.918259.

(81) Bowden, M.; Diamond, D. The Determination of Phosphorus in a Microfluidic Manifold Demonstrating Long-Term Reagent Lifetime and Chemical Stability

Utilising a Colorimetric Method. Sensors and Actuators B: Chemical **2003**, 90 (1–3), 170–174. https://doi.org/10.1016/S0925-4005(03)00024-8.

(82) To, Y. S.; Randall, C. W. Evaluation of Ascorbic Acid Method for Determination of Orthophosphates. Journal (Water Pollution Control Federation) **1977**, 49 (4), 689–692.

(83) Bowden, M. Smaller, Smarter, Faster: The Development and Application of Microfluidic Devices to the Determination of Phosphorus in Natural Waters., 2003.

(84) Katewa, S. D.; Katyare, S. S. A Simplified Method for Inorganic Phosphate Determination and Its Application for Phosphate Analysis in Enzyme Assays. Analytical Biochemistry **2003**, 323 (2), 180–187. https://doi.org/10.1016/j.ab.2003.08.024.

(85) Diamond, D.; Cleary, J.; Maher, D.; Jungho Kim; King Tong Lau. Autonomous Analyser Platforms for Remote Monitoring of Water Quality. In IECON 2011 - 37th Annual Conference of the IEEE Industrial Electronics Society; IEEE: Melbourne, Vic, Australia, 2011; pp 3516–3521. https://doi.org/10.1109/IECON.2011.6119878.

(86) Duffy, G.; Regan, F. Recent Developments in Sensing Methods for Eutrophying Nutrients with a Focus on Automation for Environmental Applications. Analyst **2017**, 142 (23), 4355–4372. https://doi.org/10.1039/C7AN00840F.

(87) RN Nordin. Water Quality Guidelines for Nitrogen (Nitrate, Nitrite, and Ammonia). **2009**, 29.

(88) Biological Nitrogen Fixation - an overview | ScienceDirect Topics https://www.sciencedirect.com/topics/earth-and-planetary-sciences/biological-nitrogen-fixation (accessed 2019 -05 -30).

(89) Kaushal, S. S.; Groffman, P. M.; Band, L. E.; Elliott, E. M.; Shields, C. A.; Kendall, C. Tracking Nonpoint Source Nitrogen Pollution in Human-Impacted Watersheds. Environ. Sci. Technol. **2011**, 45 (19), 8225–8232. https://doi.org/10.1021/es200779e.

(90) Ward, M. H.; Jones, R. R.; Brender, J. D.; de Kok, T. M.; Weyer, P. J.; Nolan, B. T.; Villanueva, C. M.; van Breda, S. G. Drinking Water Nitrate and Human Health: An Updated Review. Int J Environ Res Public Health **2018**, 15 (7). https://doi.org/10.3390/ijerph15071557.

(91) Cogan, D.; Cleary, J.; Fay, C.; Rickard, A.; Jankowski, K.; Phelan, T.; Bowkett, M.; Diamond, D. The Development of an Autonomous Sensing Platform for the Monitoring of Ammonia in Water Using a Simplified Berthelot Method. Anal. Methods **2014**, 6 (19), 7606–7614. https://doi.org/10.1039/C4AY01359J.

(92) Absalan, G.; Soleimani, M.; Asadi, M.; Ahmadi, M. B. Constructing a New Optical Sensor for Monitoring Ammonia in Water Samples Using Bis(Acetylacetoneethylendiamine)Tributylphosphin Cobalt(III) Tetraphenylborate Complex-Coated Triacetylcellulose. Anal. Sci. **2004**, 20 (10), 1433–1436. https://doi.org/10.2116/analsci.20.1433.

(93) Miranda, K. M.; Espey, M. G.; Wink, D. A. A Rapid, Simple Spectrophotometric Method for Simultaneous Detection of Nitrate and Nitrite. Nitric Oxide **2001**, 5 (1), 62–71. https://doi.org/10.1006/niox.2000.0319.

(94) Wang, S.; Lin, K.; Chen, N.; Yuan, D.; Ma, J. Automated Determination of Nitrate plus Nitrite in Aqueous Samples with Flow Injection Analysis Using Vanadium (III) Chloride as Reductant. Talanta **2016**, 146, 744–748. https://doi.org/10.1016/j.talanta.2015.06.031.

(95) Gal, C.; Frenzel, W.; Möller, J. Re-Examination of the Cadmium Reduction Method and Optimisation of Conditions for the Determination of Nitrate by Flow Injection Analysis. Microchim. Acta **2004**, 146 (2), 155–164. https://doi.org/10.1007/s00604-004-0193-7.

(96) Hydes, D. J.; Hill, N. C. Determination of Nitrate in Seawater: Nitrate to Nitrite Reduction with Copper-Cadmium Alloy. Estuarine, Coastal and Shelf Science **1985**, 21 (1), 127–130. https://doi.org/10.1016/0272-7714(85)90011-3.

(97) Wood, E. D.; Armstrong, F. A. J.; Richardsl, F. A. Determination of Nitrate in Sea Water by Cadmium-Copper Reduction to Nitrite. J. Mar. Biol. Assoc. UK **1967**, 23–31.

(98) Sandu, M.; Lupascu, T.; Tarita, A.; Goreacioc, T.; Turcan, S.; Mosanu, E. Method for Nitrate Determination in Water in the Presence of Nitrite. ChemJMold **2014**, 9 (2), 8–13. https://doi.org/10.19261/cjm.2014.09(2).01.

(99) Sequeira, M.; Diamond, D.; Daridon, A.; Lichtenberg, J.; Verpoorte, S.; Rooij, N. F. de. Progress in the Realisation of an Autonomous Environmental Monitoring Device for Ammonia. TrAC Trends in Analytical Chemistry **2002**, 21 (12), 816–827. https://doi.org/10.1016/S0165-9936(02)01205-0.

(100) Searle, P. L. The Berthelot or Indophenol Reaction and Its Use in the Analytical Chemistry of Nitrogen. A Review. Analyst **1984**, 109 (5), 549. https://doi.org/10.1039/an9840900549.

(101) Daridon, A.; Sequeira, M.; Pennarun-Thomas, G.; Dirac, H.; Krog, J. P.; Gravesen, P.; Lichtenberg, J.; Diamond, D.; Verpoorte, E.; de Rooij, N. F. Chemical Sensing Using an Integrated Micro¯uidic System Based on the Berthelot Reaction. **2001**, 9.

(102) Xylem Analytics | WTW's Analyzer https://www.xylemanalytics.com/en/products/analyzers (accessed 2019 -08 -10).

(103) 5500 sc Ammonia Monochloramine Analyzer | Hach USA - Overview | Hach https://www.hach.com/ammonia-monochloramine-analyzers/5500-sc-ammonia-monochloramine-analyzer/family?productCategoryId=35547203805 (accessed 2019 -08 -10).

(104) Ortho Phosphorus Analyzer https://www.chemscan.com/chemscan-uv-4100-process-analyzer.html (accessed 2019 -08 -10).

(105) Xylem Analytics | Ammonium-Measuring by WTW https://www.xylemanalytics.com/en/parameters/ammonium (accessed 2019 -08 -10).

(106) Mills, G.; Fones, G. A Review of in Situ Methods and Sensors for Monitoring the Marine Environment. Sensor Review **2012**, 32 (1), 17–28. https://doi.org/10.1108/02602281211197116.

(107) Ecosens Aquamonitrix https://www.ecosensaquamonitrix.eu/ (accessed 2019 -08 -10).

(108) HydroCycle PO_4 | Sea-Bird Scientific - Overview | Sea-Bird https://www.seabird.com/hydrocycle-po/product?id=54721314201 (accessed 2019 -09 -15).

(109) WIZ probe http://www.systea.it/index.php?option=com_k2&view=item&layout=item&id=223&Itemid=175&lang=en (accessed 2019 -09 -20).

(110) NPA Pro http://www.systea.it/index.php?option=com_k2&view=item&layout=item&id=221&Itemid=176&lang=en (accessed 2019 -09 -20).

(111) Bodini, S.; Sanfilippo, L.; Savino, E.; Moscetta, P. Automated Micro Loop Flow Reactor Technology to Measure Nutrients in Coastal Water: State of the Art and Field Application. In OCEANS 2015 - Genova; IEEE: Genova, Italy, 2015; pp 1–7. https://doi.org/10.1109/OCEANS-Genova.2015.7271720.

(112) Schierenbeck, T. M.; Smith, M. C. Path to Impact for Autonomous Field Deployable Chemical Sensors: A Case Study of in Situ Nitrite Sensors. Environ. Sci. Technol. **2017**, 51 (9), 4755–4771. https://doi.org/10.1021/acs.est.6b06171.

(113) Knight, C.; Davidson, J.; Behrens, S. Energy Options for Wireless Sensor Nodes. Sensors (Basel) **2008**, 8 (12), 8037–8066. https://doi.org/10.3390/s8128037.

(114) Mahmoudzadeh Andwari, A.; Pesiridis, A.; Rajoo, S.; Martinez-Botas, R.; Esfahanian, V. A Review of Battery Electric Vehicle Technology and Readiness Levels. Renewable and Sustainable Energy Reviews **2017**, 78, 414–430. https://doi.org/10.1016/j.rser.2017.03.138.

(115) Bastian, R. Temperature Effects in Differential Colorimetry. Anal. Chem. **1953**, 25 (2), 259–262. https://doi.org/10.1021/ac60074a014.

(116) Chen, L.; Ma, J.; Huang, Y.; Dai, M.; Li, X. Optimization of a Colorimetric Method to Determine Trace Urea in Seawater. Limnology and Oceanography: Methods **2015**, 13 (6), 303–311. https://doi.org/10.1002/lom3.10026.

(117) Kanno, S.; Cuyas, L.; Javot, H.; Bligny, R.; Gout, E.; Dartevelle, T.; Hanchi, M.; Nakanishi, T. M.; Thibaud, M.-C.; Nussaume, L. Performance and Limitations of Phosphate Quantification: Guidelines for Plant Biologists. Plant Cell Physiol **2016**, 57 (4), 690–706. https://doi.org/10.1093/pcp/pcv208.

(118) Okamura, K.; Kimoto, H.; Noguchi, T.; Hatta, M.; Kawakami, H.; Suzue, T. Colorimetric PH Measurement for Seawater Samples Using a Three Light-Emitting Diodes Detector and a Calibration Method for Temperature Dependence. Anal Sci **2014**, 30 (12), 1135–1141. https://doi.org/10.2116/analsci.30.1135.

(119) Miralles, V.; Huerre, A.; Malloggi, F.; Jullien, M.-C. A Review of Heating and Temperature Control in Microfluidic Systems: Techniques and Applications. Diagnostics (Basel) **2013**, 3 (1), 33–67. https://doi.org/10.3390/diagnostics3010033.

(120) Delauney, L.; Compère, C.; Lehaitre, M. Biofouling Protection for Marine Environmental Sensors. Ocean Sci. **2010**, 6 (2), 503–511. https://doi.org/10.5194/os-6-503-2010.

(121) Tang, C. Y.; Chong, T. H.; Fane, A. G. Colloidal Interactions and Fouling of NF and RO Membranes: A Review. Advances in Colloid and Interface Science **2011**, 164 (1–2), 126–143. https://doi.org/10.1016/j.cis.2010.10.007.

(122) Aoustin, E. Ultrafiltration of Natural Organic Matter. Separation and Purification Technology **2001**, 22–23 (1–2), 63–78. https://doi.org/10.1016/S1383-5866(00)00143-X.

(123) Brandt, M. J.; Johnson, K. M.; Elphinston, A. J.; Ratnayaka, D. D. Chapter 6 - Intakes. In Twort's Water Supply (Seventh Edition); Brandt, M. J., Johnson, K. M., Elphinston, A. J., Ratnayaka, D. D., Eds.; Butterworth-Heinemann: Boston, 2017; pp 205–233. https://doi.org/10.1016/B978-0-08-100025-0.00006-5.

(124) Nguyen, T.; Roddick, F.; Fan, L. Biofouling of Water Treatment Membranes: A Review of the Underlying Causes, Monitoring Techniques and Control Measures. Membranes **2012**, 2 (4), 804–840. https://doi.org/10.3390/membranes2040804.

(125) Manov, D. V.; Chang, G. C.; Dickey, T. D. Methods for Reducing Biofouling of Moored Optical Sensors. J. Atmos. Oceanic Technol. **2004**, 21 (6), 958–968. https://doi.org/10.1175/1520-0426(2004)021<0958:MFRBOM>2.0.CO;2.

(126) Song, K.; Mohseni, M.; Taghipour, F. Application of Ultraviolet Light-Emitting Diodes (UV-LEDs) for Water Disinfection: A Review. Water Research **2016**, 94, 341–349. https://doi.org/10.1016/j.watres.2016.03.003.

(127) Walker, D. I. Biofouling and Its Control for in Situ Lab-on-a-Chip Marine Environmental Sensors. **2015**. https://doi.org/10.13140/rg.2.1.4275.5040.

(128) Oct 20, P. H. |; 2015. The EXO Wiped Conductivity & Temperature Sensor Helps Eliminate Biofouling https://www.ysi.com/ysi-blog/water-blogged-blog/2015/10/the-exo-wiped-conductivity-temperature-sensor-helps-eliminate-biofouling (accessed 2019 -06 -04).

(129) McCaul, M.; Barland, J.; Cleary, J.; Cahalane, C.; McCarthy, T.; Diamond, D. Combining Remote Temperature Sensing with In-Situ Sensing to Track Marine/Freshwater Mixing Dynamics. Sensors **2016**, 16 (9), 1402. https://doi.org/10.3390/s16091402.

(130) Andres, L.; Boateng, K.; Borja-Vega, C.; Thomas, E. A Review of In-Situ and Remote Sensing Technologies to Monitor Water and Sanitation Interventions. Water **2018**, 10 (6), 756. https://doi.org/10.3390/w10060756.

(131) Chassot, E.; Bonhommeau, S.; Reygondeau, G.; Nieto, K.; Polovina, J. J.; Huret, M.; Dulvy, N. K.; Demarcq, H. Satellite Remote Sensing for an Ecosystem Approach to Fisheries Management. ICES Journal of Marine Science **2011**, 68 (4), 651–666. https://doi.org/10.1093/icesjms/fsq195.

(132) Melesse, A.; Weng, Q.; Thenkabail, P.; Senay, G. Remote Sensing Sensors and Applications in Environmental Resources Mapping and Modelling. Sensors **2007**, 7 (12), 3209–3241. https://doi.org/10.3390/s7123209.

(133) Li, J.; Pei, Y.; Zhao, S.; Xiao, R.; Sang, X.; Zhang, C. A Review of Remote Sensing for Environmental Monitoring in China. Remote Sensing **2020**, 12 (7), 1130. https://doi.org/10.3390/rs12071130.

(134) Chen, Q.; Zhang, Y.; Hallikainen, M. Water Quality Monitoring Using Remote Sensing in Support of the EU Water Framework Directive (WFD): A Case Study in the Gulf of Finland. Environ Monit Assess **2007**, 124 (1–3), 157–166. https://doi.org/10.1007/s10661-006-9215-8.

(135) Schaeffer, B. A.; Schaeffer, K. G.; Keith, D.; Lunetta, R. S.; Conmy, R.; Gould, R. W. Barriers to Adopting Satellite Remote Sensing for Water Quality Management. International Journal of Remote Sensing **2013**, 34 (21), 7534–7544. https://doi.org/10.1080/01431161.2013.823524.

(136) Wijedasa, L. S.; Sloan, S.; Michelakis, D. G.; Clements, G. R. Overcoming Limitations with Landsat Imagery for Mapping of Peat Swamp Forests in Sundaland. Remote Sensing **2012**, 4 (9), 2595–2618. https://doi.org/10.3390/rs4092595.

(137) Marshall, G. J.; Dowdeswell, J. A.; Rees, W. G. The Spatial and Temporal Effect of Cloud Cover on the Acquisition of High Quality Landsat Imagery in the European Arctic Sector. Remote Sensing of Environment **1994**, 50 (2), 149–160. https://doi.org/10.1016/0034-4257(94)90041-8.

(138) Hay, S. I. An Overview of Remote Sensing and Geodesy for Epidemiology and Public Health Application. Adv Parasitol **2000**, 47, 1–35.

(139) Sputh, B. H. C.; Faust, O.; Pettersson, L. H.; Hamre, T.; Vitulli, D.; Allen, A. R.; Spracklen, T. Integration of In-Situ and Remote Sensing Data for Water Risk Management; 2008; Vol. 1, pp 486–493.

(140) Devlin, M. J.; da Silva, E. T.; Petus, C.; Wenger, A.; Zeh, D.; Tracey, D.; Álvarez-Romero, J. G.; Brodie, J. Combining In-Situ Water Quality and Remotely Sensed Data across Spatial and Temporal Scales to Measure Variability in Wet Season Chlorophyll-a: Great Barrier Reef Lagoon (Queensland, Australia). Ecol Process **2013**, 2 (1), 31. https://doi.org/10.1186/2192-1709-2-31.

(141) Tintoré, J.; Pinardi, N.; Álvarez-Fanjul, E.; Aguiar, E.; Álvarez-Berastegui, D.; Bajo, M.; Balbin, R.; Bozzano, R.; Nardelli, B. B.; Cardin, V.; Casas, B.; Charcos-Llorens, M.; Chiggiato, J.; Clementi, E.; Coppini, G.; Coppola, L.; Cossarini, G.; Deidun, A.; Deudero, S.; D'Ortenzio, F.; Drago, A.; Drudi, M.; El Serafy, G.; Escudier, R.; Farcy, P.; Federico, I.; Fernández, J. G.; Ferrarin, C.; Fossi, C.; Frangoulis, C.; Galgani, F.; Gana, S.; García Lafuente, J.; Sotillo, M. G.; Garreau, P.; Gertman, I.; Gómez-Pujol, L.; Grandi, A.; Hayes, D.; Hernández-Lasheras, J.; Herut, B.; Heslop, E.; Hilmi, K.; Juza, M.; Kallos, G.; Korres, G.; Lecci, R.; Lazzari, P.; Lorente, P.; Liubartseva, S.; Louanchi, F.; Malacic, V.; Mannarini, G.; March, D.; Marullo, S.; Mauri, E.; Meszaros, L.; Mourre, B.; Mortier, L.; Muñoz-Mas, C.; Novellino, A.; Obaton, D.; Orfila, A.; Pascual, A.; Pensieri, S.; Pérez Gómez, B.; Pérez Rubio, S.; Perivoliotis, L.; Petihakis, G.; de la Villéon, L. P.; Pistoia, J.; Poulain, P.-M.; Pouliquen, S.; Prieto, L.; Raimbault, P.; Reglero, P.; Reyes, E.; Rotllan, P.; Ruiz, S.; Ruiz, J.; Ruiz, I.; Ruiz-Orejón, L. F.; Salihoglu, B.; Salon, S.; Sammartino, S.; Sánchez Arcilla, A.; Sánchez-Román, A.; Sannino, G.; Santoleri, R.; Sardá, R.; Schroeder, K.; Simoncelli, S.; Sofianos, S.; Sylaios, G.; Tanhua, T.; Teruzzi, A.; Testor, P.; Tezcan, D.; Torner, M.; Trotta, F.; Umgiesser, G.; von Schuckmann, K.; Verri, G.; Vilibic, I.; Yucel, M.; Zavatarelli, M.; Zodiatis, G. Challenges for Sustained Observing and Forecasting Systems in the Mediterranean Sea. Front. Mar. Sci. **2019**, 6, 568. https://doi.org/10.3389/fmars.2019.00568.

Chapter 2

Development and optimisation of a customisable benchtop sensing platform for detection of optical colorimetric chemistries

Abstract

The development, optimisation, and validation of a benchtop sensing platform for the detection of colorimetric chemistries is presented. The platform consists of a microcontroller, in house fabricated detection electronics, an optical cell with 3D printed alignment rail, and interchangeable modular LED-photodiode optics. The adaptable platform can quantify a range of colorimetric methods, the vanadomolybdophosphoric acid method for phosphate detection and the Griess method for nitrite detection are presented.

The colorimetric methods, and the benchtop sensing platform were validated and optimised. The limit of detection (LOD) and limit of quantification (LOQ) of the platform were determined to be 0.21 µM and 0.64 µM for phosphate and 0.02 µM and 0.06 µM for nitrite. The performance of this platform was assessed using a series of known concentration standards and environmental samples. Ten environmental samples were collected across a 14km transect of the river Liffey, Co. Dublin, Ireland where an average relative error of 5.3% for phosphate and 4.1% for nitrite were measured against a UV-Vis spectrometer.

Keywords: Colorimetric Chemistries; Nutrient Detection; LED; Optical Sensor; Microfluidics

2.1. Introduction

Excess levels of nutrients such as phosphates and nitrites within aquatic environments lead to algal blooms which can become toxic and damaging to aquatic ecosystems [1,2]. These blooms contribute to large volumes of organic matter which can harm aquatic ecosystems when they form anoxic and hypoxic dead zones [3]. Events related to excessive nutrient loading can also be damaging to tourism, water based recreational activities and water supply [4,5]. Nutrient loading can be caused by both anthropogenic and naturogenic activities, but events are typically related to the former from wastewater treatment discharges [6] or, agricultural run-off [7] as examples. Nutrient pollution is considered one of the most widespread and problematic challenges [8], as such it is important to regularly monitor so informed remediation strategies can be planned.

Monitoring of nutrients in natural waters remains primarily based on in frequent in-situ grab sampling followed by laboratory analysis using gold standard instrumentation and methods [9,10]. This methodology is inefficient in both time and cost [11], the possibility of on site or autonomous analysis may offer a potential solution. Combination of microfluidics with colorimetric methods and low-cost detectors can be developed which can offer this solution.

LED and photodiode-based detectors for colorimetric detection are becoming increasingly popular. LEDs are cost effective reliable light sources with long operational lifetimes [12,13]. Photodiodes are capable of being low power accurate light detectors [14–16]. Careful selection, validation and optimisation of these components is necessary to turn these low-cost components into sensitive precise optical sensors.

A benchtop sensing platform for the detection of colorimetric chemistries is presented, incorporating a prototyping microcontroller, an optical detection circuit and an optical cell consisting of an optical fluidic chip (discussed in detail in **chapters 4 and 5**), a black polylactic acid (PLA) 3D printed light box to block out external light interference and an LED - photodiode based optical detector. A 3D printed rail is used to align an optical fluidic chip between the LED and photodiode where analysis can take place.

The detection of phosphate was demonstrated, based on the colorimetric reaction with an acidified vanadomolybdophosphoric acid that produces a yellow coloured solution detectable in the UV range below 400 nm [17]. This method was chosen as it is widely used due to its long-term stability of the reagent and its ability to be adapted to microfluidic detection[18].

The detection of nitrite was also demonstrated using the Griess assay. The reaction is based on the diazotization reaction of nitrite with sulphanilamide and N-1-naphthylethylenediamine dichloride (NEDD) under acidic conditions, which results in the formation of an intense pink azo dye that can be detected spectroscopically around 540 nm [19,20].

2.2. Materials and Methods

2.2.1. Reagent and Standard Preparation

All reagents and standards were prepared using ultra high purity (UHP) water (MilliQ, Millipore, Burlington, MA, USA) and analytical grade chemicals (Sigma Aldrich, St. Louis, MO, USA).

2.2.1.1. Yellow reagent

0.351 g of ammonium metavanadate was dissolved in ~200 mL UHP water with an addition of 95 mL concentrated hydrochloric acid (37%). Following this, 7.14 g of ammonium molybdate tetrahydrate was added and the resulting solution was made up to 1000 mL using UHP water.

2.2.1.2. Griess reagent

0.5 g of Sulphanilamide was added to ~100 mL UHP water, with the addition of 5 mL of concentrated hydrochloric acid (37%). Following the dissolution of the Sulphanilamide, 0.05 g of N-(1-Naphthyl) ethylenediamine dihydrochloride (NEDD) was added and the resulting solution was made up to 500 mL using UHP water

2.2.1.3. Stock solutions

Phosphate stock solutions were prepared by dissolving known weights of potassium dihydrogen phosphate in UHP water. Nitrite stock solutions were prepared by dissolving known weights of sodium nitrite in UHP water. Serial dilutions of these stocks were carried out to make a range of known concentration solutions.

2.2.1.4. Artificial seawater

Artificial seawater matrix was prepared by dissolving 40 g of Sigma Aldrich Sea salts in 1000 mL of UHP water to give an artificial salt mixture closely resembling the composition of dissolved ocean salts.

2.2.1.5. Sample reagent ratios

For colorimetric phosphate detection equal volumes, 1:1 v/v ratio of standards/samples and yellow reagent were mixed and allowed to react at room temperature (22 °C) for 20 minutes.

For colorimetric nitrite detection, a ratio of 9:1 v/v ratio of standards/samples and Griess reagent were mixed and allowed to react at room temperature (22 °C) for 20 minutes.

2.2.2. Instrumentation

Validation of the colorimetric chemical methods for phosphate and nitrite detection were carried out using a Shimadzu UV-2600 photo spectrometer with a TCC-100 temperature-controlled cell. Benchtop sensing platform validation was carried out through reference sample measurement in tandem between the sensing platform and the UV-Vis spectrometer at matching wavelengths, 375 nm for phosphate and 545 nm for nitrite.

2.2.3. Benchtop sensing platform design

The benchtop sensing platform shown in figure 2.1. consists of on an Arduino Microcontroller, an in house fabricated read board, and an optical detection cell consisting of an LED and photodiode mounted either side of a fluidic chip.

The LED's (Roithner lasertechnik XSL-375-TF-R2 for phosphate, and Roithner LaserTechnik LED 545-33 for nitrite) and photodiode (TSL257 LF ams) chosen for testing were selected based on their advertised output and the λ_{max} of the two chosen colorimetric methods. Alternative LEDs could be integrated if another chemical method was chosen. The intensity of the LED can be controlled using a pulse width modulation (PWM) driver, the ability to change the light intensity allows for customisation of the cells pathlength and optimisation of the detection sensitivities.

The use of a Microcontroller (Arduino Mega 2560) allows for customisation of platforms operating conditions [21], when paired with a code (supplementary information figure SI.2.1.) it is used to control the experimental setup. Control of the LED intensity either measuring at a set light intensity or as a gradient, number of measurements taken, and the sampling frequency (delay) are all set within the code. The microcontroller can run independent of a computer logging measurement to an SD card, or a computer can be connected for real-time analysis of the data. The full platform can be run at 9 or 7 volts either from a domestic wall supply, battery or powered directly from a computers universal serial bus (USB) supply.

The optical cell consists of an LED and photodiode-based detector that is aligned on a 3D printed rail, this rail can be designed to suit a range of different style fluidic chips that can be positioned between the LED and photodiode. For all experimental work caried out in this chapter a two-layer tinted PMMA Fluidic chip with optically clear PMMA windows was used between the LED and Photodiode as shown in figure 2.1 D. The fluidic chip is further introduced in **chapter 4** with its fabrication, validation and optimisation discussed in detail in **chapter 5**.

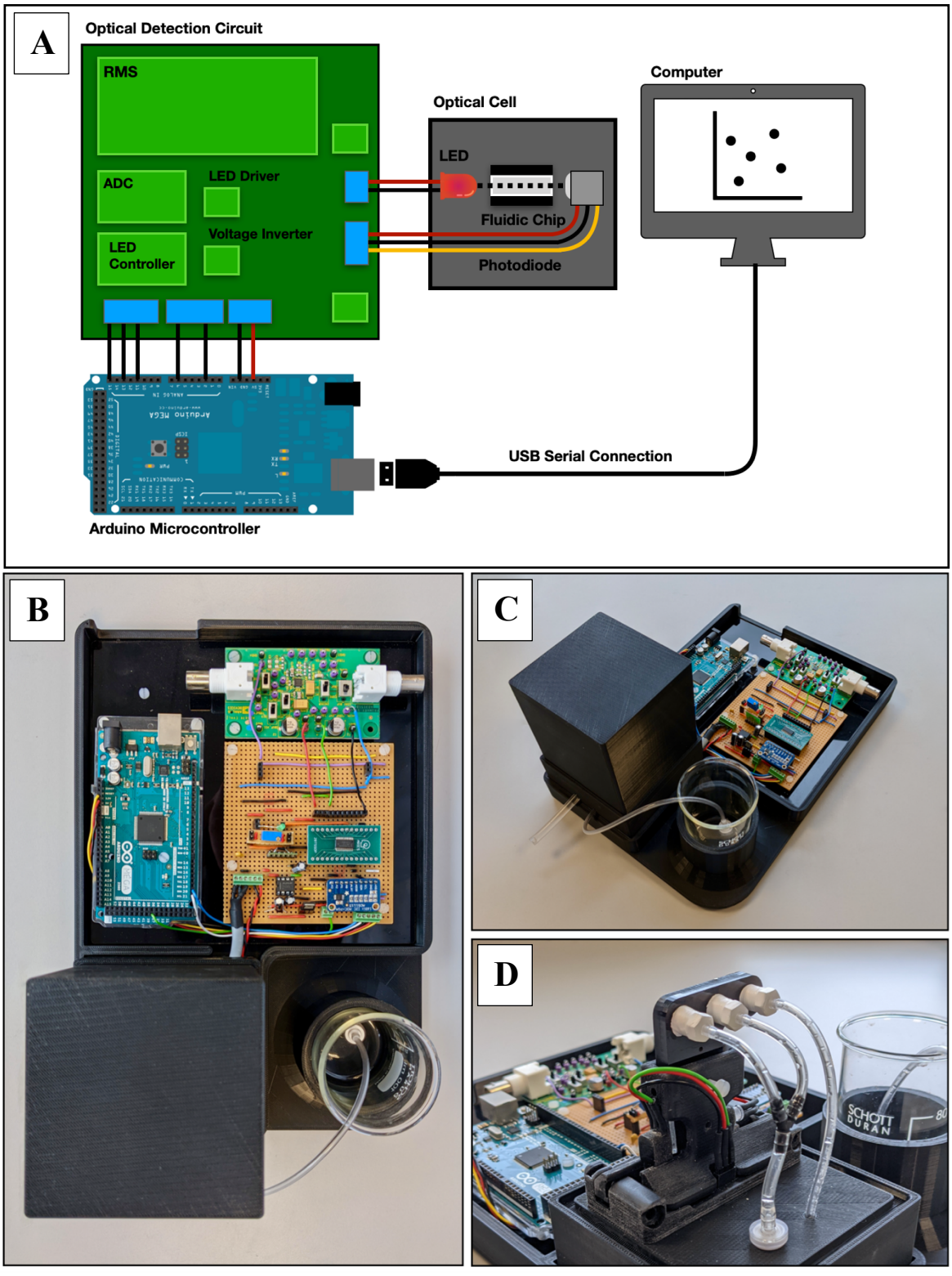

Figure 2.1. *(A) Schematic showing experimental setup of benchtop sensing platform. (B, C) images of the manufactured benchtop sensing platform and (D) optical cell consisting of a PMMA fluidic chip aligned between the LED - photodiode detector.*

2.2.3.1. Measurement control of the benchtop sensing platform

The Microcontroller sets the operation of the benchtop sensing platforms optical detection circuit. This microcontroller runs a code that has been written in house for purpose. The code has been written using open-source Arduino integrated development environment (IDE). Supplementary information figure SI.2.1. shows the initial setup function of the code that calls the libraries for components on the optical detection board, an initialisation stage, and a variables section where a user can setup their experiment by programming a set light intensity or a gradient, the number of measurements to be taken and the delay between these measurements.

Once setup the code activates the LED, and the photodiode measures the response and outputs a digital signal (bits) which is then converted to absorbance (abs). The photodiode measures the amount of light that hits it and converts it to a response, this signal will be at its highest with a blank solution in front of it. The signal is reduced when a colour is developed during a colorimetric reaction that absorbs light hitting the detector, this reduction in light intensity is then quantified. Absorbance is calculated by $Log_{10}(^{Blank}/_{Sample})$ [22] where blank is the analogue to digital convertor (ADC) reading in bits of Blank (Ultrapure Water : Reagent, either 1:1 or 9:1 v/v ratio depending on the chosen method) and Sample is the test solution (standard or sample : Reagent, 1:1 or 9:1 v/v ratio depending on the chosen method) measured under the same experimental conditions.

2.2.3.2. Optical Cell Setup

For testing, the optical cell was setup in two orientations as shown in figure 2.2.

Method 1: Benchtop sensing platform used for LED control and photodiode detection (sample measurement).

This method consists of the full function benchtop sensing platform. The microcontroller and optical detection circuit control an LED of fixed wavelength which is then detected by the onboard photodiode detector. Using this method sample measurement can be carried out using the integrated fluidic chip where test solutions can be loaded directly onto the fluidic chip (212 µL volume chip) and measured, where

an ADC signal (bits) can be converted to a static absorbance value. This method of testing is used to generate calibration curves and to obtain concentration values from unknown samples measured.

Method 2: Benchtop sensing platform used for LED control with integrated external detector (LED characterisation).

This method consists of the microcontroller and optical detection circuit controlling only the LED of fixed wavelength. The photodiode is replaced with a commercial Ocean Optics fibre optic detector which is capable of measuring wavelength and intensity. This method contains no cell (fluidic chip) and is used for characterisation of LED outputs that are controlled by the benchtop sensing platform. The ocean optics detector is used to assess the output of commercial LEDs, to evaluate their intensity, stability and the λ_{max} of the selected LED.

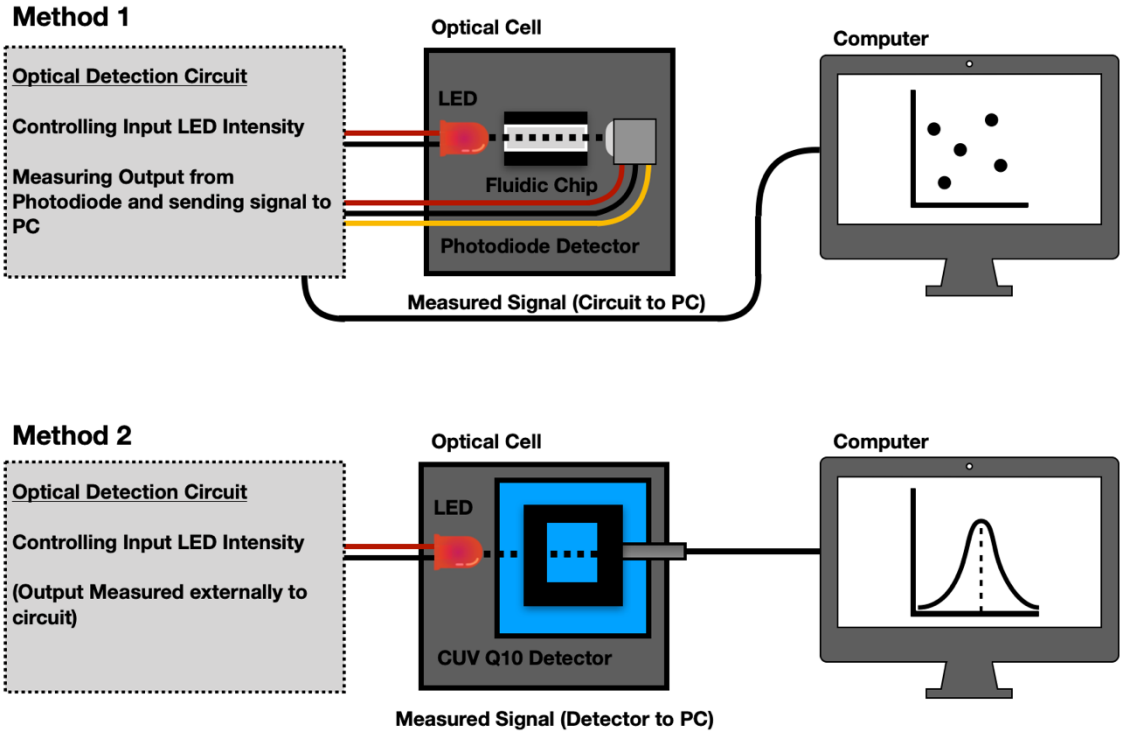

Figure 2.2. *Schematic showing experimental setup of benchtop sensing platform. Method 1 Complete benchtop sensing platform with controlled output from LED measured and converted to a signal by on board photodiode and Method 2 Output from LED controlled by benchtop sensing platform and its output measured externally using an ocean optics fibre optic detector.*

2.3. Results and Discussion

2.3.1. Characterisation of the colorimetric methods.

Prior to optimisation and validation of the benchtop sensing platform both the yellow vanadomolybdophosphoric acid method and Griess method were assessed for their performance using a Shimadzu UV-2600 UV-Vis spectrometer with TCC-100 temperature-controlled cell.

2.3.1.1. Wavelength selection – Spectrum Scan

The optimum wavelength was investigated by obtaining the absorbance spectrum for the yellow method and Griess method. Figure 2.3. shows the measured spectrums (A) 0-65 μM phosphate (PO_4^{3-}) reaction and (B) 0-10 μM nitrite (NO_2^-) reaction, measured on a Shimadzu UV-2600 Photo spectrometer. A linear trend was measured with increasing absorbance as concentration was increased. The λ_{max} of the reaction was measured at 348 nm for the yellow method and 542 nm for the Griess method, these values are consistent with literature values, which typically range from >400 nm for the yellow method [23,24], and 540-548 nm [25–27] for the Griess method.

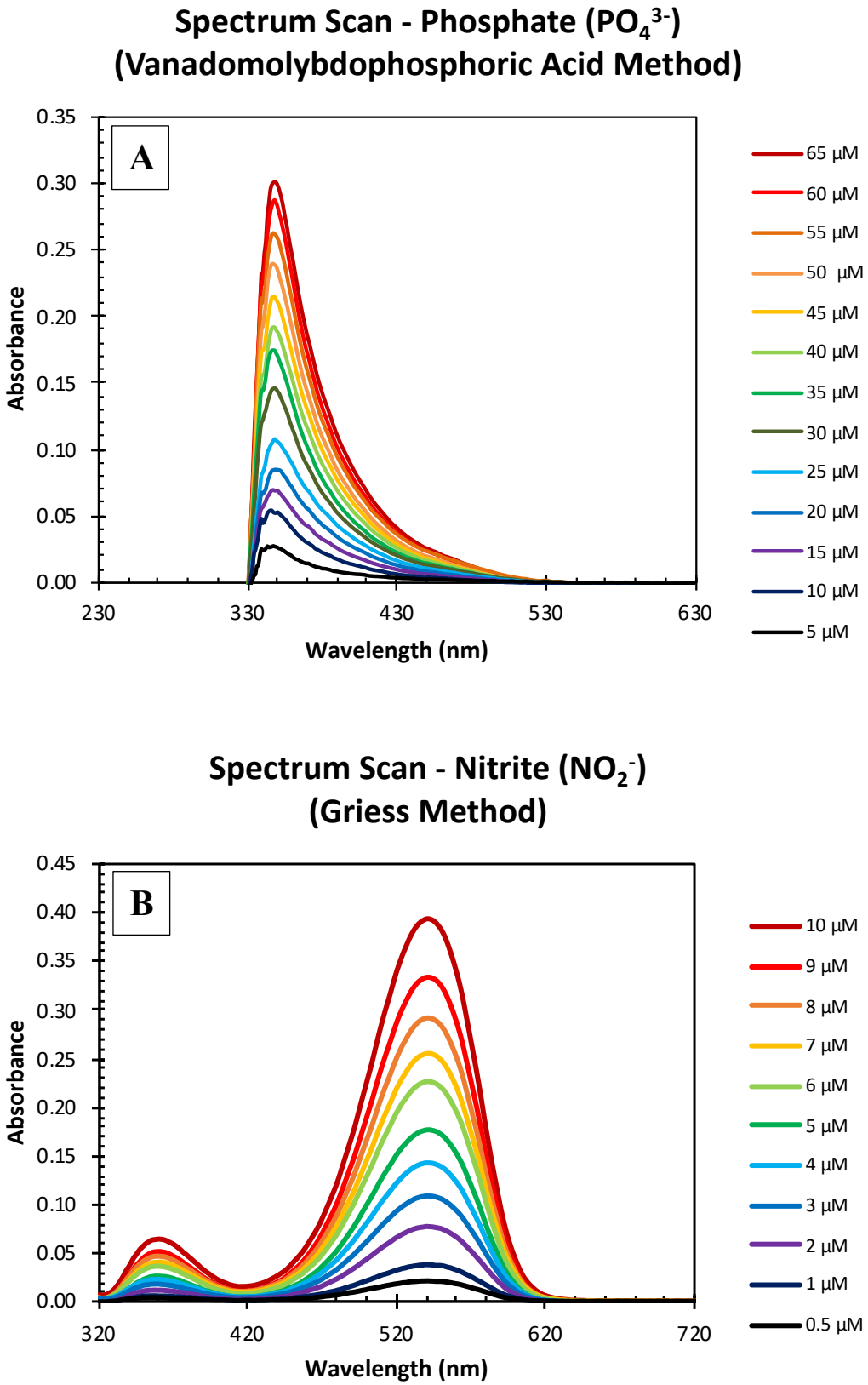

Figure 2.3. *Spectrum scan of (A) vanadomolybdophosphoric acid method of phosphate detection and (B) spectrum scan of Griess assay for nitrite detection on UV-Vis spectrometer.*

The wavelength selected for each method was selected to not only suit the λ_{max} of each colorimetric method for maximal sensitivity but also based on the material choices made for the PMMA fluidic chip. PMMA was chosen due to it having the highest transparency of all commonly used polymers [28] and being a cost effective simple material for fabrication. Figure 2.4. shows a spectrum scan of the PMMA (1.5 mm extruded precision grade - black line) used in the optical windows of the fluidic chip as well as alternative grades and thicknesses of PMMA. The PMMA begins to absorb in the UV region of the spectrum at 380 nm with two characteristic peaks at 292 and 395 nm which matched with literature values [29,30]. Each thickness will have different material composition with the 1, 2 and 3mm grades showing similar absorption patterns with an increase in absorbance as material thickness increased. The 1.5mm precision grade used within the optical chip has improved optical properties (reduced absorbance) with a significantly reduced peak at 295 nm and is optically clear in the visible region of the spectrum (see supplementary figure SI.2.2.).

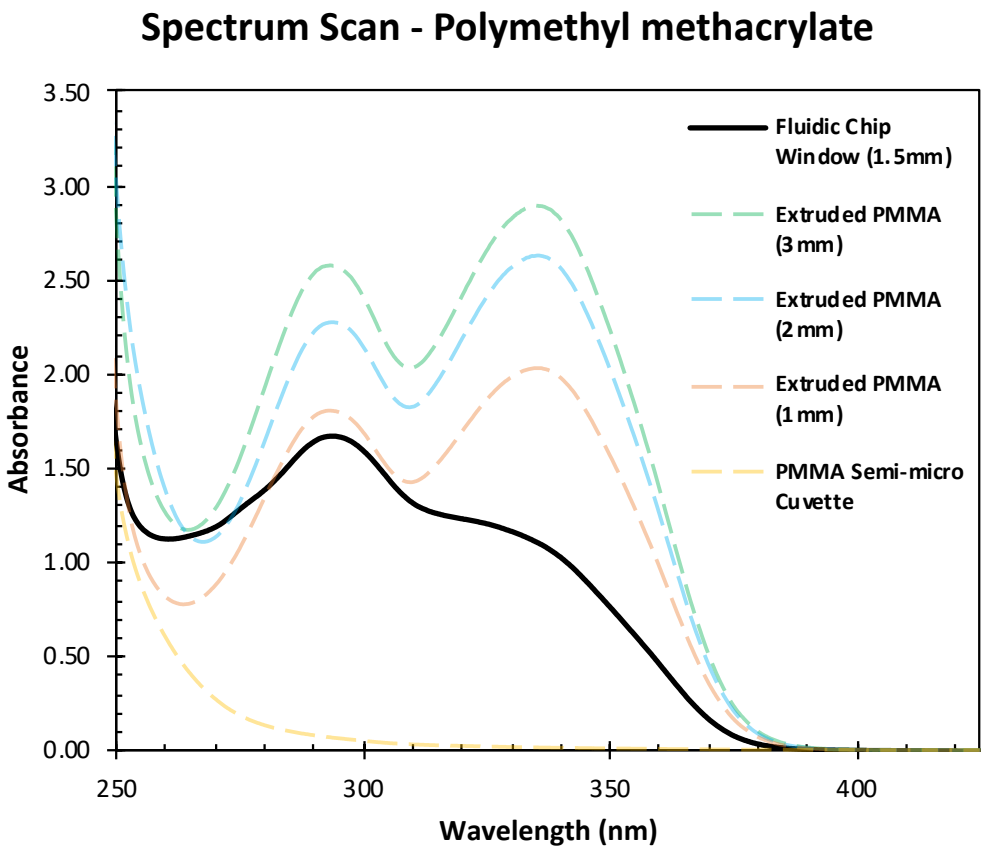

Figure 2.4. *Spectrum scan of the fluidic chip optical window (black line) and alternative variations of "clear" Polymethyl methacrylate.*

As a result of the absorbance spectrum of the PMMA, the wavelengths selected for the benchtop sensing platform were 375 nm for the yellow method (phosphate) and 545 nm for the Griess method (nitrite). All comparisons made between the benchtop sensing platform and the UV-Vis spectrometer were carried out at these wavelengths. The spectrum produced for the yellow method is broad enough to still be measured outside of its λ_{max}, however there will be a reduction in the sensitivity.

2.3.1.2. Reaction rates – Kinetics

The rate of development of the coloured complex for the yellow method and Griess method was assessed kinetically. The measurement was recorded on a Shimadzu UV-2600 with TCC-100 temperature-controlled cell. The absorbance was measured at 375 and 545 nm respectively until the development of the coloured complex had reached steady state. Figures 2.5.(A) and 2.6.(A) show the effect that temperature plays on reaction rates where a 100 µM phosphate standard and a 10 µM nitrite standard were measured between 5 to 20 °C. Figure 2.5.(B) and 2.6.(B) show varying the concentration of the standards for phosphate and nitrite at static temperature of 20 °C.

Using the yellow method for phosphate detection, the reaction was shown to occur rapidly reaching steady state after a maximum of 400 seconds at the lowest temperature measured of 5 °C with excellent stability of the coloured portion once reaching its maximum rate. Room temperature reaction results trend well with previously reported values of approximately 180 seconds (3 minutes) at room temperature by Bowden et al . [31] versus the measured value of 145 seconds at 20 °C.

Using the Griess method for nitrite detection, the reaction results in a rapid colour development for approximately the initial 600 seconds, after which the reaction rate is slowed before reaching its maximum, this result trends well with what was previously reported by O'Toole et al. [25]. The reaction was shown to occur slower in comparison to the yellow method with the reaction reaching steady state after a maximum of 2850 seconds at 5 °C. The results also showed lower maximum absorbance as temperature decreases with a 5.7% reduction seen at 5 °C in comparison to 20 °C.

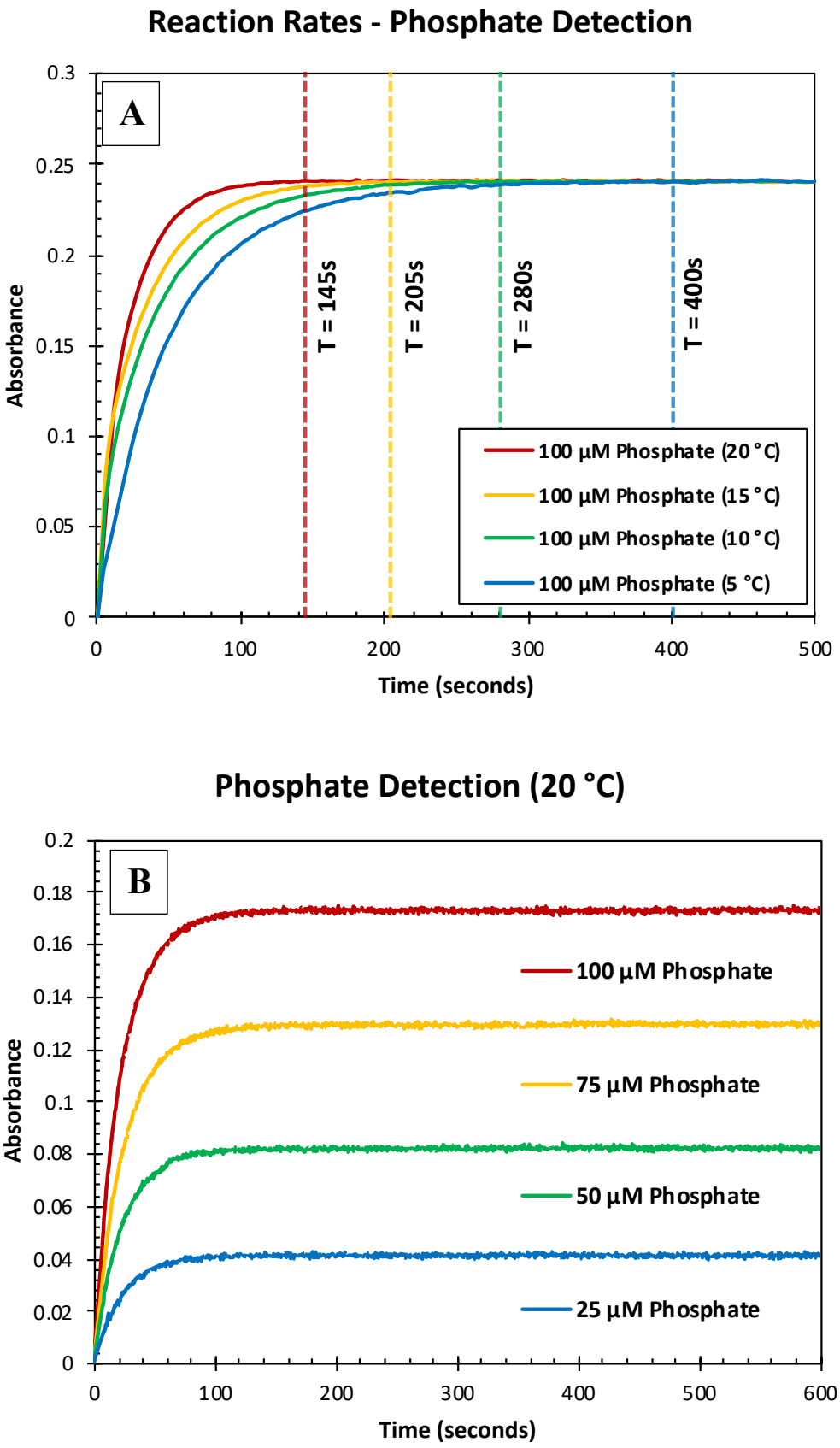

Figure 2.5. *Kinetic study of yellow reagent complex (A) varying reaction temperature and (B) varying standard concentration.*

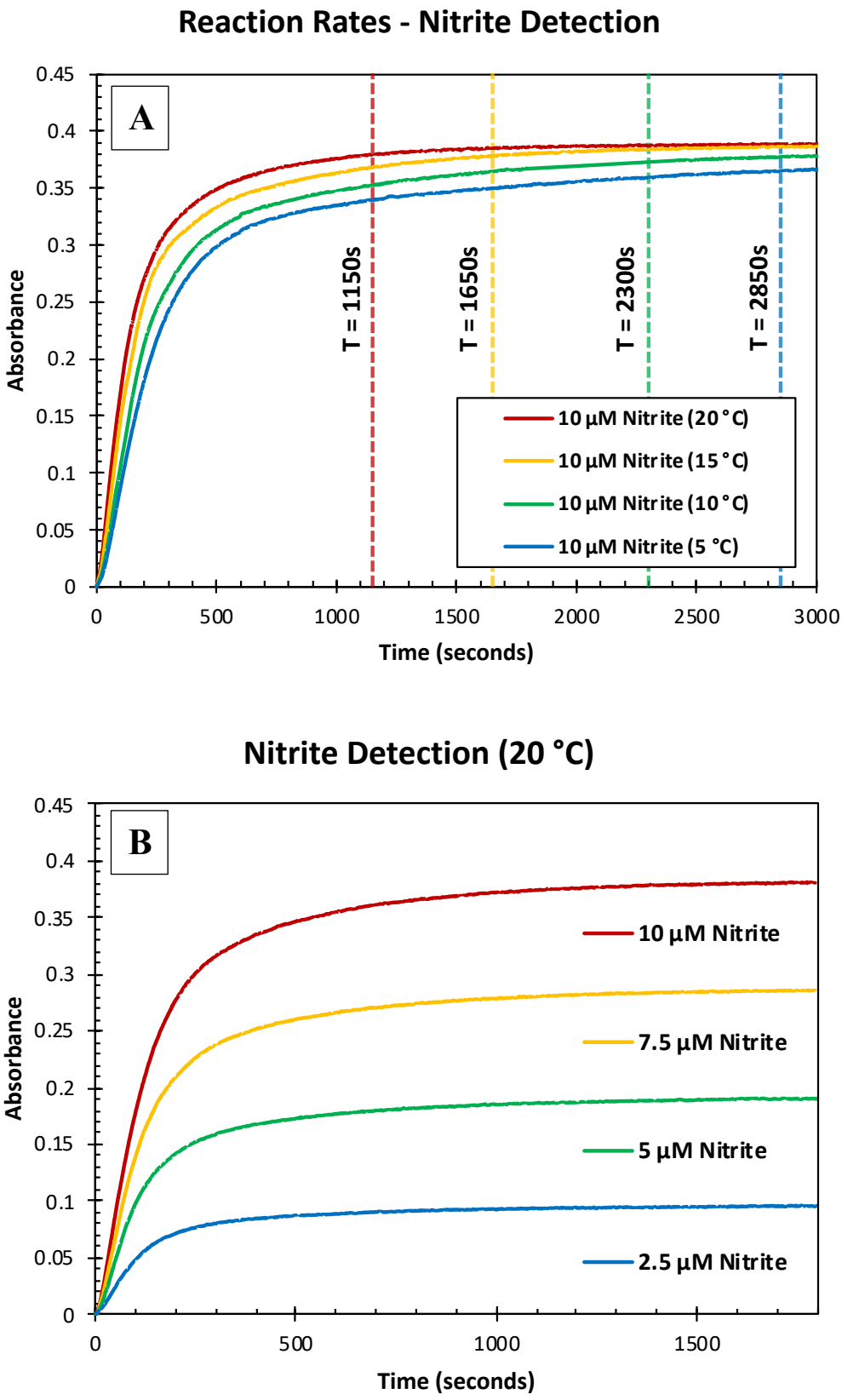

Figure 2.6. *Kinetic study of Griess reagent complex (A) varying reaction temperature and (B) varying standard concentration.*

Figures 2.5.(B) and 2.6.(B) show that a linear response between concentration and absorbance max is seen with reaction times being unaffected by concentration. Both methods show a significant temperature effect where reduction in temperature slowed the rate of reaction. This decrease in reaction rates is important to acknowledge where it could have a significant effect on results outside of temperature-controlled laboratories where fluctuating environmental temperatures become a factor in longer term analysis.

2.3.1.3. Working Range – Linear Calibration

A calibration plot was performed on UV-Vis for the detection of phosphate using the yellow method and nitrite using the Griess method with a set of known concentration standards (see supplementary figure SI.2.3.). A dynamic linear range of 0-1100 µM was measured for phosphate and 0-40 µM for nitrite. 1100 µM and 40 µM were shown to be the upper limit as at concentrations above this point the detectable difference in colour and absorbance values decreased.

The molar extinction coefficient was estimated to be 2.37 x 10^3 mol L^{-1} cm^{-1} at 375 nm for phosphate and 3.66 x 10^4 mol L^{-1} cm^{-1} at 545 nm for nitrite. An excellent correlation coefficient of 0.999 (N=3, 10 data points per replicate measured) for phosphate and nitrite was achieved with an average % relative standard deviation (RSD) of 1.03 for phosphate and 0.64 for nitrite.

The limit of detection and limit of quantification was determined by multiplying the standard deviation of the baseline of the blank. The LOD was calculated as the concentration equivalent of 3.3 x standard deviation of the blank solution (N=15, 10 data points per blank solution measured), measuring 0.44 µM for phosphate and 0.02 µM for nitrite. The LOQ was calculated at 10 x standard deviation of the blank solution (N=15, 10 data points per blank solution measured) measuring 1.33 µM for phosphate and 0.06 µM for nitrite.

2.3.1.4. Interference study – Salinity Effects

For environmental samples salinity ranges can differ significantly depending on site selection. It is therefore important to study the potential effect of salinity for both the yellow and Griess method, so that successful results can be achieved in varying sample conditions without the need for correction.

Three different marine matrices were initially selected for testing, consisting of an artificial sea salt (Red Sea Sea Salts), unrefined sea salts (Sigma Aldrich Sea Salts) and a natural sea water sample identified as having low baseline level nutrients (Seawater – Mulranny, Co Mayo). The baseline phosphate and nitrite levels were measured for these three samples and the result are summarised in table 2.1.

Table 2.1. *Phosphate and nitrite levels of three proposed test solutions for salinity interferences.*

Sample	**Phosphate:**		**Nitrite:**	
	µM	**$S_{\mu M}$**	**µM**	**$S_{\mu M}$**
Sigma Aldrich - Sea Salts	0.89	0.02	0.02	0.01
Red Sea – Sea Salt	0.67	0.05	0.07	0.01
"Natural Seawater" - Low Nutrient Source, Co. Mayo	1.37	0.06	0.13	0.01

Sigma Sea salts were selected for carrying out the salinity effect study. Although it contained higher levels of phosphate in comparison to the Red Sea salts it has the lowest levels of nitrite present. The phosphate method has a significantly higher upper limit, so it was less likely to be affected by an elevated baseline caused by preparing standards in this artificial matrix versus ultrapure water.

The effect of salinity was tested using known concentration standards made up in ultra-pure water and Sigma Aldrich Sea Salts. A concentration of 0, 20 and 40 g/L was tested to give a salinity range similar to that seen from freshwater to estuarine to marine matrices [32]. Figure 2.7. shows a calibration curve of (A) phosphate 0-50 µM and (B) nitrite 0-10 µM made up in 0, 20 and 40 g/L sea water matrix. The increased baseline from using Sigma Sea Salts versus ultrapure water was accounted for by using method blanks for each calibration.

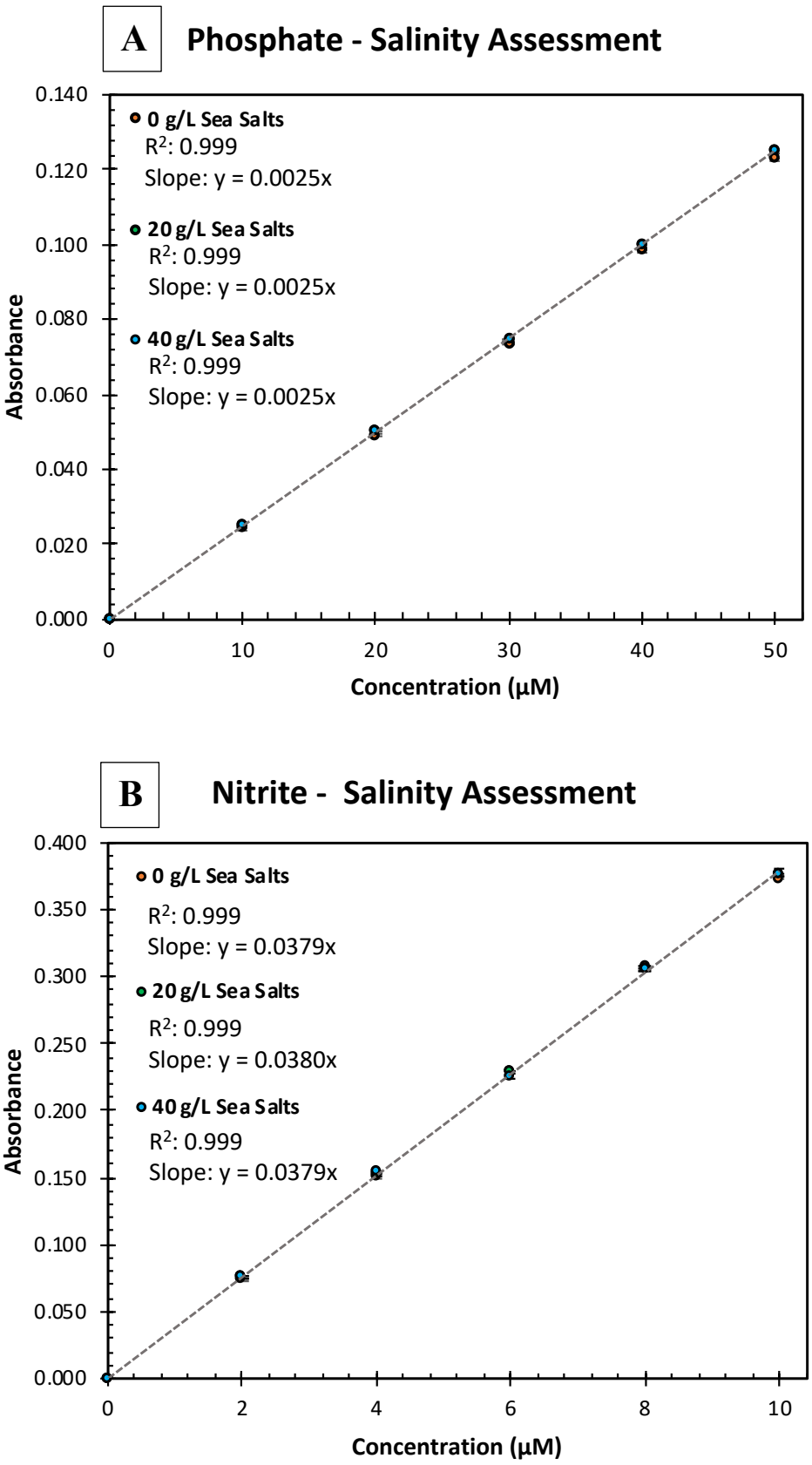

Figure 2.7. *Calibration curve of (A) phosphate standards and (B) nitrite standards tested at 0, 20 and 40 g/L Artificial Seawater matrix. The error bars represent the standard deviations for n=3.*

The Sigma Sea salts used contain ions including chloride, sodium, sulphate, potassium, calcium, carbonate, boron, magnesium, strontium, and other trace elements of less than 0.5 mg/L. The results in figure 2.7. show no interference is caused by the presence of these ions at marine levels for both the yellow method and the Griess method. As there was no significant decrease in colour intensity produced or reduction in slope both methods could be applied to not only freshwater but also estuarine and marine samples without the need for further sample pre-treatment, calibration, or complexing.

2.3.2. Detection using the Benchtop sensing platform

Following validation and optimisation of the colorimetric methods for detection of phosphate and nitrite their performance was assessed on the benchtop sensing platform and optimised.

2.3.2.1. PWM Control – LED Characterisation

The LED intensity is controlled using a Pulse Width Modulation (PWM) driver. This driver allows the LED to be controlled at PWM range from 0 (0% intensity) – 4096 (100% intensity).

Figure 2.8. shows the response of a PWM controlled LED (375 nm) between PWM 1000 – 3000 duty cycle using method 1 (see figure 2.2.) where LED control and detection is measured on the benchtop sensing platform. A stable linear step can be seen between each step cycle of 200. This shows control of the LED using the PWM driver in combination with the microcontroller and that that LEDs can be tuned so that it can be optimised for various optical methods and cell designs.

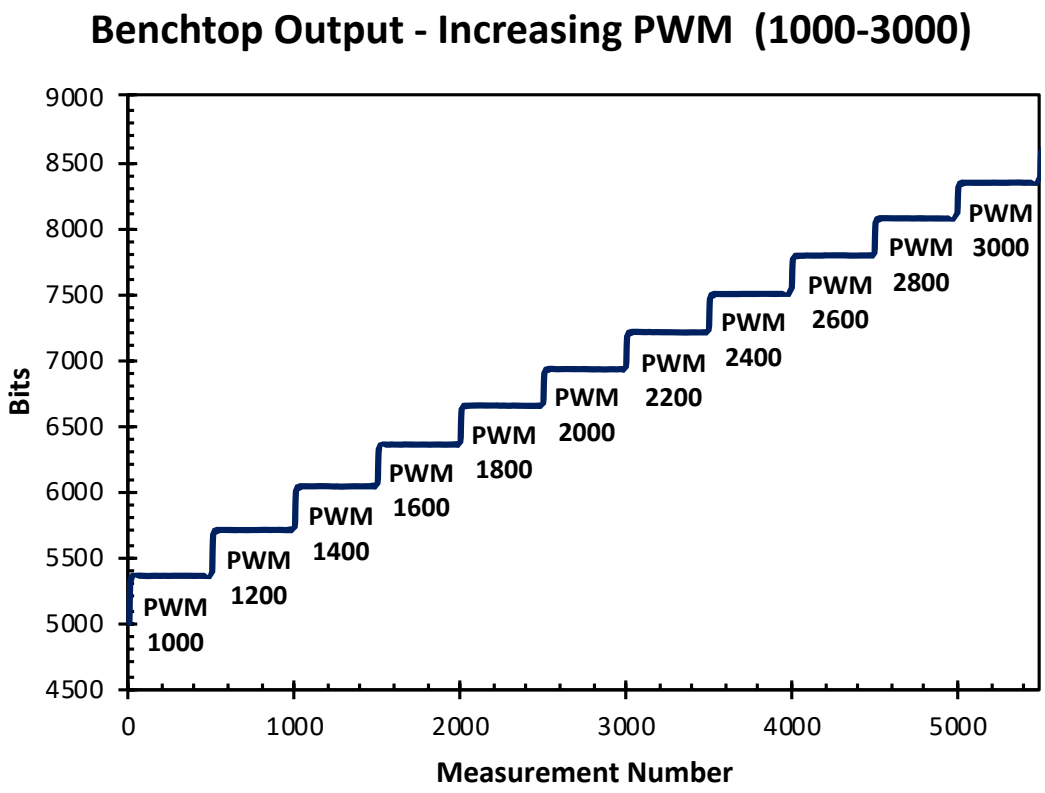

Figure 2.8. *Method 1 Digital output from the photodiode measuring PWM controlled LED intensity at a range of 1000 – 3000 PWM.*

Figure 2.9. shows the output of the LED (A) Roithner laserTechnik XSL-375-TF-R2-UV led and (B) Roithner laserTechnik LED 545-33 using the fibre optic detector described in method 2 (see figure 2.2.) when controlled by a PWM signal. This setup allows for the LEDs wavelength output to be characterised. Roithner laserTechnik XSL-375-TF-R2-UV has shown an output between 360 nm and 400 nm and has a λ_{max} of 375 nm. Roithner LaserTechnik LED 545-33 has shown an output between 500 nm and 659 nm and has a λ_{max} of 545 nm.

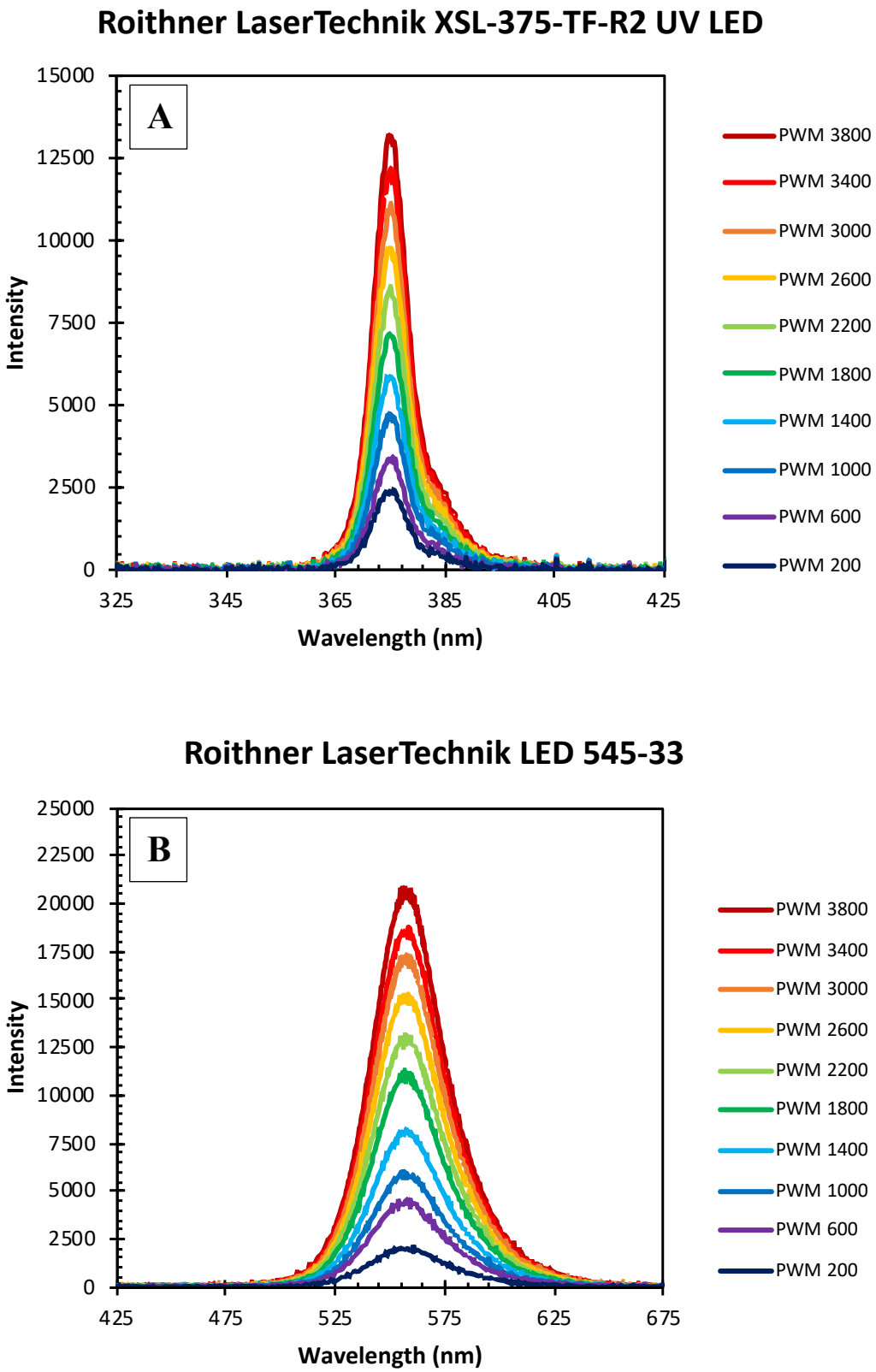

Figure 2.9. *Method 2 Measured LED output under PWM control (200-3800) using fibre optic detector with (A) showing chosen LED for phosphate detection and (B) showing chosen LED for nitrite detection.*

Method 1 (figure 2.8.) and Method 2 (figure 2.9.) show the benchtop sensing platform's ability to characterise output from commercially bought LEDs. The photodiode detector successfully measured the light from the LED as a digital signal.

The results shown in figures 2.9 show the measured output of a single Roithner laserTechnik XSL-375-TF-R2-UV LED and Roithner laserTechnik LED 545-33. Batch to batch variability of the manufactured LEDs and Photodiodes are shown in supplementary information figure SI.2.4A., SI.2.5A. and SI.2.6A. Each LED and Photodiode was measured under the same experimental conditions with a static resistance and PWM value. A variability of 6.96% (n=10) was measured for a batch of Roithner laserTechnik XSL-375-TF-R2-UV LEDs (SI 2.4A.), 17.49% (n=10) was measured for a batch of Roithner laserTechnik LED 545-33 (SI 2.5A.), and 4.20% (n=10) was measured for a batch of TSL257 LF ams Photodiodes (SI 2.6A.).

The variation in intensity emitted or detected by the LEDs and Photodiodes was calibrated for digitally in software by adjusting the PWM signal to reach a target value (10,000 bits), this could also be achieved on a hardware level by adjusting the resistance of the on-board resistor. The corrected results are presented in supplementary information figure SI.2.4B., SI.2.5B. and SI.2.6B. where after correction the variability of each LED or Photodiode was re-measured with the adjusted PWM signal where an intensity difference of 0.02% (n=10) was measured for a batch of Roithner laserTechnik XSL-375-TF-R2-UV LEDs (SI 2.4B.), 0.02% (n=10) was measured for a batch of Roithner laserTechnik LED 545-33 (SI 2.5B.), and 0.03% RSD (n=10) was measured for a batch of TSL257 LF ams Photodiodes (SI 2.6B.).

2.3.2.2. Optimization of measurement signal and LED output.

With the ability to sense the output of the LED using method 1, assessments were carried out on the output from the LED. The benchtop sensing platform was setup to take 400 rapid measurements with 1 millisecond delay between each upon initial start-up of the LED. Figure 2.10. presents the recorded measurement when the benchtop sensing platform was setup as described at a static PWM of 500 measuring a non-reactive blank solution (0 μM phosphate standard:yellow reagent, 1:1 v/v). The results show that the initial output from the LED when it is first turned on is unstable with a

substantial overshoot in intensity. This overshoot takes approximately 250 milliseconds before the intensity of the LED drops to a stable signal. This overshoot is likely due initial warm up of the LED and time necessary for stabilisation of the input voltages.

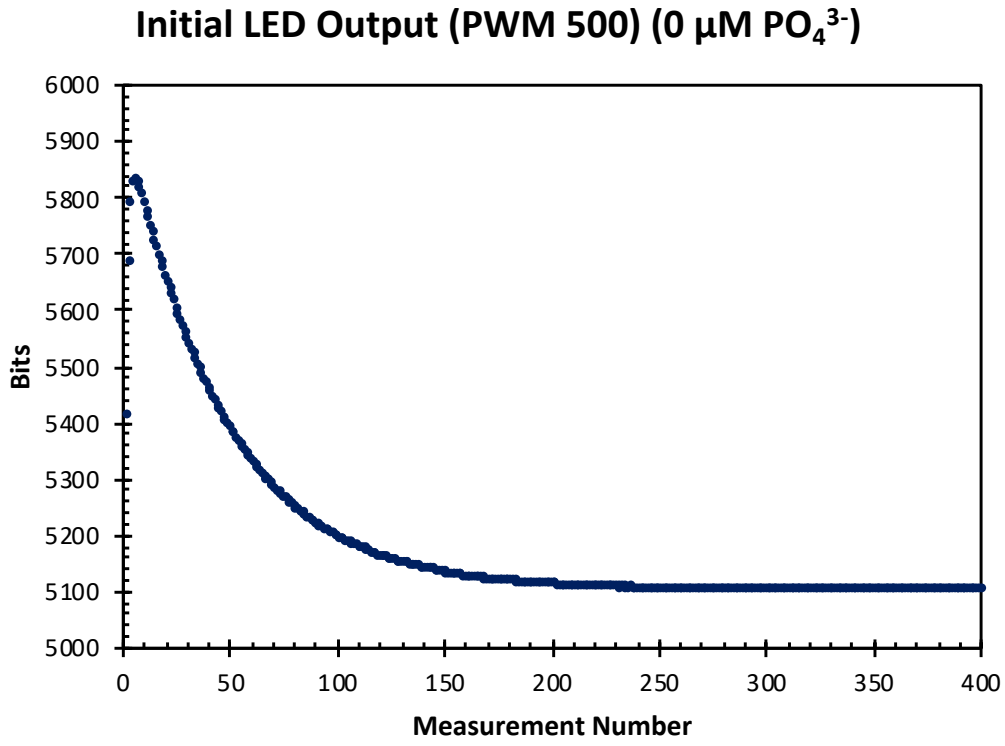

Figure 2.10. *Measured LED output at PWM 500 of a blank solution showing LED overshoot prior to stabilisation of measurement.*

Following assessment of the LEDs output a study was carried out to assess the effect of the overshoot and the improvements that could be made from averaging measurements in the linear portion versus the unstable initial portion.

Figure 2.11. presents the calibration curve generated on the benchtop sensing platform using the yellow method (vanadomolybdophosphoric acid method) for phosphate detection between 0 and 80 µM. The calibration curve was generated (n=3) with each replicate using an average of the initial 100 measurements generated. The data presented shows both (A) raw measurements (bits) and (B) converted absorbance values for each concentration standard tested.

Similarly, to figure 2.11., figure 2.12. presents the calibration curve generated on the benchtop sensing platform using the yellow Method (vanadomolybdophosphoric acid method) for phosphate detection between 0 and 80 μM. The calibration curve was generated (n=3) with each replicate using an average of the final 100 measurements generated. The data presented shows both (A) raw measurements (bits) and (B) converted absorbance values for each concentration standard tested.

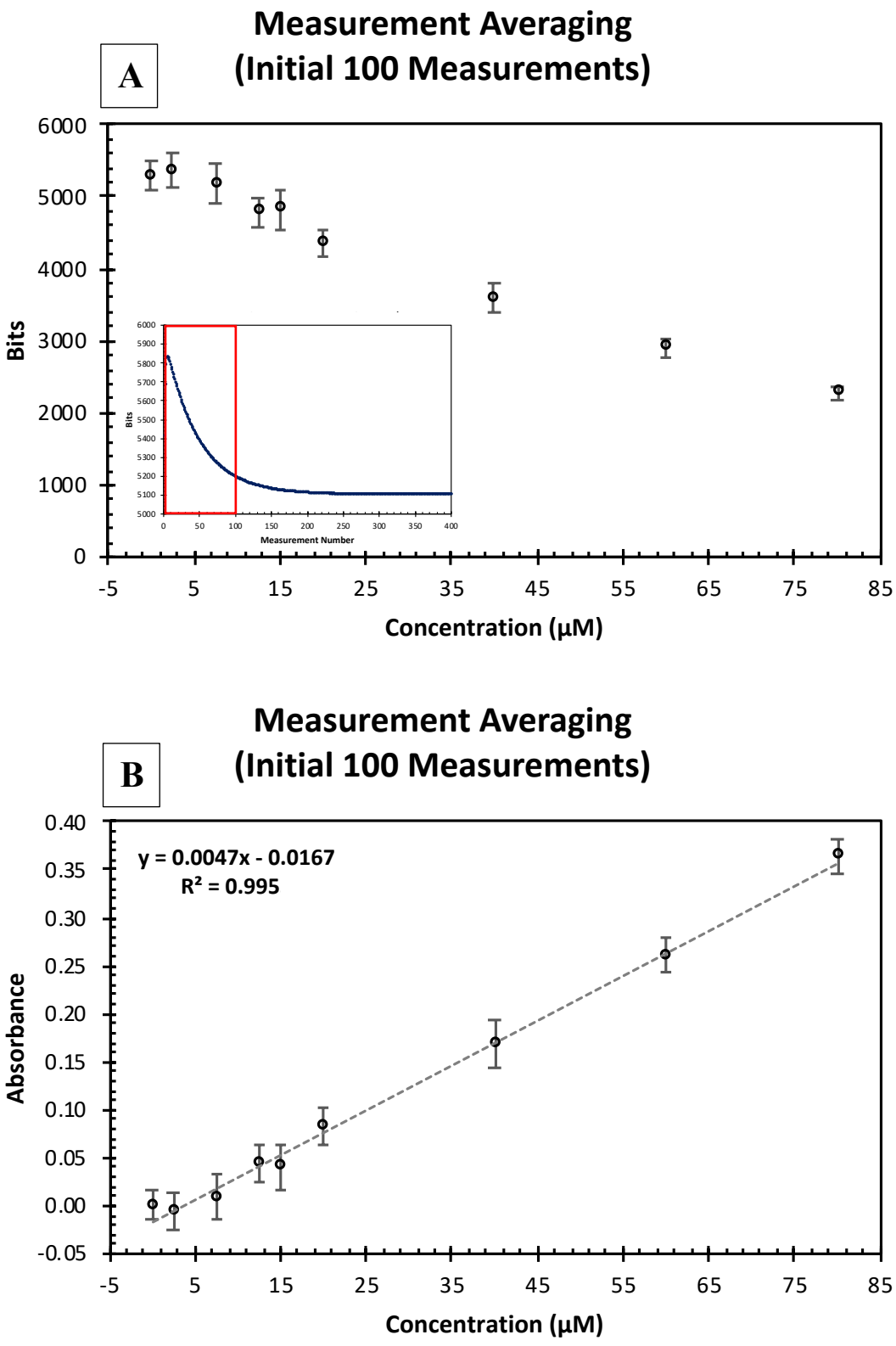

Figure 2.11. *Calibration curve for phosphate (PO_4^{3-}) presenting (A) in bits (raw data) and (B) converted absorbance using benchtop sensing platform averaging the initial 100 measurements from the unstable portion of the LED (375 nm) output.*

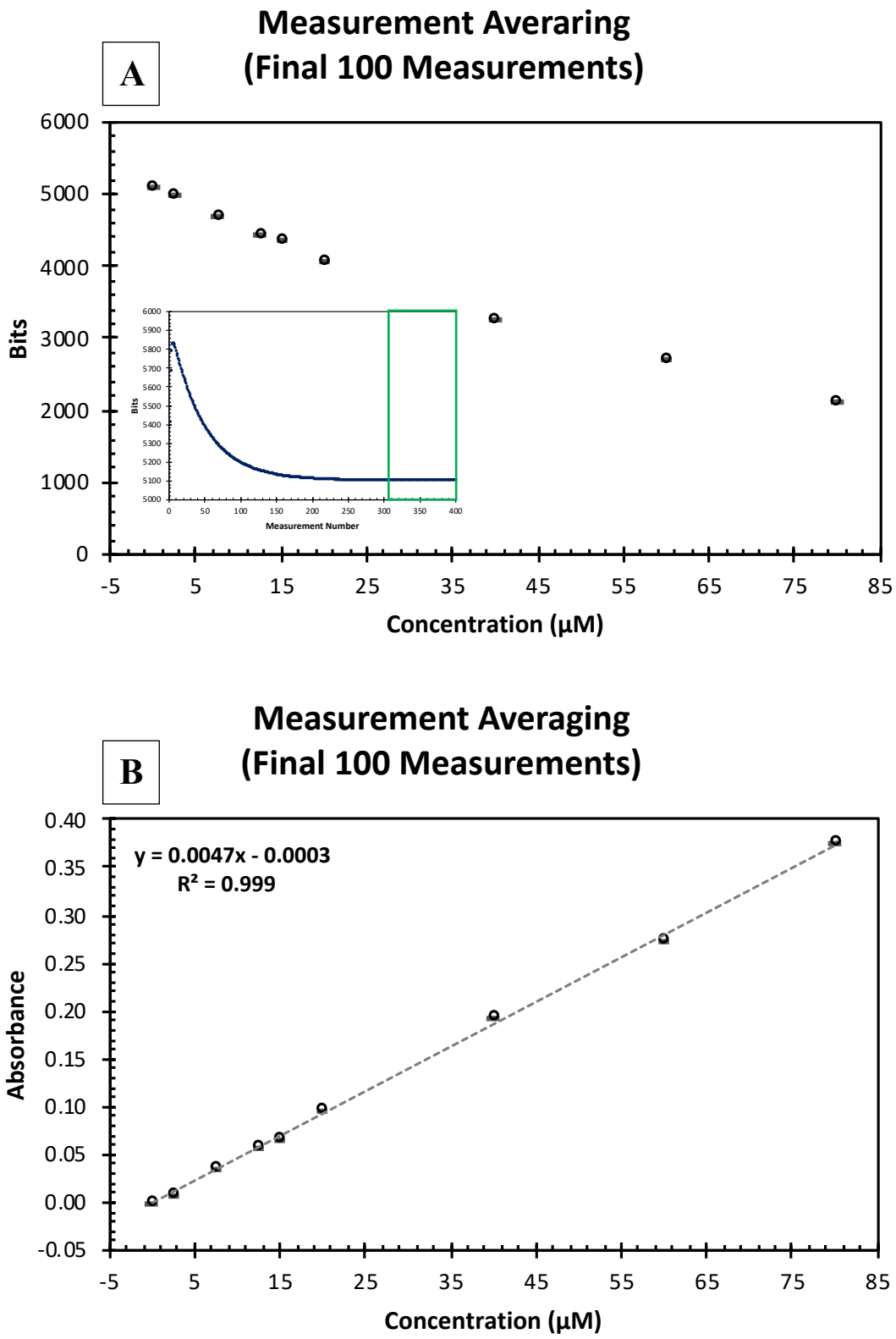

Figure 2.12. *Calibration curve for phosphate (PO_4^{3-}) (A) in bits (raw data) and (B) converted absorbance using benchtop sensing platform averaging the final 100 measurements from the stable portion of the LED (375 nm) output.*

Table 2.2. *Standard deviations shown from averaging the initial unstable 100 measurements (unoptimized) versus averaging the final stable 100 measurements (optimised) of a signal.*

Concentration PO_4^{3-} (µM)	Unoptimized		Optimised	
	S_{bits}	S_{abs}	S_{bits}	S_{abs}
0	192	0.02	1	0.00
2.5	239	0.02	1	0.00
7.5	290	0.02	1	0.00
12.5	211	0.02	1	0.00
15	276	0.02	1	0.00
20	184	0.02	1	0.00
40	209	0.02	1	0.00
60	124	0.02	1	0.00
80	93	0.02	1	0.00

The results from figures 2.11. and 2.12. and summarised in table 2.2. show that correct interpretation of the output signal is critical to achieving accurate detection. When measuring from the linear portion of the output standard deviation is reduced to ~1-bit fluctuations per sample giving stable and reproducible measurements with excellent measurement to measurement stability.

2.3.2.3. Optimization of PWM signal

The PWM drivers power delivery and signal were optimised. The driver is regulated using a resistor, this resistor controls the power delivery of the circuit and is used to set the maximum and minimum power that the controller will supply to the LED.

Figure 2.13. presents the calibration curve generated on the benchtop sensing platform using the yellow method with unoptimized PWM signal using a 47 Ω resistance measuring the stable portion of the LED output. Figure 2.14. presents the calibration curve generated on the benchtop sensing platform using the yellow method with optimized PWM signal using a 100 Ω resistance measuring the stable portion of the LED output.

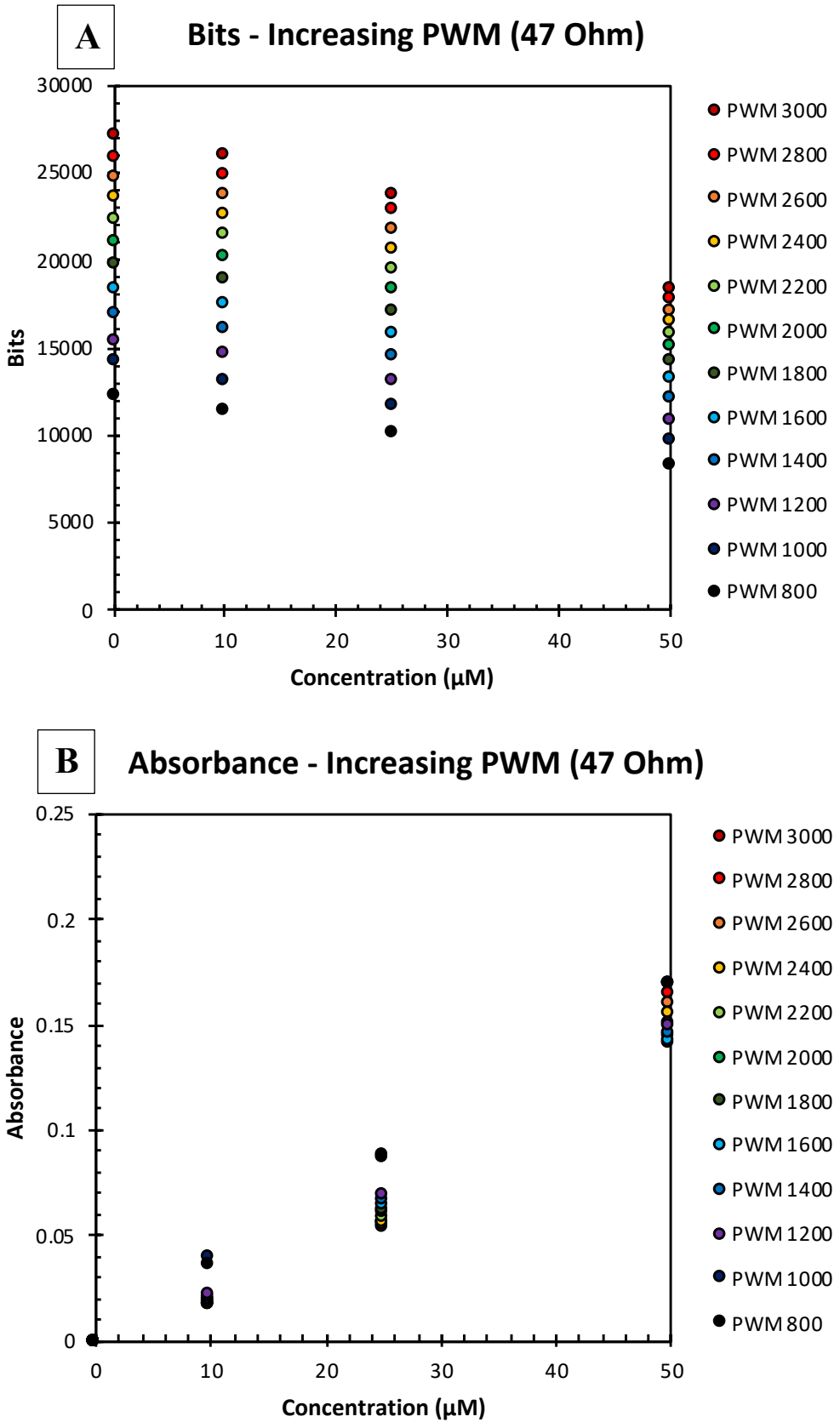

Figure 2.13. *Calibration curve for phosphate (PO_4^{3-}) presenting (A) in bits (raw data) and (B) converted absorbance using benchtop sensing platform at 47 Ω resistance.*

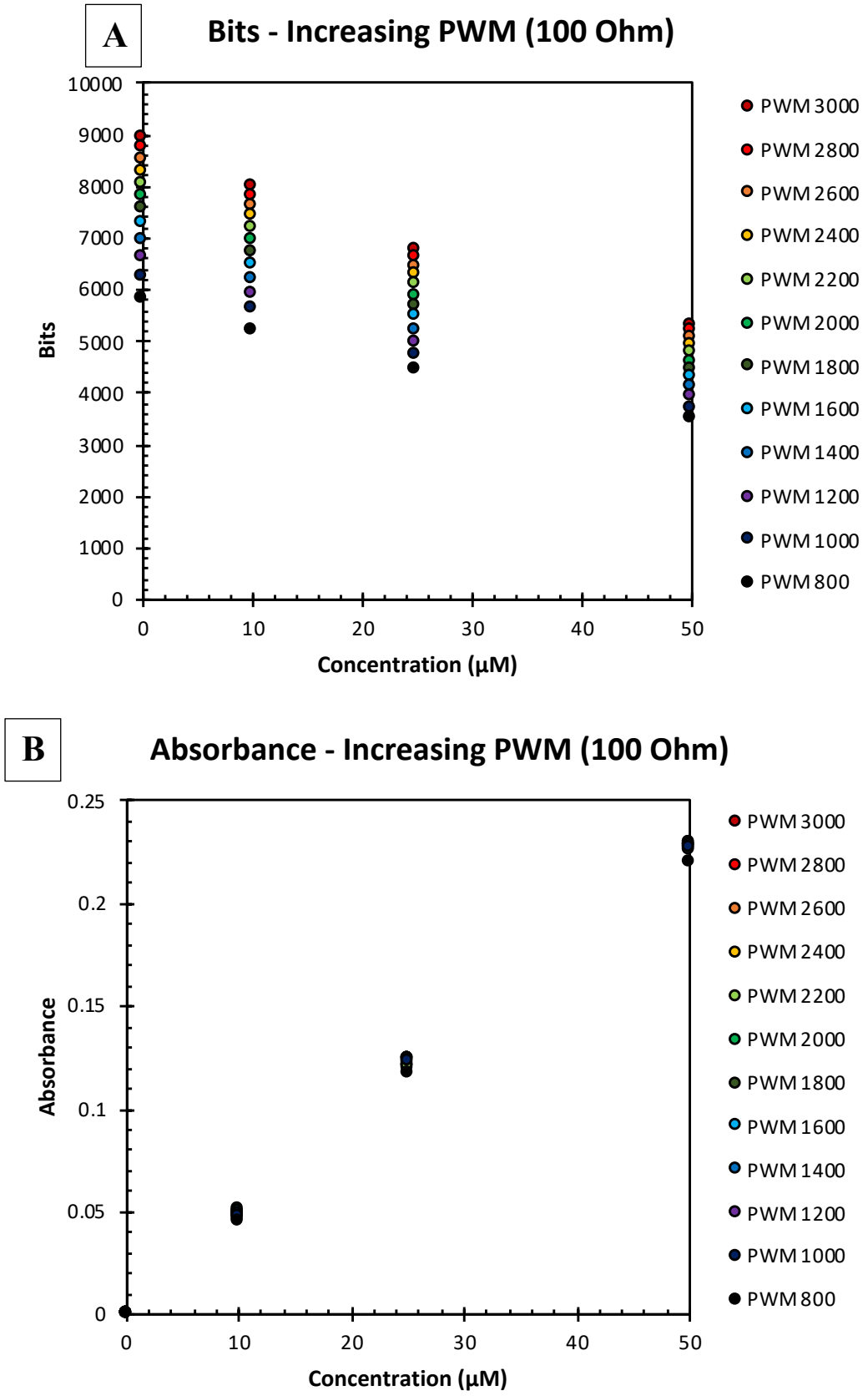

Figure 2.14. *Calibration curve for phosphate (PO_4^{3-}) presenting (A) in bits (raw data) and (B) converted absorbance using benchtop sensing platform at 100 Ω resistance.*

The results show that the optimised PWM (figure 2.14.) controller give a lower overall intensity (bits) with a distribution of 5000-9000 bits in comparison to the unoptimized (figure 2.13.) 10,000–34,0000, however this optimised range gives reproducibly sensitive absorbance values with matching linearity. This reproducible result allows for robust detection where fluctuations in power delivery or degradation of the LED over the use of the sensor will have little effect once the light intensity remains between 5000 and 9000 bits, in comparison to the lower resistance values tested which will show much greater fluctuations in measurement sensitivities. This test was reproduced for nitrite detection using the nitrite LED and shown in supplementary information figure SI.2.7. (unoptimized) and SI.2.8. (optimized).

Supplementary information figure SI.2.9. shows that following the optimisation of the measurement both through measurement averaging to account for LED warm up and hardware level refinement of the resistance values of the PWM driver a non-reactive blank solution (Yellow Reagent: 0 μM phosphate standard, 1:1 v/v) could be reproducibly measured 10 times when sampled in the stable portion of the LED output accounting for the overshoot.

2.3.3. Benchtop sensing platform performance vs UV-Vis spectrometer

Following optimisation of both the colorimetric method and the benchtop sensing platform the performance was measured against a UV-Vis spectrometer.

2.3.3.1. Calibration Curve on benchtop sensing platform versus UV-Vis spectrometer.

Figure 2.15. present the linear calibration generated on the benchtop sensing platform versus UV-Vis spectrometer with (A) phosphate standards (0-50 µM. PO_4^{3-}) using the yellow method and (B) nitrite standards (0-10 µM. NO_2^-) using the Griess method.

Both the UV-Vis spectrometer and benchtop sensing platform exhibited excellent corelation coefficients of 0.999 or greater (N=3) for detection of phosphate and nitrite. After optimisation the benchtop platform shows an enhanced sensitivity compared to the UV-Vis, likely due to the longer 2.25 cm fluidic chip detector path length compared to the standard 1 cm cuvette used with the spectrometer and the broader emission of the light source. The results are summarised in table 2.3. A dynamic linear range for the benchtop platform of 0-300 µM was measured for phosphate and 0-15 µM for nitrite, see supplementary figure SI.2.10. 300 µM and 15 µM were shown to be the upper limit for the bench top platform as at concentrations above this point the detectable difference in colour and absorbance values decreased.

The LOD was calculated for the benchtop sensing platform as the concentration equivalent of 3.3 x standard deviation of the blank solution (N=10, 25 data points per blank solution measured), measuring 0.21 µM for phosphate and 0.02 µM for nitrite. The LOQ was calculated at 10 x standard deviation of the blank solution (N=10, 25 data points per blank solution measured) measuring 0.64 µM for phosphate and 0.06 µM for nitrite.

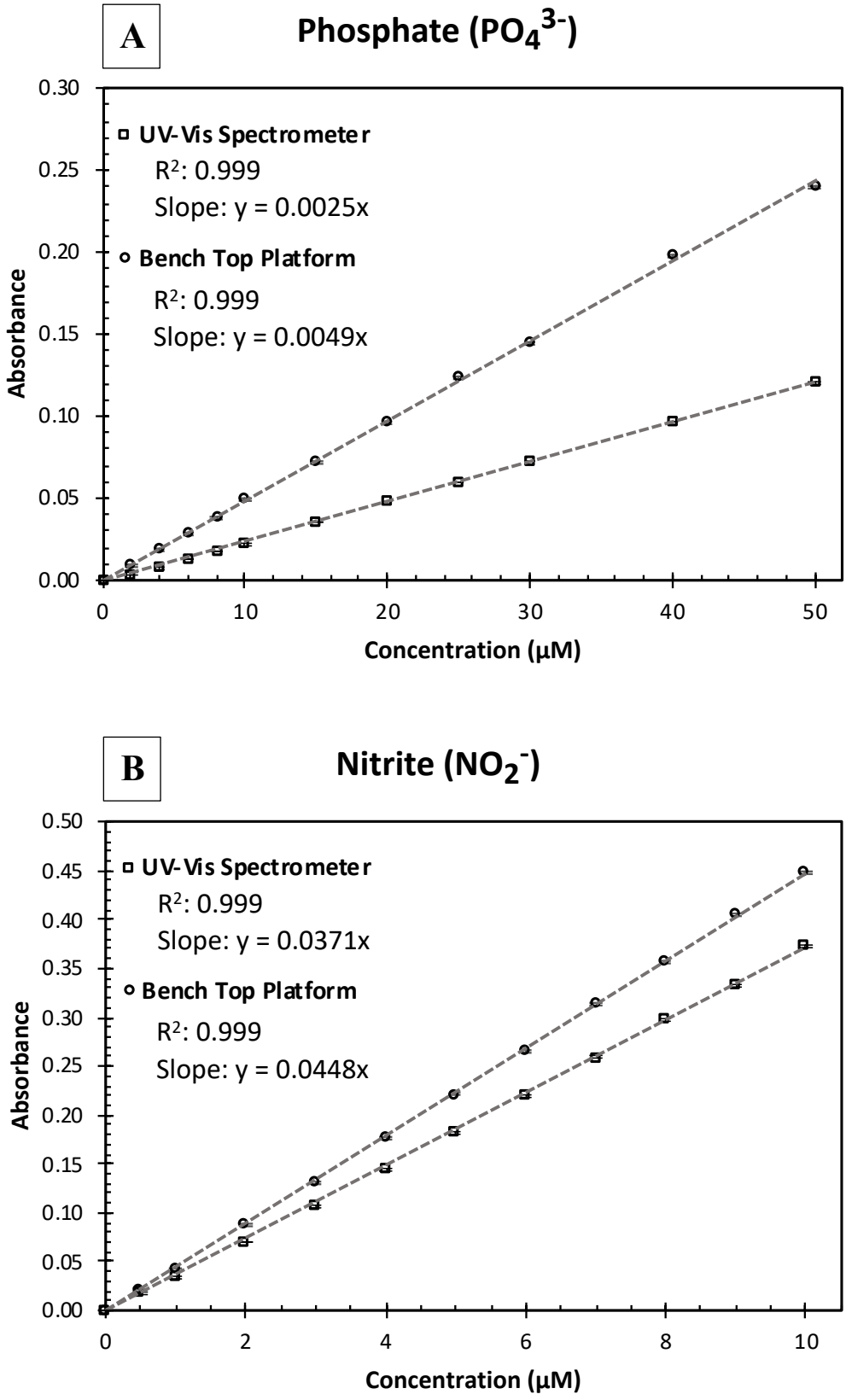

Figure 2.15. *Linear calibration curves for the detection of (A) phosphate 0-50 µM and (B) nitrite 0-10 µM on the benchtop sensing platform versus UV-Vis spectrometer.*

Table 2.3. *Analytical performance of the benchtop sensing platform based on data from figure 2.15.*

Sample	**UV-Vis Spectrometer**		**Benchtop platform**	
PO_4^{3-} (µM)	**Mean (µM) ± %RSD**	**%RE**	**Mean (µM) ± %RSD**	**%RE**
2	2.09 ± 9.42	4.39	1.86 ± 0.25	-7.04
4	3.86 ± 2.70	-3.54	3.96 ± 0.13	-1.02
6	5.88 ± 0.00	-1.96	5.96 ± 0.08	-0.61
8	7.91 ± 0.00	-0.32	7.99 ± 0.07	-0.10
10	9.75 ± 2.01	-2.48	10.37 ± 0.06	3.70
15	14.54 ± 0.00	-3.08	14.98 ± 0.04	-0.14
20	20.28 ± 0.00	1.40	19.90 ± 0.09	-0.51
25	24.79 ± 0.00	-0.83	25.38 ± 0.02	1.50
30	30.12 ± 0.00	0.42	29.68 ± 0.06	-1.06
40	39.97 ± 0.00	-0.08	40.71 ± 0.03	1.78
50	49.83 ± 0.15	-0.34	49.50 ± 0.02	-1.00

Sample	**UV-Vis Spectrometer**		**Benchtop platform**	
NO_2^- (µM)	**Mean (µM) ± %RSD**	**%RE**	**Mean (µM) ± %RSD**	**%RE**
0.5	0.48 ± 4.81	-4.59	0.49±1.33	-2.29
1	0.96 ± 1.35	-4.81	0.98 ± 0.38	-1.61
2	1.91 ± 0.00	-4.75	1.96 ± 0.10	-1.95
3	2.89 ± 0.44	-3.82	2.97 ± 0.12	-1.18
4	3.90 ± 0.35	-2.56	3.97 ± 0.23	-0.82
5	4.89 ± 0.37	-2.14	4.94 ± 0.16	-1.21
6	5.91 ± 0.21	-1.55	5.92 ± 0.27	-1.39
7	6.94 ± 0.70	-0.87	7.02 ± 0.09	0.17
8	7.97 ± 0.28	-0.34	7.95 ± 0.09	-0.59
9	8.90 ± 0.15	-1.17	9.02 ± 0.03	0.22
10	10.01 ± 0.13	0.13	9.98 ± 0.05	-0.21

2.3.3.2. Environmental Sampling

The Liffey catchment surrounds the largest population in Ireland and is characterised by a sparsely populated, upland south-eastern area with a densely populated, flat low-lying area in the remainder of the catchment basin [33]. The largest urban centre in the catchment is Dublin city with other main urban centres including Lucan and Leixlip [33]. The Liffey catchment comprises of 17 sub catchments with 77 river bodies, 6 lakes, 6 transitional and 5 coastal water bodies and 16 ground water bodies [33]. Within this catchment the river Liffey is designated as a nutrient sensitive area (NSA) [33–35] with significant pressures relating to excess nutrients primarily from agriculture both diffuse and point, but also urban and domestic wastewater [33,36] and through groundwater and urban run-off [37].

The river Liffey, rises in the Wicklow mountains south of Dublin City and flows for approximately 125 km through counties Wicklow, Kildare, and Dublin before entering Dublin Bay [38]. The river Liffey is a controlled river with a regulated flow for its final 80 km with three hydroelectric dams at, Poulaphouca, Golden Falls and Leixlip [39] as well as regulated to a lesser extent from several weirs and fish boxes [37]. Poulaphouca acts as a flood relief reservoir, with Golden falls situated about 2 km downstream from this acting as a regulating reservoir for discharges from Poulaphouca [39,40]. After passing through Golden falls the Liffey flows through Co. Kildare to Leixlip Dam and reservoir which is approximately 20 km from Dublin City. Leixlip Dam is the furthest downstream of the three dams.

Following lab validation using standards of known concentration, ten environmental samples of unknown concentration were taken from the river Liffey across a 14 km transect starting directly above Leixlip dam, Co. Kildare and finishing in Mill Lane, Palmerstown, Co. Dublin, Ireland. Figure 2.16. shows a sampling plan of the ten grab samples that were taken using weirs and common landmarks as sampling markers, supplementary information figure SI.2.11. shows a scaled version of the sampling map to give context to the site's location across the greater Liffey area. All samples taken were fully freshwater as they were upstream of the nominal tidal limit (NTL) at Island bridge weir and so were unaffected by tidal influences [37]. At the time of sampling

(30/05/2020) there was 0 mm of rainfall recorded in the previous 7 day period with river levels and flow being low (69 cm measured at the sampling location 10 [41]).

Samples were taken via kayak at a depth of 10 cm below the surface and stored on ice in the dark as they were collected. Each sample was taken using 50 mL centrifuge tubes (50 mL centrifuge tube, graduated sterile skirted purple cap, VWR 525-0024), that had been pre acid washed with 5% HCl solution and rinsed with Ultra-pure water three times, each tube was flushed three times on site with sample before a final 50 mL was collected ensuring minimal headspace within the tube. The ten samples were taken over a period of one hour and forty-five minutes with the times and location included in table 2.4. On completion of the 14 km transect, the samples were immediately frozen at -20 °C prior to analysis. On return to lab the samples were thawed, homogenised, and immediately filtered through a 0.22 µm Durapore PVDF membrane filter. The filtrate was analysed for phosphate and nitrite on both UV-Vis spectrometer (Shimadzu UV-2600 UV-Vis) and benchtop sensing platform. The results can be seen in figure 2.17. and summarised in table 2.5.

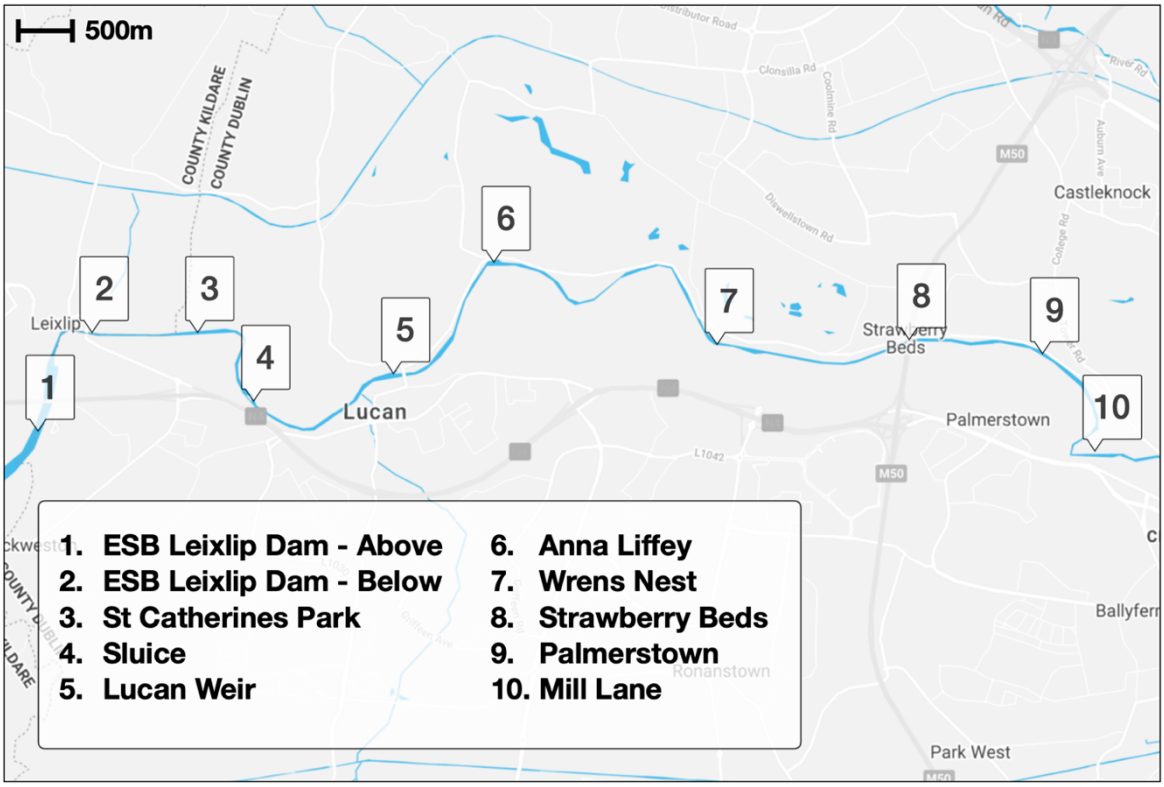

Figure 2.16. *Environmental sampling map showing ten sampling points along the river Liffey.*

Table 2.4. *Sampling log sheet showing date, time, and sampling location.*

Sample:	Date and Time:	Location:	Coordinates:
1	30/05/2020 11:48	Leixlip Dam - Above	53.35505966, -6.49223328
2	30/05/2020 12:00	Leixlip Dam - Below	53.36297944, -6.48520988
3	30/05/2020 12:11	St Catherine's Park	53.36318432, -6.47001785
4	30/05/2020 12:15	Sluice	53.35778041, -6.46521133
5	30/05/2020 12:27	Lucan Weir	53.35979532, -6.44714522
6	30/05/2020 12:48	Anna Liffey	53.36813236, -6.434327
7	30/05/2020 13:01	Wrens Nest	53.36219127, -6.40565955
8	30/05/2020 13:13	Strawberry Beds	53.36226237, -6.3694672
9	30/05/2020 13:23	Palmerstown	53.36023628, -6.36306545
10	30/05/2020 13:30	Mill Lane	53.35384161, -6.358796

Figure 2.17. shows the measured concentrations of the samples taken from the river Liffey for (A) phosphate and (B) nitrite with the results summarised in table 2.5. The results were measured both on the benchtop sensing platform and, on the UV,-Vis spectrometer. The benchtop sensing platform closely trended with the results generated on the UV-Vis with an average relative error (RE) between the two methods of 5.3% for phosphate and 4.1% for nitrite.

For phosphate measurements carried out on the UV-Vis spectrometer an average concentration of 8.00 μM was measured with a high and low of 10.15 μM at Leixlip Dam (sample 2 see figure 2.16. and table 2.4.) and 6.36 μM at St Catherine's Park (sample 3) in comparison to an average of 7.79 μM and a measurement of 9.80 μM at Leixlip Dam and 6.81 μM St Catherine's Park on benchtop sensing platform.

For nitrite measurements carried out on the UV-Vis spectrometer an average concentration of 0.91 μM was measured with a high and low of 1.70 μM (Anna Liffey) and 0.48 μM (St Catherine's Park) in comparison to an average of 0.91 μM with a high and low of 1.62 μM (Anna Liffey) and 0.47 μM (St Catherine's Park) on benchtop sensing platform.

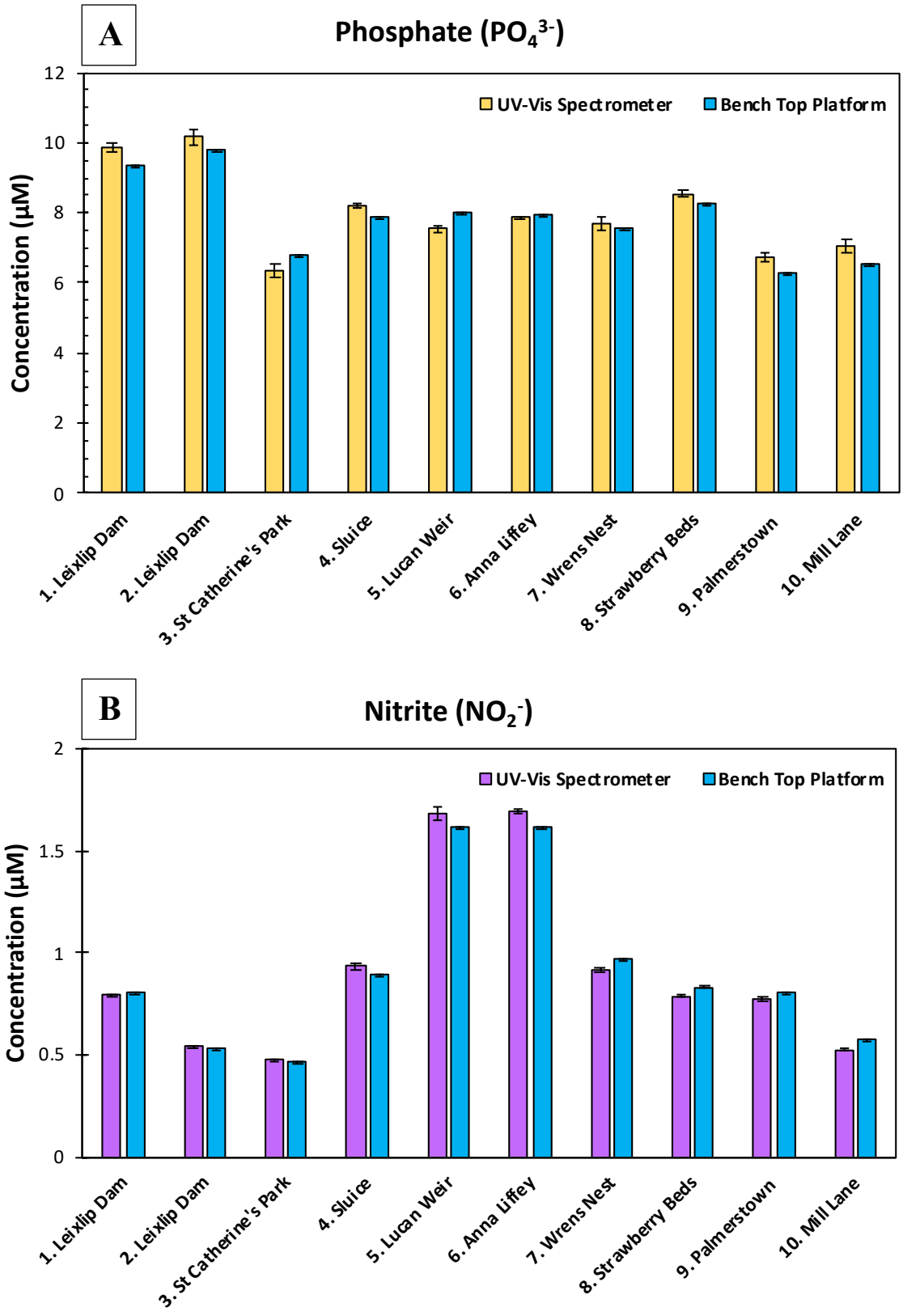

Figure 2.17. *Nutrient concentrations measured across the ten sampling points along the river Liffey for (A) phosphate and (B) nitrite.*

Table 2.5. *Summary of phosphate and nitrite concentrations measured across the ten sampling points.*

Phosphate (PO_4^{3-}) (µM)			
Sample	**UV-Vis Spectrometer**	**Benchtop Platform**	**% Relative Error**
1. Leixlip Dam - Above	9.87	9.34	-5.40
2. Leixlip Dam - Below	10.15	9.80	-3.47
3. St Catherine's Park	6.36	6.81	7.03
4. Sluice	8.18	7.91	-3.32
5. Lucan Weir	7.54	8.03	6.50
6. Anna Liffey	7.86	7.97	1.37
7. Wrens Nest	7.71	7.55	-2.00
8. Strawberry Beds	8.55	8.28	-3.05
9. Palmerstown	6.74	6.29	-6.60
10. Mill Lane	7.05	6.54	-7.18
Nitrite (NO_2^-) (µM)			
Sample	**UV-Vis Spectrometer**	**Benchtop Platform**	**% Relative Error**
1. Leixlip Dam - Above	0.79	0.81	1.30
2. Leixlip Dam - Below	0.54	0.54	-1.36
3. St Catherine's Park	0.48	0.47	-1.76
4. Sluice	0.94	0.89	-4.33
5. Lucan Weir	1.68	1.62	-3.61
6. Anna Liffey	1.70	1.62	-4.49
7. Wrens Nest	0.92	0.97	5.58
8. Strawberry Beds	0.79	0.83	5.57
9. Palmerstown	0.78	0.80	3.53
10. Mill Lane	0.52	0.57	9.05

For phosphate analysis an interesting trend was seen with the highest levels measured being found both above and below Leixlip dam (samples 1 and 2) with the lowest being recorded at the next sampling point at St Catherine's Park (sample 3) approximately

1.5 km away from this site. This result would indicate of slightly elevated levels around the reservoir and dam that had not been carried downstream due to the low river level, low rainfall, and lack of dam releases at the time of sampling. Overall levels are consistent across the ten samples with no significant indications of point sources being present at the time of sampling.

For nitrite analysis an increasing trend was seen as the samples moved downstream from Leixlip Dam towards Lucan where maximal levels were recorded between Lucan and Anna Liffey weir, following this a reducing trend was seen from Wrens Nest weir to Mill Lane, Palmerstown.

The highest levels measured for phosphate were at the earliest points at Leixlip Dam and the highest nitrite measured at Lucan weir, both sampling locations are closest to the major urban centres along the transect sampled, with Leixlip urban centre being positioned up stream of Leixlip dam and reservoir and Lucan weir being situated centrally to Lucan's urban centre. Both data sets show indicators of increased nutrient levels around populated residential areas.

2.4. Conclusion

The assessment of the performance of both the hardware and the chemical methods was essential in forming a benchtop sensing platform capable of accurate and reliable detection. The ability to alter the pathlength, chip design, LED wavelength and intensity make this platform adaptable to a range of applications and chemical methods.

The results presented show the importance of validating and optimising commercially available components when applied in a prototype configuration. Careful assessment of the LED characteristics has shown that it lacked soft start functionality resulting in an initial overshoot which had significant effect on the final values generated if unaccounted for. On a hardware level the resistance and grounding also play a significant effect on the robustness of the measurement especially during longer-term applications where an LED may dim with age, the optimised setup resulted in a more robust reliable measurement over the long term.

The performance of the platform was demonstrated using calibration standards and environmental samples which were validated against a UV-Vis spectrometer. The benchtop sensing platform showed an excellent correlation for phosphate and nitrite for both the calibration standards and environmental samples. The calibrations showed that the benchtop sensing platform gave an improved response for both phosphate and nitrite detection in comparison to the UV-Vis spectrometer with an improved limit of detection of 0.44 µM to 0.21 µM for phosphate and matching of 0.02 µM for nitrite. The increased pathlength gave improved lower range sensitivity however negatively effects the linear dynamic range of the benchtop sensing platform in comparison to the UV-Vis spectrometer with a reduction in the upper range from 1100 µM to 300 µM for phosphate and from 40 µM to 15 µM for nitrite. All environmental samples measured within this chapter were within range of these limits however this reduced upper range could have limitations especially for nitrite in highly eutrophic waters where sample dilutions may be necessary adding method complications.

The benchtop sensing platform was produced for a material cost of €234.07, see supplementary information Figure SI.2.12. for breakdown. The cost of this could significantly be reduced in the future using surface mount components, for example the route mean square (RMS) evaluation board alone costs €100.99 which consists of the RMS chipset that is required but also a series of filters are included in the evaluation board for testing which are unused in this platform adding to the cost and complexity. Use of the chipset alone as a surface mounted component would significantly reduce the cost, the same is true for the microcontroller used where an Arduino or alternative chip could be used as a standalone piece on a custom printed circuit board (PCB).

The benchtop sensing platforms modular design makes it adaptable to a wide range of testing scenarios. The platform is not only capable of measuring colorimetric optical chemistries as presented in this chapter but is also useful as a prototyping tool and test platform for sensor components. For example, the detector is completely configurable to accept cuvettes, optical cells, or microfluidic chips of varying pathlengths and form factors, the chosen LEDs and photodiode can be replaced with other LED or photodiode configurations for validation and testing, components on the electronics board can be

replaced for testing of new components including the LED Driver, on board resistor, LED controller and analogue to digital convertor. This modular configurable setup allows for complete testing of a sensor configuration in lab with minimal complexity before it is integrated into a fully autonomous sensor.

The ability to be powered and operated directly from a laptop via USB connection or from a small battery allows for use within the field however generational improvements with a focus on ruggedness and platform form factor would make this more viable. This can be realised through the movement of the electronics to a PCB design which would not only improve ruggedness but also reduce the overall scale of the platform.

The work in this chapter forms the foundations of an autonomous sensing platform capable of rapid real-time measurement. Further modification of the benchtop sensing platform with the integration of a fluid handling system to deliver reagent and sample to the fluidic chip would allow the optical detection setup to move towards autonomous operation. To enable this, further consideration for the storage and stability of reagents must be taken. The yellow method has been reported to be stable for up to 1 year [17]exhibiting excellent stability for use in autonomous sensors whereas in contrast the Griess method has been reported to be stable for up to a month at room temperature when stored out of light [42,43]. This reduction in stability limits the length an autonomous sensor can be deployed without the need for operator intervention for reagent replacement, which limits operational lifetimes as well as increasing the overall cost of the sensor. In many cases reagent stability represents a major limiting factor for long term environmental sensing.

2.5. References

(1) Wurtsbaugh, W. A.; Paerl, H. W.; Dodds, W. K. Nutrients, Eutrophication and Harmful Algal Blooms along the Freshwater to Marine Continuum. *WIREs Water* **2019**, *6* (5). https://doi.org/10.1002/wat2.1373.

(2) Heisler, J.; Glibert, P.; Burkholder, J.; Anderson, D.; Cochlan, W.; Dennison, W.; Gobler, C.; Dortch, Q.; Heil, C.; Humphries, E.; Lewitus, A.; Magnien, R.; Marshall, H.; Sellner, K.; Stockwell, D.; Stoecker, D.; Suddleson, M. Eutrophication and

Harmful Algal Blooms: A Scientific Consensus. *Harmful Algae* **2008**, *8* (1), 3–13. https://doi.org/10.1016/j.hal.2008.08.006.

(3) Anderson, D. M.; Glibert, P. M.; Burkholder, J. M. Harmful Algal Blooms and Eutrophication: Nutrient Sources, Composition, and Consequences. *Estuaries* **2002**, *25* (4), 704–726. https://doi.org/10.1007/BF02804901.

(4) Davidson, K.; Gowen, R. J.; Harrison, P. J.; Fleming, L. E.; Hoagland, P.; Moschonas, G. Anthropogenic Nutrients and Harmful Algae in Coastal Waters. *Journal of Environmental Management* **2014**, *146*, 206–216. https://doi.org/10.1016/j.jenvman.2014.07.002.

(5) Grizzetti, B.; Vigiak, O.; Udias, A.; Aloe, A.; Zanni, M.; Bouraoui, F.; Pistocchi, A.; Dorati, C.; Friedland, R.; De Roo, A.; Benitez Sanz, C.; Leip, A.; Bielza, M. How EU Policies Could Reduce Nutrient Pollution in European Inland and Coastal Waters. *Global Environmental Change* **2021**, *69*, 102281. https://doi.org/10.1016/j.gloenvcha.2021.102281.

(6) Mallin, M. A.; McIver, M. R.; Wells, H. A.; Parsons, D. C.; Johnson, V. L. Reversal of Eutrophication Following Sewage Treatment Upgrades in the New River Estuary, North Carolina. *Estuaries* **2005**, *28* (5), 750–760.

(7) Withers, P.; Neal, C.; Jarvie, H.; Doody, D. Agriculture and Eutrophication: Where Do We Go from Here? *Sustainability* **2014**, *6* (9), 5853–5875. https://doi.org/10.3390/su6095853.

(8) US EPA, O. The Issue https://www.epa.gov/nutrientpollution/issue (accessed 2021 -05 -13).

(9) Aryal, N.; Reba, M. L. Continuous Instream Monitoring of Nutrients and Sediment in Agricultural Watersheds. *J Vis Exp* **2017**, No. 127. https://doi.org/10.3791/56036.

(10) Kianpoor Kalkhajeh, Y.; Jabbarian Amiri, B.; Huang, B.; Henareh Khalyani, A.; Hu, W.; Gao, H.; Thompson, M. L. Methods for Sample Collection, Storage, and Analysis of Freshwater Phosphorus. *Water* **2019**, *11* (9), 1889. https://doi.org/10.3390/w11091889.

(11) Chapin, T. P. High-Frequency, Long-Duration Water Sampling in Acid Mine Drainage Studies: A Short Review of Current Methods and Recent Advances in Automated Water Samplers. *Applied Geochemistry* **2015**, *59*, 118–124. https://doi.org/10.1016/j.apgeochem.2015.04.004.

(12) Lau, K.-T.; Baldwin, S.; O'Toole, M.; Shepherd, R.; Yerazunis, W. J.; Izuo, S.; Ueyama, S.; Diamond, D. A Low-Cost Optical Sensing Device Based on Paired Emitter–Detector Light Emitting Diodes. *Analytica Chimica Acta* **2006**, *557* (1–2), 111–116. https://doi.org/10.1016/j.aca.2005.10.046.

(13) O'Toole, M.; Diamond, D. Absorbance Based Light Emitting Diode Optical Sensors and Sensing Devices. *Sensors* **2008**, *8* (4), 2453–2479. https://doi.org/10.3390/s8042453.

(14) Murphy, K.; Heery, B.; Sullivan, T.; Zhang, D.; Paludetti, L.; Lau, K. T.; Diamond, D.; Costa, E.; O'Connor, N.; Regan, F. A Low-Cost Autonomous Optical Sensor for Water Quality Monitoring. *Talanta* **2015**, *132*, 520–527. https://doi.org/10.1016/j.talanta.2014.09.045.

(15) Gillett, D.; Marchiori, A. A Low-Cost Continuous Turbidity Monitor. *Sensors* **2019**, *19* (14), 3039. https://doi.org/10.3390/s19143039.

(16) Siahaan, I. A.; Mutiara, G. A.; Sani, M. I. A Low-Cost Water Quality Monitoring Based on Photodiode and LDR. In *2021 IEEE Asia Pacific Conference on Wireless and Mobile (APWiMob)*; IEEE: Bandung, Indonesia, 2021; pp 141–146. https://doi.org/10.1109/APWiMob51111.2021.9435280.

(17) Bowden, M.; Diamond, D. The Determination of Phosphorus in a Microfluidic Manifold Demonstrating Long-Term Reagent Lifetime and Chemical Stability Utilising a Colorimetric Method. *Sensors and Actuators B: Chemical* **2003**, *90* (1–3), 170–174. https://doi.org/10.1016/S0925-4005(03)00024-8.

(18) Diamond, D.; Cleary, J.; Maher, D.; Jungho Kim; King Tong Lau. Autonomous Analyser Platforms for Remote Monitoring of Water Quality. In *IECON 2011 - 37th Annual Conference of the IEEE Industrial Electronics Society*; IEEE: Melbourne, Vic, Australia, 2011; pp 3516–3521. https://doi.org/10.1109/IECON.2011.6119878.

(19) Apak, R.; Çekiç, S. D.; Üzer, A.; Çapanoğlu, E.; Çelik, S. E.; Bener, M.; Can, Z.; Durmazel, S. Colorimetric Sensors and Nanoprobes for Characterizing Antioxidant and Energetic Substances. *Anal. Methods* **2020**, *12* (44), 5266–5321. https://doi.org/10.1039/D0AY01521K.

(20) Váradi, L.; Breedon, M.; Chen, F. F.; Trinchi, A.; Cole, I. S.; Wei, G. Evaluation of Novel Griess-Reagent Candidates for Nitrite Sensing in Aqueous Media Identified

via Molecular Fingerprint Searching. *RSC Adv.* **2019**, *9* (7), 3994–4000. https://doi.org/10.1039/C8RA07656A.

(21) Lockridge, G.; Dzwonkowski, B.; Nelson, R.; Powers, S. Development of a Low-Cost Arduino-Based Sonde for Coastal Applications. *Sensors* **2016**, *16* (4), 528. https://doi.org/10.3390/s16040528.

(22) Transmittance to Absorbance Table https://www.sigmaaldrich.com/IE/en/technical-documents/technical-article/analytical-chemistry/photometry-and-reflectometry/transmittance-to-absorbance (accessed 2021 -06 -23).

(23) Cleary, J.; Slater, C.; Diamond, D. Analysis of Phosphate in Wastewater Using an Autonomous Microfluidics-Based Analyser. **2009**, 4.

(24) VTW Phosphate Measurement https://www.fagerberg.dk/cgi-files/mdmgfx/26252-onl_062_069_phosphate_445-kb_us-pdf.pdf (accessed 2021 -05 -03).

(25) O'Toole, M.; Shepherd, R.; Lau, K.-T.; Diamond, D. Detection of Nitrite by Flow Injection Analysis Using a Novel Paired Emitter-Detector Diode (PEDD) as a Photometric Detector. In *Advanced Environmental, Chemical, and Biological Sensing Technologies V*; Vo-Dinh, T., Lieberman, R. A., Gauglitz, G., Eds.; International Society for Optics and Photonics: Boston, MA, 2007; p art no. 67550P. https://doi.org/10.1117/12.737791.

(26) Tsikas, D. Analysis of Nitrite and Nitrate in Biological Fluids by Assays Based on the Griess Reaction: Appraisal of the Griess Reaction in the l-Arginine/Nitric Oxide Area of Research. *Journal of Chromatography B* **2007**, *851* (1–2), 51–70. https://doi.org/10.1016/j.jchromb.2006.07.054.

(27) Griess Reagent Kit for Nitrite Determination https://tools.thermofisher.com/content/sfs/manuals/mp07921.pdf (accessed 2021 -05 -03).

(28) Kaino, T. Optical Absorption of Polymers. In *Encyclopedia of Polymeric Nanomaterials*; Kobayashi, S., Müllen, K., Eds.; Springer Berlin Heidelberg: Berlin, Heidelberg, 2014; pp 1–14. https://doi.org/10.1007/978-3-642-36199-9_118-1.

(29) Roychowdhury, T.; Shah, D.; Hilfiker, J. N.; Linford, M. R. Polymethyl Methacrylate: Optical Properties from 191 to 1688 Nm (0.735–6.491 EV) by

Spectroscopic Ellipsometry. *Surface Science Spectra* **2020**, *27* (1), 016002. https://doi.org/10.1116/1.5095422.

(30) Joram, C. Transmission curves of plexiglass (PMMA) and optical grease https://cds.cern.ch/record/1214725 (accessed 2021 -05 -03).

(31) Bowden, M.; Sequiera, M.; Krog, J. P.; Gravesen, P.; Diamond, D. Analysis of River Water Samples Utilising a Prototype Industrial Sensing System for Phosphorus Based on Micro-System Technology. *Journal of Environmental Monitoring* **2002**, *4* (5), 767–771. https://doi.org/10.1039/b200330a.

(32) Conductivity, Salinity & Total Dissolved Solids https://www.fondriest.com/environmental-measurements/parameters/water-quality/conductivity-salinity-tds/ (accessed 2021 -05 -13).

(33) EPA. Liffey catchment assessment 2010-2015 (HA 09). EPA Catchment Science Unit. https://www.catchments.ie/wp-content/files/catchmentassessments/09%20Liffey%20and%20Dublin%20Bay%20Catchment%20Summary%20WFD%20Cycle%202.pdf (accessed 2021 -06 -16).

(34) Brooks, P. R.; Nairn, R.; Harris, M.; Jeffrey, D.; Crowe, T. P. Dublin Port and Dublin Bay: Reconnecting with Nature and People. *Regional Studies in Marine Science* **2016**, *8*, 234–251. https://doi.org/10.1016/j.rsma.2016.03.007.

(35) O'Higgins, T. G.; Wilson, J. G. Impact of the River Liffey Discharge on Nutrient and Chlorophyll Concentrations in the Liffey Estuary and Dublin Bay (Irish Sea). *Estuarine, Coastal and Shelf Science* **2005**, *64* (2), 323–334. https://doi.org/10.1016/j.ecss.2005.02.025.

(36) Mockler, E. M.; Deakin, J.; Archbold, M.; Gill, L.; Daly, D.; Bruen, M. Sources of Nitrogen and Phosphorus Emissions to Irish Rivers and Coastal Waters: Estimates from a Nutrient Load Apportionment Framework. *Science of The Total Environment* **2017**, *601–602*, 326–339. https://doi.org/10.1016/j.scitotenv.2017.05.186.

(37) Peñalver, R.; Jacobs, M. R.; Hegarty, S.; Regan, F. Assessment of Anthropogenic Pollution by Monitoring Occurrence and Distribution of Chemicals in the River Liffey in Dublin. *Environ Sci Pollut Res* **2021**. https://doi.org/10.1007/s11356-021-14508-y.

(38) South Eastern River Basin District River Basin Management Plan 2009-2015 https://www.catchments.ie/download/south-easter-river-basin-management-plan-2009-2015/ (accessed 2021 -06 -16).

(39) Mangan, B., J.; Hayes, T., A. *The Reservoir as an Asset*; Thomas Telford Publishing, 1996. https://doi.org/10.1680/traaa.25288.

(40) River Liffey - Hydrometric Information https://www.esb.ie/our-businesses/generation-energy-trading-new/hydrometric-information/river-liffey (accessed 2021 -06 -16).

(41) River Gauge - River Liffey https://www.canoecentre.ie/pages/river-gauge (accessed 2020 -05 -30).

(42) Hou, C.-Y.; Fu, L.-M.; Ju, W.-J.; Wu, P.-Y. Microfluidic Colorimetric System for Nitrite Detection in Foods. *Chemical Engineering Journal* **2020**, *398*, 125573. https://doi.org/10.1016/j.cej.2020.125573.

(43) O'Dell, J. W. DETERMINATION OF NITRATE-NITRITE NITROGEN BY AUTOMATED COLORIMETRY. In *Methods for the Determination of Metals in Environmental Samples*; Elsevier, 1996; pp 464–478. https://doi.org/10.1016/B978-0-8155-1398-8.50026-4.

Chapter 3

Development of a regulated heated fluidic system for on chip detection of nutrients.

Abstract

A fluidic chip has been integrated with a 12 V silicone heating element, alongside a temperature measurement and control circuit, which has allowed for the regulation of heated reactions on chip. This setup gives improved stability and reduced reaction times of colorimetric reactions and gives the ability to stabilise reaction temperatures.

The detection setup consisted of a temperature regulated optical fluidic chip aligned between a LED and photodiode detector. The heated fluidic system was used for the detection of nitrite and nitrate with heat being used as the catalyst for the reduction of nitrate to nitrite using vanadium chloride (III), which was then detected by the Griess colorimetric assay. Standards of known concentration and a series of environmental samples taken from the river Boyne were compared using the heated fluidic sensing platform and a commercial UV-Vis spectrometer. The measurements recorded trended well with the values measured on the UV-Vis spectrometer where an average % relative error of 1.7% for nitrite and 1.4% for nitrate was seen for the environmental samples.

Keywords:

Microfluidics, Flow Injection Analysis (FIA), Colorimetric Chemistries, Nitrate, Heating on Chip

3.1. Introduction

Nitrite and nitrate are present in the environment at natural levels as part of the nitrogen cycle and are essential components of aquatic ecosystems [1]. Increasingly these ecosystems are imbalanced with excessive levels of nitrites and nitrates found in waterways [2]. Nitrogen pollution remains one of the most challenging and costly environmental problems globally [3] despite decades of regulation and remediation efforts [4]. The European Nitrate Directive was issued 30 years ago, and nitrate contamination remains a serious threat to ecosystems and human health. About half of the European monitoring stations show no significant change in nitrates [4], and 26.6% have shown an increasing trend [4].

The environmental impacts of nitrate pollution include ecological damage to waterways [5], long term loading and damage to groundwater [6], and increased demand for drinking water treatment. Excessive nutrient levels can lead to enrichment of water bodies causing harmful algal blooms capable of releasing toxins making drinking water unsafe, poisoning marine life and creating dead zones [7]. Even algal blooms without toxic secretions can cause damage where dense growth can block sunlight and starve aquatic species of oxygen as plant life decomposes [8].

Pollution of groundwater from nitrogen sources such as nitrites and nitrates is becoming an increasing concern [9]. Nitrate loss from land is common in freely draining soils where it leaches readily into groundwater before being potentially discharged into river systems and waterways, and finally reaching estuary's or coastal waters [10–12]. Nitrate contamination is a significant issue world-wide in intensively farmed regions where fertilisers are excessively used [9,13,14]. Over fertilisation of land for decades has led to excessive loading of nitrate [15], this nitrate loading of ground water will continue to be a problem unless reliable estimates can be made and improved remediation policies are put in place.

Reliably measuring nitrite and nitrate levels in the environment is critical in order to accurately quantify and estimate the potential scale of this problem [16]. Sensing technology capable of scaled sensing across a large area is necessary for estimating both point and diffuse sources of contamination. Microfluidic technology is capable of

a wide range of lab on chip applications, from sample intake in low volumes, mixing and detection. For chemical reactions that take place on chip temperature is a key factor in obtaining accurate and precise measurements. The need to control temperature is of less importance when testing is carried out in temperature-controlled laboratories however for environmental applications or reactions requiring higher than room temperature it is a critical feature.

In this chapter the development of a heated fluidic cell is demonstrated through the detection of nitrite and nitrate in known concentration standards and natural water samples. The use of vanadium chloride (III) as a reducing agent has been previously discussed by Garcia et al. and Schnetger et al. [17,18] and adapted for the testing carried out. The use of the Griess assay allows for the initial detection of nitrite, producing an intense pink colour that absorbs around 545 nm and subsequently the reduced nitrate can be detected at the same wavelength. Nitrite and nitrate contamination of aquatic ecosystems is a ubiquitous problem [14] and are key parameters to be monitored due to their potential toxicity in excess to aquatic ecosystems.

3.2. Materials and Methods

3.2.1. Reagent and Standard Preparation

All reagents and standards were prepared using ultra high purity (UHP) water (MilliQ, Millipore, Burlington, MA, USA) and analytical grade chemicals (Sigma Aldrich, St. Louis, MO, USA).

3.2.1.1. Vanadium Chloride Reduction Solution

Vanadium chloride reducing solution was prepared following the method of Schnetger et al. [18] where 800 mg VCl_3 was partly dissolved in a small amount of ultrapure water (20 mL), 8.4 mL HCl (37%) was added and the solution was subsequently diluted to 100 mL using ultrapure water.

3.2.1.2. Griess Reagent

0.5 g of Sulphanilamide was added to ~100 mL UHP water, with the addition of 5 mL of concentrated hydrochloric acid (37%). Following the dissolution of the

Sulphanilamide, 0.05 g of N-(1-Naphthyl) ethylenediamine dihydrochloride (NEDD) was added and the resulting solution was made up to 500 mL using UHP water.

3.2.1.3. Stock Solutions

Nitrate stock solutions were prepared by dissolving known weights of potassium nitrate in UHP water. Nitrite standards were prepared by dissolving known weights of sodium nitrite in UHP water. These stock solutions were further diluted to make a range of known concentration solutions.

3.2.1.4. Sample Reagent Ratios

For colorimetric nitrite detection, a ratio of 9:1 v/v ratio of standards/samples and Griess reagent were mixed and allowed to react at room temperature (22 °C for 1200 seconds.

For colorimetric nitrate detection, a ratio of 9:1:1 v/v ratio of standards/ samples, Griess reagent, and vanadium chloride (III). These were mixed and allowed to react at 60 °C for 1500 seconds. The final-coloured product accounts for both nitrite and nitrate, as a result nitrite should be measured initially and accounted for so that nitrate can be quantified from total nitrogen.

3.2.2. Instrumentation / Electronics Design

A custom-built benchtop sensing platform consisting of a microfluidic optical chip, low-cost LED – photodiode detector, and electronic detection board was used to measure the reactions on chip as previously shown in **chapter 2**. Reference measurements were taken using a Shimadzu UV-2600 photo-spectrometer. Samples measured were run in parallel on the UV-Vis spectrometer and the benchtop sensing platform at the same wavelength (545 nm).

Heating of samples was carried out using a TCC-100 temperature-controlled cell for UV-Vis spectrometer, and on chip, a custom built heater was integrated onto the fluidic chip with temperature feedback and regulation.

3.2.3. Temperature Sensor Development

To assess the performance of the microfluidic heater a temperature sensor was designed that was capable of being integrated into the surface of the fluidic chip. A thermistor based circuit was chosen using a low profile cost effective 0.1% thermistor based on the adafruit open source thermistor circuit [19]. The thermistor will give a resistance change based on temperature which can be measured [20]. Resistance was measured as a substitute for temperature which was then correlated back. The microcontroller (Arduino Mega 2560) chosen does not have a built-in resistance meter, as a proxy the on-board analogue to digital convertor (ADC) was used. To do this the resistance must first be converted from resistance to voltage which was achieved by connecting the thermistor to a resistor in series. This voltage divider circuit using a fixed resistor allows from voltage to be measured, as the resistance changes the voltage changes [21]. To convert to temperature a simplified version of the Steinhart-Hart equation is used [22] , $\frac{1}{T} = \frac{1}{T0} + \frac{1}{B}\ln(\frac{R}{R0})$ where T_0 is room temperature in kelvin, B is the coefficient of the resistor, R_0 is the resistance at room temperature and R is the resistance measured. This conversion gave temperature in Kelvin which could then be converted to Celsius. The code for temperature measurement and conversion can be seen in supplementary information Figure SI.3.1. and a circuit drawing of the temperature sensor board in figure SI.3.2.

Figure 3.1. presents the circuit layout chosen with a voltage divider circuit in place to measure the voltage change of the thermistor which can then be converted to °C. The 3.3 V track on the Arduino was chosen as an analogue reference to improve the noise generated, 3.3 V was chosen over 5 V as typically the 5 V trace on an Arduino will be noisier [19]. The 3.3V line runs through a secondary filter stage which gives it a cleaner signal. The measurement reading was also averaged in the code to further account for noise and fluctuations [19].

The error of this temperature circuit was approximated to be below ±0.5 °C where the 0.1% thermistor itself can be approximated to give an error of 0.03 °C at 25 °C and the accuracy of the ADC ±0.1 °C at 25 °C [19], this could be further improved by moving away from the Arduinos on board ADC towards an external 12 bit ADC and using an external power regulator as the analogue reference [19].

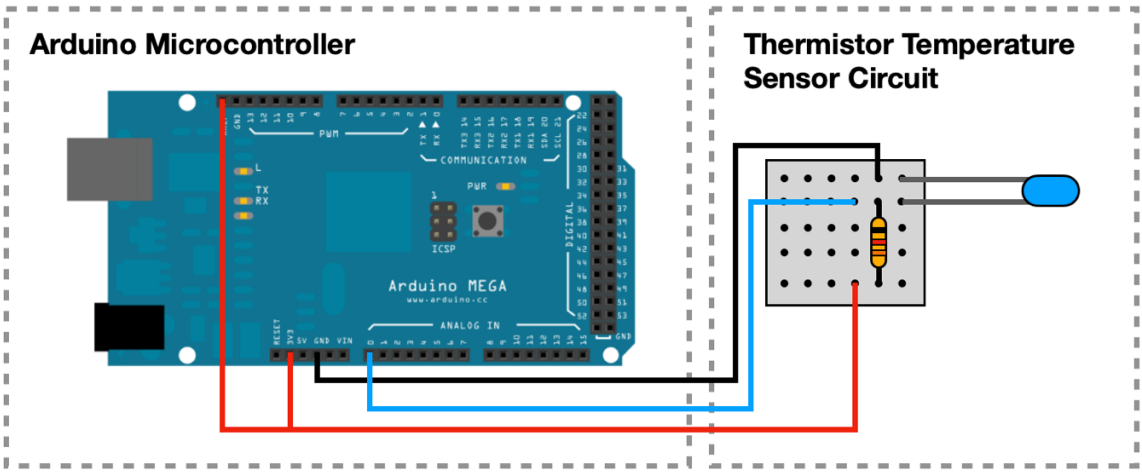

Figure 3.1. *Thermistor based temperature sensor circuit layout using an Arduino based microcontroller and a voltage divider using a thermistor and a fixed resistor in series.*

3.2.4. Integrated Fluidic heater

A silicone heater mat (RS Pro Silicone heater mat 1.25 W, 25x50 mm, 12 V DC) was chosen as the heat source for the fluidic chip. This heater was chosen due to its low profile and robust design, the heaters are composed of etched foil elements which have been embedded in glass cloth supported rubber which allows them to be both flexible, robust, and easily integrated. To characterise the heating elements, the heater was setup as shown in figure 3.2. where the foil heater was fixed using the included thermal adhesive to a PMMA fluidic chip with an embedded thermistor-based temperature sensor. The design, manufacture and characterisation of these fluidic chips are discussed in detail in **chapter 4** and **chapter 5**.

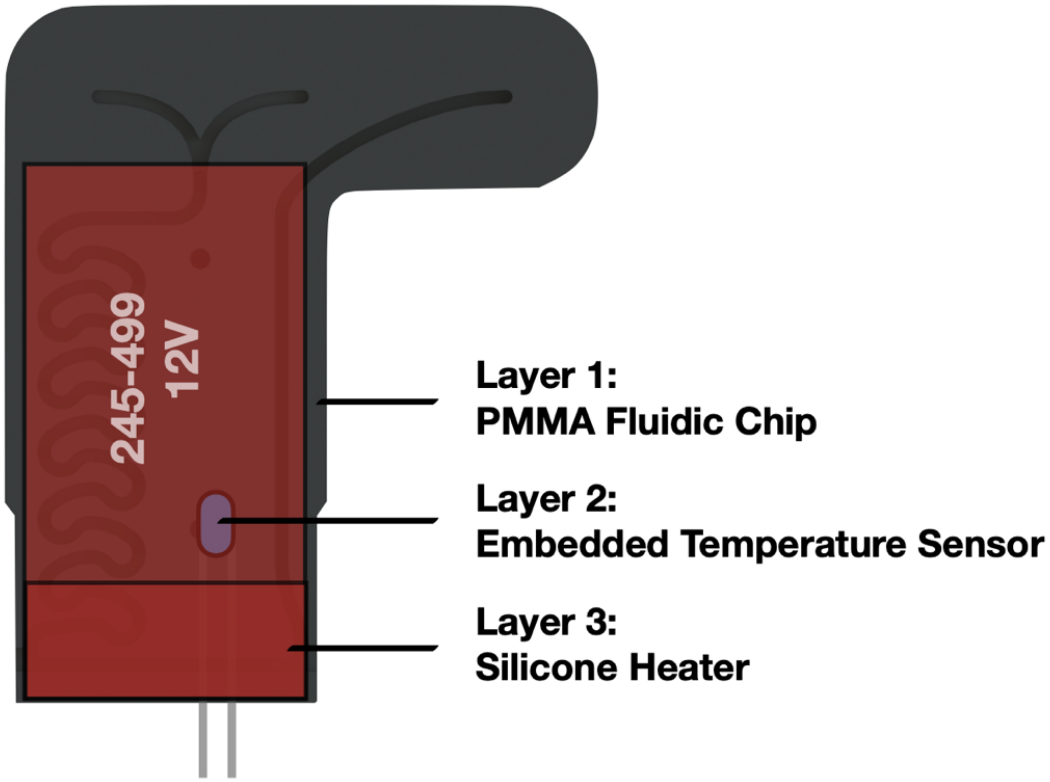

Figure 3.2. *Schematic diagram of PMMA fluidic chip with integrated heater and temperature sensor.*

3.3. Results and Discussion

3.3.1. Characterisation of the colorimetric methods.

Prior to optimisation of the fluidic chip heater and validation of the reaction on chip, the colorimetric method for nitrate detection was assessed to determine its reaction rates at elevated temperatures, working range and potential interferents using a Shimadzu UV-2600 UV-Vis spectrometer with TCC-100 temperature-controlled cell.

3.3.1.1. Wavelength selection – Spectrum Scan

The optimum wavelength was investigated by obtaining the absorbance spectrum for the complete method reducing nitrate to nitrite using VCl_3 and detecting the product using the Griess method. This was carried out to ensure the reduction step did not cause any peak shift in the λ_{max} of the reaction in comparison to what was presented in **chapter 2** for nitrite. Figure 3.3. shows the measured spectrum of 0-10 µM nitrate (NO_3^-) reaction, measured on a Shimadzu UV-2600 Photo spectrometer. A linear trend was measured with increasing absorbance as concentration was increased. The λ_{max} of

the reaction was measured at 542 nm this was consistent with literature values, which typically range from and 540-550 nm [17,18,23,24] and matched with **chapter 2's** spectrum scan of nitrite detection using the Griess assay.

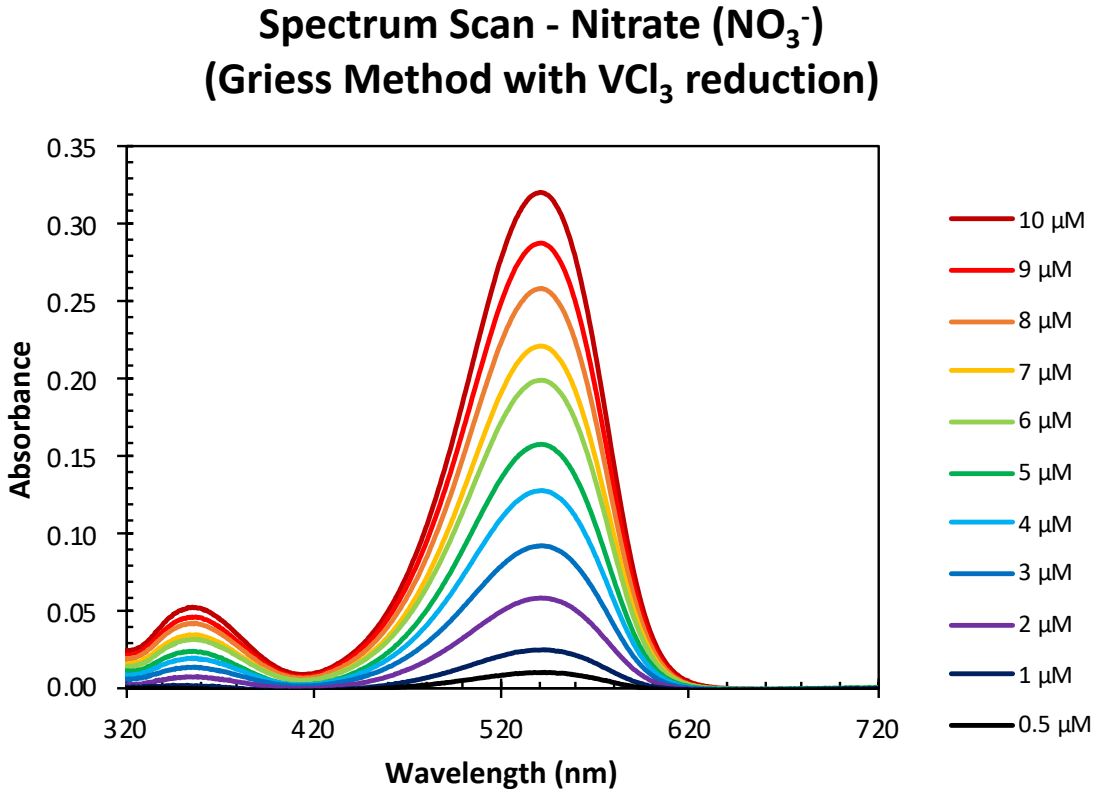

Figure 3.3. *Spectrum scan of nitrate detection using the Griess method with vanadium chloride (III) reduction step.*

3.3.1.2. Reaction rates – Kinetics

The rate of development of the coloured complex for the detection of nitrate was assessed kinetically. The measurement was recorded on a Shimadzu UV-2600 with TCC-100 temperature-controlled cell. The absorbance was measured at 545nm over a 1-hour period. A 10µM nitrate standard was measured between 40 and 70 °C as shown in Figure 3.4.

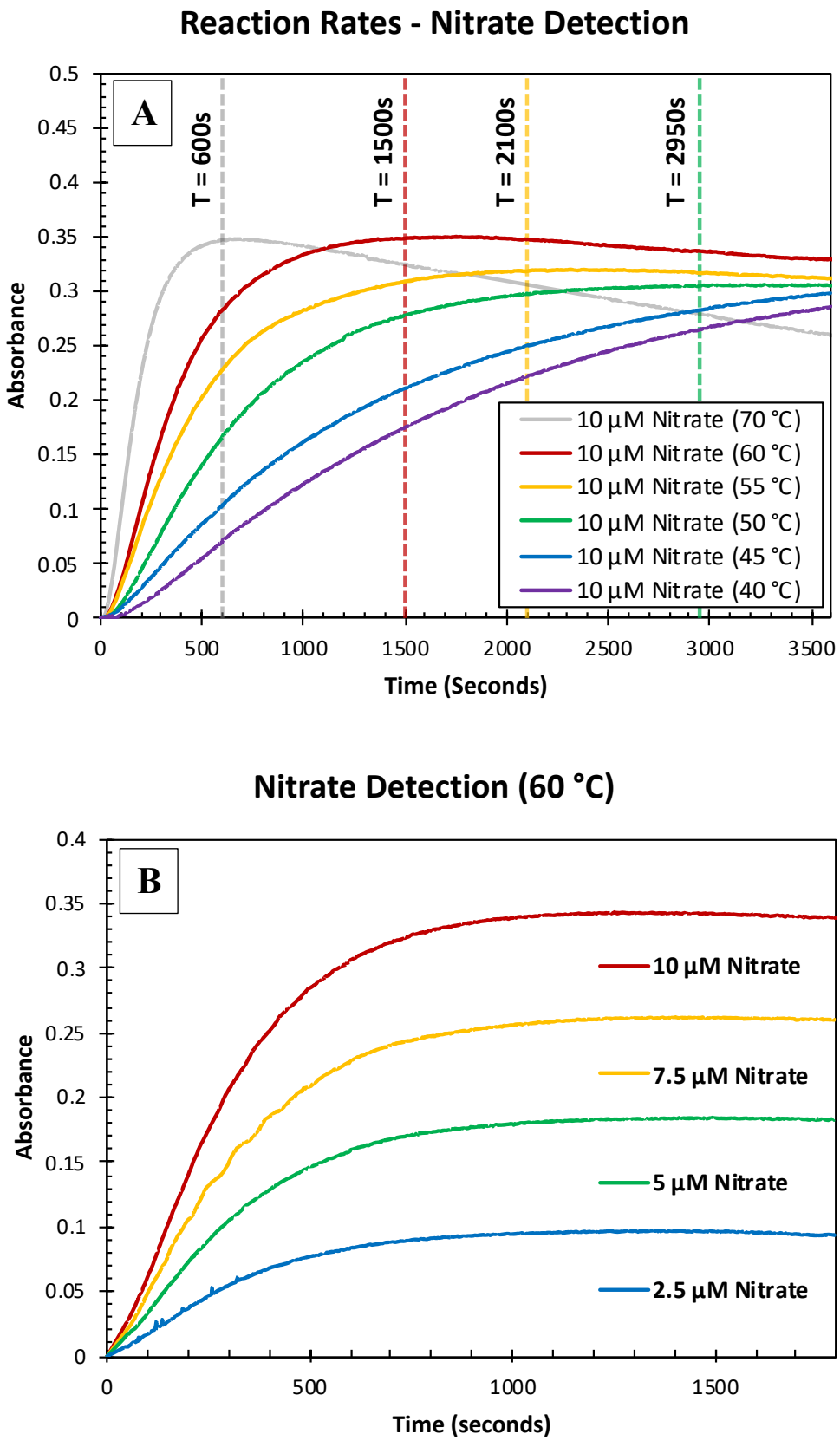

Figure 3.4. *Kinetic study of heated nitrate detection with (A) varying reaction temperature and (B) varying standard concentration.*

The reduction of nitrate requires heat as a catalyst for the reaction to reach completion without the need to wait for extended periods of time (10 - 20 hours at room temperature [18]). Below 45 °C none of the reactions completely reduced within a one-hour period, this result is consistent with results described by García-Robledo et al. [17]. 50 °C or above was required to effectively reduce nitrate to nitrite for detection within a one-hour period.

70 °C was the maximum temperature tested, at this temperature the reaction occurs rapidly under 600 seconds but also quickly degrades leaving a small window of measurement and poor stability. 60 °C resulted in rapid colour production for the first 1000 seconds before slowing to reach a maximum after 1500 seconds. At this temperature minimal degradation of the coloured product was seen over the one-hour scan period leaving a larger window of measurement. The reduction in signal over time is likely due to the decomposition of the diazonium complex formed during the Griess method [25]. 60 °C also showed an increased absorbance and sensitivity in comparison to any of the lower temperatures tested suggesting a more complete reduction of nitrate to nitrite.

Figure 3.4. B shows four concentrations (2.5 to 10 μM) of nitrate measured at 60 °C over 1800 seconds. The measurements show a linear increase in absorbance versus concentration with all concentrations reaching their maximum at the same time interval of 1500 seconds which trends well with previously reported literature values of 1200 – 1800 seconds at 60 °C [17].

3.3.1.3. Working Range – Linear Calibration

A calibration plot was performed on UV-Vis for the detection of nitrate with a set of known concentration standards (see supplementary figure SI.3.3.). A dynamic linear range of 0-40 μM for nitrate was measured, with 40 μM being the upper limit, at concentrations above this point the detectable difference in colour and absorbance values decreased.

The molar extinction coefficient was estimated to be 3.28 x 10^4 mol L^{-1} cm^{-1} at 545nm for nitrate. An excellent correlation coefficient of 0.999 (N=3, 10 data points per replicate measured) with an average %RSD of 1.04%.

The limit of detection and limit of quantification was determined by multiplying the standard deviation of the baseline of the blank. The LOD was calculated as the concentration equivalent of 3.3 x standard deviation of the blank solution (N=15, 10 data points per blank solution measured), measuring 0.03 µM. The LOQ was calculated at 10 x standard deviation of the blank solution (N=15, 10 data points per blank solution measured) measuring 0.11 µM.

3.3.1.4. Interference Study – Salinity Effects

Similarly, to **chapter 2**, three different marine matrices were selected consisting of an artificial sea salt (Red Sea Sea Salts), unrefined sea salts (Sigma Aldrich Sea Salts) and a natural sea water sample identified as having low baseline level nutrients (Seawater – Mulranny Co Mayo). Nitrate *c*oncentrations of 0.66 µM for Red Sea Sea Salts, 0.68 µM for Sigma Aldrich Sea Salts, and 1.49 µM for Natural Seawater were measured. Sigma Aldrich was chosen for the salinity interference study as it had the lowest levels of combined nitrite and nitrate of 0.70 µM versus Red Sea Sea Salts combined levels of 0.72 µM. The effect of salinity was tested using known concentration standards made up in ultra-pure water and an artificial seawater matrix using Sigma Aldrich Sea Salts.

A concentration of 0, 20 and 40 g/L was tested to give a salinity range similar to that seen from freshwater to estuarine to marine matrices [26]. Figure 3.*5.* shows a calibration curve of nitrate 0-10 µM made up in 0, 20 and 40 g/L sea water matrix. The increased baseline from using Sigma Sea Salts versus ultrapure water was accounted for by using method blanks for each calibration.

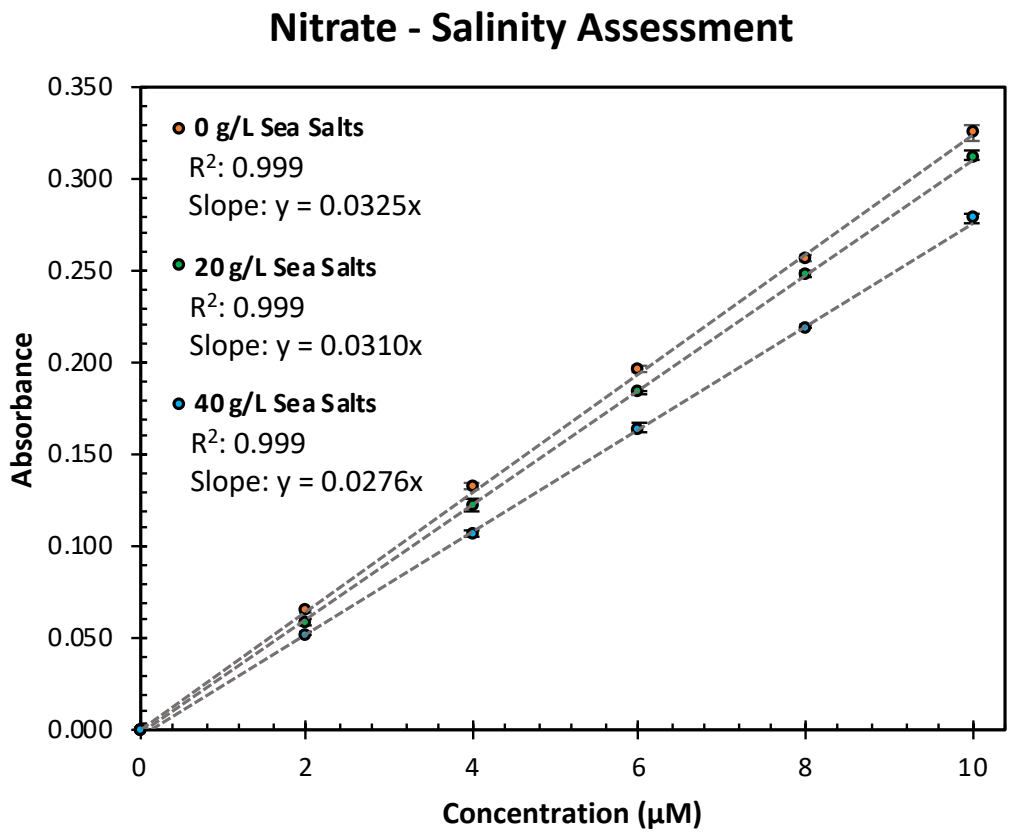

Figure 3.5. *Calibration curve of nitrate standards tested at 0, 20 and 40 g/L artificial seawater matrix. The error bars represent the standard deviations for n=3.*

The results in figure 3.5. show a reduction in the slope and colour formation of the final product as salinity levels are increased. Each calibration curve remains linear but with a decreasing sensitivity as salinity levels are increased. Figure 3.6 shows a similar decrease in absorbance of the coloured product with increasing salinity, the λ_{max} of 542 nm was consistent at concentrations of 0, 20 and 40 g/L, showing no shift in the wavelength of maximum absorbance at higher salt concentrations.

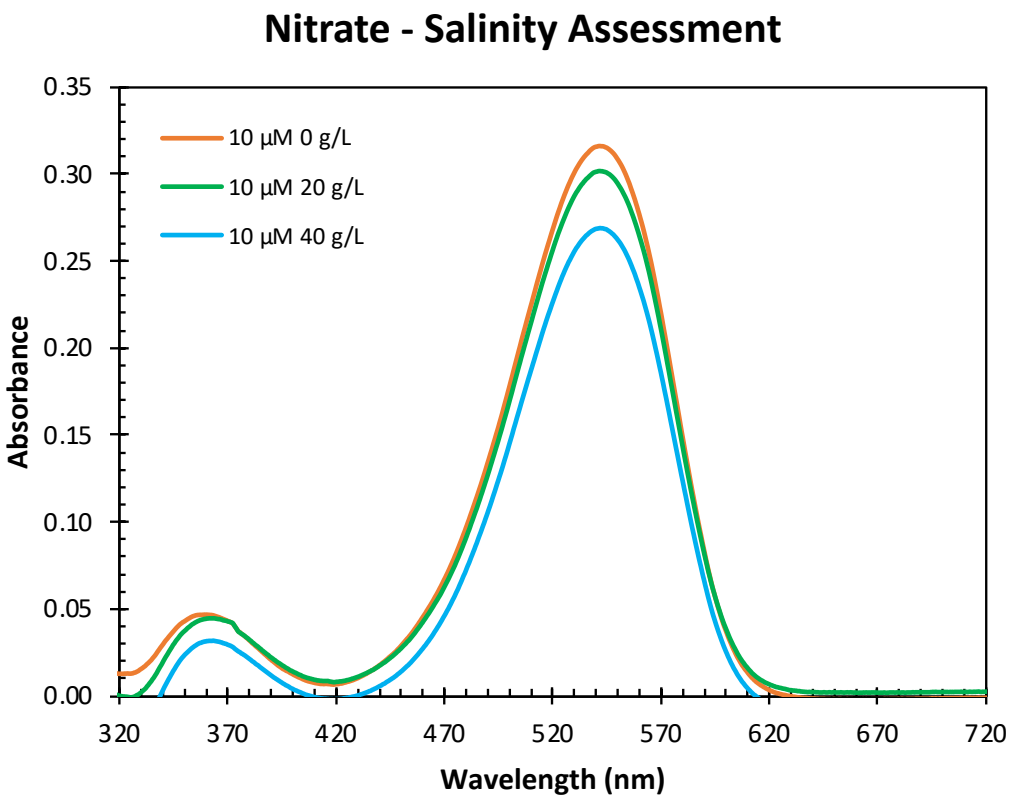

Figure 3.6. *Spectrum scan of nitrate standards tested at 0, 20 and 40 g/L artificial seawater matrix.*

This interference was not seen for the Griess method discussed in **chapter 2**, so it is likely interfering with the reduction step of the reaction where vanadium chloride (III) reduces nitrate to nitrite. The reduction in sensitivity of the reaction is most severe at 40 g/L (15.08% decrease) in comparison to the 20 g/L (4.62% decrease) calibration which is significantly closer to the 0 g/L calibration.

This interference limits the opportunity for this method to work in varied sample salinity without pre-treatment or calibration to correct for this effect. Calibration using standards of the same salinity as the sample being tested can be used to correct for this [17]. However, it is less of a concern due to the low limit of detection of the method allowing for a dilution to be carried out to reduce salinity concentrations while allowing combined nitrite and nitrate levels in the environment to still be at a detectable level.

3.3.1.5. Interference Study – Nitrite interference

The detection of nitrate relies on the reduction of nitrate to nitrite before detection, as a result the presence of nitrite in samples has the potential to interfere and contribute to the measured values if not accounted for. For the measurement of samples containing both nitrite and nitrate both analytes will contribute towards the measured absorbance.

To account for this nitrate concentration is measured as the difference between the total nitrite (nitrite + reduced nitrate) measured, and the initial nitrite measured. Nitrite is initially measured separately using Griess reagent alongside its own calibration, finally the total combined nitrite and nitrate is measured using Griess reagent and VCl_3 alongside a calibration. Nitrate can then be calculated from the total combined concentration minus the nitrite concentration measured. The combined measurement for nitrite and reduced nitrate must be lower than the upper working range of the method of 40 μM for UV-Vis Spectrometer (see SI.3.3), at levels above this a dilution is required.

For environmental sampling it is important to accurately be able to distinguish nitrite and nitrate. Typically, environmental samples of marine and freshwater systems primarily contain nitrate, with nitrite being present at low concentrations, however there are aquatic systems with elevated nitrites including marine coastal areas, oxygen minimum zones and industrial wastewater [17].

Figure 3.7 shows the measurement of three sets of calibration standards: nitrite standards (0, 5, 10, 15, 20 μM), nitrate standards (0, 5, 10, 15, 20 μM), and a mixed standard containing equal concentrations of nitrite and nitrate (0, 5, 10, 15, 20 μM nitrite and 0, 5, 10, 15, 20 μM nitrate).

Figure 3.7 (A) presents the initial measurement of nitrite using the Griess assay . The results show no reaction from the nitrate standards in the presence of Griess reagent, the nitrite standards and the mixed standards show matching absorbance signal as only the nitrite reacts in the mixed standard. The presence of nitrate in the mixed sample causes no inerferece with the detection of nitrite as shown by its matching

sensitivity to the nitrite standards measured. 3.7 (B) presents the measurement of the combined measurement of nitrite and nitrate using Griess reagent and VCl_3. The results show complete reaction of the nitrate showing matching absorbance signal to the nitrite standards. The mixed standard shows an increased absorabance in comparison to the other two standards due to the contribution from both the nitrite and nitrate present in the sample.

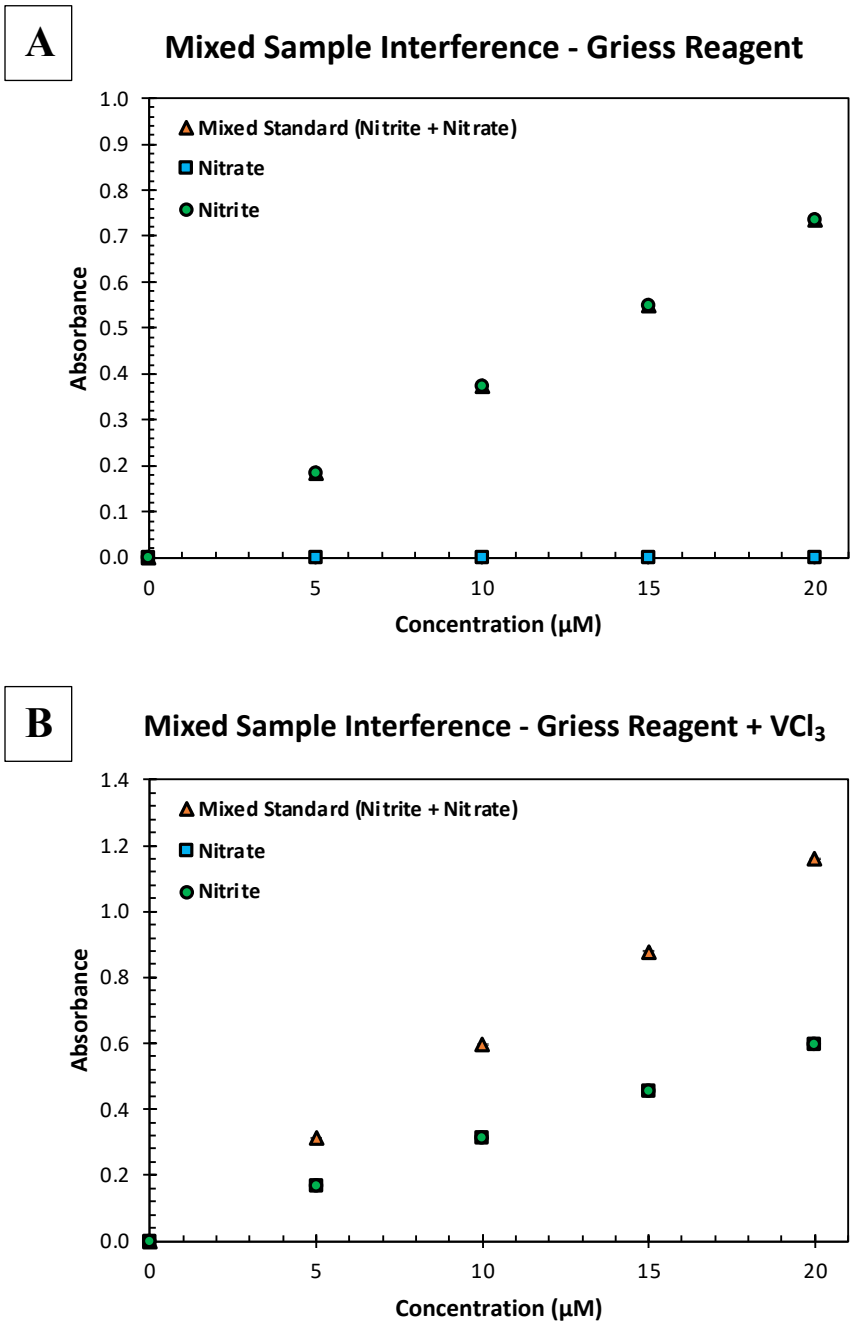

Figure 3.7. *Calibration curve of nitrite, nitrate and mixed standards, showing (A) nitrite detection and (B) combined nitrite and nitrate detection. The error bars represent the standard deviations for n=3.*

Figure 3.8 and table 3.1 shows the determination of nitrate in a mixed sample from the measurement of nitrite using the griess assay and the combined absorbance measured using Greiss reagent and vanadium chloride III as described above. The results show that nitrate can be accuaretly quantified in the presence of nitrite with the proposed *two-part* method with an average % Relative Error of 0.38% between the calculated concentration and the expected concentration.

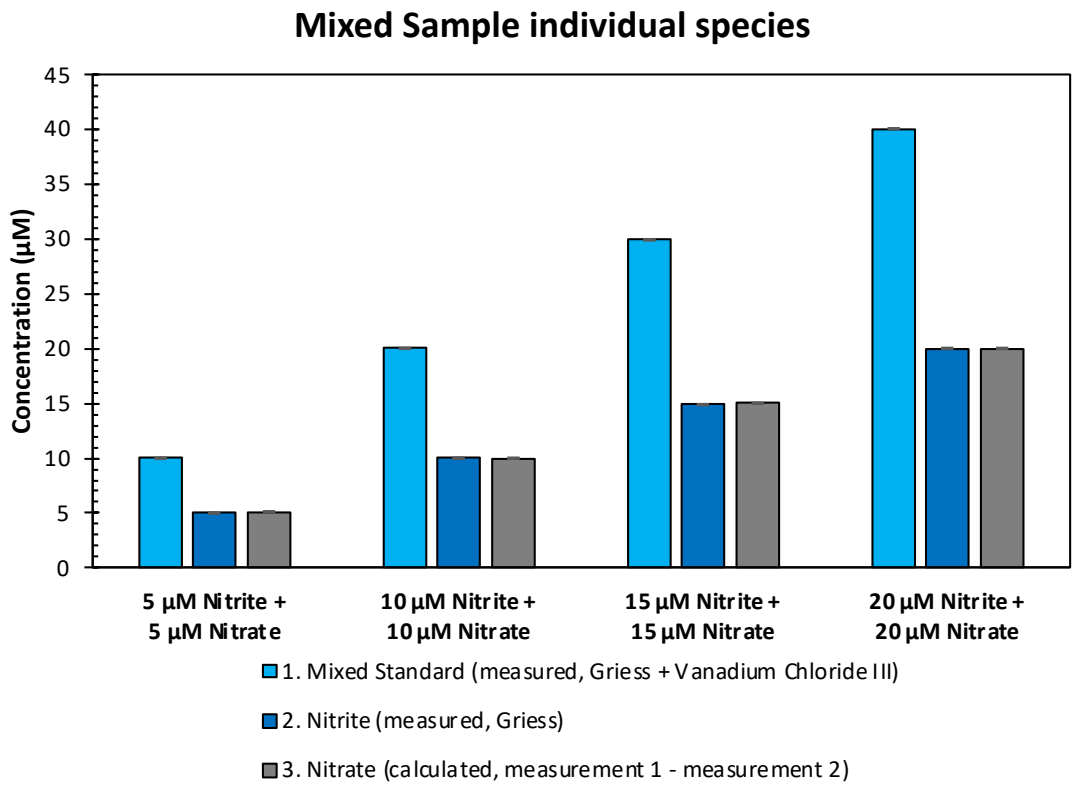

Figure 3.8. *Determination of individual species in mixed samples containing nitrite and nitrate.*

Table 3.1. *Summary of calculated nitrate from measured nitrite and measured combined nitrite + nitrate.*

Mixed Samples (Nitrite + Nitrate)				
Sample	Mixed Standard	Nitrite	Nitrate	Nitrate %RE
5 µM Nitrite + 5 µM Nitrate	10.08	5.00	5.08	1.56
10 µM Nitrite + 10 µM Nitrate	20.02	10.03	9.99	-0.15
15 µM Nitrite + 15 µM Nitrate	29.99	14.97	15.02	0.12
20 µM Nitrite + 20 µM Nitrate	40.01	20.02	19.99	-0.02

3.3.2. Heater Selection and Characterisation

Following characterisation of the colorimetric method for nitrate detection the heated fluidic cell was validated and optimised.

3.3.2.1. Heater Characterisation – Voltage Control

Using a Power Supply Unit (Aim TTi EL183R 18V 3A Power Supply) the heat output of the silicone heater mat (RS Pro Silicone heater mat 1.25 W, 25x50mm, 12 V DC) was recorded over a one-hour period at a series of voltages, 3.3 V, 6 V, 9 V, 12 V and 14.4 V. The voltages selected were chosen due to the availability of common power regulators at these values. This test was carried out in an uninsulated open bench setup with a room temperature of 22 °C. Figure 3.9. presents the temperature output of the heated PMMA chip at each described voltage and is summarised in table 3.2. There was a linear increase between temperature and voltage at the tested values when sufficient current (unlimited) was allowed to be drawn at the selected voltages. A boost convertor can also be attached to the circuit to increase the max temperature and speed of heat generated; a comparison can be seen in supplementary information figure SI.3.4.

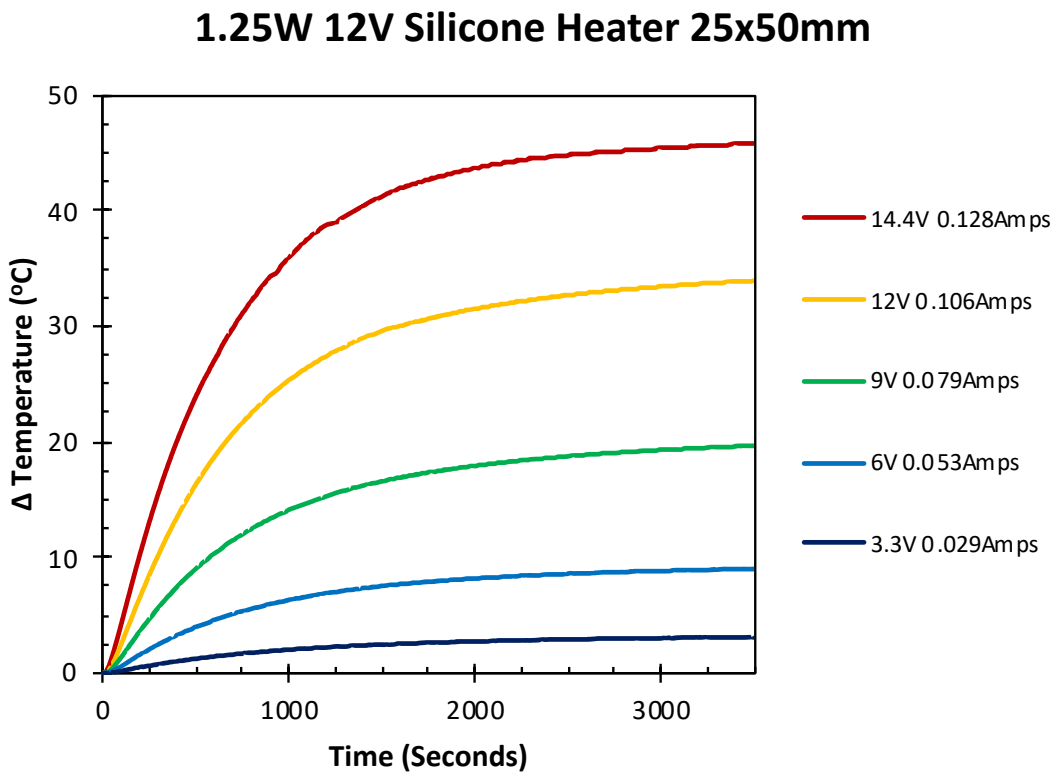

Figure 3.9. *Measured output of silicone heater attached to PMMA fluidic chip at 3.3 V, 6 V, 9 V, 12 V and 14.4 V over a period of one hour.*

Table 3.2. *Measured output of silicone heater attached to PMMA fluidic chip at 3.3 V, 6 V, 9 V, 12 V and 14.4 V over a period of one hour.*

Set Voltage	Power Draw (amps)	Max heat output (°C)
3.3	0.029	3.12
6	0.053	9.19
9	0.079	19.75
12	0.106	34.03
14.4	0.128	45.84

3.3.2.2. Temperature Regulation and Validation (feedback thermostat loop)

It was important to regulate temperature digitally rather than by current allowing for the selection of a desired value which could be maintained regardless of changing external environment temperatures. This was important if the heating element was to be used in non-temperature-controlled laboratory settings such as environmental deployments where changing weather conditions and day and night cycles would affect the external temperature around the sensor/heater.

The code for the initial temperature regulation circuit can be seen in supplementary information Figure SI.3.5. The temperature regulator was setup in a feedback loop where an upper and lower temperature limit would be set, this value would be measured by the temperature sensor and the microcontroller would turn the heater on or off if the temperature was below or above the defined limits. This setup is summarised in figure 3.10. below.

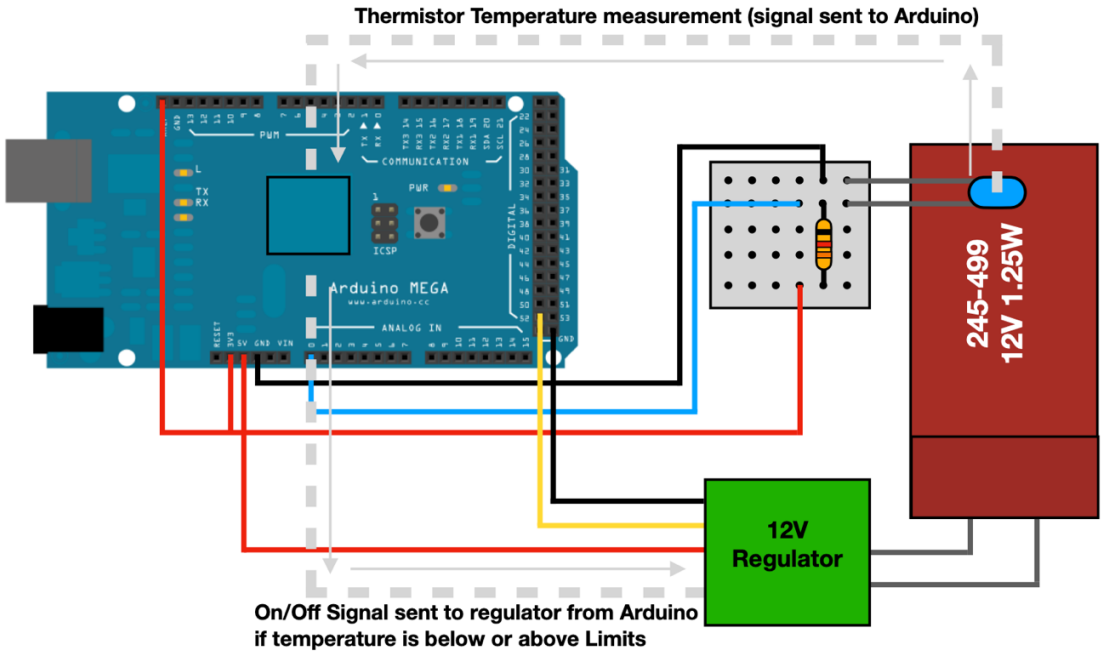

Figure 3.10. *Schematic for feedback loop for temperature regulation using a microcontroller and temperature sensor to trigger the heater on or off.*

Following circuit design the setup was tested using a 12 V regulator to power the heater with an upper limit of 50 °C and a lower limit of 49.5 °C. This experiment was carried out in an uninsulated setup, the heater could be made more efficient using insulation to minimize heat loss during operation and improve power consumption. Figure 3.11. shows performance of the setup with setpoint regulation, an average temperature of 48.93 °C was reached with a high of 50.10 °C and low of 45.05 °C. Due to the open-air uninsulated setup the heat loss when off was quicker than the heat gain, with the heater needing to stay active for 86% of the time. The results showed that using feedback it was possible to regulate the heaters output, but further refinement was necessary beyond on or off setpoints due to the lag in the heater being turned on and it returning to temperature.

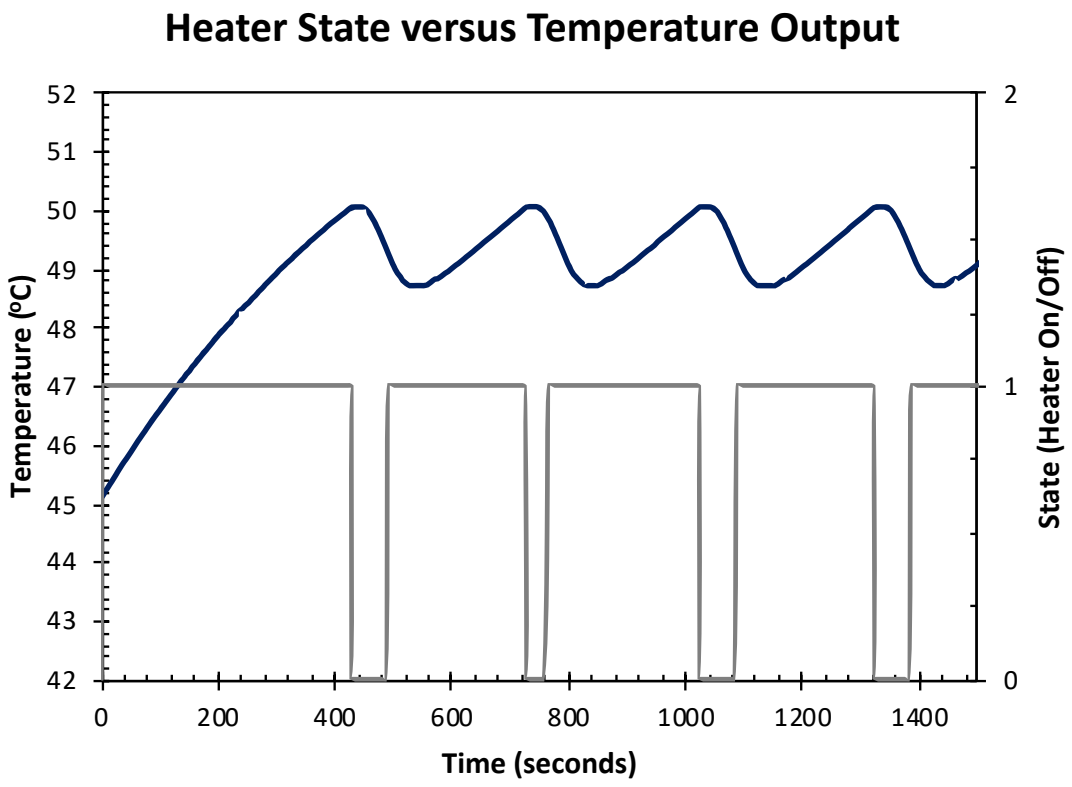

Figure 3.11. *Measured heat of the PMMA fluidic device versus the heaters state (on or off) using the feedback loop.*

3.3.2.3. Integration of PID refinement

Following the initial tests further refinement of the regulation circuit was necessary. This was carried out by using a proportional integral derivative (PID) signal versus a static on or off limit. The PID code can be seen in supplementary information figure SI.3.6. Figure 3.12. shows the improvements made while using PID as well as a comparison of the two methods of regulation in figure 3.13.

The ability to control the power output of the heater within a range gives much higher performance than an on / off programmed setpoint. With PID control the heater held an average temperature of 49.91 °C with a high of 50.17 °C and low of 49.68 °C. With PID control the heater averaged a power output of 55% total usage throughout the run showing greater efficiency than the previous temperature regulation method tested.

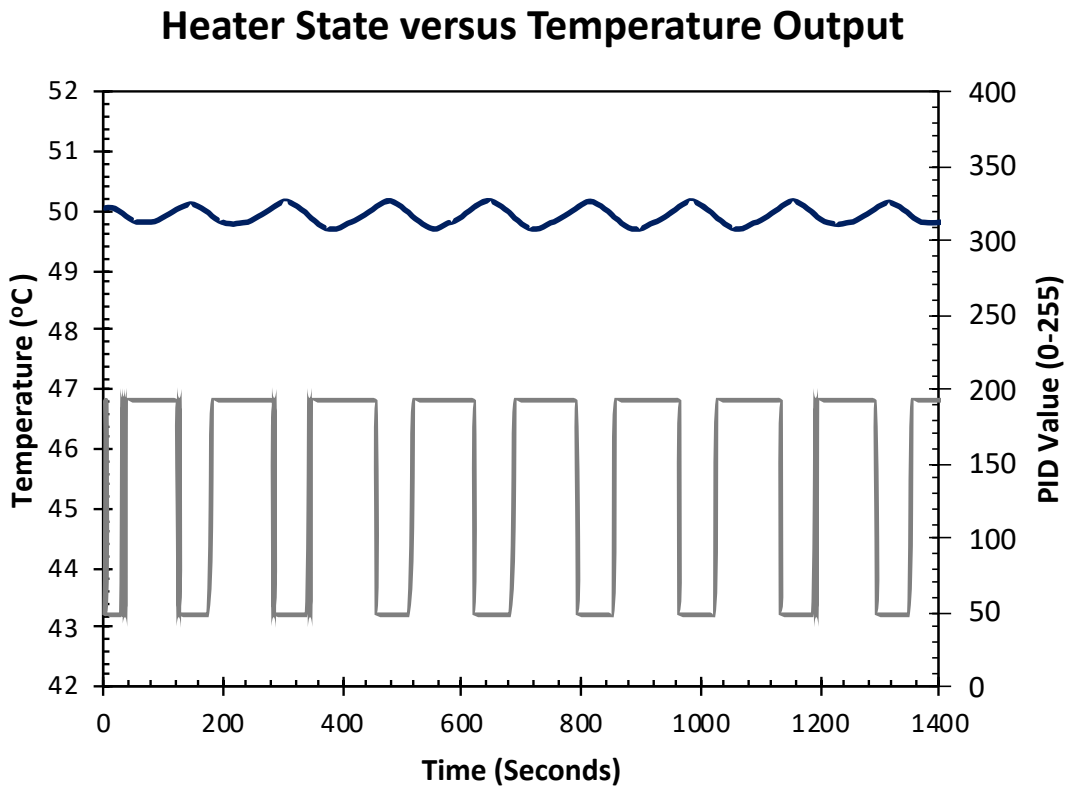

Figure 3.12. *Measured heat of the PMMA fluidic device versus the heaters output using PID control.*

Figure 3.13. shows the improvements made using a PID controller. Further improvements to the PID values could improve the responsiveness of the regulation but overall, a more stable wave was generated. With the on off feedback system there was a greater slope for the heater off phase than the on phase, in the uninsulated setup showing that with the heater off heat was lost quicker than could be gained when turning on the heater, this meant that while uninsulated the heater had to remain on for a longer period than off. With the use of PID and controlling the overall power the slope during cool down and heating up are similar leading to a more stable controlled system. With both regulation methods used temperatures stayed stable with drops in temperature upon sample addition due to the low thermal mass of the cell however these quickly recover (see supplementary information Figure SI.3.7.).

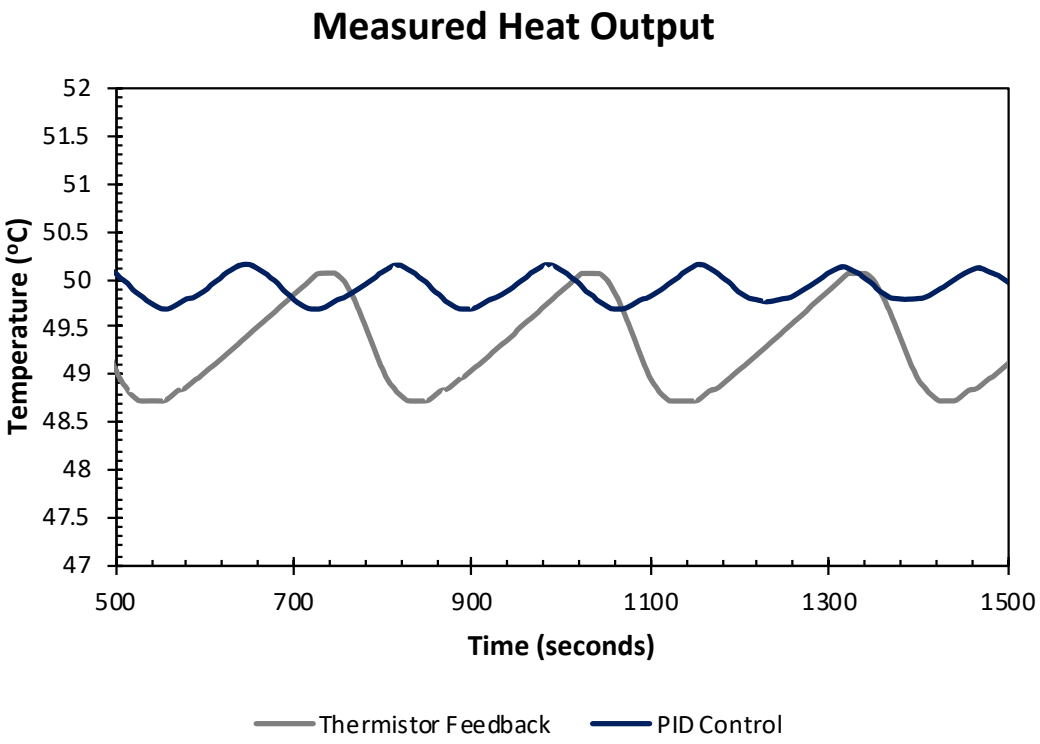

Figure 3.13. *Comparison of the two tested methods of heater regulation, thermistor feedback versus PID control.*

3.3.3. Heated Platform Performance vs UV-Vis Spectrometer

Following optimisation of both the colorimetric method and the heated cell the performance could be compared against a UV-Vis spectrometer.

3.3.3.1. Calibration curve on benchtop sensing platform versus UV-Vis spectrometer.

With the heating characterised detection and nitrate was tested out on the benchtop fluidic system. The heated fluidic chip was set to 60 °C and solutions were loaded on to the chip for detection. Standards of nitrate were loaded onto the chip with vanadium chloride (III) and Griess reagent (9:1:1 v/v) and allowed to react for 1500 seconds before measurement values were taken. Reference measurements were taken in parallel to the benchtop measurements by reacting the same known standards at 60 °C in a temperature-controlled cell before being measured on a UV-Vis spectrometer (Shimadzu UV2600 Photo spectrometer, TCC-100 Temperature controlled cell). 60 °C was chosen based on the kinetic results shown, at temperatures above this bubble generation occurred more frequently within the cell affecting measurements (see

supplementary information figure SI.3.8.). Both benchtop and UV-vis spectrometer measurements were measured at 545nm.

Figure 3.14. shows the on-chip detection of nitrate vs the UV-Vis spectrometer using known standards in a range from 0 – 10 µM and the values are summarised in table 3.2. Both set of results showed a linear response with a correlation coefficient of 0.999. The measurements taken on the Benchtop platform show an increased sensitivity, this is likely due to the greater pathlength of the optical chip (2.25 cm for the fluidic chip and 1 cm for the UV-Vis spectrometer). A dynamic linear range for the benchtop platform of 0-15 µM for nitrate was measured, see supplementary figure SI.3.9. 15 µM was shown to be the upper limit as at concentrations above this point the detectable difference in colour and absorbance values decreased.

The LOD was calculated for the benchtop platform as the concentration equivalent of 3.3 x standard deviation of the blank solution (N=10, 25 data points per blank solution measured), measuring 0.04 µM. The LOQ was calculated at 10 x standard deviation of the blank solution (N=10, 25 data points per blank solution) measuring 0.11 µM.

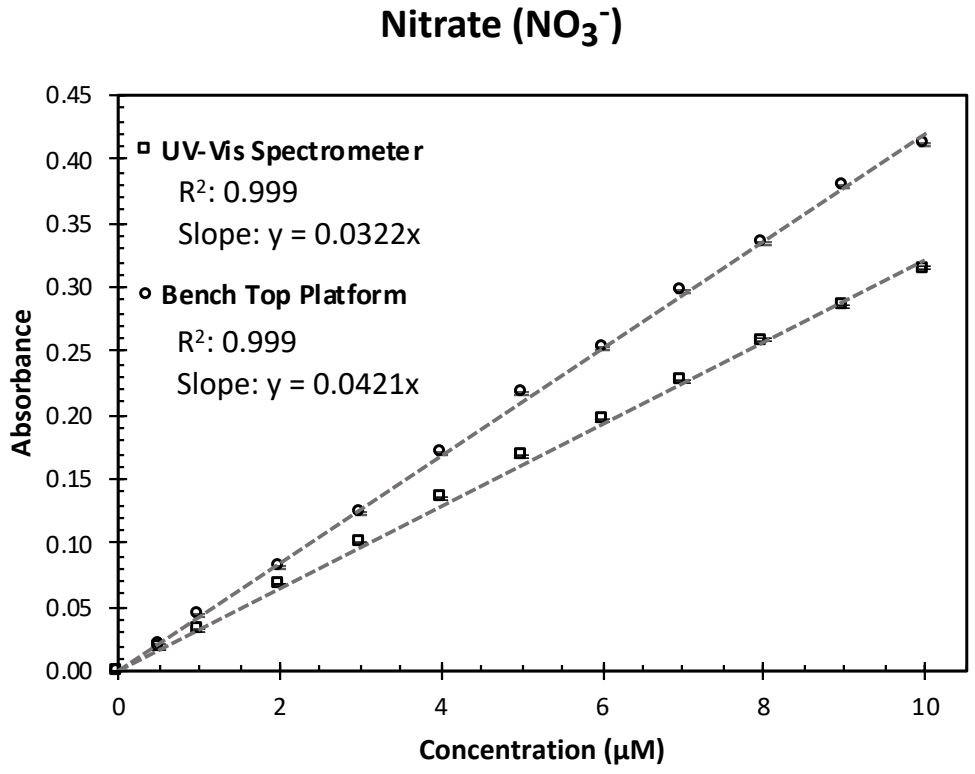

Figure 3.14. *Linear calibration curves for the detection of nitrate 0-10 µM using VCl_3 and Griess reagent on the heated benchtop sensing platform vs UV-Vis spectrometer at 545 nm.*

Table 3.3. *Analytical performance of the heated sensing platform based on data from Figure 3.14.*

Sample	UV-Vis Spectrometer		Bench Top Platform	
NO_3^- (µM)	Mean (µM) ± %RSD	%RE	Mean (µM) ± %RSD	%RE
0.5	0.54 ± 3.87	8.22	0.52 ± 2.34	-3.33
1	1.06 ± 2.26	5.72	1.09 ± 1.06	9.34
2	2.13 ± 1.33	6.59	1.97 ± 0.02	-1.50
3	3.19 ± 1.07	6.62	3.00 ± 0.48	-0.1
4	4.24 ± 0.66	6.16	4.11 ± 0.30	2.63
5	5.29 ± 0.60	5.76	5.22 ± 0.28	4.45
6	6.21 ± 0.56	3.54	6.05 ± 0.16	0.90
7	7.15 ± 0.59	2.20	7.10 ± 0.29	1.44
8	8.17 ± 0.12	2.217	8.03 ± 0.36	0.32
9	9.00 ± 0.37	-0.05	9.09 ± 0.24	1.02
10	9.95 ± 0.65	0.52	9.89 ± 0.34	-1.06

3.3.3.2. Environmental Sampling

The Boyne catchment comprises of 20 sub-catchments with 114 river bodies, 11 lakes, 1 transitional and 3 coastal water bodies, and 25 ground water bodies [27]. The catchment includes a total draining area of 2694 km^2 including the area drained by the river Boyne [27]. The river Boyne is a river in Leinster, Ireland which is 112 km long and rises at Trinity Well, Newberry hall, Co. Kildare and flows northeast through Co. Meath before reaching the Irish sea between Mornington, Co. Meath, and Baltray, Co. Louth [28]. The river Boyne has significant pressures relating to agriculture, peat drainage works, domestic and industrial waste water and diffuse urban sources [27].

Following lab validation using standards of known concentration, six environmental samples of unknown concentration were taken from the river Boyne across a 7 km transect starting at Stackallen Weir, Stackallen, Co. Meath and finishing at Slane Bridge, N2, Fennor, Co. Meath, Ireland. The river Boyne was chosen as it was previously identified as being a potential nutrient sensitive area for nitrate pollution in the EU Commissions nitrates directive and urban waste water treatments directive [29]. Figure 3.15. shows a sampling plan of the six grab samples that were taken using weirs

and common landmarks as sampling markers, supplementary information figure SI.3.10. shows a scaled version of the sampling map to give context to the site's location across the greater Boyne catchment. The samples were taken using the same method as **chapter 2** where samples were taken via kayak at a depth of 10cm below the surface and stored on ice in the dark as they were collected. Each sample was taken using prewashed 50 mL centrifuge tubes (50 mL centrifuge tube, graduated sterile skirted purple cap, VWR 525-0024), the six samples were taken over a one-and-a-half-hour period with the times and location included in table 3.3.

At the time of sampling (01/01/2021) there was 12.9 mm of rainfall recorded in the previous 7 day period and 84.4 mm of rainfall in previous 30 day period [30] with river levels and flow being high as a result (171 cm measured at the sampling location 5 [31]). On completion of the transect, the samples were immediately frozen at -20 °C prior to analysis. On return to lab the samples were thawed, homogenised, and immediately filtered through a 0.22 µm Durapore PVDF membrane filter. The filtrate was analysed for nitrite and nitrate on both UV-Vis spectrometer (Shimadzu UV-2600 UV-Vis) and the heated benchtop sensing platform. The results can be seen in figure 3.16. and summarised in table 3.4.

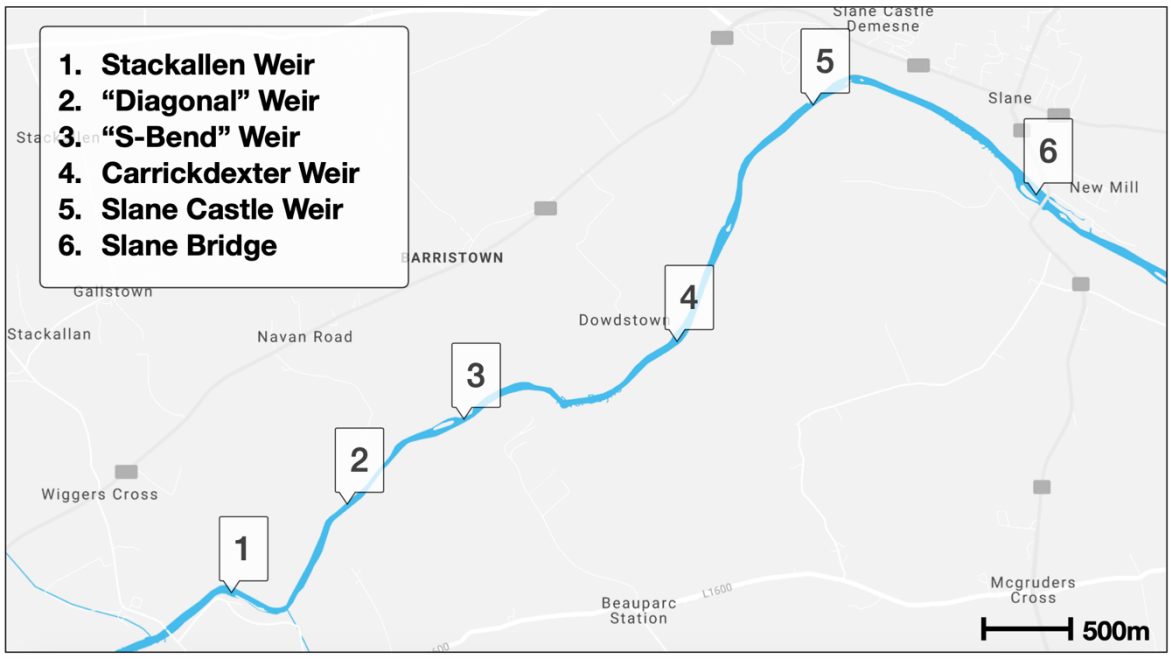

Figure 3.15. *Environmental Sampling map showing ten sampling points along the river Boyne.*

Table 3.4. *Sampling log sheet showing date, time, and sampling location.*

Sample:	Date and Time:	Location:	Coordinates:
1	01/01/2021 09:12	Stackallen Weir	53.68552527864036, -6.6050148010253915
2	01/01/2021 09:28	"Diagonal Weir"	53.689794812945905, -6.595745086669923
3	01/01/2021 09:39	"S-Bend" Weir	53.69392274609994, -6.586647033691407
4	01/01/2021 10:01	Carrickdexter Weir	53.69945049710343, -6.56810760498047
5	01/01/2021 10:20	Slane Castle Weir	57.70534457578036, -6.564159393310548
6	01/01/2021 10.40	Slane Bridge	57.70402346924484, -6.541328430175782

Figure 3.16. shows the measured concentrations of the samples taken from the river Boyne for (A) nitrite and (B) nitrate, supplementary information figure SI.3.11. shows the combined measured value for nitrite and nitrate. Nitrate results were generated using samples that had been diluted 1:10 prior to analysis to fit within the working range of the calibration curve. The results were measured both on the heated benchtop sensing platform and, on the UV-Vis spectrometer. The results for both methods trend well together with the results summarised in table 3.4. An average of 1.7% relative error was seen for nitrite and an average of 1.4% relative error was seen for nitrate when analysed on the heated benchtop platform in comparison to the UV-Vis spectrometer. The results showed low levels of nitrites and nitrates at the time of sampling the six points measured with an average nitrite concentration of 0.66 µM and an average nitrate concentration of 41.66 µM on the heated benchtop sensing platform.

An increasing trend in nitrates was seen as the samples moved downstream towards Slane urban centre and surrounding agricultural land.

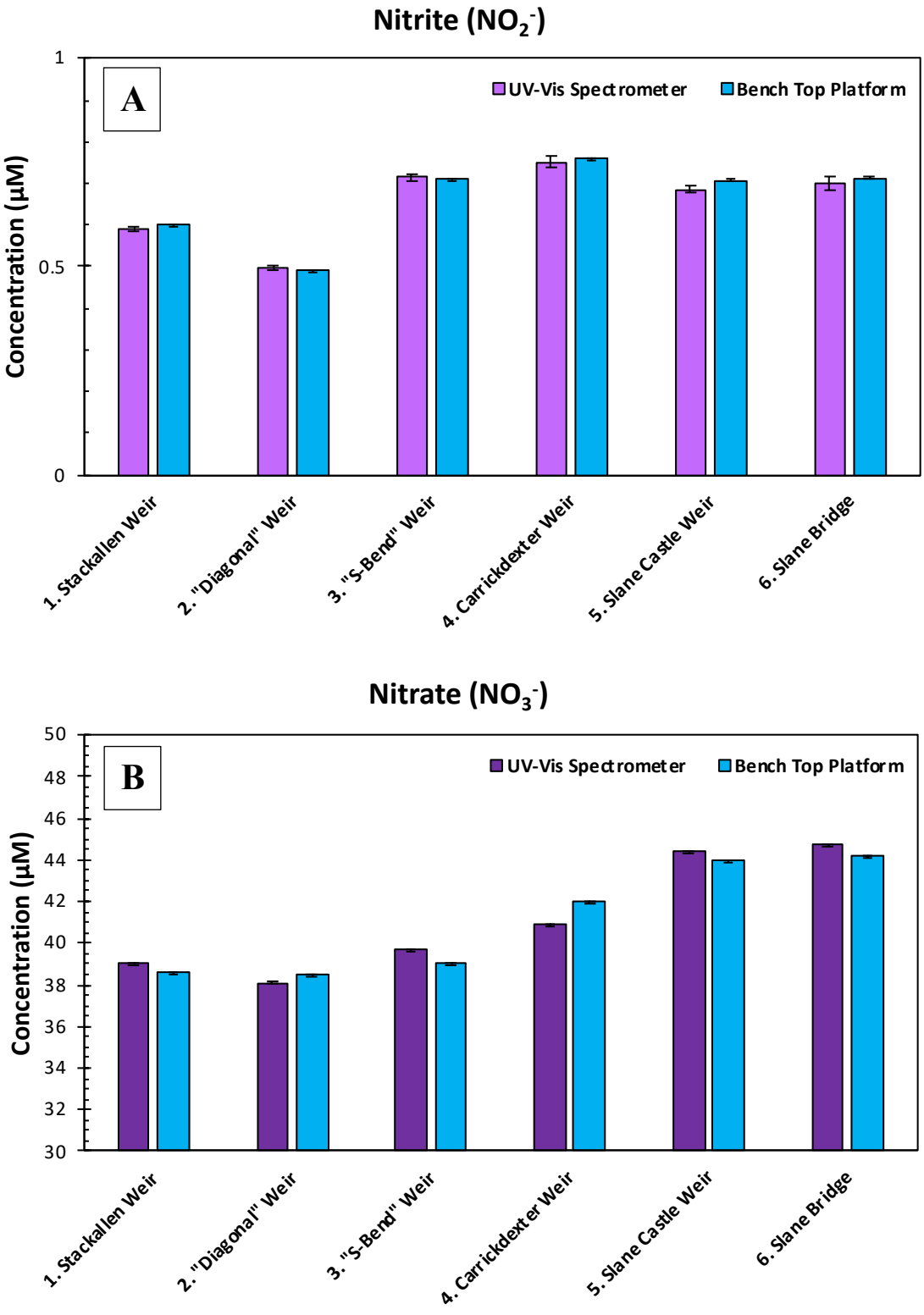

Figure 3.16. *Nutrient concentrations measured across the six sampling points along the river Boyne for (A) nitrite and (B) nitrate.*

Table 3.5. *Summary of nitrite and nitrate concentrations measured across the six sampling points.*

Nitrite (NO_2^-) (µM)			
Sample	**UV-Vis Spectrometer**	**Bench Top Platform**	**% Relative Error**
1. Stackallen Weir	0.59	0.60	1.41
2. "Diagonal" Weir	0.50	0.49	-1.74
3. "S-Bend" Weir	0.72	0.71	-0.61
4. Carrickdexter Weir	0.75	0.76	1.41
5. Slane Castle Weir	0.69	0.71	3.08
6. Slane Bridge	0.70	0.71	1.72
Nitrate (NO_3^-) (µM)			
Sample	**UV-Vis Spectrometer**	**Bench Top Platform**	**% Relative Error**
1. Stackallen Weir	39.00	38.86	-1.11
2. "Diagonal" Weir	38.11	38.48	0.97
3. "S-Bend" Weir	39.70	39.61	-1.74
4. Carrickdexter Weir	40.93	41.11	2.66
5. Slane Castle Weir	44.38	43.97	-0.92
6. Slane Bridge	44.80	44.90	-1.23

3.4. Conclusion

The development of a heated fluidic cell was presented. The heating element was characterised, and the output was evaluated. A temperature measurement and regulation circuit and code were developed to further enhance the performance of the heater. With this addition the heated cell could maintain regulated temperature regardless of external conditions once sufficient power and current were given. The use of heat within the cell allowed for regulation of room temperature reactions such as the detection of nitrite as well as allowing for reactions that require higher temperatures such as the reduction of nitrate to nitrite using VCl_3.

The combination of the heated fluidic cell with a benchtop sensing platform allowed for the detection of nitrite and nitrate on chip with both known standard solutions and

environmental samples. The heated benchtop sensing platform showed an excellent correlation for nitrite and nitrate for the 11 standards and 6 river samples that were measured with results that trended well versus a UV-Vis spectrometer.

The calibrations showed that the benchtop sensing platform gave an improved response for nitrate detection in comparison to the UV-Vis spectrometer. The benchtop sensing platform showed a reduced linear dynamic range in comparison to the UV-Vis spectrometer with a reduction in the upper range from 40 μM to 15 μM for nitrate, the same result as seen in chapter 2 for nitrite. This lower working range restricts the ability to measure samples on the benchtop sensing platform with a combined concentration above 15 μM without the need for sample dilution. It was required to carry out a dilution of the environmental samples tested to bring the combined nitrite and nitrate concentrations within the working range of both the UV-Vis spectrometer and benchtop sensing platform. This need for dilutions in areas above the working range will complicate automation of future sensors, this complication could be reduced with improvements to the working range or partial reaction of the samples to produce a less intense colour portion.

The methods presented show potential for moving towards flow through autonomous sensors however with significant complications. The use of multiple reagents further complicates autonomous sensing with the need for individual storage of each reagent as well as requiring complex fluidics to accurately transport these reagents and sample to the fluidic chip. The procedure can be simplified by using a single mixed reagent consisting of combined Griess and vanadium chloride III [18,32–34]. With this approach the fluidics can be simplified however the stability of the mixed reagent must then be considered as a potential limiting factor for extended deployments. Wang et al. has reported that at room temperature the mixed reagent is stable for up to nine days and can be used for a further 4 weeks but with a reduction in sensitivity up to 50%, similarly O et al. reports a stability of two weeks [34] and Schnetger et al reports a mixed reagent stability of one month [18]. Purging of the mixed reagent and storage out of light have been suggested to extend the stability of the reagent [32,33]. The work presented in this chapter highlights the possibility of direct detection of heated

colorimetric reactions on chip however further refinement is necessary to reduce complication when moving towards autonomous sensing platforms.

3.8. References

(1) *Guidelines for Drinking-Water Quality*, 4th ed.; World Health Organization, Ed.; World Health Organization: Geneva, 2011.

(2) Ward, M. H.; Jones, R. R.; Brender, J. D.; de Kok, T. M.; Weyer, P. J.; Nolan, B. T.; Villanueva, C. M.; van Breda, S. G. Drinking Water Nitrate and Human Health: An Updated Review. *Int J Environ Res Public Health* **2018**, *15* (7). https://doi.org/10.3390/ijerph15071557.

(3) Bijay-Singh; Craswell, E. Fertilizers and Nitrate Pollution of Surface and Ground Water: An Increasingly Pervasive Global Problem. *SN Appl. Sci.* **2021**, *3* (4), 518. https://doi.org/10.1007/s42452-021-04521-8.

(4) Musacchio, A.; Re, V.; Mas-Pla, J.; Sacchi, E. EU Nitrates Directive, from Theory to Practice: Environmental Effectiveness and Influence of Regional Governance on Its Performance. *Ambio* **2020**, *49* (2), 504–516. https://doi.org/10.1007/s13280-019-01197-8.

(5) Wang, H.; Gao, J.; Li, X.; Zhang, S.; Wang, H. Nitrate Accumulation and Leaching in Surface and Ground Water Based on Simulated Rainfall Experiments. *PLoS ONE* **2015**, *10* (8), e0136274. https://doi.org/10.1371/journal.pone.0136274.

(6) Feng, W.; Wang, C.; Lei, X.; Wang, H.; Zhang, X. Distribution of Nitrate Content in Groundwater and Evaluation of Potential Health Risks: A Case Study of Rural Areas in Northern China. *IJERPH* **2020**, *17* (24), 9390. https://doi.org/10.3390/ijerph17249390.

(7) US EPA, O. The Effects: Dead Zones and Harmful Algal Blooms https://www.epa.gov/nutrientpollution/effects-dead-zones-and-harmful-algal-blooms (accessed 2021 -06 -17).

(8) Nitrate Water Pollution https://storymaps.arcgis.com/stories/e7e6ec676acb4cc58d3d35e914efc207 (accessed 2021 -06 -17).

(9) Sahoo, P. K.; Kim, K.; Powell, M. A. Managing Groundwater Nitrate Contamination from Livestock Farms: Implication for Nitrate Management Guidelines. *Curr*

Pollution Rep **2016**, *2* (3), 178–187. https://doi.org/10.1007/s40726-016-0033-5.

(10) Government of Ireland, Department of Housing, Planning and Local Govenment. Significant Water Management Issues in Ireland - Public Consultation Document https://assets.gov.ie/78373/30d96d3b-a09c-431c-a3ee-790668e35e57.pdf (accessed 2021 -06 -10).

(11) Mellander, P.-E.; Jordan, P.; Bechmann, M.; Fovet, O.; Shore, M. M.; McDonald, N. T.; Gascuel-Odoux, C. Integrated Climate-Chemical Indicators of Diffuse Pollution from Land to Water. *Sci Rep* **2018**, *8* (1), 944. https://doi.org/10.1038/s41598-018-19143-1.

(12) Mockler, E. M.; Deakin, J.; Archbold, M.; Gill, L.; Daly, D.; Bruen, M. Sources of Nitrogen and Phosphorus Emissions to Irish Rivers and Coastal Waters: Estimates from a Nutrient Load Apportionment Framework. *Science of The Total Environment* **2017**, *601–602*, 326–339. https://doi.org/10.1016/j.scitotenv.2017.05.186.

(13) Howden, N. J. K.; Burt, T. P.; Worrall, F.; Mathias, S.; Whelan, M. J. Nitrate Pollution in Intensively Farmed Regions: What Are the Prospects for Sustaining High-Quality Groundwater?: NITRATE POLLUTION IN INTENSIVELY FARMED REGIONS. *Water Resour. Res.* **2011**, *47* (6). https://doi.org/10.1029/2011WR010843.

(14) Mas-Pla, J.; Menció, A. Groundwater Nitrate Pollution and Climate Change: Learnings from a Water Balance-Based Analysis of Several Aquifers in a Western Mediterranean Region (Catalonia). *Environ Sci Pollut Res* **2019**, *26* (3), 2184–2202. https://doi.org/10.1007/s11356-018-1859-8.

(15) Sebilo, M.; Mayer, B.; Nicolardot, B.; Pinay, G.; Mariotti, A. Long-Term Fate of Nitrate Fertilizer in Agricultural Soils. *Proceedings of the National Academy of Sciences* **2013**, *110* (45), 18185–18189. https://doi.org/10.1073/pnas.1305372110.

(16) Wick, K.; Heumesser, C.; Schmid, E. Groundwater Nitrate Contamination: Factors and Indicators. *Journal of Environmental Management* **2012**, *111*, 178–186. https://doi.org/10.1016/j.jenvman.2012.06.030.

(17) García-Robledo, E.; Corzo, A.; Papaspyrou, S. A Fast and Direct Spectrophotometric Method for the Sequential Determination of Nitrate and

Nitrite at Low Concentrations in Small Volumes. *Marine Chemistry* **2014**, *162*, 30–36. https://doi.org/10.1016/j.marchem.2014.03.002.

(18) Schnetger, B.; Lehners, C. Determination of Nitrate plus Nitrite in Small Volume Marine Water Samples Using Vanadium(III)Chloride as a Reduction Agent. *Marine Chemistry* **2014**, *160*, 91–98. https://doi.org/10.1016/j.marchem.2014.01.010.

(19) Thermistor https://learn.adafruit.com/thermistor/overview (accessed 2021 -03 -09).

(20) Kaye, J. E.; Zaidi, A. J.; Nostedt, J. M. SCIENTIFIC MONITORING TECHNIQUES FOR EVALUATING THE PERFORMANCE OF SOLAR HOT WATER HEATING SYSTEMS. In *Energy Developments: New Forms, Renewables, Conservation*; Curtis, F. A., Ed.; Pergamon, 1984; pp 163–168. https://doi.org/10.1016/B978-0-08-025407-4.50036-3.

(21) Kim, J.; Kim, J. D. Voltage Divider Resistance for High-Resolution of the Thermistor Temperature Measurement. *Measurement* **2011**, *44* (10), 2054–2059. https://doi.org/10.1016/j.measurement.2011.08.004.

(22) Ali, A. S.; Zanzinger, Z.; Debose, D.; Stephens, B. Open Source Building Science Sensors (OSBSS): A Low-Cost Arduino-Based Platform for Long-Term Indoor Environmental Data Collection. *Building and Environment* **2016**, *100*, 114–126. https://doi.org/10.1016/j.buildenv.2016.02.010.

(23) O'Toole, M.; Shepherd, R.; Lau, K.-T.; Diamond, D. Detection of Nitrite by Flow Injection Analysis Using a Novel Paired Emitter-Detector Diode (PEDD) as a Photometric Detector. In *Advanced Environmental, Chemical, and Biological Sensing Technologies V*; Vo-Dinh, T., Lieberman, R. A., Gauglitz, G., Eds.; International Society for Optics and Photonics: Boston, MA, 2007; p art no. 67550P. https://doi.org/10.1117/12.737791.

(24) Tsikas, D. Analysis of Nitrite and Nitrate in Biological Fluids by Assays Based on the Griess Reaction: Appraisal of the Griess Reaction in the l-Arginine/Nitric Oxide Area of Research. *Journal of Chromatography B* **2007**, *851* (1–2), 51–70. https://doi.org/10.1016/j.jchromb.2006.07.054.

(25) Miranda, K. M.; Espey, M. G.; Wink, D. A. A Rapid, Simple Spectrophotometric Method for Simultaneous Detection of Nitrate and Nitrite. *Nitric Oxide* **2001**, *5* (1), 62–71. https://doi.org/10.1006/niox.2000.0319.

(26) Conductivity, Salinity & Total Dissolved Solids https://www.fondriest.com/environmental-measurements/parameters/water-quality/conductivity-salinity-tds/ (accessed 2021 -05 -13).

(27) EPA. Boyne Catchment Assessment 2010-2015 (HA 07) EPA Catchment Science Unit. https://catchments.ie/wp-content/files/catchmentassessments/07%20Boyne%20Catchment%20Summary%20WFD%20Cycle%202.pdf (accessed 2021 -06 -17).

(28) Quinn, R.; Boland, D. The Role of Time-Lapse Bathymetric Surveys in Assessing Morphological Change at Shipwreck Sites. *Journal of Archaeological Science* **2010**, *37* (11), 2938–2946. https://doi.org/10.1016/j.jas.2010.07.005.

(29) European Commission, DG Environment Verification of Vulnerable Zones Identified under the Nitrates Directive and Sensitive Areas Identified under the Urban Wastewater Treatment Directive IRELAND https://ec.europa.eu/environment/water/water-urbanwaste/pdf/ireland.pdf (accessed 2021 -02 -01).

(30) Historical Data - Met Éireann - The Irish Meteorological Service https://www.met.ie/climate/available-data/historical-data (accessed 2021 -01 -01).

(31) Realtime waterlevel https://waterlevel.ie/0000007012/0001/week/ (accessed 2021 -01 -01).

(32) Doane, T. A.; Horwáth, W. R. Spectrophotometric Determination of Nitrate with a Single Reagent. *Analytical Letters* **2003**, *36* (12), 2713–2722. https://doi.org/10.1081/AL-120024647.

(33) Wang, S.; Lin, K.; Chen, N.; Yuan, D.; Ma, J. Automated Determination of Nitrate plus Nitrite in Aqueous Samples with Flow Injection Analysis Using Vanadium (III) Chloride as Reductant. *Talanta* **2016**, *146*, 744–748. https://doi.org/10.1016/j.talanta.2015.06.031.

(34) O, I.; Maa, A.-B.; L, H.; Jl, F.; Ml, R.; Jh, M. Validation of a Spectrophotometric Procedure for Determining Nitrate in Water Samples. *J Environ Toxicol Stud* **2018**, *2* (1). https://doi.org/10.16966/2576-6430.113.

Chapter 4

Development of a Cost-Effective Sensing Platform for Monitoring Phosphate in Natural Waters

---

Andrew Donohoe [a], Gareth Lacour [a], Peter McCluskey [a], Dermot Diamond [a] and Margaret McCaul [a].

[a.] Insight Centre for Data Analytics National Centre for Sensor Research, Dublin City University, Glasnevin, Dublin 9, Ireland

Development of a Cost-Effective Sensing Platform for Monitoring Phosphate in Natural Waters, ***published in:*** *Chemosensors* **2018**, *6* (4), 57–69
https://doi.org/10.3390/chemosensors6040057

Abstract

A sensing platform for the in situ, real-time analysis of phosphate in natural waters has been realised using a combination of microfluidics, colorimetric reagent chemistries, low-cost LED-based optical detection, and wireless communications. Prior to field deployment, the platform was tested over a period of 55 days in the laboratory during which a total of 2682 autonomous measurements were performed (854 each of sample, high standard, and baseline, and 40 × 3 spiked solution measurements). The platform was subsequently field deployed in a freshwater stream at Lough Rea, Co. Galway, Ireland, to track changes in phosphate over a five-day period. During this deployment, 165 autonomous measurements (55 each of sample, high standard, and baseline) were performed and transmitted via general packet radio service (GPRS) to a web interface for remote access. Increases in phosphate levels at the sampling location coincident with rainfall events (min 1.45 μM to max 10.24 μM) were detected during the deployment. The response was found to be linear up to 50 μM PO_4^{3-}, with a lower limit of detection (LOD) of 0.09 μM. Laboratory and field data suggest that despite the complexity of reagent-based analysers, they are reasonably reliable in remote operation, and offer the best opportunity to provide enhanced in situ chemical sensing capabilities. Modifications that could further improve the reliability and scalability of these platforms while simultaneously reducing the unit cost are discussed.

Keywords: Water quality; Nutrients; Phosphate; Eutrophication; Colorimetric chemistries; Fluidics; Autonomous analysers.

4.1. Introduction

Excessive nutrient loading in both fresh and marine ecosystems can have adverse effects on aquatic ecosystems [1]. Eutrophication as a result of elevated nutrients levels can result in the formation of harmful algal blooms leading to oxygen depletion, the release of algal toxins, formation of dead zones and contamination of drinking water supplies [2]. Impacts to drinking water supplies and aquatic ecosystems caused by excessive nutrient concentrations are estimated to cost US $210 billion annually in the US alone [3]. Traditionally, phosphate levels in natural water are taken by manual collection and subsequent laboratory analysis [4]. This process is not only labour intensive and costly but provides limited information regarding the spatial and temporal variation of the nutrient concentrations within the waterbody. Real-time monitoring provides reliable in situ measurements, which can provide spatial data that can enhance our understanding of the processes that drive increases in nutrient levels [5]. This data can be used to strengthen the development of projection models for mitigation measures to reduce economic and environmental impacts caused by nutrient stresses [6]. In recent years, advances in rapid prototyping related to 3D printing and fabrication technologies have dramatically improved the efficiency of producing in situ reagent-based analysers for monitoring key environmental parameters, such as phosphate levels in natural waters [7,8]. This improved prototyping efficiency is opening the way to more effective analytical platforms, combined with lower unit costs, higher frequency sampling, and longer service intervals for sensing platforms for nutrients (PO_4^{3-}, NO_2^- and NO_3^-) and other analytical targets in natural waters. Despite these advances, measurement uncertainty, reliability, robustness, and cost of in situ analysers for long term deployments still significantly inhibit wide scale deployments necessary to generate data with enhanced spatial and temporal frequency to meet user and regulatory requirements. For example, the Marine Strategy Framework Directive (MSFD) and Water Framework Directive states that all member states must implement cost effective measures to obtain good environmental status (GES) by 2020 [9,10], thus driving the need for devices capable of providing in situ data at an acceptable unit cost. In this chapter, the development of an autonomous sensing platform for the detection of phosphate in natural waters with significantly improved operational performance and potentially much reduced cost of ownership is described. In comparison to earlier work [11,12],

key components have been further optimised in terms of design and performance using rapid prototyping techniques such as 3D printing, laser ablation and microfabrication. The sensing platform is completely autonomous, incorporating sampling, automatic calibration, waste containment, and wireless communication. Automation is achieved via Arduino microcontrollers, while low-cost pumps and solenoid valves allow precise fluidic handling. Microfluidic technologies have been employed for sample–reagent (1:1) mixing using shear forces in a serpentine channel, followed by colorimetric detection via an integrated 2.25 cm path length flow cell using a pulse width modulated LED, coupled with an in-line photodiode detector. The sensing platform has a linear detectable range up to 50μM PO_4^{3-} and a limit of detection (LOD) of 0.09 μM PO_4^{3-}.

4.2. Materials and methods

The sensing platform presented in Figure 4.1. is designed to fully automate the molybdovanadophosphoric 'yellow' colorimetric method for detection of soluble orthophosphate. Orthophosphate rapidly reacts with the reagent under acidic conditions to form a yellow vanamolybdphosphoric acid product with a strong absorbance below 400 nm (λ_{max} = 348 nm). The reagents are stable in storage for at least 12 months, which is a major consideration for autonomous analyser platforms [7].

4.2.1. Reagents and standard preparation

All reagents and standards were prepared using ultra high purity (UHP) water (MilliQ, Millipore, Burlington, MA, USA) and analytical grade chemicals (Sigma Aldrich, St. Louis, MO, USA). The yellow reagent was prepared by dissolving 0.351 g of ammonium metavanadate (Sigma Aldrich) in ~200 mL UHP water with an addition of 95 mL concentrated hydrochloric acid (Sigma Aldrich). Following this, 7.14 g of ammonium molybdate tetrahydrate was added and the resulting solution was made up to 1 L using UHP water. The phosphate standards were prepared by dissolving 0.408 g potassium dihydrogen phosphate (Sigma Aldrich) in UHP water in a 1 L volumetric flask to make a 3 mM stock phosphate solution. This stock solution was further diluted to make up solutions of the known concentration (range 0.05–50 μM). Equal volumes (1:1 ratio) of yellow reagent and standards/samples were mixed and left for 20 minutes to

develop at room temperature. The blank contained equal volumes of yellow reagent and UHP water with no phosphate added. All reagent and standard solutions were tested and validated against reference measurements generated from spectra obtained with a VWR UV-1600PC spectrometer using a wavelength of 375 nm.

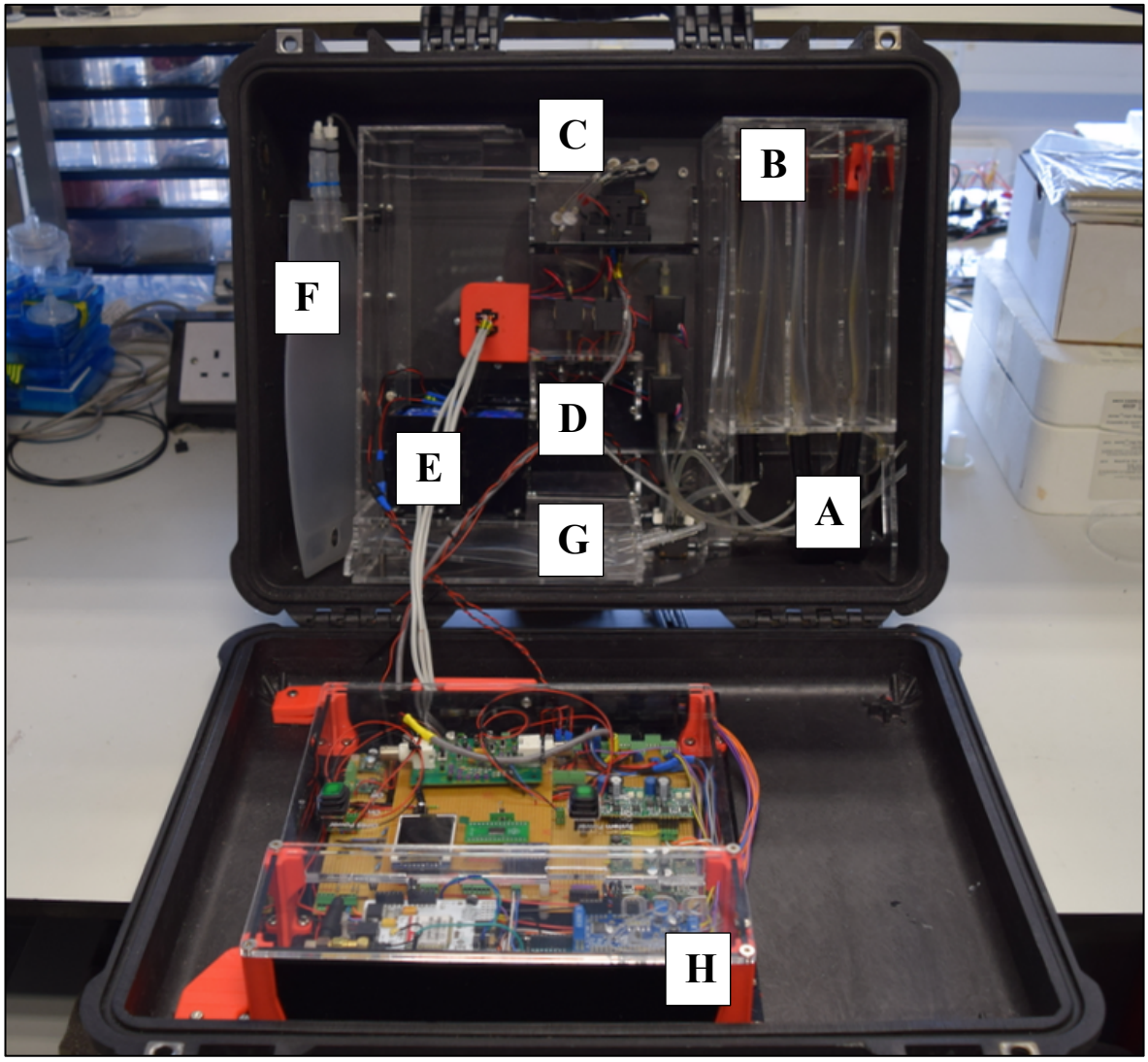

Figure 4.1. *Picture of the autonomous sensing platform. (A) inlet system, (B) bags holding sample, high calibration standard, and low calibration standard, (C) detection chamber housing the microfluidic chip, LED (375 nm), and photodiode, (D) poly (methyl methacrylate) (PMMA) fluidic board, (E) battery, (F) reagent bag, (G) waste bag and (H) electronics.*

4.2.2. Fluidic handling

Fluidic control (see Figure 4.2.) was managed through two 2/2 (hit and hold) and two 3/2 (latching) solenoid valves while pumping was achieved using two piezo electric diaphragm pumps (Figure 4.1.D). The pumps were tested and optimised to deliver a

precise and stable 1:1 ratio to the fluidic chip (Figure 4.1.C) via the sample/standards and reagent input lines (Figure 4.2.). Between measurements, the system was cleaned with UHP water followed by flushing with the standard/sample to minimise any carry over between measurements. The inlet pump (Gardner Denver Thomas GmbH, Germany) was used to draw samples from the external environment through a 0.45 µm, 47 mm Durapore (polyvinylidene difluoride) PVDF filter membrane (Millipore, Burlington, MA, USA) held within a filter holder (Millipore, Burlington, MA, USA) placed on the inlet. During sampling, approximately 300 mL of sample was introduced into a sample reservoir (Figure 4.1.B), from which it was passively drained (Figure 4.1.A). All components were mounted on a laser cut poly methyl methacrylate (PMMA) fluidic board (Figure 4.1.D) using bespoke 3D printed holders.

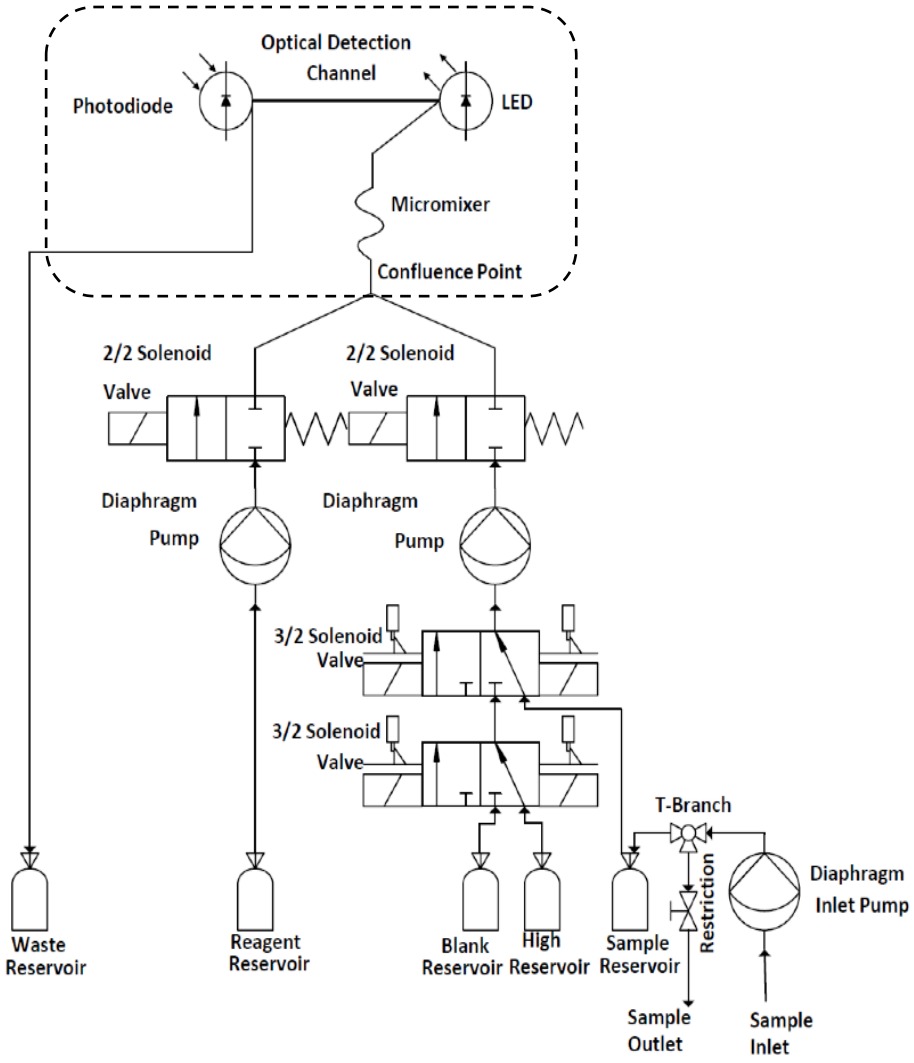

Figure 4.2. *Schematic diagram illustrating the sensing platform fluidic system. The portion including the fluidic chip is within the area bounded by the dashed line.*

4.2.3. Fluidic chip and optical detection

The sensing platform incorporated a detection chamber (Figure 4.1.C) housing the two-layer microfluidic chip (Figure 4.3.) fabricated from opaque PMMA. All channels were micro-machined on the bottom layer using a Datron CAT3D-M6 (Micro Machining Centre). The mixing channel and outlet channel (Figure 4.3.A) were 1000 µm wide × 500 µm deep, and the detection channel was 22.5 mm in length, 1000 µm wide × 1000 µm deep. The top layer sealed the channels and was milled to provide two inlets (sample and reagent) and one outlet (waste). The two opaque PMMA layers were thermally bonded, and the optical windows of the flow cell formed using laser cut 2 mm thick clear PMMA, which were thermally bonded at both ends of the detection channel. The completed chip has a size 52 mm × 22.5 mm × 6 mm (H x W x D) and an internal volume of 212 µL. A 375 nm LED (XSL-375-TF-R2 UV LED, Roithner, Wien, Austria) and photodiode (TSL257-LF, AMS) were used for absorbance detection. Alignment of the LED, chip and photodiode was achieved through a 3D printed (Stratasys Objet260 Connex1) custom designed alignment rail (Figure 4.3.B). A significant design improvement is the incorporation of a rail in the microfluidic chip mount, through which the LED photodiode can be easily removed and replaced while maintaining alignment. This improves the detector's kinematic stability, reduces unit costs, and simplifies servicing of the detection unit.

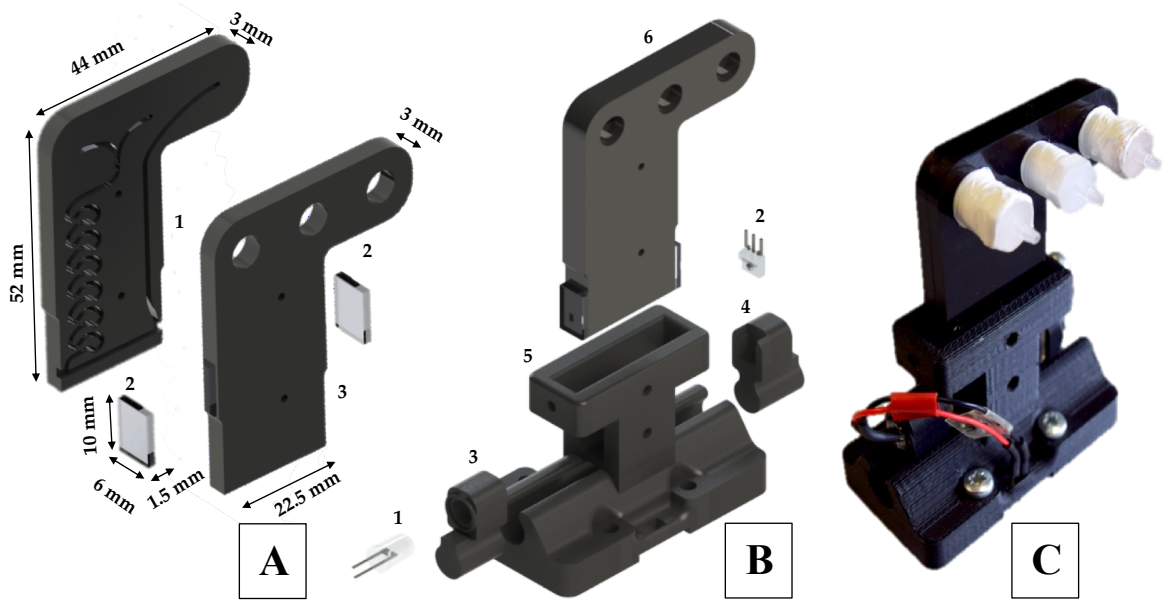

Figure 4.3. *(A) Exploded render of the microfluidic chip showing 1) the top PMMA layer with the milled reagent/sample inlet and waste outlet, 2) the clear PMMA optical windows at each side of the optical channel and 3) the capping layer of the PMMA chip. (B) Render of the microfluidic chip custom 3D printed alignment rail and sliders with detector components: 1) 375 nm UV LED; 2) photodiode; 3) LED slider; 4) photodiode slider; 5) microfluidic chip mount and alignment rail; and 6) microfluidic chip. (C) Image of the fluidic chip integrated into the alignment rail.*

4.2.4. Chassis, housing, and tubing

The sensor platform chassis was fabricated from 4 mm thick clear PMMA panels which were laser cut (Epilog Zing Laser) and solvent bonded together (1,2-Dichloroethane, Sigma Aldrich). The chassis was mounted onto a marine grade stainless steel back plate and housed within a ruggedized casing (Pelican Case 1560) to protect the sensor from liquid ingress and weather. A 1/16″ Tygon™ tubing was used for transport of the analytical fluids to and from the microfluidic chip. Finally, 1/8″ polyethylene tubing was used to convey samples from the external environment into the sensor platform.

4.2.5. Electrical control and transmittance

System control (Figure 4.1.H) was achieved via an Arduino Mega 2560 microcontroller board. The 2/2 solenoid valves and inlet pump were activated through a MOSFET triggering circuit and power regulators, and the 3/2 solenoid valves were controlled through an Arduino Motor Shield. Raw data was transmitted to an online interface via a general packet radio service (GPRS) module (SIM900 GPRS/GSM Shield, Maplin),

controlled through a secondary slave Arduino circuit. The data string transmitted the platform's internal temperature, humidity,pressure via integrated sensors, and bit values for sample and standard measurements. Short range wireless communication was achieved via an integrated Bluetooth module, while an 8 GB SD card connected via a Data Logger Arduino Shield was used for local data storage and data backup.

4.2.6. Analytical performance

The analytical performance of the system was evaluated via laboratory tests using two methods:

Method 1. *Off-Chip Solution Mixing*: Test solutions of known concentrations (0.05–45μM PO_4^{3-}) were pre-mixed off-chip with yellow reagent (1:1 *v*/*v* ratio). The premixed solution was directly infused into the fluidic chip, using a microprocessor-controlled syringe pump (KD Scientific Model 210), at a constant flow rate of 1 mL/min. The flow was then stopped for 1200 seconds to ensure the reaction reached a steady-state condition in the detection channel [8]. For each test solution measurement, an associated blank measurement was obtained (no phosphate present), and the resulting data pairs converted to absorbance using the Beer-Lambert equation [9]: $A = \log (I_o/I)$ where A is absorbance, I_o the blank intensity, and I is the standard intensity. For method validation, the absorbance of the same test solutions was measured using a VWR UV-1600PC photo spectrometer at a wavelength of 375 nm, and the results compared with the absorbance obtained using the fluidic chip (Figure 4.4.).

Method 2. *Chip-based Solution Mixing:* Test solutions of known concentrations (0 μM, 25 μM, and 50 μM PO_4^{3-}) were held in 25 L tanks and automatically introduced into the platform through the inlet pump. Test solutions and yellow reagent mixing (1:1 *v*/*v* ratio) and detection occurred on the fluidic chip. The same stopped flow approach used in Method 1, described above, was applied to allow formation of the yellow phosphate reagent reaction product (1200 seconds) and the absorption was calculated as for Method 1.

4.2.7. Long-term laboratory assessment of the sensing platform in fully autonomous mode

The sensor was allowed to run autonomously within the laboratory with service intervals every 112 readings to evaluate the effect of continuous operation on system components, optimise the platform operational settings, and check reagent/waste volumes (half a day per service). During the testing period (total period 55 days), the nutrient sensor sampled every 70 minutes, with a complete measurement cycle involving measurement of a blank solution (0 μM PO_4^{3-}), followed by a high concentration calibration solution (50 μM PO_4^{3-}), followed by the filtered samples drawn from tanks filled with test solutions of known phosphate concentrations (5.5 μM, 8 μM, 12.5 μM, 25 μM PO_4^{3-}). To prevent any carry over between measurements, the blank/standard lines were flushed with sample or standard to be measured for 1 min prior to each measurement at a flow rate of 1.0 mL/min (fluidic chip dead volume ca. 212 μL). To ensure homogeneity within the tanks, water was continually circulated using aquarium pumps. Aliquots from each tank (test sample), along with aliquots from the internal calibration standard (50 μM PO_4^{3-}) and internal low calibration standard (0 μM PO_4^{3-}) were taken at regular intervals and analysed in parallel with the VWR UV-1600PC spectrometer using a wavelength of 375 nm.

4.2.8. Field deployment

The prototype platform was deployed at Lough Rea, County Galway, Ireland (Figure 4.4.), from the 5th–9th of December 2017. Lough Rea is a circular lake with a radius of approximately 1 km (2.5 km at its longest axis) and a surface area of approximately 3.2 km^2. The underlying geology of the lake is carboniferous limestone. It is fed by springs and a stream, with the main input stream flowing into the southern end of the lake and exiting from the northern end of the lake [10]. Lough Rea lake is designated as a Natural Heritage Area with international importance for waterfowl, and blue flag accreditation for the period 2001–2018 [11]. The prototype nutrient sensor was deployed on a raised platform 50 cm above the water surface located at Lough Rea angler's fish hatchery, which is located at the northern end of the lake approximately 100 m from the lake boundary. The sampling inlet was positioned 1 m below the surface of the water. During deployment, samples were automatically taken and analysed by the platform every 95 minutes. Contemporaneous rainfall data were obtained from the nearby Athenry Met Eireann weather monitoring station [12].

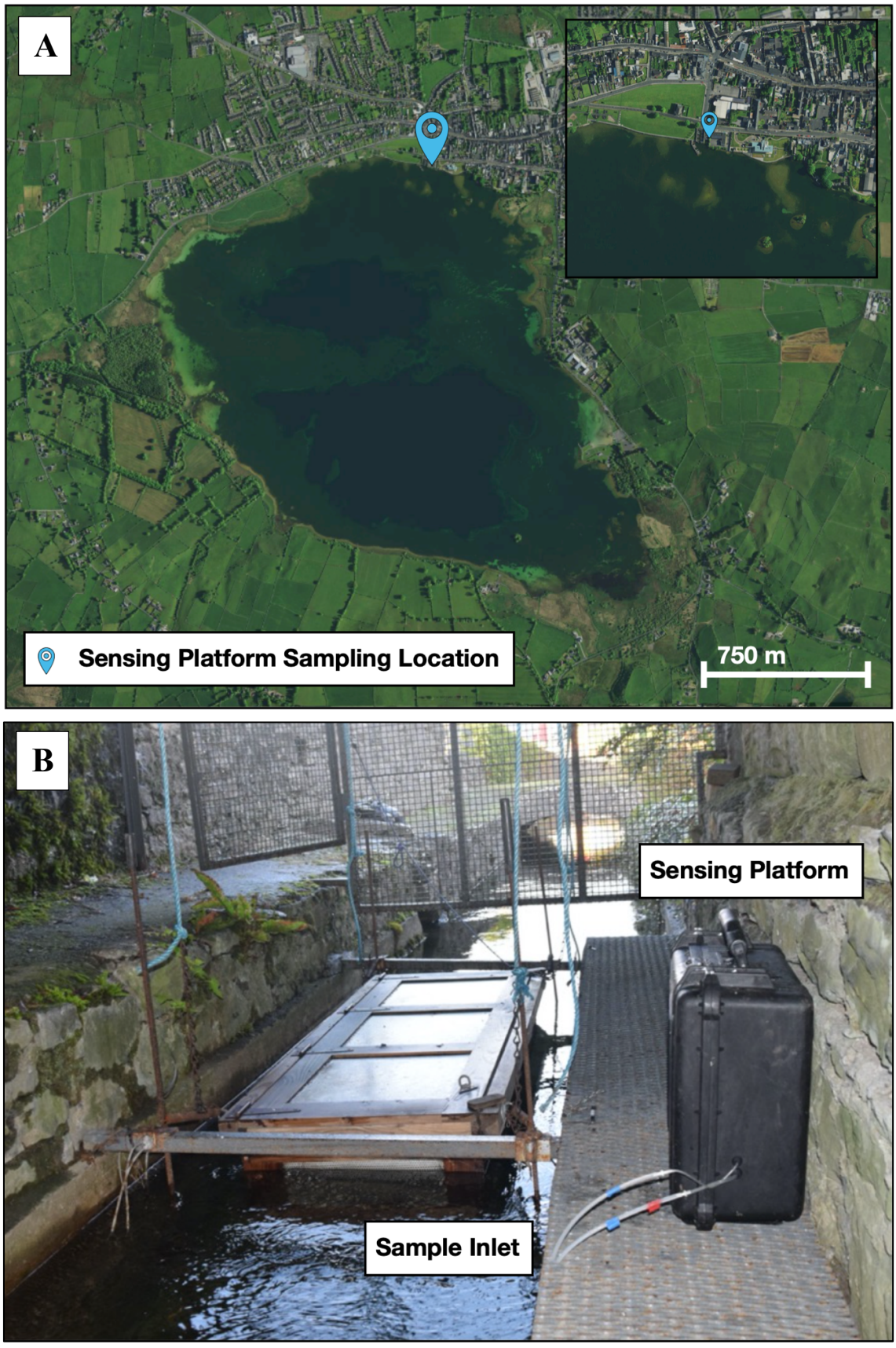

Figure 4.4. *(A) Satellite image of the sampling location at Loughrea Co. Galway, Ireland. (53°11′47.5″ N: 8°34′6.8″ W) [13]. (B) Picture of the prototype sensing platform deployment at Lough Rea angler's fish hatchery, Loughrea Co. Galway, Ireland.*

4.3. Results and discussion

4.3.1. Validation of sampling and optical detection (methods 1 and 2)

Figure 4.5. presents the linear calibrations generated from the validation of the colorimetric chemistries and their integration into the fluidic chip. Figure 4.5.A shows results obtained using off-chip pre-mixed solutions (Method 1). These demonstrate that both the benchtop microfluidic detection and the UV-Vis spectrometer measurements have excellent linearity, with the microfluidic chip exhibiting enhanced sensitivity compared to the UV-Vis spectrometer, due to the longer 2.25 cm fluidic chip detector path length compared to the standard 1 cm cuvette used with the spectrometer. Figure 4.5.B presents calibration plots obtained using the prototype platform with on-chip autonomous mixing of the sample solutions and reagents (Method 2). Method 1 (off-chip sample/reagent mixing) was repeated using the same samples as Method 2 for comparison. A high correlation and excellent linear range is evident with automated sampling and reagent mixing on-chip (0.09 to 50 µM PO_4^{3-}, R^2 = 0.999, n = 10 at each concentration) in all cases. In Figure 4.5., the tightness of the error bars (n = 10 replicates) for all graphs indicates the excellent precision of the methods (see also summary analytical data presented in Table 4.1.). The limit of detection (LOD) of the sensing platform was estimated using three times the standard deviation (n = 10) of the lowest concentration test solution, corrected with the blank measurement, and was found to be 0.09 µM.

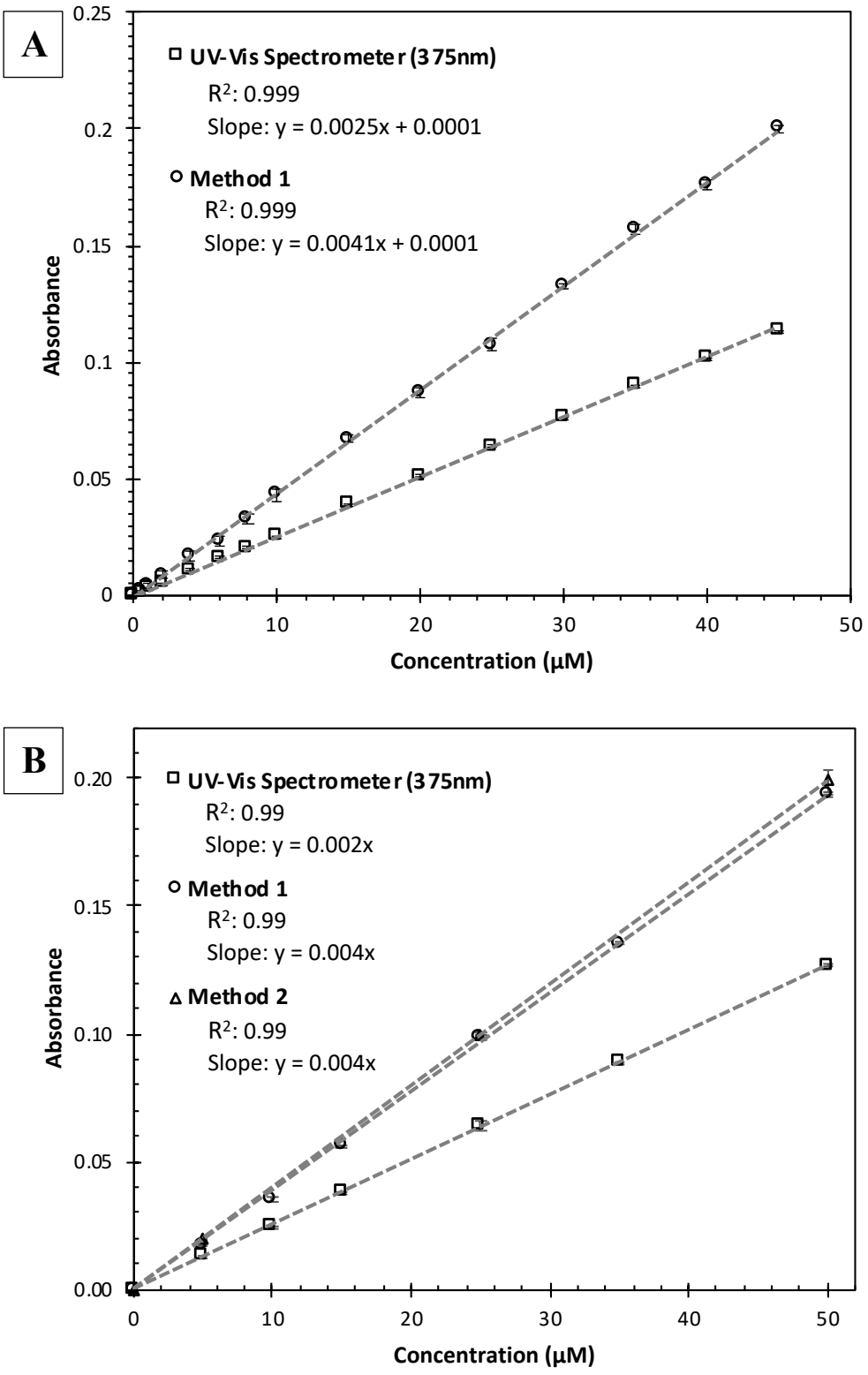

Figure 4.5. *(A) Comparison of phosphate linear calibrations (0–50 µM) obtained using the UV-Vis spectrophotometer and the fluidic chip detector with off-chip pre-mixed solutions (Method 1); (B) comparison of phosphate linear calibrations obtained using the UV-Vis spectrophotometer and the fluidic chip detector with automated sampling and on-chip mixing (Method 2). Method 1 (off-chip solution mixing) was also repeated with the same solutions for comparison. The excellent precision is evidenced by masking of error bars (standard deviations for n = 10 replicate measurements) by the point symbols.*

The analytical performance of each approach is summarised in Table 4.1. The results confirm excellent correlations for all linear calibrations (R^2 = 0.999) in all cases (see Figure 4.5.). The reproducibility and accuracy of measurements obtained using both off-chip solution mixing (Method 1) and chip-based solution mixing (Method 2) is impressive, with mean relative standard deviation (RSD) of 0.93% and 1.23%, respectively, and an average relative error (RE) of 4.53% and 0.23%, respectively.

Table 4.1. *Analytical performance of the sensing platform based on data from Figure 4.5.B.*

PO_4^{3-} (µM)	Reference PO_4^{3-}		Method 1 PO_4^{3-}		Method 2 PO_4^{3-} **	
	Mean (µM) ± %RSD *	%RE	Mean (µM) ± %RSD *	%RE	Mean (µM) ± %RSD *	%RE
5	5.07 ± 1.98	1.40	4.44 ± 2.23	−11.16	5.03 ± 0.81	0.52
10	9.71 ± 0.46	−2.90	8.98 ± 2.03	−10.19	-	-
15	14.86 ± 0.95	−0.93	14.38 ± 0.38	−4.12	-	-
25	25.35 ± 3.28	1.40	25.17 ± 0.84	0.69	25.04 ± 0.59	0.15
35	34.91 ± 0.58	−0.26	34.56 ± 0.34	−1.25	-	-
50	49.89 ± 0.28	−0.22	49.44 ± 0.12	−1.13	50.01 ± 2.30	0.01

* *n* = 10 at each concentration. ** Only three concentrations were analysed using Method 2 due to the large volume tanks used in preparation for the long-term laboratory validation study. RSD = relative standard deviation; RE = relative error.

4.3.2. Long-term laboratory assessment of the sensing platform in fully autonomous mode

The purpose of this study was to stress-test and optimise the platform in fully autonomous operational mode prior to initiating field deployments. The measurement cycle (ca. 90 minutes) consisted of (i) a blank solution measurement (0 µM PO_4^{3-}), (ii) a high standard measurement (50 µM PO_4^{3-}), and (iii) a sample measurement. During the study, the platform automatically generated 854 measurements of each test solution, blank and high standard, totalling 2562 measurements, along with a further 40 spiked solution measurements of varying concentration ranges (with associated blank and standard high calibrations, i.e., 120 measurements) at regular intervals to

test the system response (not shown for clarity), totalling 2682 measurements in all. The concentration of PO_4^{3-} in the 25 L sampling tanks was varied in the sequence between 25.0 µM, 8.5 µM, 5.5 µM and 11.5 µM PO_4^{3-} to validate the response of the platform. Figure 4.6. shows the platform response obtained over the entire test period. The red dots, representing the PO_4^{3-} concentrations determined using the UV-Vis Spectrophotometer reference method, are clearly in excellent agreement with the concentrations determined by the sensing platform (see also Table 4.2.). Overall, the response of the platform was encouraging, with the response remaining reasonably consistent with the reference measurements throughout. However, several issues were identified that had to be addressed through fault finding, software debugging and component changes during the study (see below).

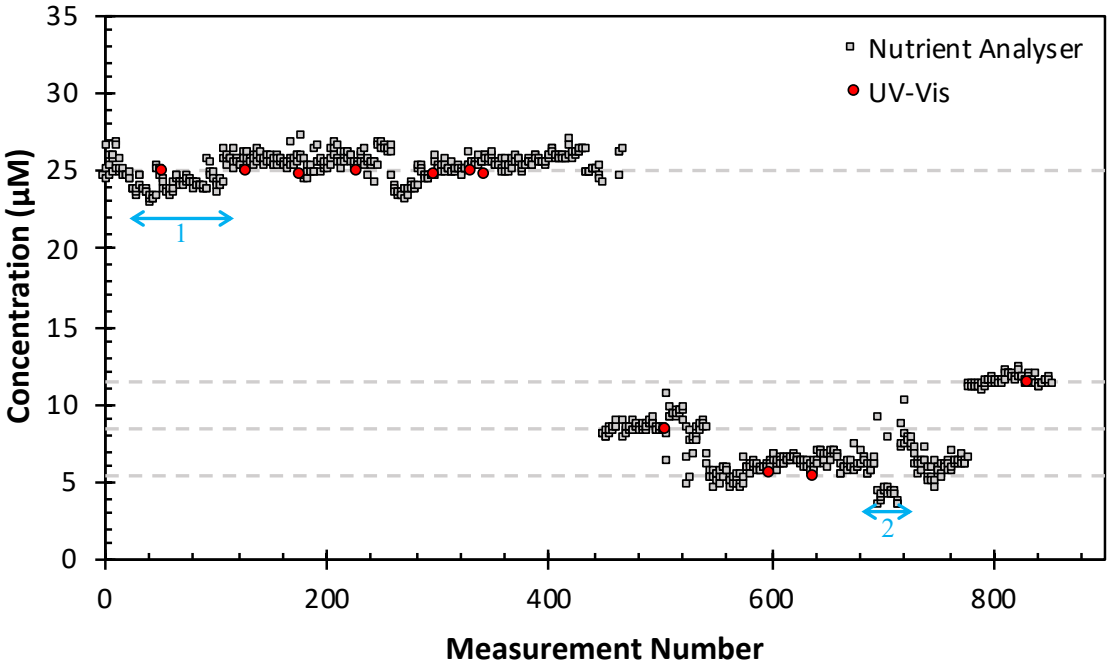

Figure 4.6. *Laboratory analysis of phosphate standards (PO_4^{3-}) with the autonomous sensing platform (grey dots) and the UV-Vis spectrophotometer reference method (red dots). Performance issues Sections 1 and 2 (blue line).*

Table 4.2. *Summary of the analytical performance of the sensing platform during laboratory testing * n=10.*

PO_4^{3-} (μM)	Reference PO_4^{3-}		Sensing Platform PO_4^{3-}	
	Mean (μM) ± %RSD *	**%RE**	**Mean (μM) ± %RSD**	**%RE**
5.5	5.81 ± 3.27	5.64	5.77 ± 13.45 (*n* = 223)	4.91
8.5	8.48 ± 2.82	−0.24	8.49 ± 6.12 (*n* = 90)	−0.12
11.5	11.49 ± 0.78	−0.09	11.40 ± 2.42 (*n* = 69)	−0.87
25.0	24.97 ± 0.48	−0.12	25.12 ± 3.36 (*n* = 462)	0.48

Weekly routine maintenance and system checking (downtime typically ca. 0.5 days) were carried out every 112 readings and involved checking for leaks, refilling reagent bags, and removal of waste. On occasion, a more substantial service was required to improve the system software and hardware, and address performance issues. For example, a rapid decrease in the signal from the photodetector observed during the initial phase of the experiment (ca. 0–100 readings; see Figure 4.6. Section 1) was rectified by replacement of the photodiode detector and modifying the system software. Interestingly, the effect of this decrease in signal arising from the photo-detector components was almost entirely cancelled out using ratio metric measurements of the calibration (blank and high) and sample solutions. However, as the cycle for the three measurements was 70 minutes, the detector artefact was not entirely removed, and manifested as a slight negative error over this period (mean phosphate concentration = 24.31 μM, mean %RE = −2.77, %RSD = 3.24, *n* =100, range 1–100). After the repair, the equivalent results were recorded (mean phosphate concentration = 25.33 μM, mean %RE = +1.32, %RSD = 1.29, *n* =100, range 301–400). Instability in the data from ca. 700–750 readings (Figure 4.6. Section 2) was traced to a connection that had become faulty on the electronics board (mean phosphate concentration = 6.83 μM, mean %RE = 5.32, %RSD = 12.66, *n* =25, range 718–742). The system performance was again restored following repair of the faulty connection (mean phosphate concentration = 11.19 μM, mean %RE = −1.23, %RSD = 1.80, *n* =25, range 780–804).

4.3.3. Preliminary Field Assessment of the Sensing Platform

Following extensive lab trials, the system field performance was assessed through a deployment during which it operated in completely autonomous mode at a location around 150 miles from the laboratory. Figure 4.7. shows the phosphate concentration data generated during the deployment at Loughrea lake, Co. Galway, Ireland. During the five-day deployment, a total of 165 in situ measurements (i.e., 55 sample, 55 blank (0 µM) and 55 high standard (50 µM)) were obtained. Data were transmitted wirelessly to an online interface via a GPRS module and stored on an 8 GB SD card connected via a Data Logger Arduino Shield as backup. The sample was filtered through a 0.45 µM filter membrane at the inlet which remained un-changed throughout the deployment. During the deployment, the phosphate concentrations measured by the platform ranged from 1.45 to 10.24 µM, with an average concentration during this time of 3.13 µM. Of particular interest is the observation that the highest phosphate concentrations between the 6th –7th of December 2017 coincided with rainfall events (Figure 4.7.).

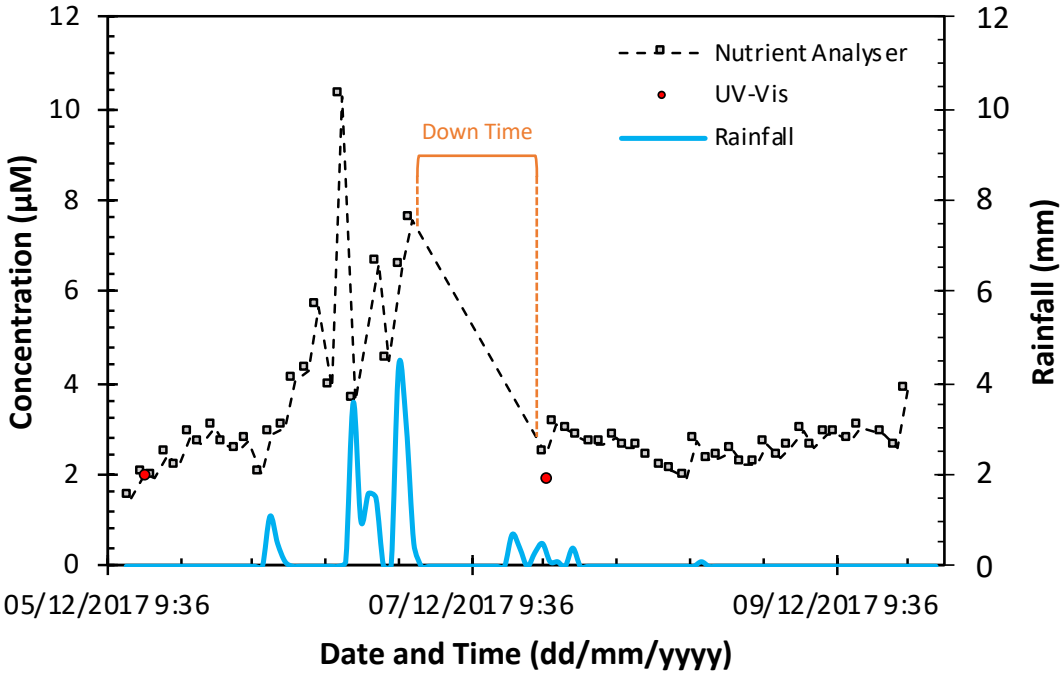

Figure 4.7. *Variation in phosphate concentration (PO_4^{3-}) measurements in Lough Rea over the 5-day deployment. The red dots represent concentrations of PO_4^{3-} in grab samples collected at the site during the deployment and measured with the lab-based UV-Vis reference method.*

During the deployment, a down time of 16 hours occurred due to failure of a power regulator in the sensor (highlighted in Figure 4.7.). This was replaced on-site, and the sensor platform thereafter continued to operate for the duration of the deployment. Grab samples (n = 5) were taken at the sampling point on two occasions during the deployment (day 1 and day 4), and the concentration of phosphate in these was determined using the UV-Vis spectrometer reference method. The first sample taken at the initial deployment of the nutrient platform gave a result of 2.00 ± 0.05 μM PO_4^{3-} via the spectrometer reference method, compared to the in-situ prototype sensor reading of 2.03 μM PO_4^{3-}. The second grab sample, taken on Day 3 after the servicing visit, returned a concentration of 1.93 ± 0.03 μM PO_4^{3-} via the spectrometer reference method, compared to 2.42 μM PO_4^{3-} obtained from the prototype sensor platform.

4.4. Discussion

Even though the duration of this deployment was relatively short, the increasing trend in PO_4^{3-} concentration on the 6th of December from ca. 3.0 to ca. 7.5 μM was an interesting outcome, as it coincided with a major rainfall event. Unfortunately, the component failure mentioned previously occurred just after this feature, and following repair, measurements returned to the more usual value of ca. 3.0 μM. While the second grab sample suggests that the system was still functioning properly, more extensive field measurements are required to determine whether the apparent rise in PO_4^{3-} concentration is a real event, and if so, whether there is a causal relationship between this event and local rainfall.

Overall, the analytical performance of the sensing platform is very encouraging, capable of achieving mean relative errors and standard deviations of 1–2% during completely autonomous operation. However, building these reagent-based chemical sensing platforms for long-term autonomous operation is a challenging task. The need to provide a means for in situ calibration means that these devices must incorporate components that provide fluidic handling (pumps, valves, reservoirs, fluidic interconnects), along with electronics for data harvesting, processing, storage, power management, and communications, all housed within a rugged enclosure and located securely in position. The platform design presented comprises 488 components and interconnectors, mostly electronics (138, including 20 major components such as LED,

photodiode, temperature sensor, GPRS module, Arduino units, power regulators, and driver boards, along with 118 minor components—resistors, capacitors, etc.), but also encompassing 34 fluidics components (16 interconnecting tubing, fluidic chip, pumps, valves, filter etc.) and 29 mechanical components (case, internal chassis, 27 customised 3D printed unit locators). Reliable in situ operation depends on effective continuous functioning of all these components, and the stability of reagents/standards used to generate the analytical response. Producing these platforms, even at a modest scale-up level (10–20 units), and validating their performance, is a formidable challenge for research teams due to the complex inter-disciplinary nature of the work, costs involved, and time required. The total component cost of this design is slightly under €2000, not including labour, which mainly involved assembly and fabrication of the fluidic chip via micro-milling. There is no doubt that adoption of industry production approaches will drive down the overall cost and improve reliability through automation of assembly, and more complete integration of electronics and fluidics. A particularly important improvement would be the use of automated methods for production of the fluidic chip (e.g., injection moulding or 3D printing). This is the subject of a recently launched project called 'Holifab', funded under the H2020-NMBP-PILOTS-2017 call (see https://cordis.europa.eu/project/rcn/212839_en.html). When faults arise, as occurred in these trials, locating of the fault source can be difficult and time consuming, and can result in significant downtime and maintenance costs. This makes the translation from platforms designed and built-in universities to commercial devices that present disruptive improvements in the 'performance/cost of ownership' ratio very challenging, as it requires long-term commitment and investment of significant resources. However, the migration of emerging rapid prototyping technologies into universities and industry is creating an interesting opportunity to bridge this gap, by dramatically reducing the design/fabricate/evaluate iteration cycle. These developments will in turn encourage stronger university–industry cooperation, and significantly de-risk involvement from industry's perspective. We are continuing to improve the platform design to improve reliability and incorporate emerging fabrication technologies to enhance the analytical performance and reduce costs. Further laboratory validation studies and in situ deployments of these platforms are currently in progress.

4.5. Conclusions

Reagent-based analyser platforms offer a route to delivering reliable long-term measurements of important chemical markers of water quality. A portable reagent-based analyser platform capable of continuous operation has been developed and extensively tested in laboratory trials, and in a preliminary in situ trial. The component cost is under €2000, and the analytical performance overall is very promising. Data generated can be remotely accessed and shared, offering a route to future integration with other sources of important environmental data. However, despite several significant design improvements over previous platforms, these systems remain relatively complex, and difficulties related to reliability can therefore arise. Despite this, we are confident that improvements arising from increasingly automated fabrication, more fully integrated electronics and fluidics, and closer cooperation between industry and university research teams will produce dramatic improvements in the performance/cost ratio, opening the way to the emergence of large scale environmental in situ (chemical) sensor networks.

4.6. References

(1) Zamparas, M.; Zacharias, I. Restoration of Eutrophic Freshwater by Managing Internal Nutrient Loads. A Review. *Science of The Total Environment* **2014**, *496*, 551–562. https://doi.org/10.1016/j.scitotenv.2014.07.076.

(2) Johnson, A. G.; Glenn, C. R.; Burnett, W. C.; Peterson, R. N.; Lucey, P. G. Aerial Infrared Imaging Reveals Large Nutrient-Rich Groundwater Inputs to the Ocean. *Geophysical Research Letters* **2008**, *35* (15). https://doi.org/10.1029/2008GL034574.

(3) Schierenbeck, T. M.; Smith, M. C. Path to Impact for Autonomous Field Deployable Chemical Sensors: A Case Study of in Situ Nitrite Sensors. *Environmental Science & Technology* **2017**, *51* (9), 4755–4771. https://doi.org/10.1021/acs.est.6b06171.

(4) Warwick, C.; Guerreiro, A.; Soares, A. Sensing and Analysis of Soluble Phosphates in Environmental Samples: A Review. *Biosensors and Bioelectronics* **2013**, *41*, 1–11. https://doi.org/10.1016/j.bios.2012.07.012.

(5) Blaen, P. J.; Khamis, K.; Lloyd, C. E. M.; Bradley, C.; Hannah, D.; Krause, S. Real-Time Monitoring of Nutrients and Dissolved Organic Matter in Rivers: Capturing

Event Dynamics, Technological Opportunities and Future Directions. *Science of The Total Environment* **2016**, *569–570*, 647–660. https://doi.org/10.1016/j.scitotenv.2016.06.116.

(6) Sanseverino, I.; Conduto, D.; Pozzoli, L.; Dobricic, S.; Lettieri, T.; European Commission; Joint Research Centre. *Algal Bloom and Its Economic Impact.*; Publications Office: Luxembourg, 2016.

(7) Bowden, M.; Diamond, D. The Determination of Phosphorus in a Microfluidic Manifold Demonstrating Long-Term Reagent Lifetime and Chemical Stability Utilising a Colorimetric Method. *Sensors and Actuators B: Chemical* **2003**, *90* (1–3), 170–174. https://doi.org/10.1016/S0925-4005(03)00024-8.

(8) O'Toole, M.; Lau, K. T.; Shepherd, R.; Slater, C.; Diamond, D. Determination of Phosphate Using a Highly Sensitive Paired Emitter–Detector Diode Photometric Flow Detector. *Analytica chimica acta* **2007**, *597* (2), 290–294.

(9) Cleary, J.; Slater, C.; McGraw, C.; Diamond, D. An Autonomous Microfluidic Sensor for Phosphate: On-Site Analysis of Treated Wastewater. *IEEE Sensors Journal* **2008**, *8* (5), 508–515.

(10) McCarthy, V.; Irvine, K. A Test of Stoichiometry across Six Irish Lakes of Low-Moderate Nutrient Status and Contrasting Hardness. *Journal of Plankton Research* **2010**, *32* (1), 15–29. https://doi.org/10.1093/plankt/fbp103.

(11) Galway County Council http://www.galway.ie/en/services/environment/environmentalprotectionbeachesburialgrounds/beaches/blueflagandgreencoastawards/ (accessed 2018 -09 -06).

(12) Historical Data - Met Éireann - The Irish Meteorological Service https://www.met.ie/climate/available-data/historical-data (accessed 2018 -06 -26).

(13) Interactive, N. Zoom Earth - Explore satellite and aerial images of the Earth https://zoom.earth/ (accessed 2018 -08 -14).

Chapter 5

Fabrication of Rugged and Reliable Fluidic Chips for Autonomous Environmental Analysers using combined thermal and pressure bonding of Polymethyl Methacrylate layers

---

Andrew Donohoe [a], Gareth Lacour [a], D. Jed Harrison [b], Dermot Diamond [a] and Margaret McCaul [a].

a. Insight Centre for Data Analytics National Centre for Sensor Research, Dublin City University, Glasnevin, Dublin 9, Ireland

b. Department of Chemistry, University of Alberta, Edmonton, Alberta, T6G 2G2, Canada

Fabrication of Rugged and Reliable Fluidic Chips for Autonomous Environmental Analysers using combined thermal and pressure bonding of Polymethyl Methacrylate layers, ***published in:*** *ACS Omega* **2019**, *4* (25), 21131–21140.
https://doi.org/10.1021/acsomega.9b01918

Abstract

The fabrication of highly reliable and rugged fluidic chips designed for use in autonomous analysers for nutrient monitoring is described. The chips are based on a two-layer configuration, with the fluidic channels produced in one layer using precision micro-milling. The second capping layer contains through holes for sample/standard and reagent addition, and waste removal post-analysis. Two optically clear PMMA windows are integrated into the opaque PMMA chip, orthogonal to a 22.5 mm long section of the channel downstream from a serpentine reagent and sample/standard mixing region. An LED source is coupled into the channel through one of the windows, and the light intensity monitored with a photodiode located at the distal end of the channel outside the second optically clear window. Efficient coupling of the source through the channel to the detector is achieved using custom designed alignment units produced using 3D printing. In contrast to chips produced using solvent adhesion, the thermal/pressure bonded chips show no evidence of leakage throughout extensive lab and field trials. Optimisation of the thermal/pressure conditions leads to very strong adhesion between the PMMA layers, requiring forces in the region of 2,000 N to separate them. Profilometry imaging shows minimal evidence of channel distortion after bonding.

Fluidic chips integrated into prototype nutrient analysers display no evidence of leakage in extensive lab tests involving 2,500 phosphate measurements using the yellow (Vanadomolybdophosphoric Acid) method. Similarly, excellent analytical performance is reported for a 28-day field trial comprising 188 in-situ autonomous phosphate measurements (564 measurements in total including calibration).

Keywords: PMMA; Fluidic Chips; Profilometry; Colorimetric Analysis; Water quality; Nutrient Sensing Phosphate.

5.1. Introduction

The ability to monitor the chemical status of environmental waters requires sensing devices that can function in a wide variety of deployment scenarios, ranging from single-use disposable devices for on-the-spot measurements, to much more sophisticated analyser platforms that provide continuous data from remote locations to databases [1–4]. These sensing devices either complex or single use commonly utilise microfluidics. The ability to reliably fabricate these microfluidic chips plays a critical role in an analyser's performance and function. Analysers are typically deployed by specialists from environmental agencies, the water industry, and university research teams due to unit costs and the need for considerable background experience and knowledge due to the complexity of these devices. The data generated from autonomous analysers is increasingly augmented by satellite remote sensing data, opening the way towards much more comprehensive real-time and historical (trending) information that can be visualised and modelled via complex algorithms that feed into predictions of future water status [5–7]. Autonomous environmental analyser platforms are expensive to buy and to manage in deployments, due to the often-hostile conditions these devices experience when in use [8–10]. The high cost of these analysers arises from the need to produce a device that incorporates reagents, at least one standard for checking calibration, pumps and valves for flow control, waste storage, non-fouling sampling port, fluidic system, selective detection, electronics for data acquisition and wireless communications, and power source/management [11]. Cost-of-ownership is primarily driven by short service intervals, the need for specialist staff, maintenance/use of expensive facilities and boats/ribs, and replacement of devices/parts/reagents. This use model is obviously very expensive and has contributed to the slow uptake of autonomous sensors for tracking water chemistry [12,13].

Producing an inexpensive analyser platform that can be left in deployment for several months unattended remains a significant challenge. For example, the recent global Nutrient Challenge targeted a unit cost to buy of $5,000 or less, compared to the typical $20,000 or more for such devices, as this lower price point would lead to a much larger uptake by state agencies and industry [14,15]. A key challenge is to make every aspect of the device and the analytical method very reliable in use, as failure of any single

component renders the device faulty and requires a service visit to repair or replace the device. For the reagent based colorimetric methods often used in these devices, reagent stability and compatibility within the fluidic system must be balanced with method sensitivity, as more stable reagents can provide for longer service intervals and lower maintenance costs [16]. Likewise, power supply and management strategy must be considered, although major international research efforts driven largely by the e-car industry will advance this technology rapidly [17].

Clearly, extending the service interval from days to months will dramatically drive down the cost of ownership, and enable many more units to be deployed. The service interval depends on many interrelated variables, including reagent/standard stability, reagent capacity (number of assays), sampling frequency, power demand/availability, and reliability of the numerous components. In this chapter, the reliability of the fluidic chip is focused on, due to its critical role in the device operation, and the impact of leakage of the often-aggressive reagents on the system. The proposed fabrication method using micro-milling provides the means to quickly prototype and test various fluidic designs in small scale batches during optimisation of the fluidic layout. Micro-milling enables the design to be produced directly in the polymer layer without the need to reproduce expensive moulds if design changes are required between batches [18].

Polymethyl-methacrylate (PMMA) is a useful material for producing prototype fluidic chips due to its broad chemical compatibility, thermal stability and its availability in opaque and transparent forms [19]. PMMA is compatible with a range of manufacturing techniques including direct machining or moulding. Direct machining techniques suitable for use include laser ablation and micro-milling and applicable moulding techniques include hot and cold embossing and thermoforming [20,21]. Micromachining provides the flexibility to rapidly produce and test various modifications to the fluidic design, and thereby optimise the proposed method on-chip before moving to a higher volume method such as injection moulding for low-cost production of the final chip design. In addition, opaque PMMA reduces the potential impact of stray light on the colorimetric detection approach used in this method.

In this chapter, a simple method for bonding a two-layer PMMA chip is presented that results in very strong adhesion between the PMMA layers, and no evidence of chip failure/leakage during lab and field trials. These chips improve the reliability of the system fluidics, and in so doing, significantly enhance the overall platform ruggedness and reliability during testing cycles and in real deployments.

5.2. Materials and Methods

5.2.1. Analytical Method

Colorimetric detection of phosphate (PO_4^{3-}) using the Yellow Method (Vanadomolybdophosphoric Acid Method) was chosen to evaluate the performance of the chip, in view of the excellent reagent stability of 12 months or more [18], and demonstrated compatibility with microfluidic analysers [22]. The prototype analyser used for testing and integration of the fluidic chip housed method reagent, calibration standards (0 µM/blank and 50µM PO_4^{3-}), and sample taken either from the environment during in-situ field testing, or from a sampling tank during in-lab testing. Flow control was carried out using an in-house produced fluidic board comprising two 2/2 (hit and hold) and two 3/2 (latching) solenoid valves, and two piezo electric pumps to deliver reagent and calibration standard/sample to the fluidic chip in a 1:1 v/v ratio.

All reagents and standards were prepared using ultra high purity (UHP) water (MilliQ, Millipore, Burlington, MA, USA) and analytical grade chemicals (Sigma Aldrich, St. Louis, MO, USA), as described previously [11]. Briefly, the Yellow Reagent was prepared by dissolving 0.351 g of ammonium metavanadate (Sigma Aldrich) in ~200 mL UHP water with an addition of 95 mL concentrated hydrochloric acid (Sigma Aldrich). Following this, 7.14 g of ammonium molybdate tetrahydrate was added and the resulting solution was made up to 1 L using UHP water. The phosphate standards were prepared by dissolving 0.408 g potassium dihydrogen phosphate (Sigma Aldrich) in UHP water in a 1 L volumetric flask to make a 3 mM stock phosphate solution. This stock solution was further diluted to make up the 50 µM high calibration standard used within the prototype analyser. The blank solution contained equal volumes of yellow reagent and UHP. All reagent and standard solutions were tested and validated against reference spectra obtained with a VWR UV-1600PC photo spectrometer using a wavelength of 375 nm.

Figure 5.1. shows the fluidic chip design and channel arrangement. It is a two-layer configuration comprising a lower 'channel' layer and an upper 'capping' layer. Fabrication of the two fluidic layers was carried out using a series of manufacturing techniques including laser ablation and precision micro-milling as illustrated in figure 5.2. Plates of commercially available opaque 3 mm PMMA were initially cut to the dimensions of the micro-mill bed (145 mm x 145 mm) using a CO_2 Laser Cutter (Epilog Zing 16). The features comprising the fluidic chip were micro-milled (Datron CAT3D-M6 Micro-mill) into the opaque PMMA to create the two-layer prototype design. This comprised ca. 1 mm depth/width channels milled in the channel layer and three through-holes (⌀ 6.5 mm) in the capping layer. The three through holes were configured to receive 6.5 mm threaded barbed liquid connectors used for connection of tubing (1/16th inch internal diameter Tygon®) between the fluidic chip and the fluid board of the prototype analyser.

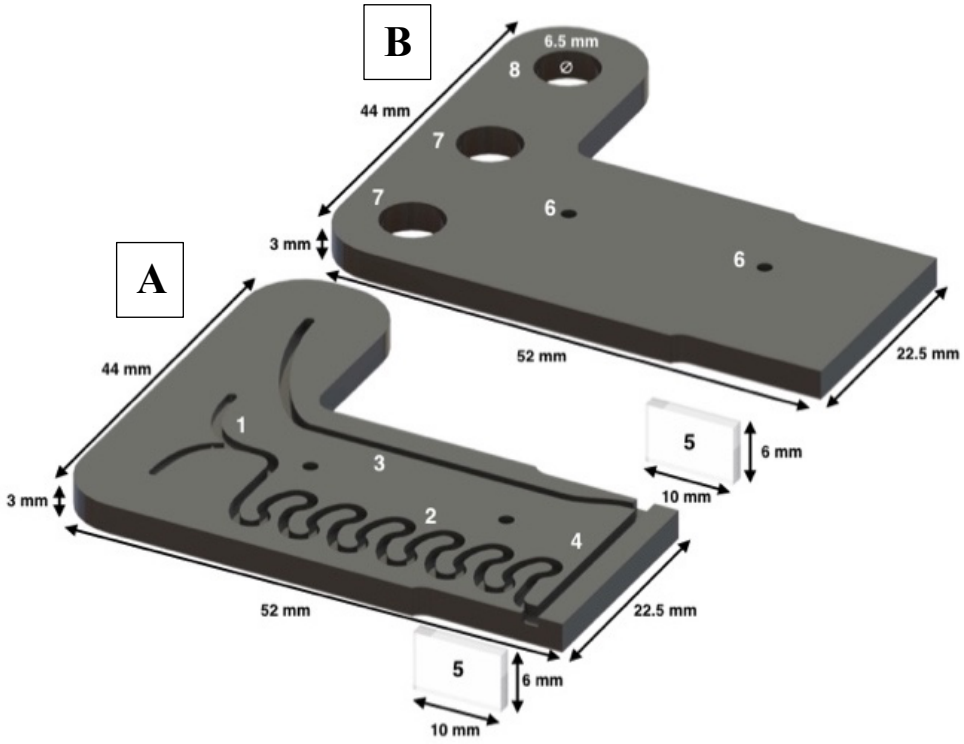

Figure 5.1. *The two-layer design showing; (A) bottom channel layer containing milled fluidic channels incorporating a merging point (1) for sample and reagent inputs, a serpentine mixing region (2) for mixing of sample and reagent, an outlet line (3) for flushing of waste after analysis, and optical channel (4) for detection on chip, and two optically clear windows (5) for coupling light into and out of the detection channel. (B) Upper capping layer incorporating two holes (6) to house alignment pins for the two layers during bonding, and three 6.5 mm circular through holes, two inlets for sample and reagent intake (7) and one outlet (8) for waste.*

Two holes were drilled into both layers of the chip to ensure precise alignment during bonding of the chip. During use, reagent and sample/calibrant enter via the inputs (Figure 5.1., 7), merge (Figure 5.1., 1) and mix in the serpentine channel (Figure 5.1., 2). The colour developed via the reagent and analyte reaction is measured by means of a LED and Photodiode arranged at opposite ends of a 22.5 mm optical detector channel (Figure 5.1., 4). Light is coupled into and out of the detector via transparent PMMA windows (Figure 5.1., 5). From the detection channel, the mixture is conveyed to the waste outlet (figure 5.1., 8) via the outlet channel (Figure 5.1., 3) for external storage.

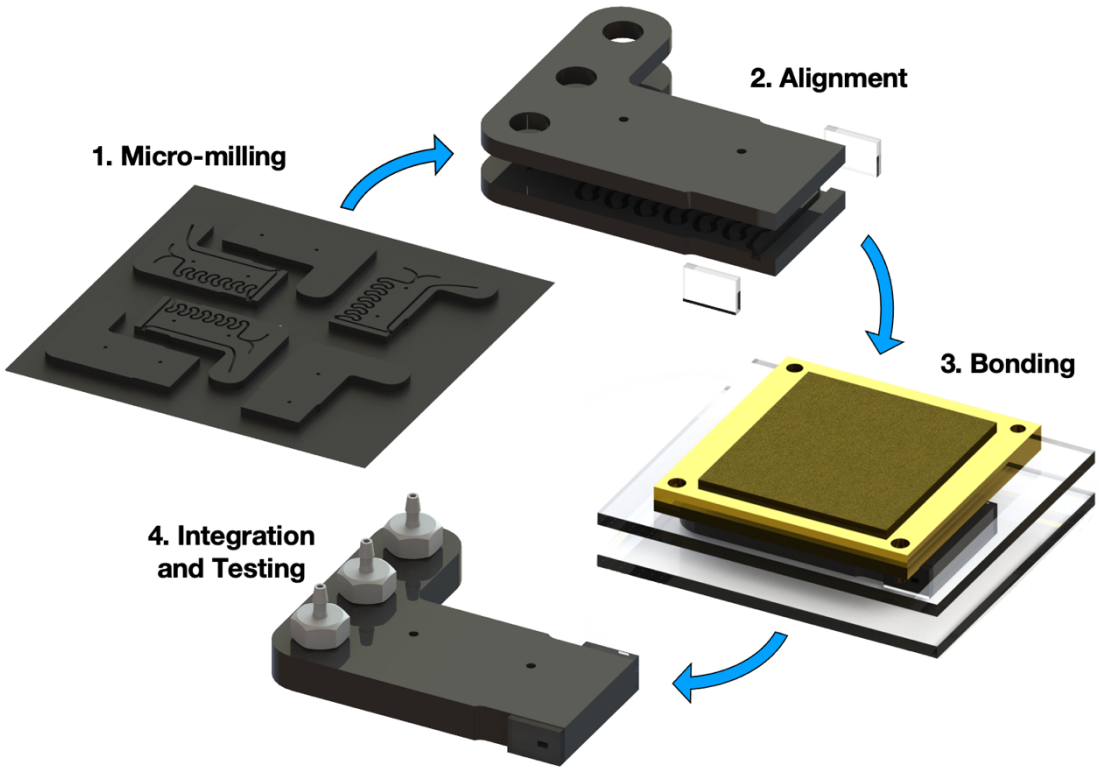

Figure 5.2. *Manufacturing scheme for prototyping of two-layer PMMA fluidic chips. (1) micro-milling is used to produce a batch of two layer fluidic chips (x3) from a 145 x 145 mm laser cut PMMA milled plate, (2) the cleaned capping, channel layer and optically clear windows are aligned to fluidic chip design, (3) bonding is carried out using heat and pressure with the aligned fluidic chip positioned between two glass compression plates and a brass weight on top and (4) barbed liquid connectors are integrated and the fluidic chips are leak tested prior to use.*

5.2.2. Bonding Procedure

A simple bonding method employing an external weight in combination with thermal and vacuum conditions was used to effectively seal the two-layer fluidic chip. Prior to bonding the two layers were cleaned using an ultrasonic bath to remove debris and residues left over from the micro-milling, and swarf build up within the channels or through holes of the chip. Thermal/vacuum bonding of the two-layer PMMA chips was performed under optimised conditions (see supplementary information table SI.5.1.) using a vacuum Oven (Gallenkamp vacuum oven) set at the glass transition temperature of this particular PMMA (~165 °C) [23] and a vacuum of 200 mBar. A 220 g brass weight (A) was placed on top of two glass compression plates (B) with the two aligned layers of the PMMA fluidic Chip (C) positioned between these plates (see Supplementary Information Figure SI.5.1.). Adhesion of the two layers occurred under these conditions for a period of 20 minutes.

5.2.3. PMMA Fluidic Chip Characterisation

Characterisation was carried out to assess the reproducibility of the fabricated fluidic chips using a series of techniques including optical profilometry, stylus profilometry and optical microscopy. Inspection and visualisation of micro-milled channels was carried out using a Keyence 3D microscope equipped with a composite 50-500x lens. Depths and profile measurements were carried out using complimentary profilometers, a Bruker DektakXT stylus profilometer and a Bruker ContourGT optical profilometer. The stylus profilometry was carried out at a range of 65.5μm, tracking surface features with a 2.5 μm stylus tip. Both approaches were used to create surface profiles of both fluidic layers at the same targeted areas covering the merging point, serpentine mixing region, waste outlet and optical channel (see figure 5.3.). These measurements were performed before and after thermal bonding to assess the accuracy and precision of the fabrication techniques, and the extent of any channel deformation associated with the thermal bonding procedure.

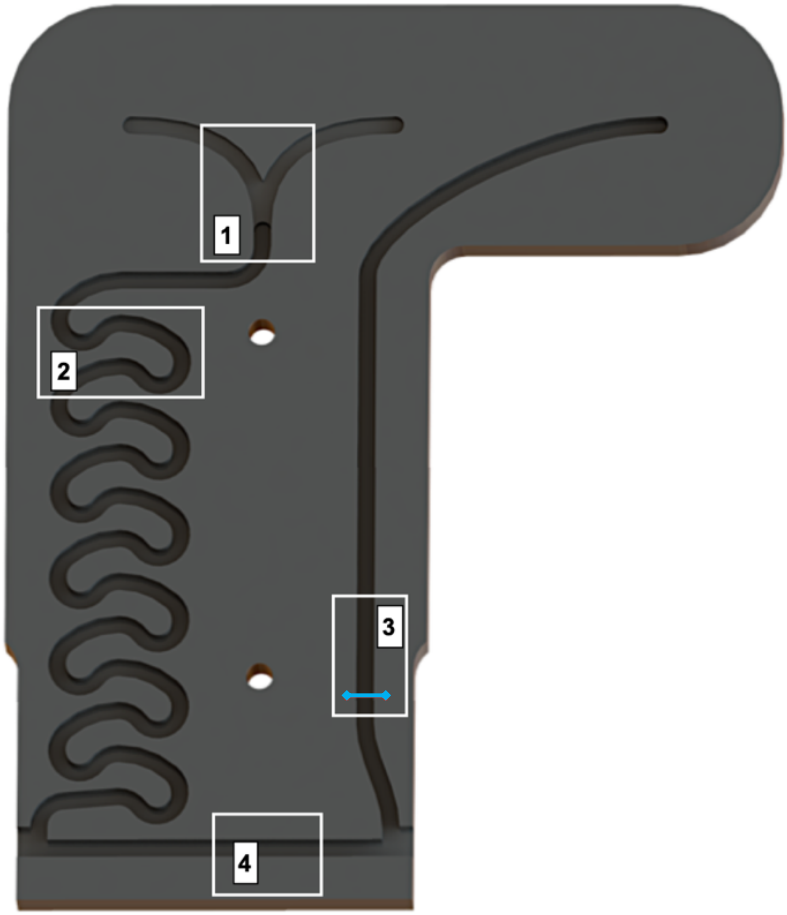

Figure 5.3. *Channel layout and the target areas used for characterisation of the channels in the channel layer of the Fluidic chip. 1) sample and reagent inlet where sample and reagent merge after intake onto the chip, 2) initial portion of the serpentine mixing region where the sample and reagent mix on chip prior to measurement, 3) waste outlet channel through which sample and reagent are flushed after analysis and 4) optical channel for colorimetric detection of the sample/reagent mixture. These regions are discussed further (see Figure 5.8.). The blue line in the waste outlet channel (3) is the location used to obtain the section shown in figure 5.7.*

5.2.4. Chip Leak Testing

To optimise bonding of the chip layers, temperature, vacuum, and time were varied systematically (see supplementary information Table SI.5.1.). The so-produced chips were tested for leakage following bonding and cooling prior to integration into the prototype analyser. A 60 mL syringe was used to pump UHP water through each chip for one hour, refilling the syringe as needed. Flow rates of 3.0 mL, 6.0 mL and 12.0 mL per minute were applied while the chips were visually checked for any signs of leakage

throughout testing. Particular attention was paid to potential failure points including seams, optical windows, and fluidic connectors. In order to minimise potential distortion of the fluidic channels, the selected conditions were the least extreme that exhibited no evidence of leakage (temperature = 165 °C, oven pressure = 200 mBar, time = 20 minutes). After this preliminary testing, the fluidic chips were integrated into a prototype water nutrient analyser for further lab assessment and testing, during which reagent and sample were delivered to the fluidic chips at a flow rate of 3.0 mL/min for 1 hour, mimicking the operational flow rate of the analyser in field deployments. The analyser was then setup to run in fully autonomous mode for further in-lab and in-situ field testing (see section 5.3.4).

5.2.5. Inter-Layer Tensile Strength Measurements

Quantitative measurements of fluidic chip inter-layer bond strength were carried out using a Zwick tensile strength test system. Figure 5.4. shows the experimental setup designed to assess the strength of the chip layer bonding wherein each face of the thermally bonded chip was fixed to an aluminium plate using a two-part epoxy adhesive (araldite® rapid). The aluminium plates were attached to the instrument and the force, and the stress applied to attempt to separate the fluidic layers was measured.

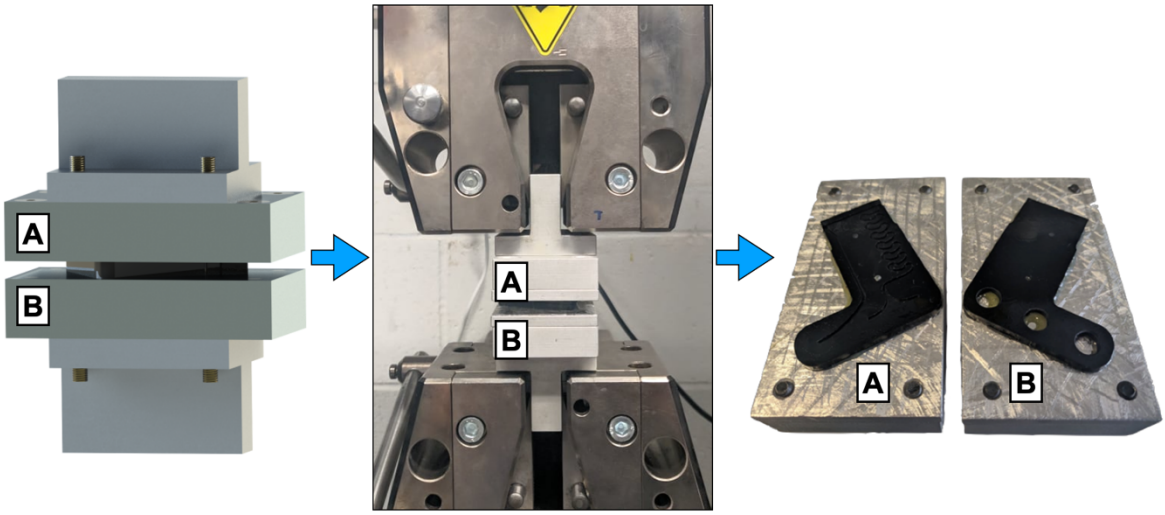

Figure 5.4. *Experimental setup for bond strength testing with two-layer chip fixed between two clamps used to apply tension; Left: rendering of the test rig with the upper (A) and lower (B) clamps; Middle: photo of the test rig in position prior to pull-apart testing; Right: chip after pull-apart test showing channel layer (A) and capping layer (B).*

5.3. Results and Discussion

5.3.1. Chip Inter-Layer Bond Strength Analysis

Three methods were carried out to assess the fluidic chip bond strength (see Figure 5.5. and Table 5.1.).

Method 1: The fluidic chips were directly adhered to the aluminium base plates using two-part epoxy. During testing of this method, forces in excess of 300 N were applied. The fluidic chips failed at the interface between the epoxy adhesive and the fluidic chip, not at the interface between the chip layers. Alternative epoxies (Araldite® Instant, Standard and Rapid) were tested using the above method, all giving similar results.

Method 2: Modification of the fluidic chip surface was carried out by manually roughening the surface in contact with the epoxy using 1000 grit sandpaper, to further improve adhesion of the epoxy adhesive between the chip and the metal support. Bond strength testing was again carried out using greater forces in excess of 1500 N. Once again, failure occurred at the at the epoxy interface between the chip and the metal plate, not at the interface between the chip layers.

Method 3: In addition to the chip surface roughing as per method 2, the surface of the metal plate was scored and roughened manually using a hand file to further increase the strength of the bond between the epoxy, the metal plate, and the fluidic chip. The tests were repeated for a further set of chips and under these conditions, the inter-layer bond in the fluidic chips failed at forces in the range 1,878.88-2,076.47 N, indicating the high degree of inter-layer adhesion generated by the simple bonding process.

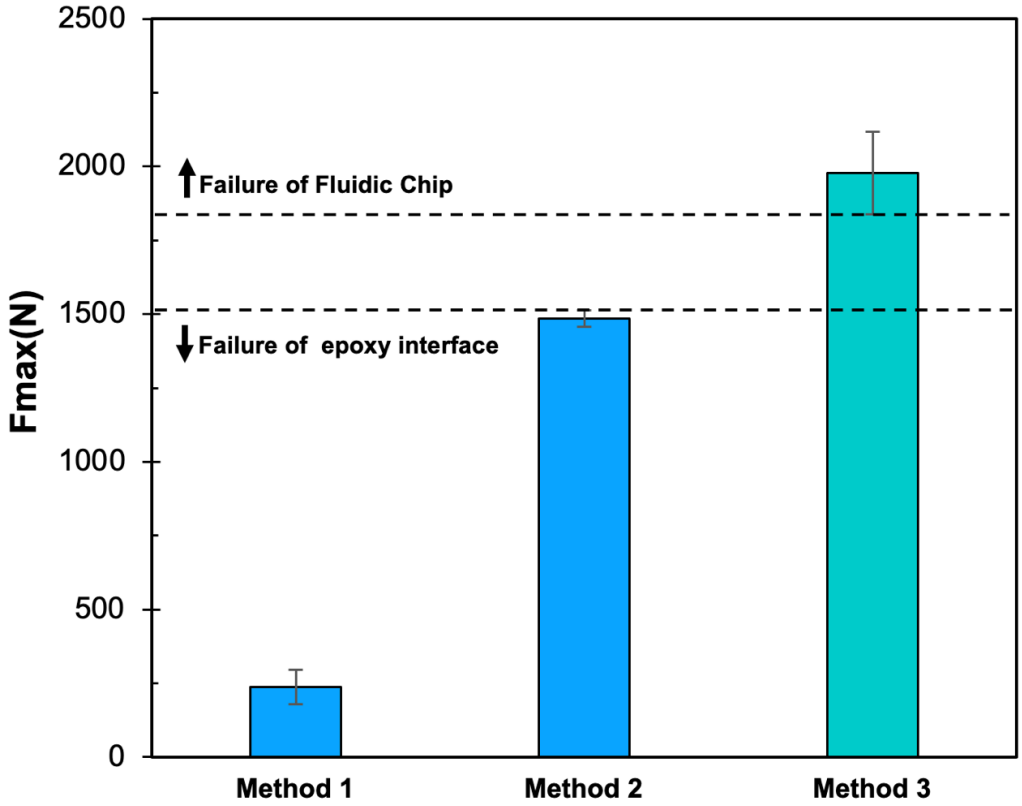

Figure 5.5. *Bond strength analysis carried for methods (1) fluidic chip adhered directly to metal plates using epoxy, failure was seen at the epoxy interface, (2) fluidic chip with roughened surface adhered to metal plates using epoxy, failure was seen at the epoxy interface and (3) fluidic chip with roughened surface adhered to metal plate with roughened and scored surface using epoxy, failure occurred at the bond between the fluidic chip layers.*

Table 5.1. *Summary of Bond Strength testing carried out with surface modifications and method optimisation carried out for methods 1 – 3.*

Method	Mean F_{max} (N)	%RSD	Failure Point
Method 1: Fluidic chip adhered to metal plate using epoxy	237.29	24.92	Epoxy Interface between the fluidic chip and plate
Method 2: Fluidic chip adhered to metal plate using epoxy with surface of fluidic chip roughened	1485.66	1.92	Epoxy Interface between the fluidic chip and plate
Method 3: Fluidic chip adhered to metal plate using epoxy with surface of fluidic chip roughened and metal plate scored	1977.68	7.06	Bond between the two layers of the bonded fluidic chip

5.3.2. Post-Bonding Fluidic Chip Channel Characterisation

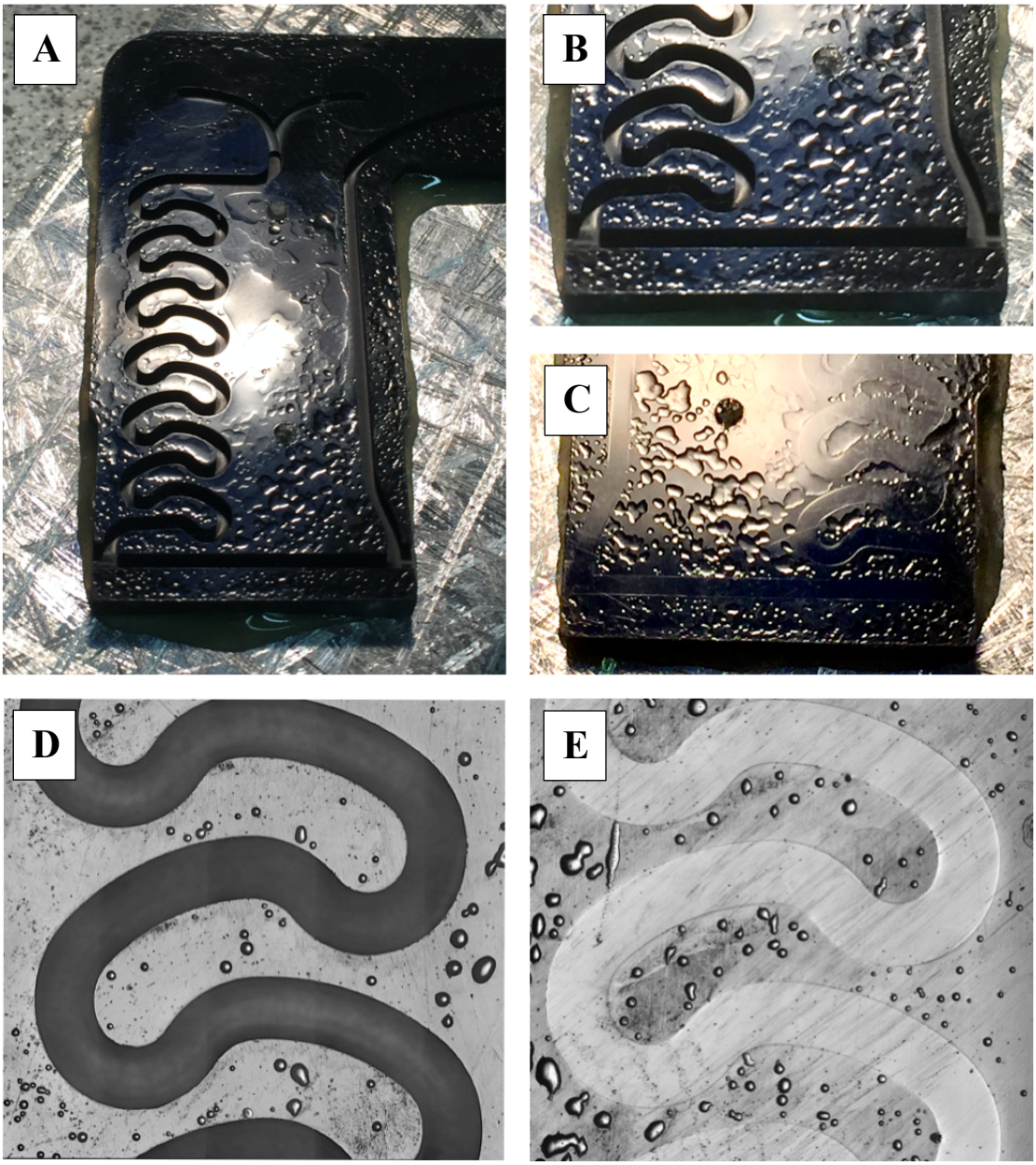

Figure 5.6. *Images of chips after layer separation; (A) photo of the bottom fluidic layer showing channels; close up photos of the bottom layer (B) and top layer (C) showing the channel layout imprinted on the top layer; Keyence microscope images the lower layer showing a section of the serpentine mixing channel (D) and its imprint (E) on the same region of the top layer.*

The imprint of the lower fluidic layer channel layout appearing in the upper layer shown in Figure 5.6. is an effect arising from the temperature and vacuum conditions combined with the external weight used during the bonding process. Sections across the channel and equivalent imprint locations on the capping and channel layers (Figure

5.7.) show that the capping layer protrudes slightly into the channel (ca. 3.0 µm), forming a very tight seal at the channel edges in the process.

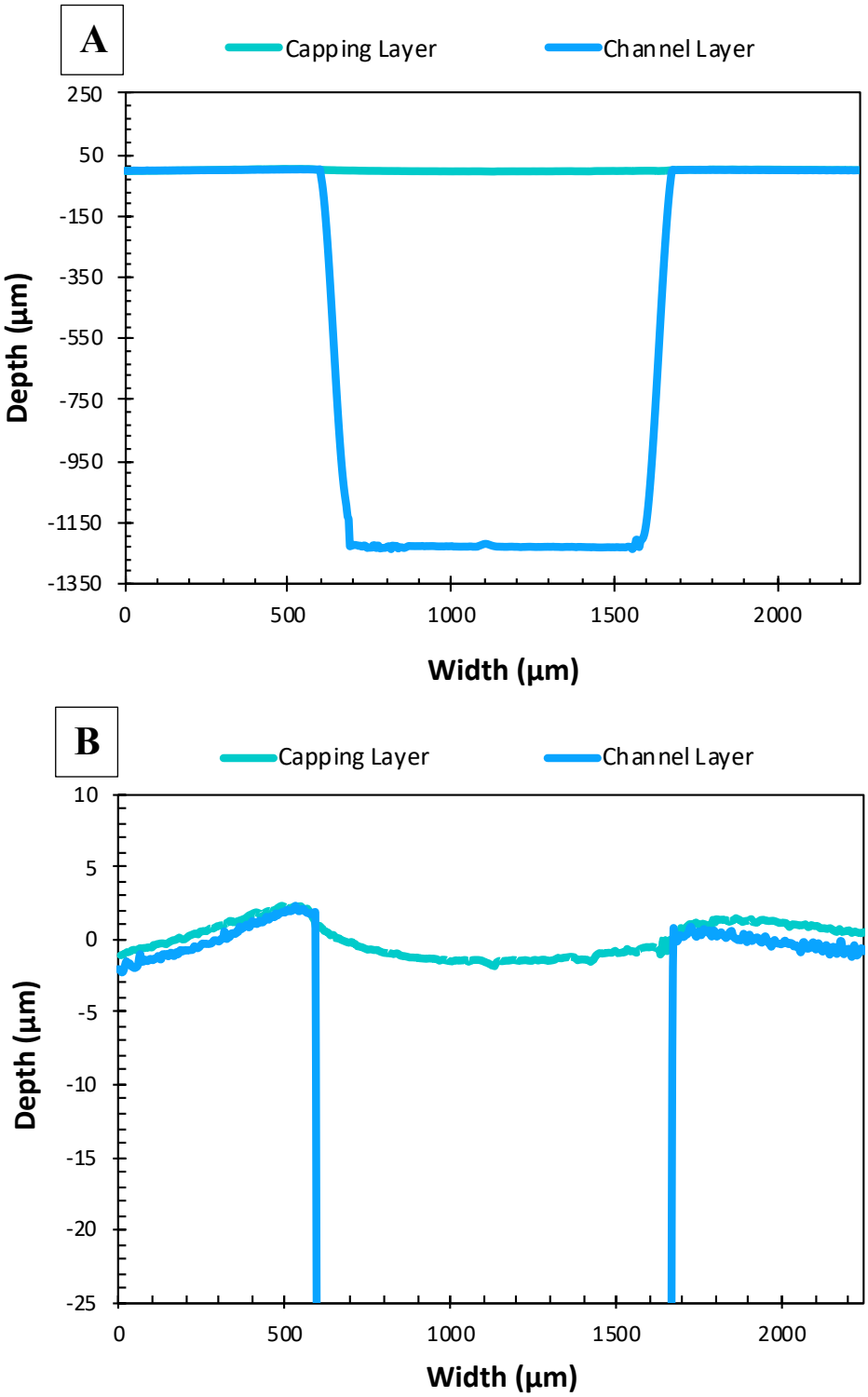

Figure 5.7. *Section across the lower layer channel (blue) and the equivalent section of the upper layer imprint (teal) at the location marked in teal in figure 5.3. Data obtained using the Bruker ContourGT Optical Profilometer.*

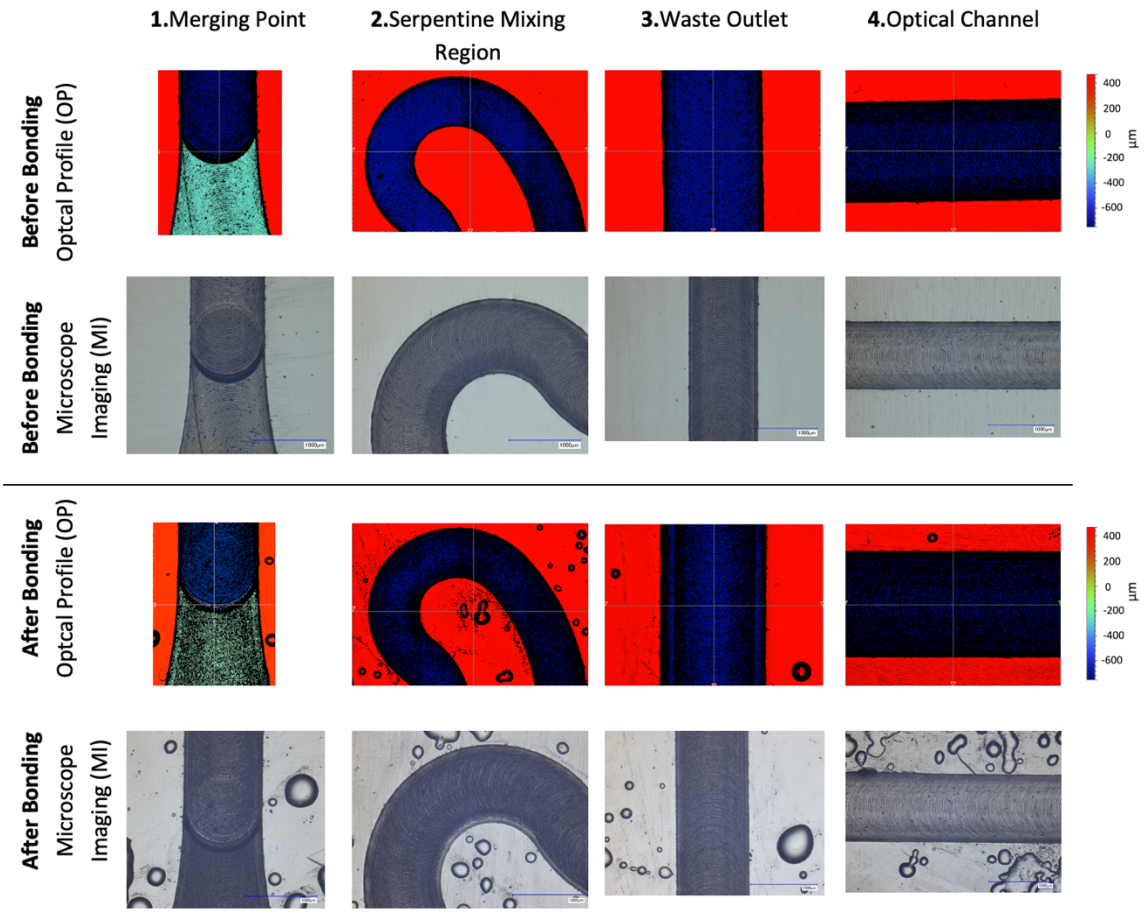

Figure 5.8. *Optical profile and microscope images of channel layer before and after bonding of the (1) merging point, (2) mixing channel, (3) waste outlet, (4) optical channel (see Figure 5.3.).*

Figure 5.8. shows characterisation carried out on the target areas (see figure 5.3.) of the fluidic chips channel layer using optical profilometry (Bruker contourGT) and microscopic imaging (Keyence 3D microscope). Optical profilometry was used to generate 3D maps of the surfaces from which channel widths and depths could be measured before and after bonding (see supplementary information figure SI.5.2. and SI.5.3.).

Table 5.2. *Optical profilometry measurements of fluidic chip at target areas (figure 5.3.) before thermal bonding.*

	Merging Point (mm)	Mixing Channel (mm)	Waste Outlet (mm)	Optical Channel (mm)	Total Chip Profile (channel layer) (mm)	Total chip Profile (capping layer) (mm)
Channel Depth Average	1.244	1.157	1.207	1.187	N/A	N/A
Channel Depth Standard Deviation (N=3)	$4x10^{-4}$	$4x10^{-4}$	$3.1x10^{-3}$	$3.1x10^{-3}$	N/A	N/A
Surface Roughness Sz	0.012	0.016	$5.1x\ 10^{-3}$	$5.5x10^{-3}$	0.549	0.061
Channel Width	1.045	N/A	1.045	1.045	N/A	N/A

Table 5.3. *Optical profilometry measurements of fluidic chip at target areas (figure 5.3.) after thermal bonding.*

	Merging Point (mm)	Mixing Channel (mm)	Waste Outlet (mm)	Optical Channel (mm)	Total Chip Profile (channel layer) (mm)	Total chip Profile (capping layer) (mm)
Channel Depth Average	1.130	1.149	1.137	1.089	N/A	N/A
Channel Depth Standard Deviation (N=3)	$5.8x10^{-4}$	$2.5x10^{-4}$	$3.8x10^{-3}$	$1.3x10^{-3}$	N/A	N/A
Surface Roughness Sz	0.0239	0.0351	$5.8x10^{-3}$	0.0167	0.110	0.248
Channel Width	1.105	N/A	1.087	1.109	N/A	N/A

Tables 5.2. and 5.3. summarise typical measurements of Average Depth, Average Width, Depth Standard Deviation and Surface Roughness (Sz). These techniques were used to assess if residues or swarf build up from the milling process could be seen and to determine the extent of any channel deformation caused by the layer bonding process. Table 5.2. shows low standard deviation for channel depth at each of the target areas measured and low channel roughness.

Improved surface roughness measurements were recorded for the milled channels (merging point, mixing channel, waste outlet, and optical channel) in comparison to the un-milled surfaces of the chip (chip profile capping and channel layer). The milled channels measured an average deviation between the highest and lowest measured points (Sz, see table 5.2) of 12 μm in comparison to the un-milled PMMA surfaces which averaged 179 μm deviation. This improvement seen due to the milling process within the channel areas is important to note as an increased channel roughness can lead to turbulent flow causing dead zones and sample carry over within the chip. Increased surface roughness can also contribute to higher rates of biofouling due to the larger internal surface area. No evidence of channel fouling was observed during testing carried out in section 5.3.4, this result is aided by the low channel roughness minimizing chances for adhesion, however any potential for biofouling within the channels of the fluidic chip are largely mitigated due to the low pH (pH 0.74) of the reagent used within the vanadomolybdophosphoric acid method tested.

The results from table 5.2 and 5.3 show that micro-milling is a suitable method of fabrication and can produce accurate and precise channels in the PMMA chips at the required dimensions with acceptable tolerances. Comparisons before and after bonding show a small increase in channel width and decrease in channel depth, due to the impact of the weight and vacuum used during the bonding method to ensure strong adhesion between the two PMMA layers.

Figure 5.8. also shows that after thermal bonding, the channels remained clear with no blockages or damage occurring, the mill marks remain present on the surface of the channels both before and after bonding (compare for example the microscope images of the waste channel before and after bonding). The inclusions at the interface between

the layer after bonding are most likely due to small amounts of air trapped during the bonding process in this interfacial region. However, these do not give rise to any leakage, apparently due to the formation of a tight seal between the channel and the capping layer (figure 5.7.).

5.3.3. Fluidic Chip Characterisation - Leak testing

Leak testing showed no evidence of any leakages or failure points from ten replicates chips assessed at flow rates of 3.0 ,6.0 and 12.0 mL per minute over a period of 1 hour. When integrated into the prototype analyser, no evidence of failure or leakage occurred over 1 hour of testing using a flow rate of 3.0 mL a minute. The chips were further tested with the analyser running in fully autonomous mode during which 2,500 in-lab phosphate measurements were taken using the yellow method without chip failure (see Donohoe et al., 2018, **chapter 4**).

5.3.4. Performance of Fluidic Chip in prototype Nutrient analyser

5.3.4.1. In-lab testing

In-lab testing was carried out on the integrated fluidic chip on the prototype analyser using a series of phosphate calibration standards (0-25 µM PO_4^{3-}) that were autonomously loaded onto the chip using the fluidic handling of the analyser. Standards of known concentration were measured optically on chip using the integrated 375 nm LED coupled with a photodiode-based detector, and the results compared against a UV-Vis spectrophotometer employing the same method.

The fluidic chip had two inlets, the first taking in the phosphate standard and the second taking in Yellow Reagent, at a 1:1 v/v ratio of sample to reagent. As the two solutions were pumped through the chip, mixing occurred within the serpentine mixing region, see figure 5.3. Once the chip had been fully filled and the reaction mixture was present in the optical channel, pumping was paused for 20 minutes to allow the reaction to come to completion at room temperature [24]. Optical measurements were then taken using the LED and Photodiode. Figure 5.9. and Table 5.3. present the linear calibrations generated and the analytical performance summaries for the phosphate sample detection on chip versus the UV-Vis spectrometer.

Both methods have excellent linearity (0.9999 UV-Vis reference method, 0.9999 Prototype Analyser) as seen in figure 5.9. The UV-Vis reference method had a mean %RSD of 1.74 and a mean %RE of 1.63 (N=90), compared to the prototype analyser which had a slightly better performance, with a mean %RSD of 1.05 and mean %RE of 1.25 (N=90). The results summarised in table 5.4. and shown in figure 5.9. also show an increased sensitivity for the analyser (y=0.043x) in comparison to the UV-Vis spectrometer (y=0.026x). This can be accounted for by the longer 22.5 mm detector pathlength of the fluidic chip in comparison to the 10 mm cuvette used in the UV-Vis spectrometer.

Table 5.4. *Analytical Performance of the Prototype analyser Vs UV-Vis Spectrometer (n=10 per measurement).*

PO_4^{3-} (µM)	UV-Vis Spectrometer		Prototype Analyser	
	Mean (µM) ± %RSD	**%RE**	**Mean (µM) ± %RSD**	**%RE**
1	1.07 ± 3.93	6.65	0.99±4.01	-0.70
2	2.00 ± 3.34	0.01	2.06 ± 2.03	2.76
4	3.91± 1.60	-2.33	3.93 ± 1.04	-1.74
6	6.23 ± 2.04	3.85	5.89 ± 0.77	-1.82
8	8.07 ± 1.50	0.84	7.84 ± 0.59	-1.94
10	10.05 ± 1.00	0.52	9.93 ± 0.52	-0.65
15	15.05 ± 1.18	0.35	15.08 ± 0.05	0.50
20	20.01 ± 0.61	0.07	20.11 ±0.24	0.57
25	25.02 ± 0.45	0.07	24.86 ± 0.21	-0.56
Mean (n=90)	1.74	1.63	1.05	1.25

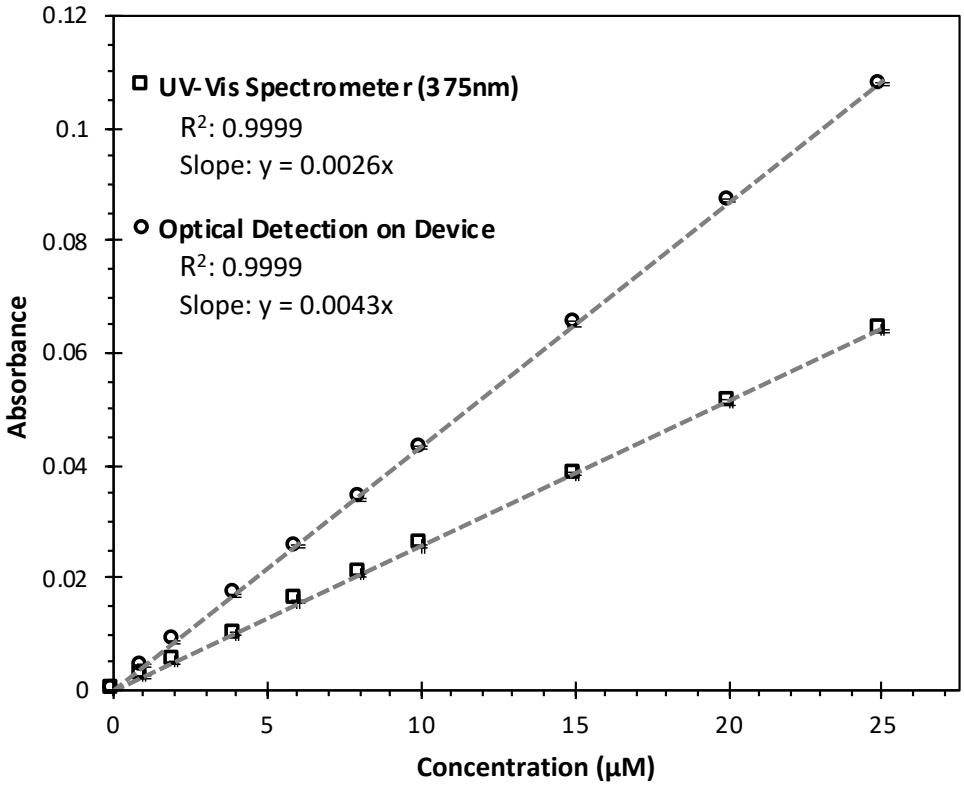

Figure 5.9. *Optical detection for phosphate (PO_4^{3-}) using the yellow method comparing the Prototype Analyser incorporating the fluidic chip and the UV-Vis spectrometer (375nm).*

5.3.4.2. In-Situ Field Testing

A further field study was arranged to test the prototype analyser, incorporating the fluidic chip, under real deployment conditions. The analyser was deployed at the river Liffey, Co. Dublin (figure 5.10.), and its field performance assessed over a period of 28 days (21/02/2018 to 20/03/2018). During this time the analyser functioned in a completely autonomous manner, obtaining, and analysing samples, as well as performing 2-point calibrations between each sample measurement.

Throughout the period of the deployment, samples were measured every 3 hours, comprising a total of 564 measurements, including environmental sample and internal sensor calibration measurements. Occasional grab samples were taken to validate the analyser performance via the UV-Vis lab-based reference method. The internal temperature of the analyser was also monitored, along with the external environmental temperature and water level throughout the deployment, see figure 5.11.

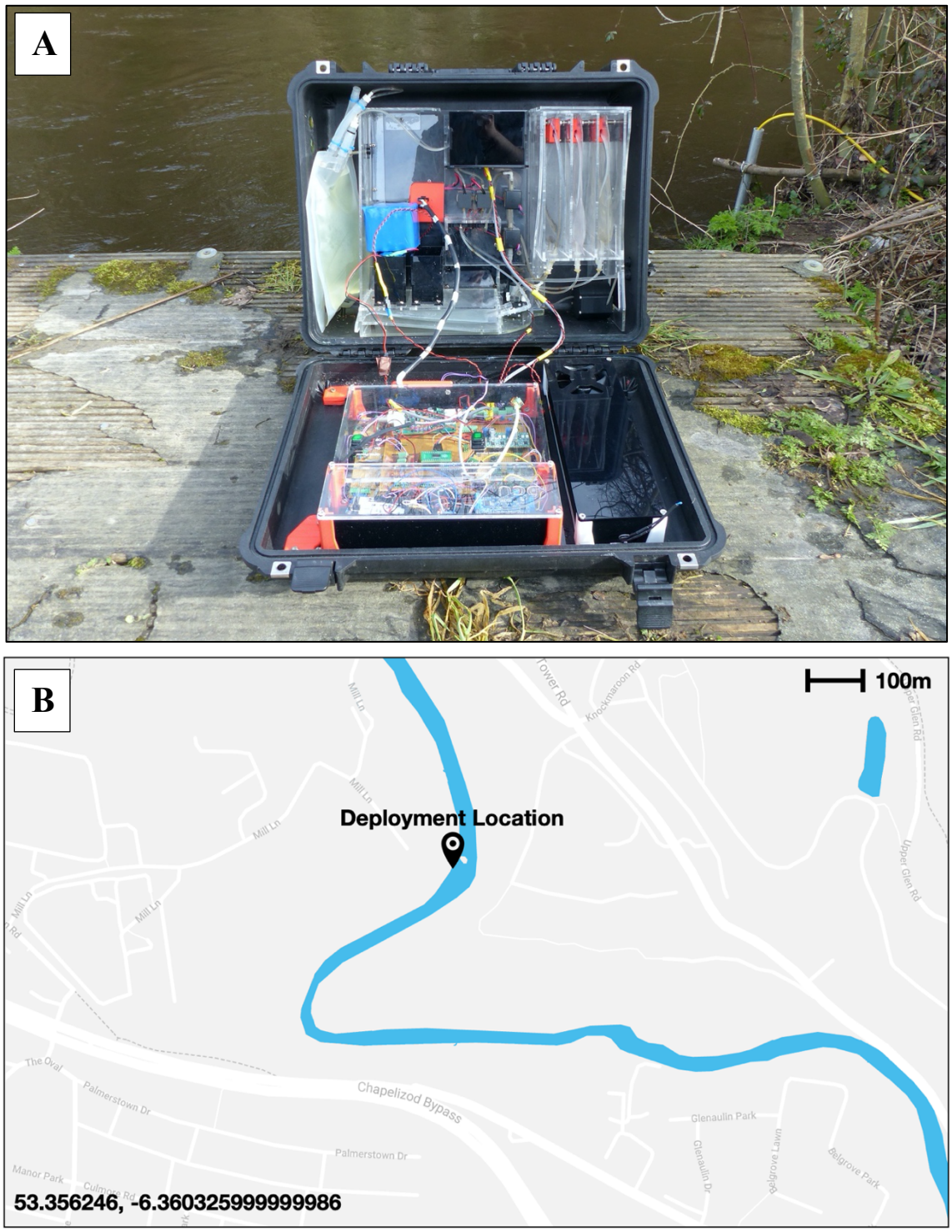

Figure 5.10. *(A) Picture of the prototype sensing platform deployment at Liffey deployment location, Co. Dublin, Ireland (B) Satellite image of the sampling location at Palmerstown, Co. Dublin, Ireland. (Coordinates 53.356246, -6.360325999999986).*

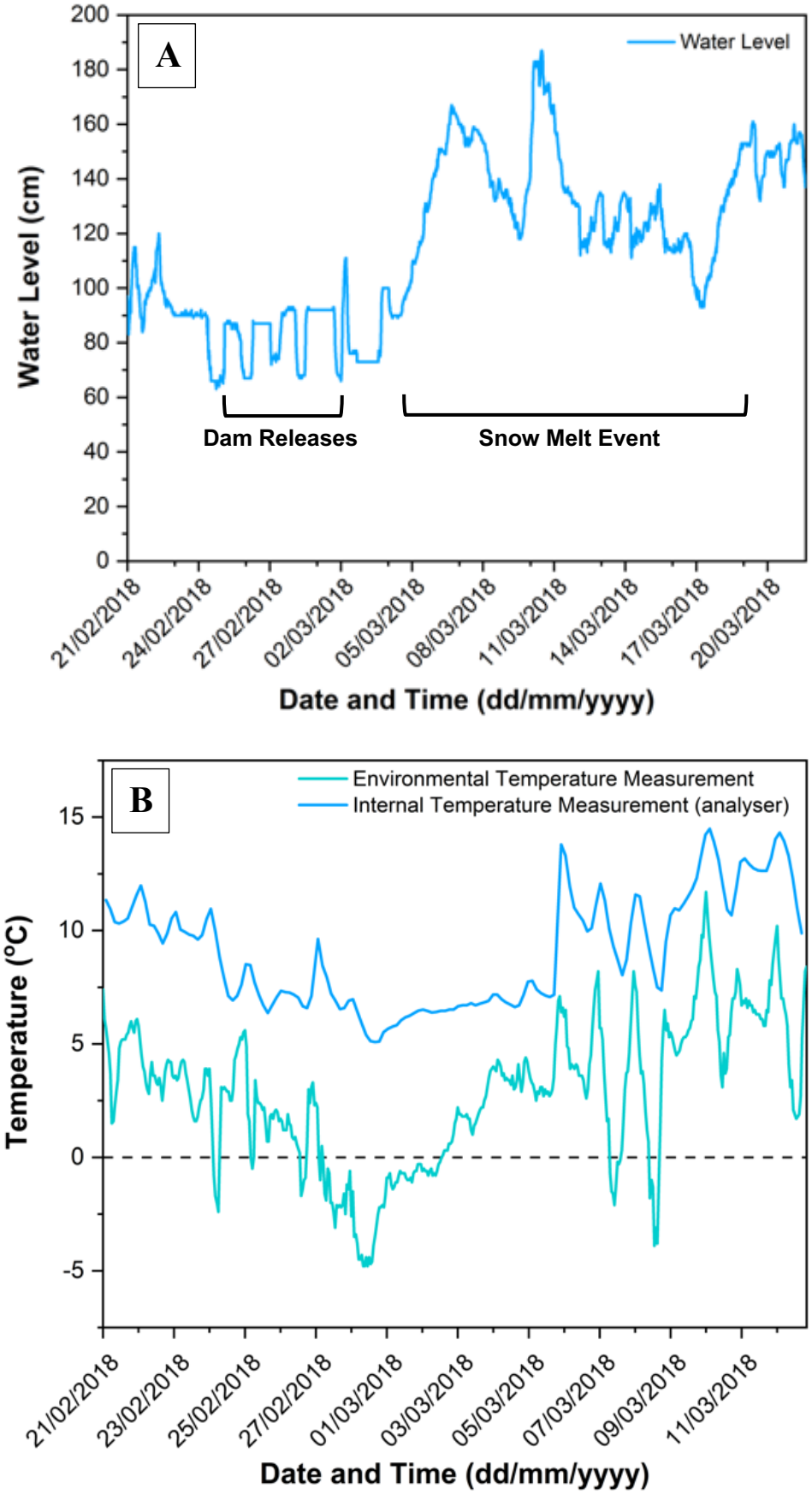

Figure 5.11. *In-Situ environmental monitoring. (A) water level (cm) from 21/02/2018 to 20/03/2018, (B) external and internal temperature (°C) from 21/02/2018 to 11/03/2018.*

The river Liffey is dam controlled with regular releases upstream of the deployment site being carried out by the Electricity Supply Board at Golden Falls and Leixlip. Figure 5.11. (A) shows the environmental monitoring of the river level using a depth gauge deployed alongside the analyser. During the 28-day deployment river levels ranged between 63 to 187 cm in depth. Dam releases can be seen during the period 25/02/18 to 02/03/18. A heavy snow fall occurred from the 24/02/18, with a subsequent melt beginning from 04/03/18. As a result, a rapid rise in water level was recorded (70 to 170 cm) before reaching a maximum level of 187 cm on 11/03/18. The average water level was 115 cm during the period of the deployment.

The prototype analyser was insulated to minimize heat loss and to prevent internal freezing within the platform. Figure 5.11. (B) shows the elevated temperature internally versus external environmental temperatures measured, due to the insulation of the analyser and small amounts of heat generated internally by the electronics. The internal temperature dropped to a low of 5.1 °C in comparison to a low of -4.8 °C being recorded externally (night of 28/02/18). Due to this insulation, the internal temperature changes are also dampened compared to the more rapid external fluctuations (e.g., see the changes from 05/03/18). From the 27/03/18 to 03/03/18 a major sub-zero temperature event occurred with the external temperature dropping to -5.0 °C, and thereafter rising rapidly to 11.7 °C. A series of much shorter sub-zero sharp temperature drops can be seen at 24/02/18, 07/03/18 and 09/03/18.

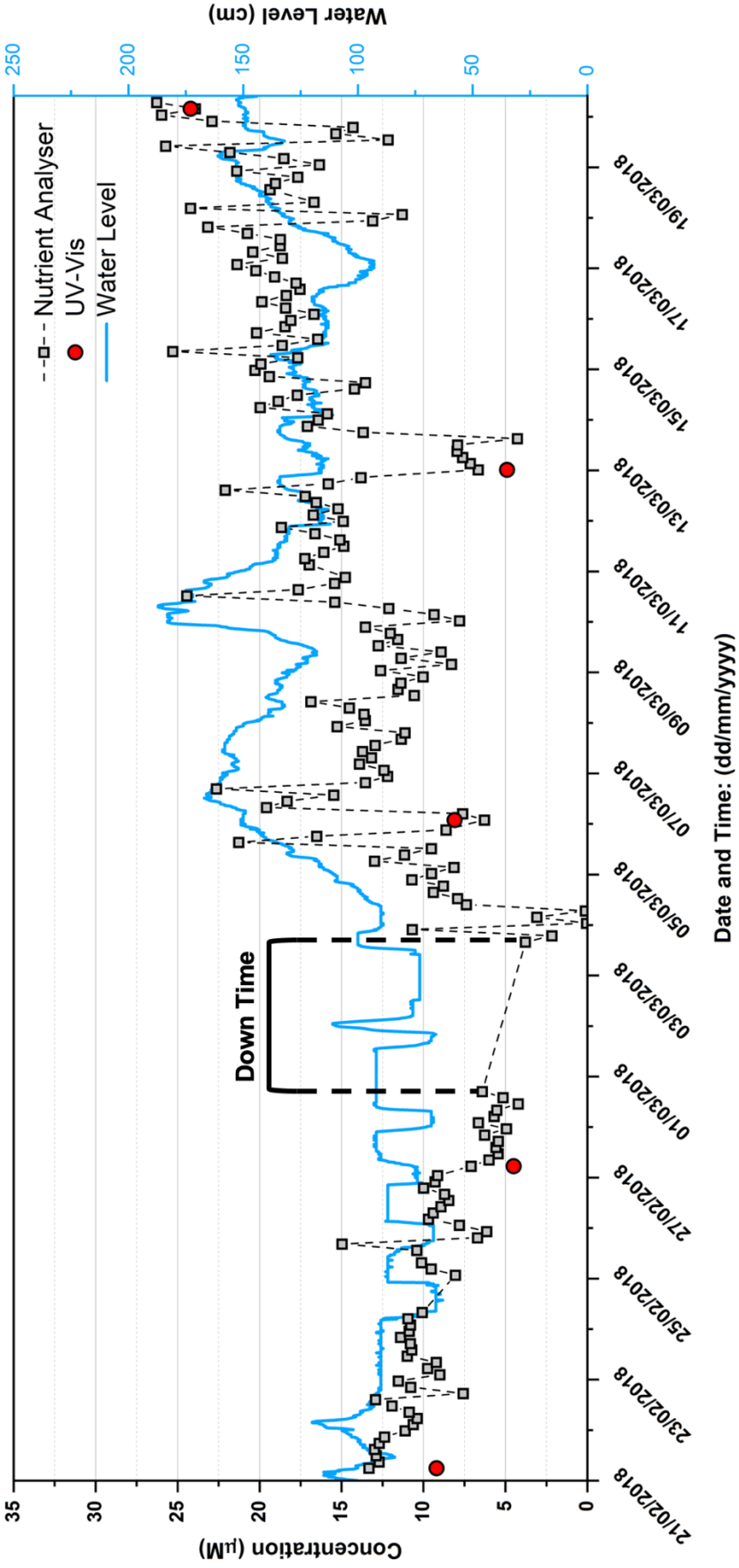

Figure 5.12. *Prototype analyser with integrated fluidic chip, phosphate (PO_4^{3-}) detection at the deployment site over a 28-day period.*

Figure 5.12. presents the results of the 28-day deployment to track variations in phosphate concentration during the deployment (grey squares), along with lab validation measurements (red circles) and water level (blue line). A total of 188 environmental phosphate measurements were recorded over the 28-day deployment (i.e., 564 measurements in total including 2-point calibration), using the fluidic chip in the analyser. During the deployment, the phosphate water concentrations together with the calibration data were transmitted to a cloud database for remote access.

There appears to be a general correlation between the phosphate concentration and the water level, which could in turn be linked to wash out of nutrients from fields into the river. The effect of run-off caused by the snow melt into the river from the surrounding area can be seen through the increased water levels from 05/03/18, which is coincident with gradual increase in phosphate concentration. A number of grab sample values correlate reasonably well with measured levels recorded from the in-situ analyser. The maximum detected phosphate (PO_4^{3-}) level during this deployment was 26.26 µM with an average of 13.0 µM detected over the 28-day period.

During the deployment, the analyser did not generate valid sample measurements during the period 01/03/2018 to 03/03/2018, highlighted in black in figure 5.12. This was due to a significant freezing event during which the external sampling line froze at the intake point, preventing the prototype analyser from acquiring samples. However, despite this, the internal functions were unaffected (reagents, pumps, electronics, power), and the platform continued to perform valid calibrations and transmit data. After 03/03/2018 the external sampling line thawed and recommenced acquiring samples as before, with no servicing or external intervention needed.

5.4. Conclusion

A methodology for combined thermal and vacuum bonding has been developed for the fabrication of fluidic chips. These manufactured chips were designed for rugged and reliable performance in environmental analysers. The chips were characterised, and performance assessed through several in-lab and in-situ field tests of the chips before and after integration into a prototype environmental analyser. Careful optimisation of

temperature and pressure during bonding of the two chip layers produced very strong adhesion with no observed leakage or failures throughout extensive testing.

The fluidic chips produced accurate and reproducible optical measurements for the detection of nutrients using colorimetric chemistries. The design allows for sample and reagent intake, mixing and detection all to be carried out on-chip. An environmental analyser incorporating one of these chips functioned successfully over a 28-day period during which time it was exposed to sub-zero fluctuating temperatures. Throughout this deployment no blockages, leakages or other types of failures occurred. The ruggedness and reliability of these chips will enhance the analyser system fluidics and in so doing, significantly improve the overall platform ruggedness and reliability in field deployments.

5.5. References

(1) Grand, M. M.; Clinton-Bailey, G. S.; Beaton, A. D.; Schaap, A. M.; Johengen, T. H.; Tamburri, M. N.; Connelly, D. P.; Mowlem, M. C.; Achterberg, E. P. A Lab-On-Chip Phosphate Analyzer for Long-Term In Situ Monitoring at Fixed Observatories: Optimization and Performance Evaluation in Estuarine and Oligotrophic Coastal Waters. *Frontiers in Marine Science* **2017**, *4*. https://doi.org/10.3389/fmars.2017.00255.

(2) Legiret, F.-E.; Sieben, V. J.; Woodward, E. M. S.; Abi Kaed Bey, S. K.; Mowlem, M. C.; Connelly, D. P.; Achterberg, E. P. A High Performance Microfluidic Analyser for Phosphate Measurements in Marine Waters Using the Vanadomolybdate Method. *Talanta* **2013**, *116*, 382–387. https://doi.org/10.1016/j.talanta.2013.05.004.

(3) Jońca, J.; León Fernández, V.; Thouron, D.; Paulmier, A.; Graco, M.; Garçon, V. Phosphate Determination in Seawater: Toward an Autonomous Electrochemical Method. *Talanta* **2011**, *87*, 161–167. https://doi.org/10.1016/j.talanta.2011.09.056.

(4) Vuillemin, R.; Sanfilippo, L.; Moscetta, P.; Zudaire, L.; Carbones, E.; Maria, E.; Tricoire, C.; Oriol, L.; Blain, S.; Bris, N. L.; Lebaron, P. Continuous Nutrient Automated Monitoring on the Mediterranean Sea Using in Situ Flow Analyser. 8.

(5) Sputh, B. H. C.; Faust, O.; Pettersson, L. H.; Hamre, T.; Vitulli, D.; Allen, A. R.; Spracklen, T. Integration of In-Situ and Remote Sensing Data for Water Risk Management. 8.

(6) McCaul, M.; Barland, J.; Cleary, J.; Cahalane, C.; McCarthy, T.; Diamond, D. Combining Remote Temperature Sensing with In-Situ Sensing to Track Marine/Freshwater Mixing Dynamics. *Sensors* **2016**, *16* (9), 1402. https://doi.org/10.3390/s16091402.

(7) Chebud, Y.; Naja, G. M.; Rivero, R. G.; Melesse, A. M. Water Quality Monitoring Using Remote Sensing and an Artificial Neural Network. *Water, Air, & Soil Pollution* **2012**, *223* (8), 4875–4887. https://doi.org/10.1007/s11270-012-1243-0.

(8) Bourgeois, W.; Romain, A.-C.; Nicolas, J.; Stuetz, R. M. The Use of Sensor Arrays for Environmental Monitoring: Interests and Limitations. *Journal of Environmental Monitoring* **2003**, *5* (6), 852. https://doi.org/10.1039/b307905h.

(9) Al-Turjman, F. M.; Hassanein, H. S.; Ibnkahla, M. A. Efficient Deployment of Wireless Sensor Networks Targeting Environment Monitoring Applications. *Computer Communications* **2013**, *36* (2), 135–148. https://doi.org/10.1016/j.comcom.2012.08.021.

(10) Jang, A.; Zou, Z.; Lee, K. K.; Ahn, C. H.; Bishop, P. L. State-of-the-Art Lab Chip Sensors for Environmental Water Monitoring. *Measurement Science and Technology* **2011**, *22* (3), 032001. https://doi.org/10.1088/0957-0233/22/3/032001.

(11) Donohoe, A.; Lacour, G.; McCluskey, P.; Diamond, D.; McCaul, M. Development of a Cost-Effective Sensing Platform for Monitoring Phosphate in Natural Waters. *Chemosensors* **2018**, *6* (4), 57. https://doi.org/10.3390/chemosensors6040057.

(12) Byrne, R.; Diamond, D. Chemo/Bio-Sensor Networks. *Nature Materials* **2006**, *5* (6), 421–424. https://doi.org/10.1038/nmat1661.

(13) Sacks, L.; Britton, M.; Wokoma, I.; Marbini, A.; Adebutu, T.; Marshall, I.; Roadknight, C.; Tateson, J.; Robinson, D.; Velazquez, A. G. The Development of a Robust, Autonomous Sensor Network Platform for Environmental Monitoring. 6.

(14) Pellerin, B. A.; Stauffer, B. A.; Young, D. A.; Sullivan, D. J.; Bricker, S. B.; Walbridge, M. R.; Clyde, G. A.; Shaw, D. M. Emerging Tools for Continuous Nutrient Monitoring Networks: Sensors Advancing Science and Water Resources Protection. *JAWRA Journal of the American Water Resources Association* **2016**, *52* (4), 993–1008. https://doi.org/10.1111/1752-1688.12386.

(15) Alliance for Coastal Technologies - Nutrient Sensor Challenge http://www.act-us.info/nutrients-challenge/About.php (accessed 2019 -03 -26).

(16) Diamond, D.; Cleary, J.; Maher, D.; Jungho Kim; King Tong Lau. Autonomous Analyser Platforms for Remote Monitoring of Water Quality. In *IECON 2011 - 37th Annual Conference of the IEEE Industrial Electronics Society*; IEEE: Melbourne, Vic, Australia, 2011; pp 3516–3521. https://doi.org/10.1109/IECON.2011.6119878.

(17) Mahmoudzadeh Andwari, A.; Pesiridis, A.; Rajoo, S.; Martinez-Botas, R.; Esfahanian, V. A Review of Battery Electric Vehicle Technology and Readiness Levels. *Renewable and Sustainable Energy Reviews* **2017**, *78*, 414–430. https://doi.org/10.1016/j.rser.2017.03.138.

(18) Bowden, M.; Diamond, D. The Determination of Phosphorus in a Microfluidic Manifold Demonstrating Long-Term Reagent Lifetime and Chemical Stability Utilising a Colorimetric Method. *Sensors and Actuators B: Chemical* **2003**, *90* (1–3), 170–174. https://doi.org/10.1016/S0925-4005(03)00024-8.

(19) Zhang, W.; Lin, S.; Wang, C.; Hu, J.; Li, C.; Zhuang, Z.; Zhou, Y.; Mathies, R. A.; Yang, C. J. PMMA/PDMS Valves and Pumps for Disposable Microfluidics. *Lab on a Chip* **2009**, *9* (21), 3088. https://doi.org/10.1039/b907254c.

(20) Guckenberger, D. J.; de Groot, T. E.; Wan, A. M. D.; Beebe, D. J.; Young, E. W. K. Micromilling: A Method for Ultra-Rapid Prototyping of Plastic Microfluidic Devices. *Lab on a Chip* **2015**, *15* (11), 2364–2378. https://doi.org/10.1039/C5LC00234F.

(21) Matellan, C.; del Río Hernández, A. E. Cost-Effective Rapid Prototyping and Assembly of Poly(Methyl Methacrylate) Microfluidic Devices. *Scientific Reports* **2018**, *8* (1). https://doi.org/10.1038/s41598-018-25202-4.

(22) Cleary, J.; Slater, C.; Diamond, D. Analysis of Phosphate in Wastewater Using an Autonomous Microfluidics-Based Analyser. **2009**, 4.

(23) Ashby, M. F. *Materials Selection in Mechanical Design*, 3rd ed.; Butterworth-Heinemann: Amsterdam ; Boston, 2005.

(24) Bowden, M.; Sequiera, M.; Krog, J. P.; Gravesen, P.; Diamond, D. Analysis of River Water Samples Utilising a Prototype Industrial Sensing System for Phosphorus Based on Micro-System Technology. *Journal of Environmental Monitoring* **2002**, *4* (5), 767–771. https://doi.org/10.1039/b200330a.

Chapter 6

Summary and Conclusions

6.1. Introduction

Despite decades of legislation and remediation efforts, water remains a scarce natural resource with declining quality due to naturogenic and increasing anthropogenic pressures [1]. This decline is widely acknowledged yet key events largely go unnoticed. Excess nutrient loading of waterways and aquatic ecosystems remains a persistent problem within the environment. Traditional sampling techniques and lab-based analysis continue to be the primary source of information on water quality [2], but this approach is not scalable and cannot produce data with sufficient spatial and temporal resolution. Improved sensing technologies are therefore critically important to meet these challenges, allowing more frequent sampling, at more locations, to provide real-time, high-quality data for more informed water management strategies.

6.2. Aims and achievements

The aim of this thesis was to develop, optimise and validate customisable environmental sensing platforms capable of accurately and robustly measuring key nutrients within the environment with improved temporal data resolution. Within the work presented in this thesis, two configurations of sensor were developed and extensively characterised, a benchtop sensing platform and an autonomous sensing platform.

The benchtop sensing platform was developed and used to gain insight into the function of the optics, detection circuitry and colorimetric methods and the relationship between them. The work showed that hardware and software level optimisation was necessary for a basic LED-photodiode detector to become an accurate and reliable sensor. The versatile design showed its capability to be adapted to a wide range of methods, with the addition of a powered heated regulated cell further broadening its application. The sensing platform was capable of accurately detecting phosphate, nitrite and nitrate in both calibration and real-world samples. The optimisation and validation of the benchtop sensing platforms measurement formed the foundations of the autonomous sensing platform.

A fluidic chip was extensively characterised and a fabrication methodology using thermal and vacuum bonding was developed. The fabrication focused on the

development of robust fluidics with a high bond strength to minimize leakage, large channel dimensions to improve optical properties and prevent blockages and improve the overall reliability of sensing platforms that are integrated with this fluidic chip.

The autonomous sensing platform realised the final goal of an operational autonomous sensing platform that was not only capable of functioning accurately and reliably in lab but also within the field. The reagent-based sensing platform was extensively validated and shown to be capable of continuous operation within the field on both a preliminary field deployment as well as an extended deployment lasting over 28 days. Both deployments demonstrated the autonomous sensing platform's ability to work under challenging conditions, with the extended deployment operating in harsh sub-zero temperatures. Data generated was capable of being remotely accessed and shared, offering a route to future integration with other sources of environmental data

6.3. Limitations to in-situ remote sensing

Unattended long-term deployment of chemical sensing platforms remains a challenge. The duration of autonomous operation remains a limitation for remote deployments of autonomous chemical sensing platforms. Therefore, ways to extend deployment lifetimes should be a significant focus. The main shortcomings remain power and battery lifetimes, sensor fouling, and consumables in the case of chemical sensing platforms.

Renewable energy sources such as solar energy offers a reliable source of power capable of extending deployment lifetimes [3]. Solar cells offer the potential to produce a net positive increase in battery with minimal need for maintenance. These improvements can be easily integrated removing one of the major limitations of sensing platforms. Combination of renewable energy sources and improved battery technology alongside energy efficient electronics will allow for long-term deployments without power and battery life limitations.

For reagent based chemical sensing, consumables such as reagents, calibration standards, and flush solutions remain a limiting factor requiring the need for frequent routine maintenance [4]. This remains a challenge especially in areas of remote

deployments. To develop a low demand sensing platform with minimal need for routine maintenance focus should be given to the miniaturisation and simplification of both the chemical methods as well as the internal fluidics.

Biofouling is a ubiquitous challenge to sensor deployment within the environment [5]. Several solutions are widely used to extend the maintenance periods due to fouling including wipers and cleaning brushes, and prefiltration and back flushing steps [6]. Continued research into anti fouling materials will further advance this area and aid in remediating this challenge [7].

6.4. Research drivers

The Covid-19 pandemic has given an insight into the environmental recovery that can be made through drastic habitual changes [8]. Improvements to air and water quality were reported globally [9]. Water pollution in Venice, Italy was significantly reduced due to lockdown with canals visually clear when compared to pre lockdown [10]. Similarly, several beaches have reported water quality improvements due to reduction in footfall and tourism [10]. Improvements have also been reported in areas typically exposed to industrial related pollution. Chakraborty et al. [11] reported a reduction in total nitrogen and phosphorus in the river Damodar, India, which pre-covid was highly eutrophic. Yunus et al. [12] reported an average reduction in suspended particulate matter of 15.9% compared to pre covid levels in the Vembanad lake, India. Cherif et al. [13] reported that Tangier coastal environment, Morocco, showed a positive impact on its water quality following decreasing industrial discharge due to lockdown.

However short term this effect is, it points to the potential for the environment to rapidly recover from a declining status if well informed and appropriately targeted action is taken. While lockdown measures introduced in response to the Covid-19 pandemic have led to cleaner air, waters, and reduced noise, it has also negatively influenced economic activities. The EU Green deal aims to have similar environmental improvements however its response revolves around boosting the efficient use of resources by moving to a clean, circular economy [14]. The aim is to have a resource efficient economy with no net emissions of greenhouse gases where economic growth is unhindered. The deal has recognised that current environmental measures will not

suffice to meet targets and that disruptive change is needed [15]. It sets out an integrated plan where pollution is reduced to levels that are no longer harmful to human health and natural ecosystems by 2050. The plan outlines several flagship initiatives and actions including, reviewing the standards for the quality of water in EU rivers and seas , and the "farm to fork" strategy [16] which will also aid in pollution reduction in natural waters as it aims to reduce the use of fertilizers by 20% and reduce nutrient loss by at least 50%.

The EU Horizon Europe program is the European Union's flagship research and innovation programme and has a total budget of €95.5 billion for 2021-2027, an increase of 30% over the previous program, Horizon 2020 [17]. The goal for Horizon Europe is to stimulate and accelerate research, development, and innovation activities. 30% of the total budget will be allocated towards green technology research, in this there will be focuses on healthy oceans, seas, coastal and inland waters [18] with cluster five of the programme aiming to fight climate change by better understanding its causes, evolution, risks, and impacts [19].

This demonstrates the increasing impact of growing environmental awareness and recognition of the importance of the global climate emergency facing humanity. Climate and Biodiversity emergency declarations, Global and European environmental directives, and research and development programmes are all key steps towards addressing and mitigating damage to the environment and waterways globally [20]. These initiatives will help to drive the demand to develop, accurate and reliable monitoring strategies. For regulations to be followed and remediation efforts to be tailored an increased effort must be made to sense and detect environmental change so that these efforts can be tracked

6.5. Future progress of the autonomous sensing platform

The autonomous sensing platform demonstrated in chapters 4 and 5 represents a considerable effort in terms of platform development, validation and deployment however there is still significant potential for future progress.

In the short term generational prototyping and developmental refinements should continue with a focus on platform robustness, miniaturisation and deployment longevity to address the limitations presented in section 6.3. With the success of the sensing platform deployments, the major emphasis should be towards continued long-term deployment and field testing with a focus on extending the length of deployment as well as the number of deployed sensing platforms aiming for improved spatial and temporal resolution at key locations.

In the longer term a focus on manufacturing scale up towards commercialisation should be considered. Progress should be made towards component selection that allows for low cost, large scale manufacture with an emphasis on ease of assembly. With validation completed the manufacturing techniques could shift to methods less suited to prototyping but more favourable to scale up. For example the electronics could move from hand soldered prototyping boards to fully integrated PCB boards [21], and the fluidic chip could move from micro milling to high volume manufacturing techniques such as hot embossing or injection moulding [22].

A secondary goal should be expansion of the applicable colorimetric methods utilised in the autonomous sensing platform. The focus was primarily on phosphate detection within the autonomous sensing platform due to its ease of integration and excellent method and reagent stability. The success of this platform opens the route towards further integration of alternative applicable colorimetric methods for the detection of other key nutrients such as those presented for nitrite and nitrate in chapters 2 and 3.

6.6. Challenges to further development and progress

Aside from the current limitations to autonomous in-situ remote sensing there are also several challenges towards further development of the autonomous sensing platforms presented in chapters 4 and 5.

For research groups large scale environmental monitoring campaigns can be a significant undertaking when collecting in situ environmental data. Chemical based autonomous sensing platforms demand high levels of work from skilled staff with the need for continual maintenance, validation and data interpretation. When aiming to

increase the spatial and temporal distribution of these autonomous sensing platforms a proportionally greater allocation of resources and manpower is also necessary, as a result the temporal and spatial scale of water quality monitoring is largely determined by financial and logistical constraints [21].

Similarly scale up towards large scale manufacture requires significant effort, the fabrication of multiple units requires a significant workload involving not only fabrication but calibration and validation of each sensing platform. In order for scale up to be successful the sensing platforms design must have moved passed small scale manufacture where the final layout and configuration has been chosen to avoid conflict between development and fabrication [23].

6.7. Strategies for achieving further progress

For a sensing platform to gain significant improvements in robustness, miniaturisation and deployment longevity, significant breakthroughs in technology that provide innovative and disruptive solutions need to be achieved. Future impact from new fabrication technologies may revolutionize sensor manufacturing where unit production cost can be reduced while maintaining or improving reliability [24]. Miniaturisation of fluidic systems remains limited by the scale of currently manufactured pumps and valves for fluidic control. New fundamental approaches to fluidic control such as the work presented by Pandurangan et al. [25] showing the use of stimuli responsive actuators capable of direct integration into fluidic devices may offer potential in the future as ground breaking solutions for further minimizing component and sensing platform scale.

For developing prototype sensing platforms the leap from lab testing to environmental deployment can be significant. Promotion of deployments through improved infrastructure and site access in key environmental areas of interest may help bridge the gap. Availability of reference testing sites [23] with access to power, communications and a secure deployment location would encourage the move from lab to field for many research groups. These sites could act as standardised locations for field testing with improved sample validation efforts. This effort could also further improve integration and collaboration between researchers.

There remains a clear need to improve data integration and sharing, moving away from isolated individual datasets towards collaborative open access systems to create comprehensive multiparameter rich datasets [26]. Open access data and increasing multidisciplinary collaboration from research groups advances this effort, allowing for improved data sets that minimize duplications of research.

6.8. Advancing Sensor Networks

Internet of Things (IoT) networks have advanced rapidly in recent years due to improved multidisciplinary research in communications, cloud infrastructure, data analytics and smart sensing [27]. Further integration in these areas alongside reliable sensing platforms will allow for the realisation of networked IoT sensing platforms, allowing for autonomous operation and communication in real time or near real time.

In its current state direct in-situ sensing alone will not have sufficient resolution to measure water status globally. This can only be achieved through combined research efforts into combination sensing. The combination of in-situ and satellite remote sensing could be a powerful tool for water quality estimation. In-situ sensing can provide validated high frequency measurements of the local concentration of specific analytes [4] and remote sensing is capable of large-scale generalised measurement [28]. This complementary approach can provide the ability to actively monitor water processes at a global scale and at a resolution that enables highly localized behaviour to be visualized.

This proposed approach offers a feasible real-world solution utilizing in situ sensing, satellite remote sensing and cloud-based communication equipment alongside data processing. This would provide the ability to predict and map much more complicated processes such as origins of pollution events, the severity of the event and the direction of spreading that may occur and will allow for understanding of how local events contribute to the global environment.

6.9. References

(1) Khatri, N.; Tyagi, S. Influences of Natural and Anthropogenic Factors on Surface and Groundwater Quality in Rural and Urban Areas. *Frontiers in Life Science* **2015**, *8* (1), 23–39. https://doi.org/10.1080/21553769.2014.933716.

(2) Kianpoor Kalkhajeh, Y.; Jabbarian Amiri, B.; Huang, B.; Henareh Khalyani, A.; Hu, W.; Gao, H.; Thompson, M. L. Methods for Sample Collection, Storage, and Analysis of Freshwater Phosphorus. *Water* **2019**, *11* (9), 1889. https://doi.org/10.3390/w11091889.

(3) Krejcar, O.; Mahdal, M. Optimized Solar Energy Power Supply for Remote Wireless Sensors Based on IEEE 802.15.4 Standard. *International Journal of Photoenergy* **2012**, *2012*, e305102. https://doi.org/10.1155/2012/305102.

(4) Daniel, A.; Laës-Huon, A.; Barus, C.; Beaton, A. D.; Blandfort, D.; Guigues, N.; Knockaert, M.; Munaron, D.; Salter, I.; Woodward, E. M. S.; Greenwood, N.; Achterberg, E. P. Toward a Harmonization for Using in Situ Nutrient Sensors in the Marine Environment. *Front. Mar. Sci.* **2020**, *6*. https://doi.org/10.3389/fmars.2019.00773.

(5) Delauney, L.; Compère, C.; Lehaitre, M. Biofouling Protection for Marine Environmental Sensors. *Ocean Sci.* **2010**, *6* (2), 503–511. https://doi.org/10.5194/os-6-503-2010.

(6) Bixler, G. D.; Bhushan, B. Biofouling: Lessons from Nature. *Proc. R. Soc. A* **2012**, *370* (1967), 2381–2417. https://doi.org/10.1098/rsta.2011.0502.

(7) Delgado, A.; Briciu-Burghina, C.; Regan, F. Antifouling Strategies for Sensors Used in Water Monitoring: Review and Future Perspectives. *Sensors* **2021**, *21* (2), 389. https://doi.org/10.3390/s21020389.

(8) Manzanedo, R. D.; Manning, P. COVID-19: Lessons for the Climate Change Emergency. *Science of The Total Environment* **2020**, *742*, 140563. https://doi.org/10.1016/j.scitotenv.2020.140563.

(9) Shakil, M. H.; Munim, Z. H.; Tasnia, M.; Sarowar, S. COVID-19 and the Environment: A Critical Review and Research Agenda. *Science of The Total Environment* **2020**, *745*, 141022. https://doi.org/10.1016/j.scitotenv.2020.141022.

(10) Mousazadeh, M.; Paital, B.; Naghdali, Z.; Mortezania, Z.; Hashemi, M.; Karamati Niaragh, E.; Aghababaei, M.; Ghorbankhani, M.; Lichtfouse, E.; Sillanpää, M.; Hashim, K. S.; Emamjomeh, M. M. Positive Environmental Effects of the

Coronavirus 2020 Episode: A Review. *Environ Dev Sustain* **2021**, 1–23. https://doi.org/10.1007/s10668-021-01240-3.

(11) Chakraborty, B.; Roy, S.; Bera, A.; Adhikary, P. P.; Bera, B.; Sengupta, D.; Bhunia, G. S.; Shit, P. K. Eco-Restoration of River Water Quality during COVID-19 Lockdown in the Industrial Belt of Eastern India. *Environ Sci Pollut Res* **2021**, *28* (20), 25514–25528. https://doi.org/10.1007/s11356-021-12461-4.

(12) Yunus, A. P.; Masago, Y.; Hijioka, Y. COVID-19 and Surface Water Quality: Improved Lake Water Quality during the Lockdown. *Science of The Total Environment* **2020**, *731*, 139012. https://doi.org/10.1016/j.scitotenv.2020.139012.

(13) Cherif, E. K.; Vodopivec, M.; Mejjad, N.; Esteves da Silva, J. C. G.; Simonovič, S.; Boulaassal, H. COVID-19 Pandemic Consequences on Coastal Water Quality Using WST Sentinel-3 Data: Case of Tangier, Morocco. *Water* **2020**, *12* (9), 2638. https://doi.org/10.3390/w12092638.

(14) A European Green Deal https://ec.europa.eu/info/strategy/priorities-2019-2024/european-green-deal_en (accessed 2021 -06 -25).

(15) The European Green Deal - communication from the commission https://eur-lex.europa.eu/legal-content/EN/TXT/HTML/?uri=CELEX:52019DC0640&from=EN (accessed 2021 -06 -25).

(16) From Farm to Fork https://ec.europa.eu/info/strategy/priorities-2019-2024/european-green-deal/actions-being-taken-eu/farm-fork_en (accessed 2021 -06 -25).

(17) Horizon Europe https://ec.europa.eu/info/research-and-innovation/funding/funding-opportunities/funding-programmes-and-open-calls/horizon-europe_en (accessed 2021 -06 -25).

(18) Mission area: Healthy oceans, seas, coastal and inland waters https://ec.europa.eu/info/research-and-innovation/funding/funding-opportunities/funding-programmes-and-open-calls/horizon-europe/missions-horizon-europe/healthy-oceans-seas-coastal-and-inland-waters_en (accessed 2021 -06 -25).

(19) Cluster 5: Climate, Energy and Mobility https://ec.europa.eu/info/research-and-innovation/funding/funding-opportunities/funding-programmes-and-open-

calls/horizon-europe/cluster-5-climate-energy-and-mobility_en (accessed 2021 -06 -25).

(20) Grizzetti, B.; Vigiak, O.; Udias, A.; Aloe, A.; Zanni, M.; Bouraoui, F.; Pistocchi, A.; Dorati, C.; Friedland, R.; De Roo, A.; Benitez Sanz, C.; Leip, A.; Bielza, M. How EU Policies Could Reduce Nutrient Pollution in European Inland and Coastal Waters. *Global Environmental Change* **2021**, *69*, 102281. https://doi.org/10.1016/j.gloenvcha.2021.102281.

(21) Chan, K.; Schillereff, D. N.; Baas, A. C.; Chadwick, M. A.; Main, B.; Mulligan, M.; O'Shea, F. T.; Pearce, R.; Smith, T. E.; van Soesbergen, A.; Tebbs, E.; Thompson, J. Low-Cost Electronic Sensors for Environmental Research: Pitfalls and Opportunities. *Progress in Physical Geography: Earth and Environment* **2021**, *45* (3), 305–338. https://doi.org/10.1177/0309133320956567.

(22) Scott, S.; Ali, Z. Fabrication Methods for Microfluidic Devices: An Overview. *Micromachines* **2021**, *12* (3), 319. https://doi.org/10.3390/mi12030319.

(23) Regan, F.; Lawlor, A.; McCarthy, A.; Ireland; Environmental Protection Agency; Marine Institute (Galway, I.; EPA STRIVE Programme. *SmartCoast Project: Smart Water Quality Monitoring System : (AT-04-01-06) : Synthesis Report*; Environmental Protection Agency: Wexford, 2009.

(24) Diamond, D. Grand Challenges and Opportunities in Sensor Science and Technology. *Front. Sens.* **2020**, *1*, 2. https://doi.org/10.3389/fsens.2020.00002.

(25) Pandurangan, K.; Barrett, R.; Diamond, D.; McCaul, M. Fluidic Platforms Incorporating Photo-Responsive Soft-Polymers Based on Spiropyran: From Green Synthesis to Precision Flow Control. *Front. Mater.* **2021**, *7*, 615021. https://doi.org/10.3389/fmats.2020.615021.

(26) Mao, F.; Khamis, K.; Krause, S.; Clark, J.; Hannah, D. M. Low-Cost Environmental Sensor Networks: Recent Advances and Future Directions. *Front. Earth Sci.* **2019**, *7*, 221. https://doi.org/10.3389/feart.2019.00221.

(27) Kumar, S.; Tiwari, P.; Zymbler, M. Internet of Things Is a Revolutionary Approach for Future Technology Enhancement: A Review. *J Big Data* **2019**, *6* (1), 111. https://doi.org/10.1186/s40537-019-0268-2.

(28) Dubovik, O.; Schuster, G. L.; Xu, F.; Hu, Y.; Bösch, H.; Landgraf, J.; Li, Z. Grand Challenges in Satellite Remote Sensing. *Front. Remote Sens.* **2021**, *2*. https://doi.org/10.3389/frsen.2021.619818.

Supplementary Information

Chapter 2

Development and optimisation of a customisable benchtop sensing platform for detection of optical colorimetric chemistries.

Figure SI.2.1. shows a sub section of the in-house code for the benchtop sensing platform where system variables can be modified. The code written through Arduino IDE contains all the setup variables and libraries to control the benchtops operation, sets up all hardware components (LED, ADC, Serial command, SD Card), and contains the serial command functions for Launching data acquisition manually.

```
#include <Adafruit_ADS1015.h>
#include <Adafruit_PWMServoDriver.h>
#include <Wire.h>
#include <SPI.h>
#include <SD.h>

Adafruit_ADS1115 ads(0x48); // sets up an iteration of the Analog to Digital library
Adafruit_PWMServoDriver pwm = Adafruit_PWMServoDriver(0x40);  // sets up an iteration of the PWM driver

// EDIT FOR TESTING
const float uM_conc = 0;
int
ohm_R = 470,
PWMStart = 0,
PWMEnd = 4000,
PWMStep = 200,
N_meas = 500,
delay_measures = 5;

// SYSTEM PARAMETERS
const int
LEDChannel = 0,
LED_OFF_PWM = 4096,
SD_CS = 53,
TRIG_PIN = 38,
PWMFreq = 1000;
const float SerialFreq = 115200;

// GLOBAL VARIABLES
int titleFlag = 0, PWMValue, ADC_A0, ADC_A2, n =0;
bool file_End=false;
bool typing_possible=false;
bool finish_setup=false;
bool begin_prog=true;

// Creates the logFile with the number increasing each time
char* fileName = "SD_log.csv"; // character array storing file name (max 8 letters name)
```

Figure SI.2.1. *Initial setup code for microcontroller function with modifiable system variables.*

Figure SI.2.2. shows a medium speed spectrum scan of a selected grades and thicknesses of PMMA from 250-700 nm showing the optical clarity of PMMA in the visible region of the spectrum.

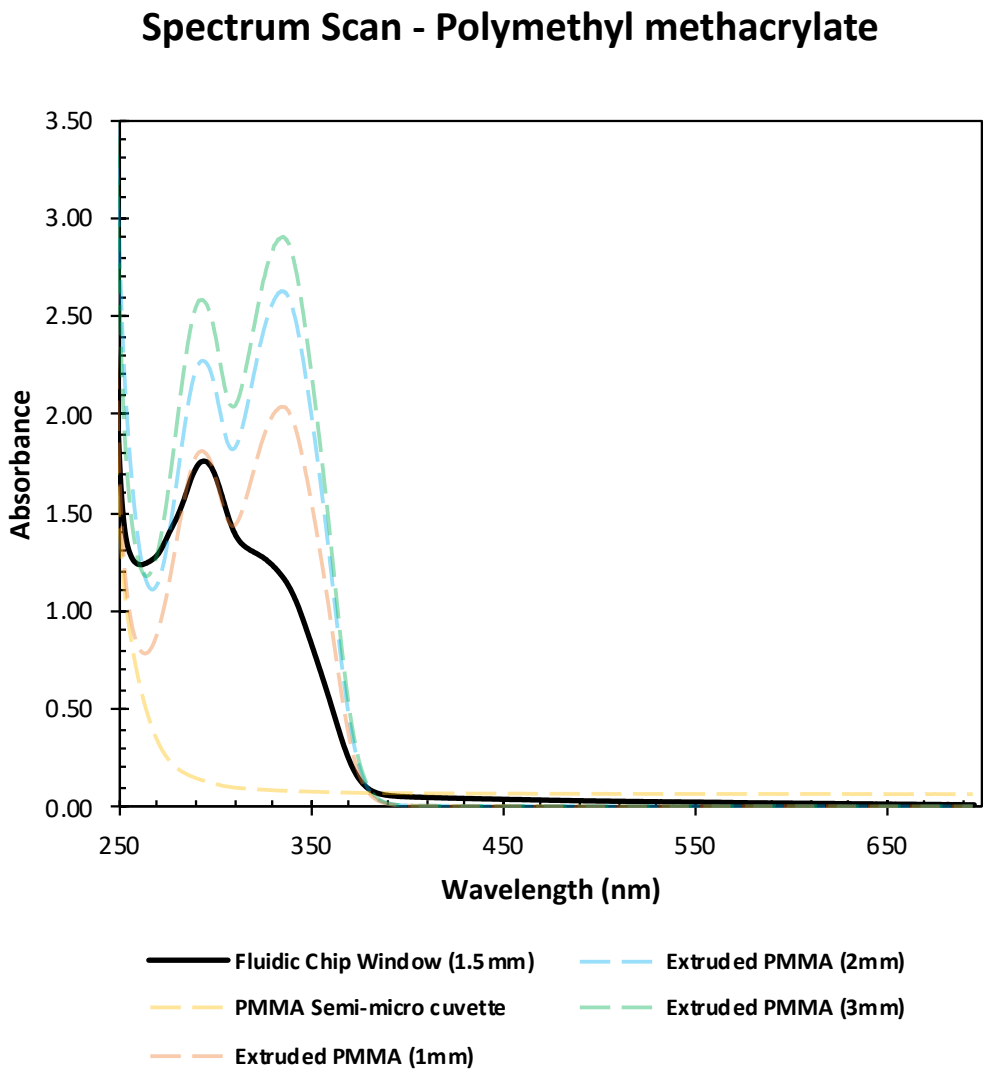

Figure SI.2.2. *Spectrum scan of fluidic chip optical window (Black Line) and alternative variations of "clear" Polymethyl methacrylate.*

Figure SI.2.3. shows the calibration curves used to demonstrate the linear dynamic range on UV-Vis photo spectrometer in chapter 2 section 2.3.1.3. These calibrations for phosphate and nitrite were used as the sample data sets for the generation of the molar extinction coefficients, upper limits, and correlation coefficients.

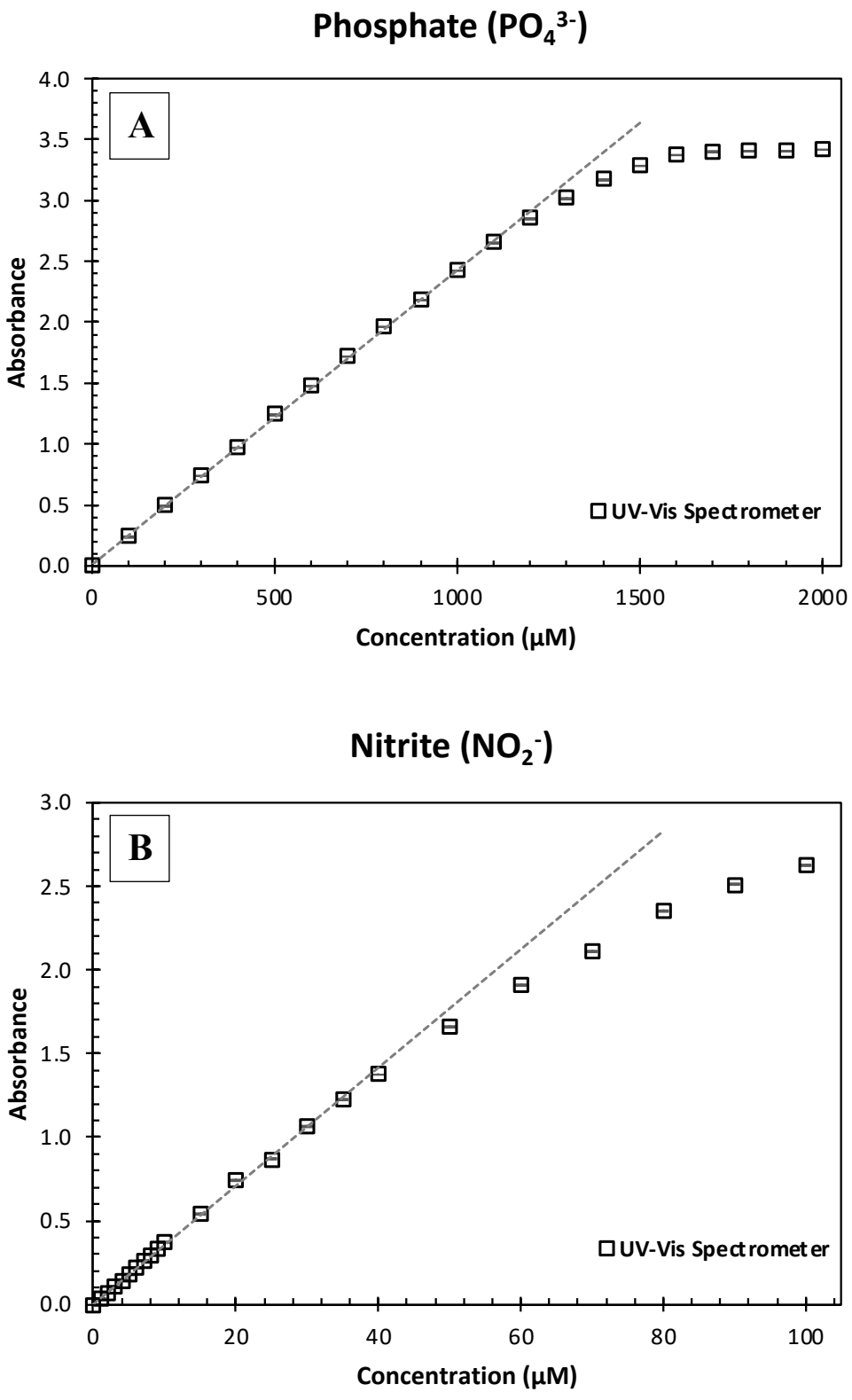

Figure SI.2.3. *Calibration curve of (A) phosphate standards ranging from 0-2000 µM and (B) nitrite standards ranging from 0-100 µM carried out on UV-Vis Spectrometer. The error bars represent the standard deviations for n=3.*

Figure SI.2.4. shows (A) the variation in light intensity from a batch (N=10) of Roithner LaserTechnik XSL-375-TF-R2 UV LEDs with each measured under the same experimental conditions of a static PWM signal and resistance and (B) matching light intensity when corrected for using a target value and a varied PWM signal. Variation in intensity before correction is measured as a %RSD of 6.96 (average bits value of 10757.42 with standard deviation of 749.00 bits) and after correction is measured as a %RSD of 0.02 (average bits value of 10001.49 with standard deviation of 2.20 bits).

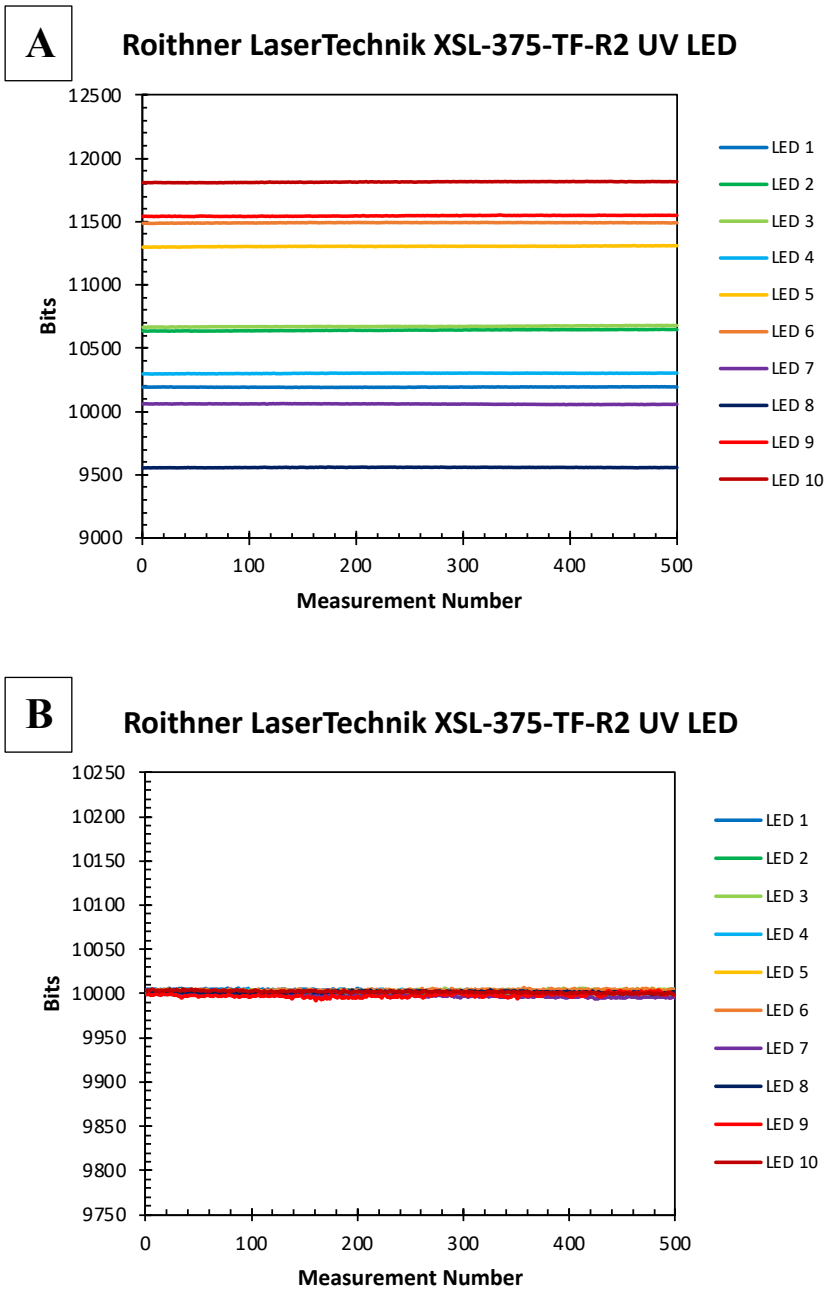

Figure SI.2.4. *Roithner LaserTechnik XSL-375-TF-R2 UV LED (A) LED batch to batch intensity variation and (B) corrected LED intensity (N=10)*

Figure SI.2.5. shows (A) the variation in light intensity from a batch (N=10) of Roithner LaserTechnik LED 545-33 with each measured under the same experimental conditions of a static PWM signal and resistance and (B) matching light intensity when corrected for using a target value and a varied PWM signal. Variation in intensity before correction is measured as a %RSD of 17.49 (average bits value of 10722.74 with standard deviation of 1876.29 bits) and after correction is measured as a %RSD of 0.02 (average bits value of 10001.44 with standard deviation of 2.33 bits).

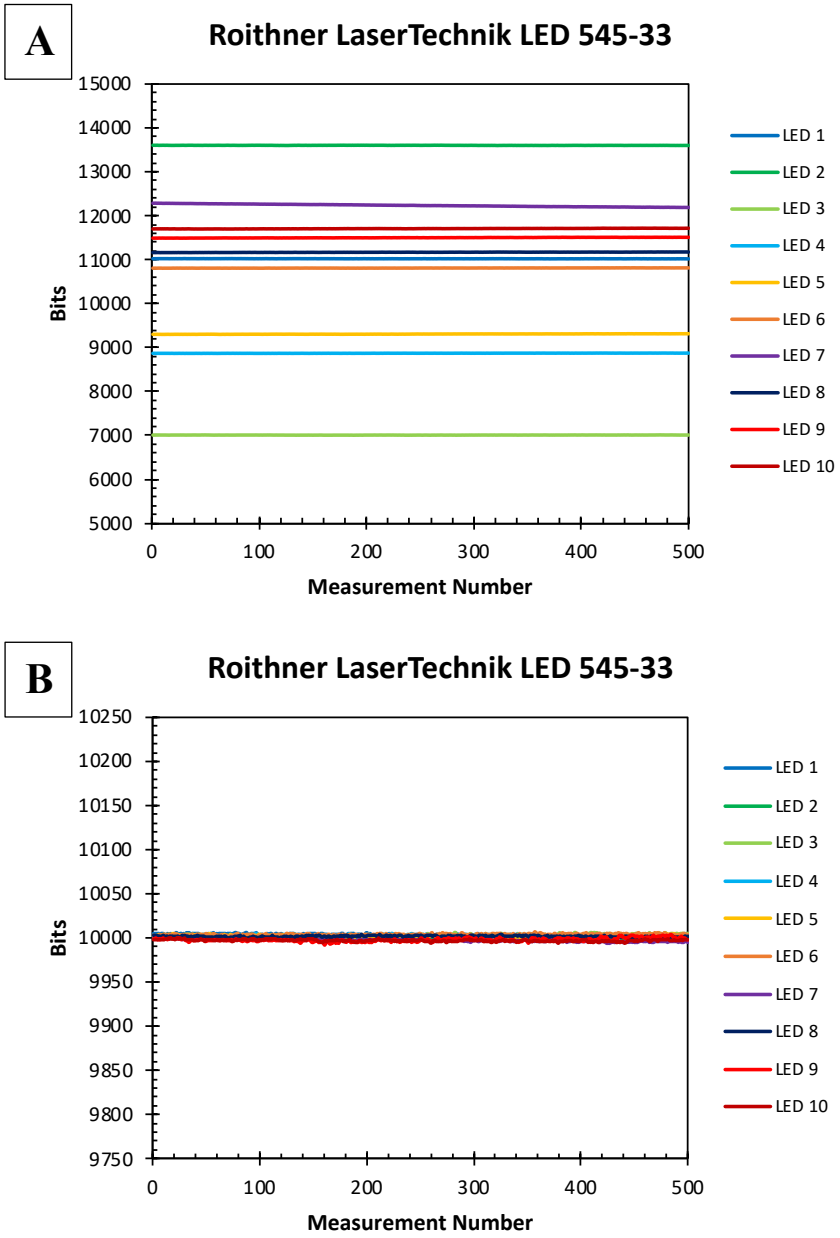

Figure SI.2.5. *Roithner LaserTechnik LED 545-33 (A) LED batch to batch intensity variation and (B) corrected LED intensity (N=10)*

Figure SI.2.6. shows (A) the variation in measured light intensity from a batch (N=10) of TSL257 LF ams Photodiodes with each measured under the same experimental conditions of an LED emitting a set light intensity with static PWM signal and resistance and (B) matching measured light intensity when corrected for using a target value and a varied PWM signal. Variation in intensity before correction is measured as a %RSD of 4.20 (average bits value of 8565.62 with standard deviation of 360.00 bits) and after correction is measured as a %RSD of 0.03 (average bits value of 10000.52 with standard deviation of 3.40 bits).

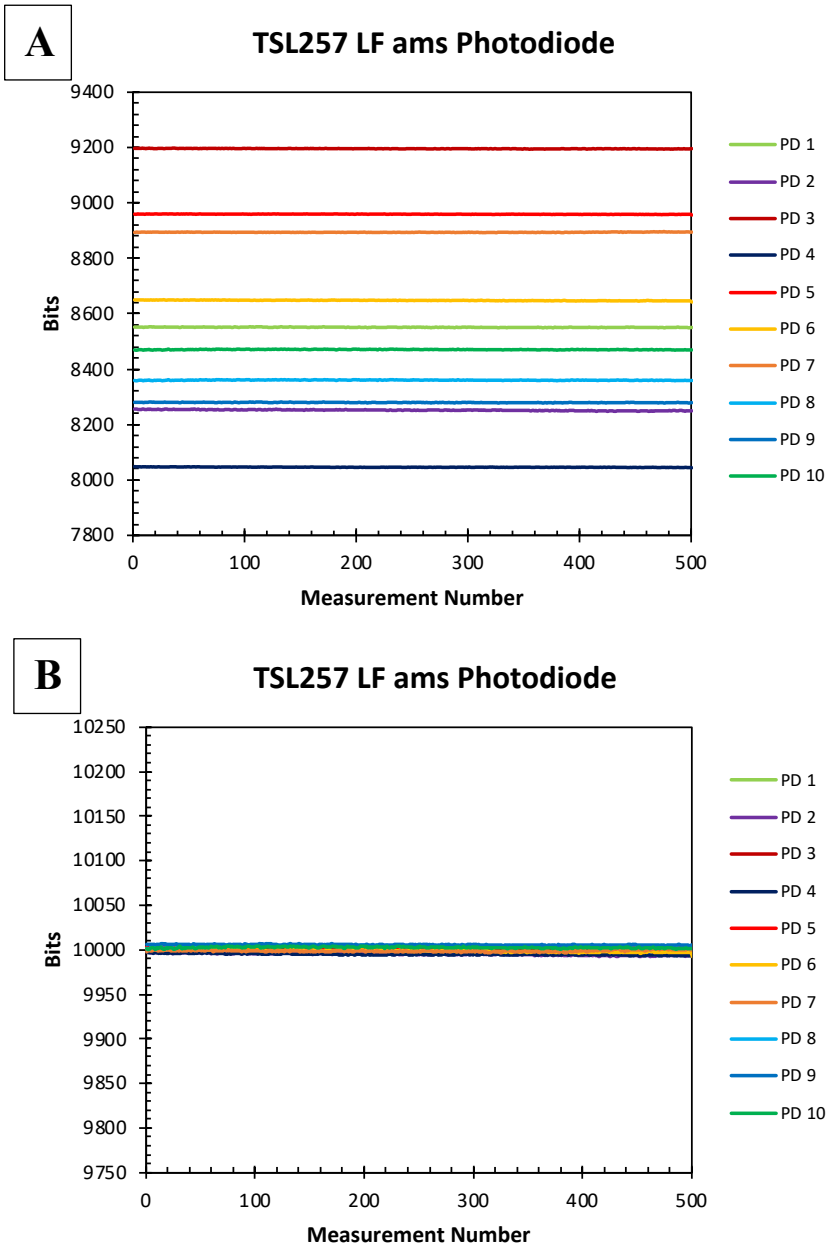

Figure SI.2.6. *TSL257 LF ams Photodiode (A) Photodiode batch to batch intensity measurement variation and (B) corrected Photodiode measurement (N=10)*

Optimisation on a hardware level through tuning of the on-board resistor was tested for phosphate in Chapter 2. The results below show the reproduction of this work for nitrite using the alternative 545 nm LED chosen for the Griess assay. The results show that the optimised PWM (SI.2.8.) controller give a lower overall intensity (bits) with a distribution of 4000-8000 bits in comparison to the unoptimized (SI2.7.) 8,000 – 28,0000 but with a significant better grouping of slopes, showing uniform sensitivity at a range of light intensities (4000-8000).

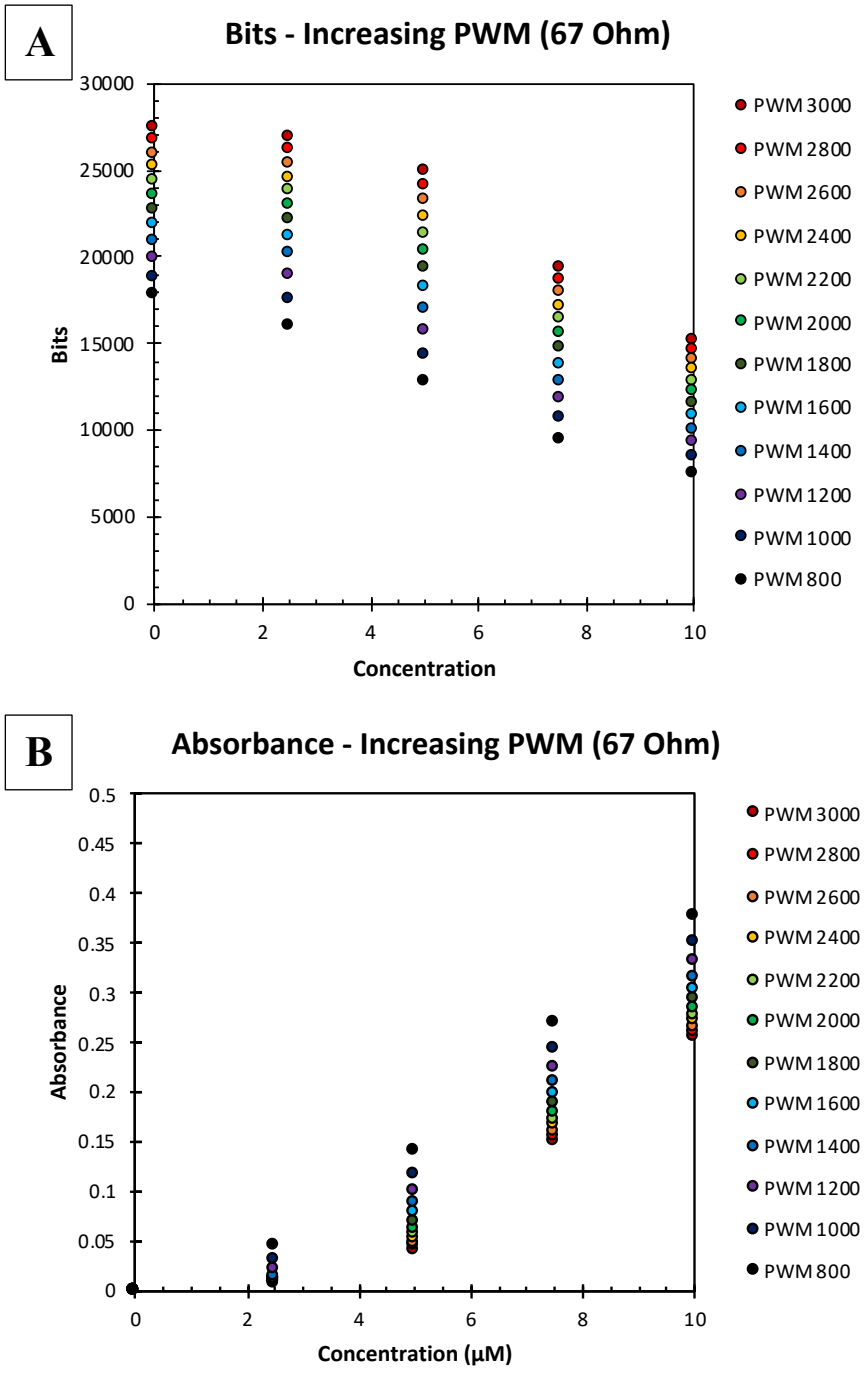

Figure SI.2.7. *Calibration curve for nitrite (NO_2^-) presenting (A) in bits (raw data) and (B) converted absorbance using benchtop detection platform at 67 Ω resistance.*

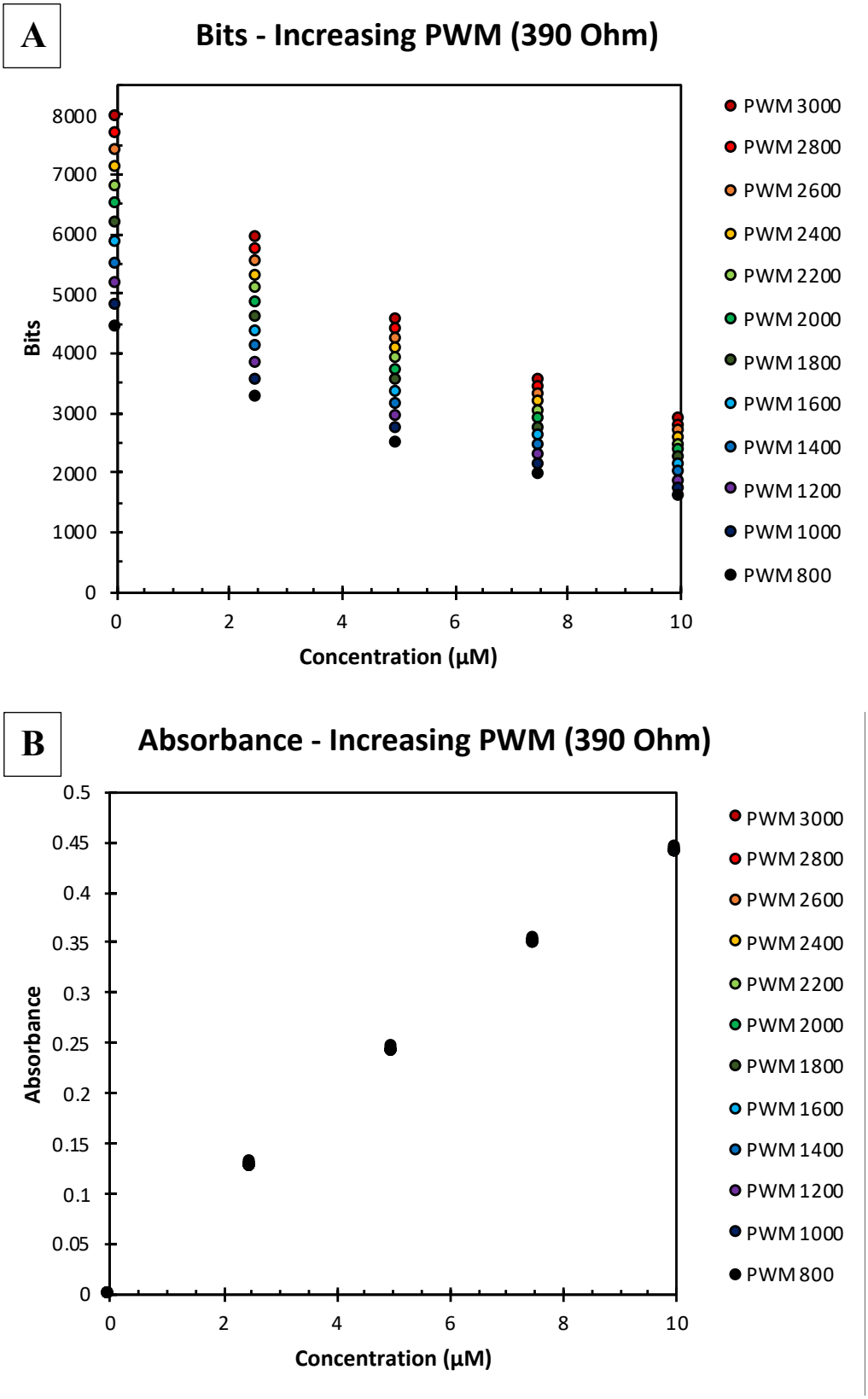

Figure SI.2.8. *Calibration curve for nitrite (NO_2^-) presenting (A) in bits (raw data) and (B) converted absorbance using benchtop detection platform at 390 Ω resistance.*

Figure SI.2.9. shows reproducible measurements of a non-reactive blank solution (Yellow Reagent: 0µM Phosphate standard, 1:1 v/v) reproducibly measured 10 times (100 measurements were taken at a rate of 50 ms) when sampled in the stable portion of the LED output accounting for the overshoot and with optimised resistance settings.

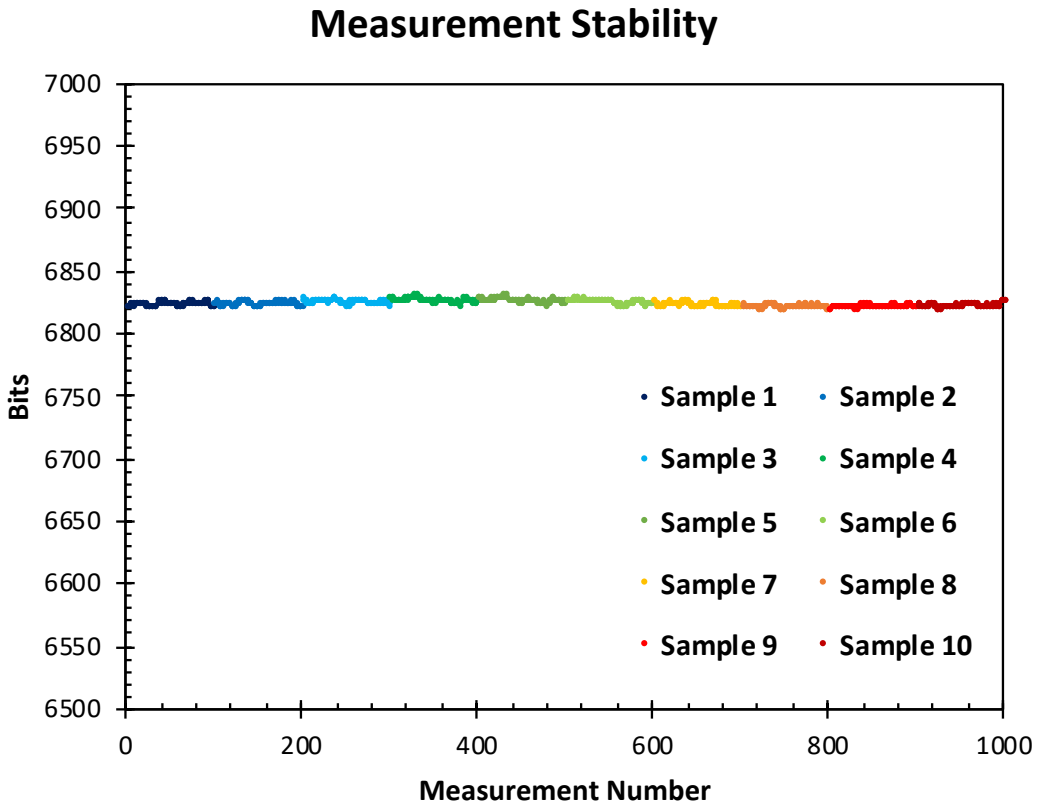

Figure SI.2.9. *Measurement stability accounting for initial LED overshoot prior to data acquisition.*

Figure SI.2.10. shows the calibration curves used to demonstrate the linear dynamic range on the benchtop sensing platform in chapter 2 section 2.3.3.1. A dynamic linear range of 0-300 µM was measured for phosphate and 0-15 µM for nitrite. 300 µM and 15 µM were shown to be the upper limit for the bench top platform, at concentrations above this point the detectable difference in colour and absorbance values decreased.

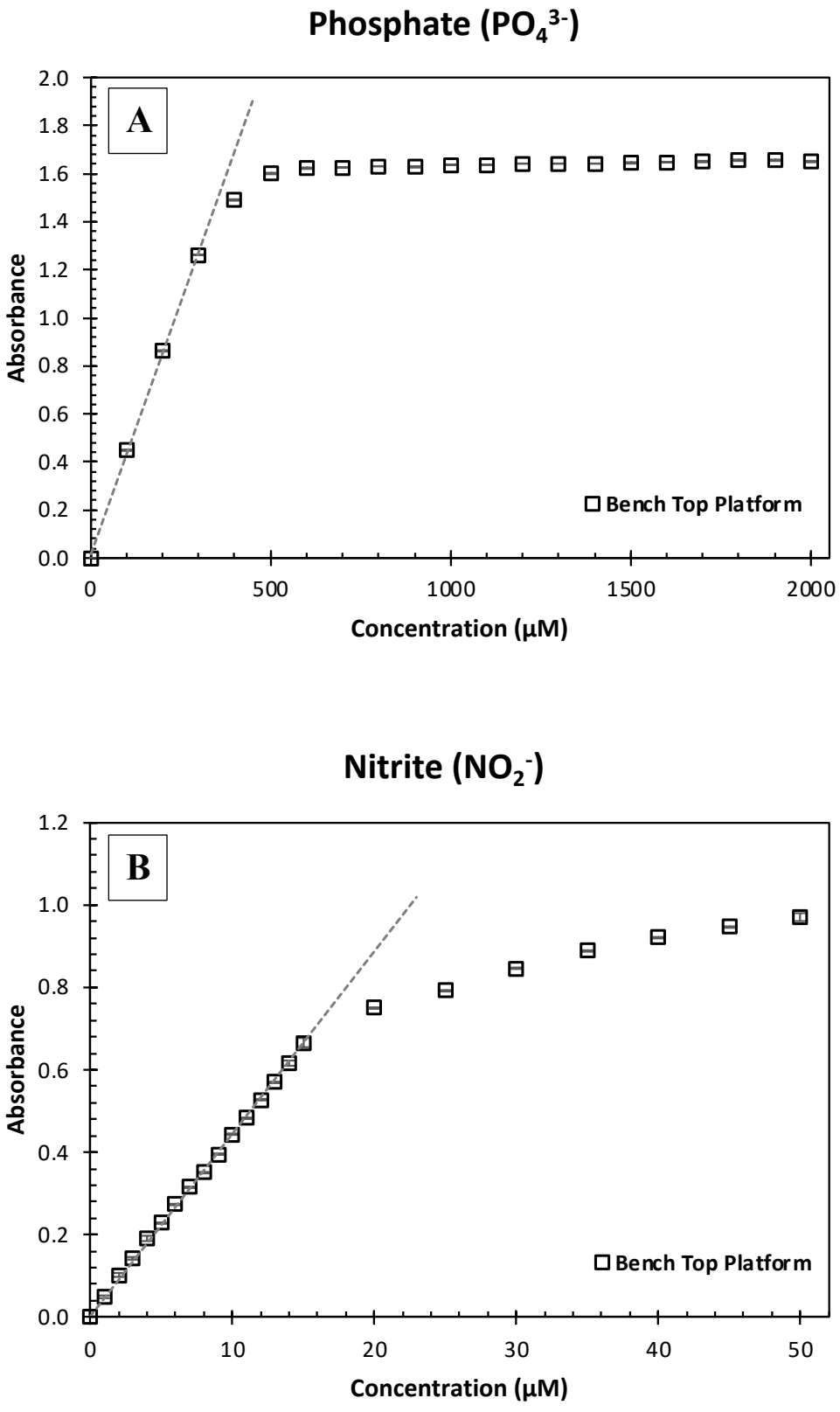

Figure SI.2.10. *Calibration curve of (A) phosphate standards ranging from 0-2000 µM and (B) nitrite standards ranging from 0-50 µM carried out on Benchtop sensing platform. The error bars represent the standard deviations for n=3.*

Ten environmental samples of unknown concentration were taken from the river Liffey across a 14 km transect starting above Leixlip dam, Co. Kildare and finishing in Mill Lane, Palmerstown, Co. Dublin, Ireland. Figure SI.2.11. shows a scaled version of the sampling map to give context to the site's location across the greater Liffey catchment.

Figure SI.2.11. *Environmental sampling map showing the start and end point of the samples collected across the 14 km transect of the river Liffey.*

Figure SI.2.12. component cost breakdown for the benchtop sensing platform at the time of manufacture. This costing does not account for manufacturing time, tooling, or equipment use. The platform was fully developed in house using available, 3D printers, soldering stations, precision micro mills and vacuum ovens.

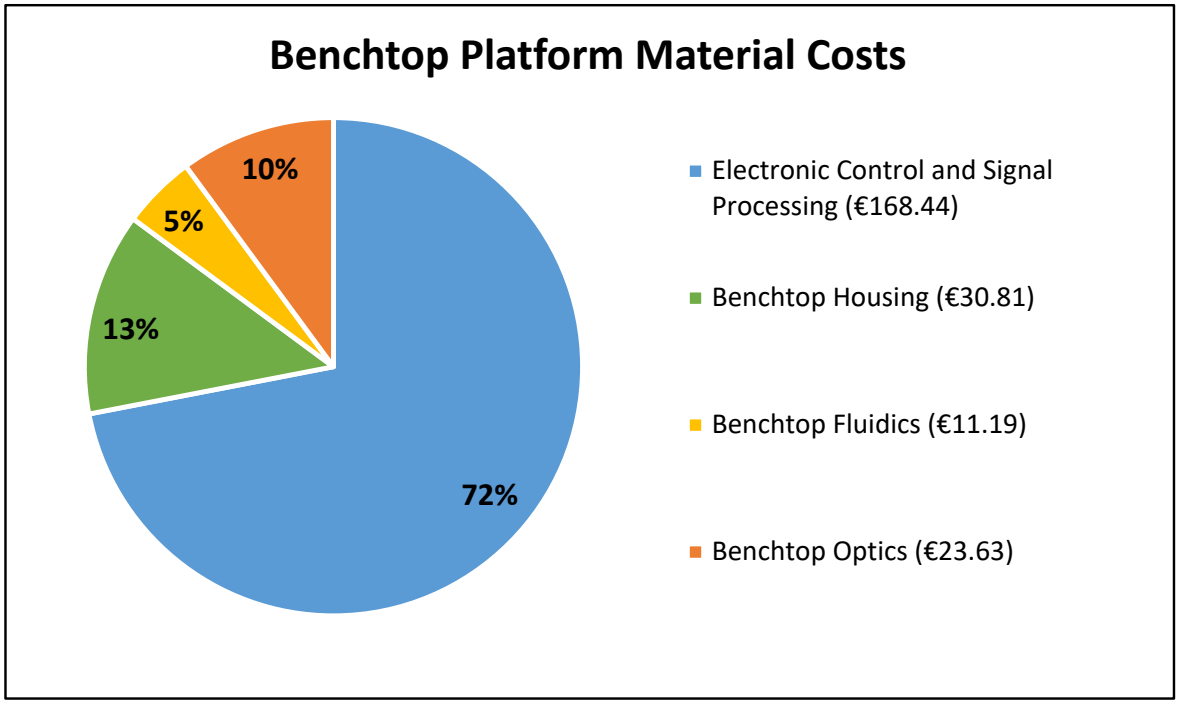

Figure SI.2.12. *Component cost breakdown of benchtop platform.*

Chapter 3

Development of regulated heated fluidic system for on chip detection of nutrients.

Figure SI.3.1. shows the code for thermistor-based temperature measurement and conversion using the simplified Steinhart equation.

```
// which analog pin to connect
#define THERMISTORPIN A0
// resistance at 25 degrees C
#define THERMISTORNOMINAL 10000
// temp. for nominal resistance (almost always 25 C)
#define TEMPERATURENOMINAL 25
// how many samples to take and average, more takes longer
// but is more 'smooth'
#define NUMSAMPLES 5
// The beta coefficient of the thermistor (usually 3000-4000)
#define BCOEFFICIENT 3950
// the value of the 'other' resistor
#define SERIESRESISTOR 10000

int samples[NUMSAMPLES];

void setup(void) {
  Serial.begin(9600);
  analogReference(EXTERNAL);
}

void loop(void) {
  uint8_t i;
  float average;

  // take N samples in a row, with a slight delay
  for (i=0; i< NUMSAMPLES; i++) {
   samples[i] = analogRead(THERMISTORPIN);
   delay(10);
  }

  // average all the samples out
  average = 0;
  for (i=0; i< NUMSAMPLES; i++) {
     average += samples[i];
  }
  average /= NUMSAMPLES;

  Serial.print("Average analog reading ");
  Serial.println(average);

  // convert the value to resistance
  average = 1023 / average - 1;
  average = SERIESRESISTOR / average;
  Serial.print("Thermistor resistance ");
  Serial.println(average);
```

```
  float steinhart;
  steinhart = average / THERMISTORNOMINAL;     // (R/Ro)
  steinhart = log(steinhart);                  // ln(R/Ro)
  steinhart /= BCOEFFICIENT;                   // 1/B * ln(R/Ro)
  steinhart += 1.0 / (TEMPERATURENOMINAL + 273.15); // + (1/To)
  steinhart = 1.0 / steinhart;                 // Invert
  steinhart -= 273.15;                         // convert to C

  Serial.print("Temperature ");
  Serial.print(steinhart);
  Serial.println(" *C");

  delay(1000);
}
```

Figure SI.3.1. *Code of resistance-based temperature measurement and conversion of ADC value to Celsius using the Steinhart equation.*

Figure SI.3.2. shows the circuit diagram with voltage divider using a fixed resistor to measure voltage as a proxy for resistance.

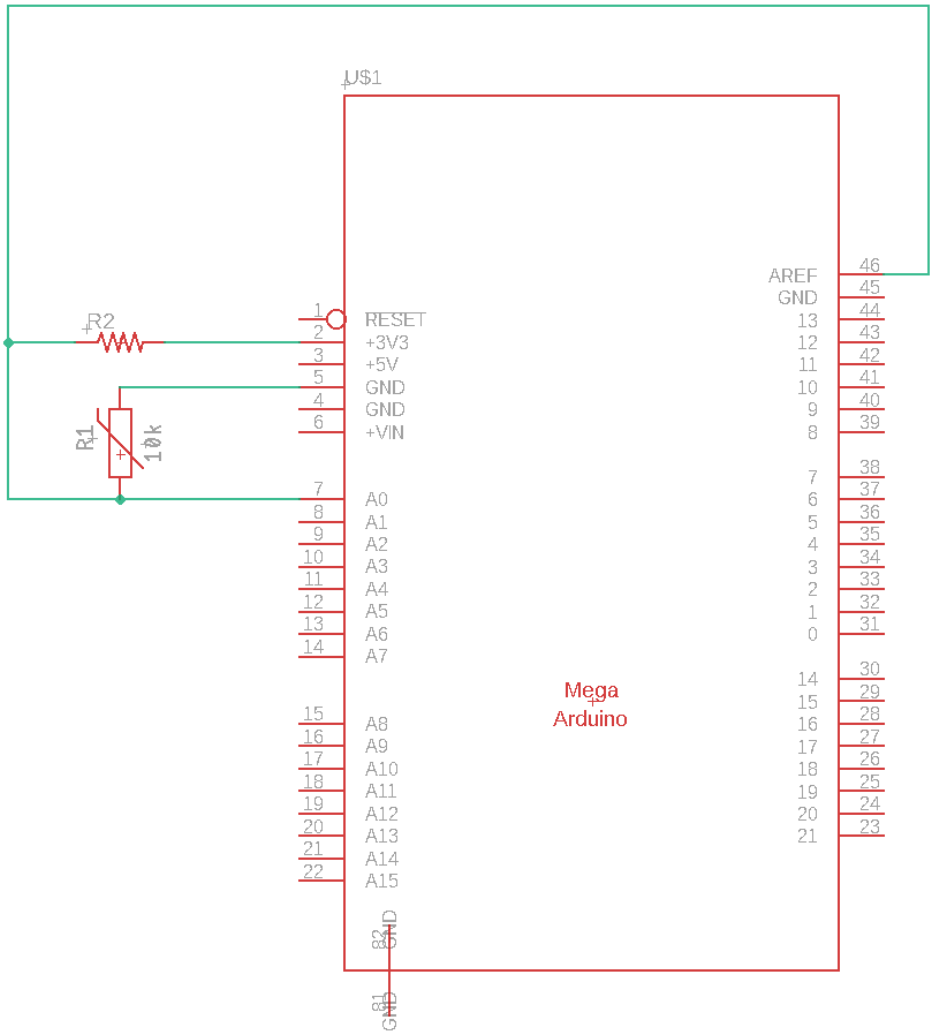

Figure SI.3.2. *Circuit diagram of temperature sensor schematic.*

Figure SI.3.3. shows the linear calibration curve used to demonstrate the working range in chapter 3. This data set was used as the sample data sets for the generation of the molar extinction coefficients, upper limits, and correlation coefficients. A dynamic linear range of 0-40 μM for nitrate was measured, with 40 μM being the upper limit, at concentrations above this point the detectable difference in colour and absorbance values decreased.

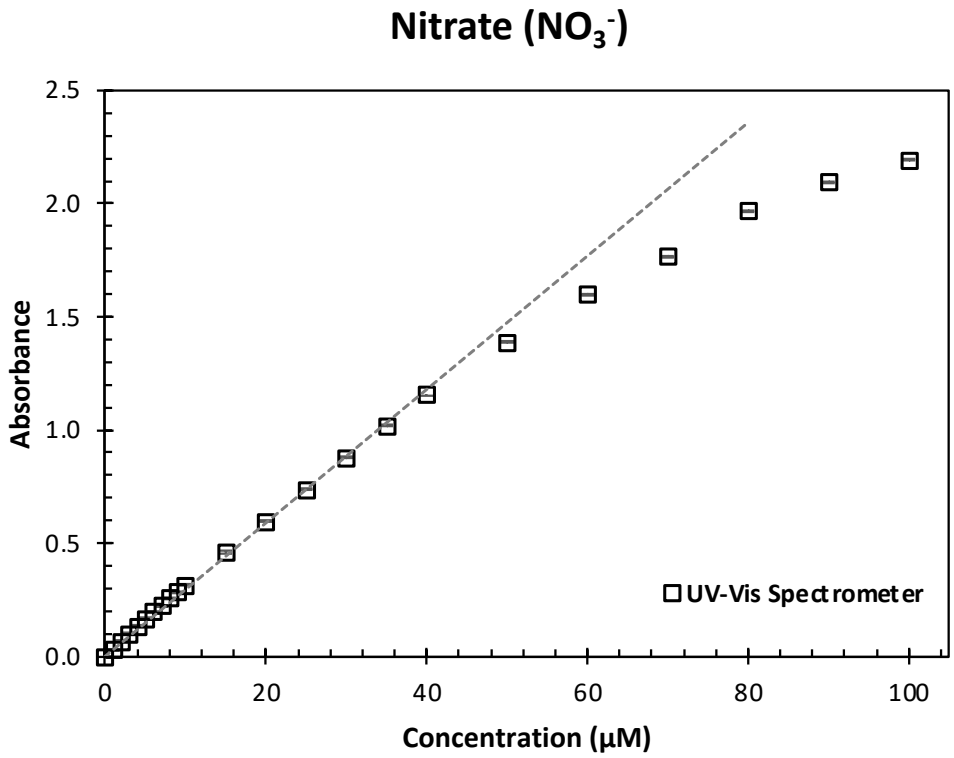

Figure SI.3.3. *Calibration curve for nitrate detection using standards ranging from 0-100 μM carried out on UV-Vis Spectrometer. The error bars represent the standard deviations for n=3.*

Figure SI.3.4. shows results for an integrated boost convertor vs without, the boost convertor shows improved response and maximum heat output.

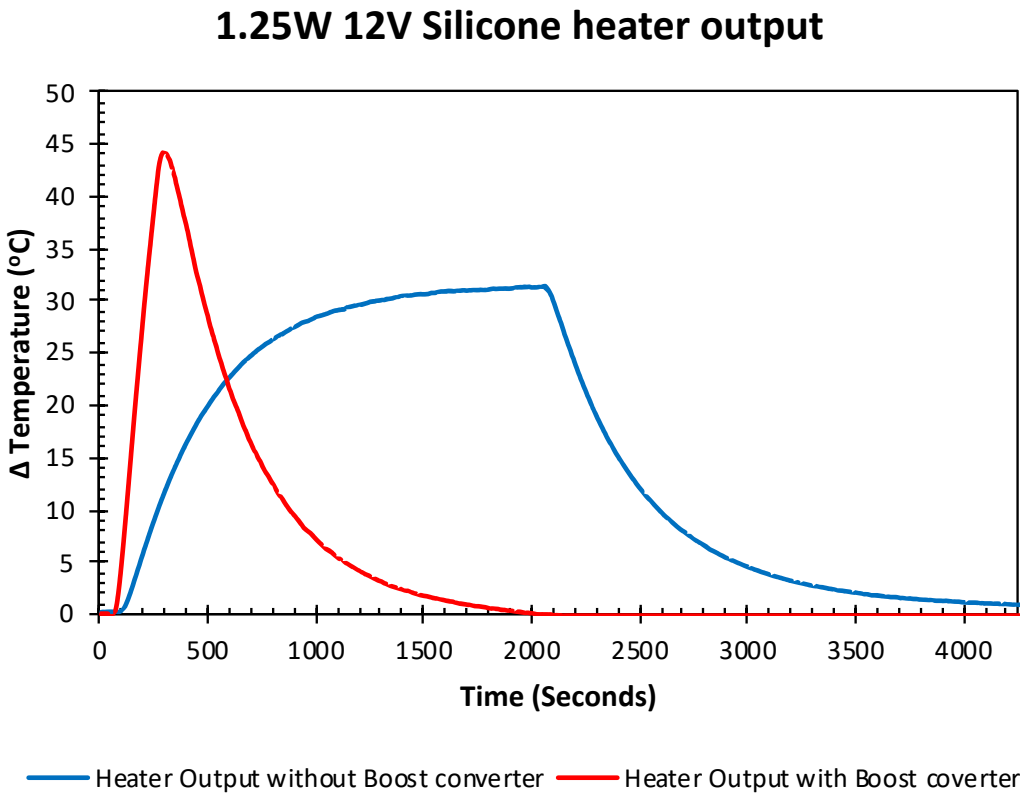

Figure SI.3.4. *Comparison of temperature output with and without an integrated boost convertor.*

Figure SI.3.5. shows the initial temperature regulation code with on off based upper and lower limits for thermostat style control.

```
#include <SPI.h>
#include <SD.h>
#include <Wire.h>

File logfile;

#include "RTClib.h"
RTC_DS1307 RTC;
DateTime now;
float average;
#define  SD_CS  10          // CS pin for the data logger shield

// char array to print to the screen
char sensorPrintout1[10];
float oldStein;
// which analog pin to connect
#define THERMISTORPIN A0
// resistance at 25 degrees C
#define THERMISTORNOMINAL 3000
// temp. for nominal resistance (almost always 25 C)
#define TEMPERATURENOMINAL 25
// how many samples to take and average, more takes longer
// but is more 'smooth'
#define NUMSAMPLES 5
// The beta coefficient of the thermistor (usually 3000-4000)
```

```
#define BCOEFFICIENT 3969
// the value of the 'other' resistor
#define SERIESRESISTOR 2500

int samples[NUMSAMPLES];
float lastval;

int HeatTrigger = 53;
float targetu = 50;
float targetl = 49.5;

void setup(void) {
 Serial.begin(115200);
 Wire.begin();
 RTC.begin();
 SD_Setup();
 analogReference(EXTERNAL);
 pinMode(HeatTrigger, OUTPUT);
 digitalWrite(HeatTrigger, LOW);
 Serial.print("Temperature \t");
 Serial.print("Heater Status \t");
 Serial.println("Time_Hr_Min_Sec");
}

void SD_Setup(){
 Serial.print("Initializing SD card...");
 pinMode(SD_CS, OUTPUT);
   // see if the card is present and can be initialized:

   delay(1000);
 if (!SD.begin(SD_CS))
 {
  Serial.println("Card failed, or not present");
  // don't do anything more:
//    while (1);!!!!!!!!!!!!!!!!!
 }
 Serial.println("card initialized.");

 //Creates the logfile with the number increasing each time
 char filename[] = "LOGDAT00.CSV";
 for (uint8_t i = 0; i < 100; i++) {
  filename[6] = i / 10 + '0';
  filename[7] = i % 10 + '0';
  if (! SD.exists(filename)){
    // only open a new file if it doesn't exist
    logfile = SD.open(filename, FILE_WRITE);
    break;  // leave the loop!
  }
 }
 if (! logfile){
  Serial.print("Could not create file");
  // while (1);     !!!!!!!!!!!!!!!!!!!!!!!!!!!!!!!!!!!!!!!!!!!!!!!!!!!!!!!!!!!!!!!!!!!!!!!!!!!
 }
 Serial.print("Logging to: ");
 Serial.println(filename);
 //Outputs if the real time clock isn't running
 if (! RTC.begin()) {
```

```
   Serial.println("RTC is NOT running!");
  }
  else
     Serial.println("RTC is running!");
  logfile.println("Date,Time,Temperature");
  logfile.flush();
}

void Log_to_SD(float steinhart, int ONOFF){
  DateTime Initial = RTC.now();
  logfile.print(Initial.year(),   DEC);
  logfile.print('/');
  logfile.print(Initial.month(),  DEC);
  logfile.print('/');
  logfile.print(Initial.day(),    DEC);
  logfile.print(" , ");
  logfile.print(Initial.hour(),   DEC);
  logfile.print(':');
  logfile.print(Initial.minute(), DEC);
  logfile.print(':');
  logfile.print(Initial.second(), DEC);
  logfile.print(" , ");
  logfile.print(steinhart);
  logfile.print(" , ");
  logfile.print(ONOFF);
  logfile.println();
  delay(250);
  logfile.flush();
}

void loop() {

  // take N samples in a row, with a slight delay
  for (uint8_t i=0; i<NUMSAMPLES; i++) {
   average += analogRead(THERMISTORPIN);
   delay(100);
  }
  average /= NUMSAMPLES;
  //Serial.print("Average analog reading ");
  //Serial.println(average);
  // convert the value to resistance
  average = 1023 / average - 1; // 10 bit Arduino ADC
  float resistance = SERIESRESISTOR / average;
  //Serial.print("Thermistor resistance ");
  //Serial.println(resistance);
  float steinhart = resistance / THERMISTORNOMINAL; // (R/Ro)
  steinhart = log(steinhart);                  // ln(R/Ro)
  steinhart /= BCOEFFICIENT;                   // 1/B * ln(R/Ro)
  steinhart += 1.0 / (TEMPERATURENOMINAL + 273.15); // + (1/To)
  steinhart = 1.0 / steinhart;                 // Invert
  steinhart -= 273.15;                         // convert to *C
  //Serial.print("Temperature ");
  Serial.print(steinhart);
  //Serial.print(" *C");
  Serial.print("\t");
  bool ONOFF;
  if (steinhart <= targetl) {
```

```
   digitalWrite(HeatTrigger, HIGH);
   ONOFF = 1;
   Serial.print("\t");
   Serial.print(ONOFF);
   Serial.print("\t");
   Serial.print("\t");
  }
  else if (steinhart >= targetu) {
   digitalWrite(HeatTrigger, LOW);
   ONOFF = 0;
   Serial.print("\t");
   Serial.print(ONOFF);
   Serial.print("\t");
   Serial.print("\t");
  }
  DateTime Initial = RTC.now();
  Serial.print(Initial.hour(), DEC);
  Serial.print(":");
  if(Initial.minute()<10)
  {
   Serial.print("0");
  }
  Serial.print(Initial.minute(), DEC);
  Serial.print(":");
  if(Initial.second()<10)
  {Serial.print("0");
   }
  Serial.println(Initial.second(), DEC);
  Log_to_SD(steinhart, ONOFF);
  delay(10);
}
```

Figure SI.3.5. *Code of temperature regulation using limits and feedback from the integrated temperature sensor.*

Figure SI.3.6. shows the improved temperature regulation circuit with PID based temperature regulation.

```
#include <SPI.h>
#include <SD.h>
#include <Wire.h>

File logfile;

#include "RTClib.h"
RTC_DS1307 RTC;
DateTime now;
float average;
#define  SD_CS  10          // CS pin for the data logger shield

// char array to print to the screen
char sensorPrintout1[10];
float oldStein;
// which analog pin to connect
#define THERMISTORPIN A0
// resistance at 25 degrees C
#define THERMISTORNOMINAL 3000
// temp. for nominal resistance (almost always 25 C)
#define TEMPERATURENOMINAL 25
// how many samples to take and average, more takes longer
// but is more 'smooth'
#define NUMSAMPLES 5
// The beta coefficient of the thermistor (usually 3000-4000)
#define BCOEFFICIENT 3969
// the value of the 'other' resistor
#define SERIESRESISTOR 2500

int samples[NUMSAMPLES];
float lastval;
int HeatTrigger = 13;              //Digital PWM Output port 2-13
float targetu = 50;
float targetl = 49;
float set_temperature = 100;       //Desired Temperature in Degree celcius
float PID_error = 0;
float previous_error = 0;
float elapsedTime, Time, timePrev;
int PID_value = 0;
```

```
//PID variables
int kp = 9.1;   int ki = 0.3;   int kd = 1.8;
int PID_p = 0;    int PID_i = 0;    int PID_d = 0;

void setup(void) {
 Serial.begin(115200);
 Wire.begin();
 RTC.begin();
 SD_Setup();
 analogReference(EXTERNAL);
 pinMode(HeatTrigger, OUTPUT);
 digitalWrite(HeatTrigger, LOW);
 Serial.print("Temperature \t");
 Serial.print("Heater Status 0-255 \t");
 Serial.println("Time_Hr_Min_Sec");
 Time = millis();
}

void SD_Setup(){
 Serial.print("Initializing SD card...");
 pinMode(SD_CS, OUTPUT);
  // see if the card is present and can be initialized:

  delay(1000);
 if (!SD.begin(SD_CS))
 {
  Serial.println("Card failed, or not present");
  // don't do anything more:
  // while (1);!!!!!!!!!!!!!!!!!
 }
 Serial.println("card initialized.");

 //Creates the logfile with the number increasing each time
 char filename[] = "LOGDAT00.CSV";
 for (uint8_t i = 0; i < 100; i++) {
  filename[6] = i / 10 + '0';
  filename[7] = i % 10 + '0';
  if (! SD.exists(filename)){
   // only open a new file if it doesn't exist
   logfile = SD.open(filename, FILE_WRITE);
   break;  // leave the loop!
  }
 }
 if (! logfile){
```

```
   Serial.print("Could not create file");
   // while (1);     !!!!
```

```
average /= NUMSAMPLES;
//Serial.print("Average analog reading ");
//Serial.println(average);
// convert the value to resistance
average = 1023 / average - 1; // 10 bit Arduino ADC
float resistance = SERIESRESISTOR / average;
//Serial.print("Thermistor resistance ");
//Serial.println(resistance);
float steinhart = resistance / THERMISTORNOMINAL; // (R/Ro)
steinhart = log(steinhart);                  // ln(R/Ro)
steinhart /= BCOEFFICIENT;                   // 1/B * ln(R/Ro)
steinhart += 1.0 / (TEMPERATURENOMINAL + 273.15); // + (1/To)
steinhart = 1.0 / steinhart;                 // Invert
steinhart -= 273.15;                         // convert to *C
//Serial.print("Temperature ");
Serial.print(steinhart);

PID_error = set_temperature - steinhart;
//Calculate the P value
PID_p = kp * PID_error;
//Calculate the I value in a range on +-3
if(-3 < PID_error <3)
{
  PID_i = PID_i + (ki * PID_error);
}

//For derivative we need real time to calculate speed change rate
timePrev = Time;                        // the previous time is stored before the actual time read
Time = millis();                        // actual time read
elapsedTime = (Time - timePrev) / 1000;
//Now we can calculate the D calue
PID_d = kd*((PID_error - previous_error)/elapsedTime);
//Final total PID value is the sum of P + I + D
PID_value = PID_p + PID_i + PID_d;

//We define PWM range between 0 and 255
if(PID_value < 0)
{    PID_value = 0;    }
if(PID_value > 255)
{    PID_value = 255;  }
//Now we can write the PWM signal to the mosfet on digital pin D3
analogWrite(HeatTrigger,255-PID_value);
previous_error = PID_error;     //Remember to store the previous error for next loop.
delay(300);
```

```
 //Serial.print(" *C");
/* bool ONOFF;
 if (steinhart < targetl) {
  digitalWrite(HeatTrigger, HIGH);
  ONOFF = 1;
  /*Serial.print("\t");
  Serial.print(ONOFF);
  Serial.print("\t");
  Serial.print("\t");
 } else if (steinhart > targetu) {
  digitalWrite(HeatTrigger, LOW);
  ONOFF = 0;
  /*Serial.print("\t");
  Serial.print(ONOFF);
  Serial.print("\t");
  Serial.print("\t");
 }
  Serial.print("\t");
  Serial.print(ONOFF);
  Serial.print("\t");
  Serial.print("\t");*/
 DateTime Initial = RTC.now();
 Serial.print("\t");
 Serial.print(255-PID_value);
 Serial.print("\t");
 Serial.print("\t");
 Serial.print(Initial.hour(), DEC);
 Serial.print(":");
 Serial.print(Initial.minute(), DEC);
 Serial.print(":");
 Serial.println(Initial.second(), DEC);
//  Log_to_SD(steinhart, ONOFF);
 delay(100);
}
```

Figure SI.3.6. *Code of temperature regulation using PID control.*

Figure SI.3.7. demonstrates the heating system can hold temperature within the microfluidic system, the introduction of cooler samples to the cell temporally reduces the cells temperature. This drop in temperature is caused by the temperature of the solution being injected and the total volume being flushed through the fluidic cell. The results show the effect of flushing a 5 mL solution at room temperature through the fluidic channels at two points. This addition of new sample for measurement resulted in an average drop of 6.9 °C which return to the set point temperature of the cell following addition. This temperature drop could be improved by lowering the volume of sample introduced to the cell and the time to recover could be improved by increasing the voltage of the heater and tuning the PID values.

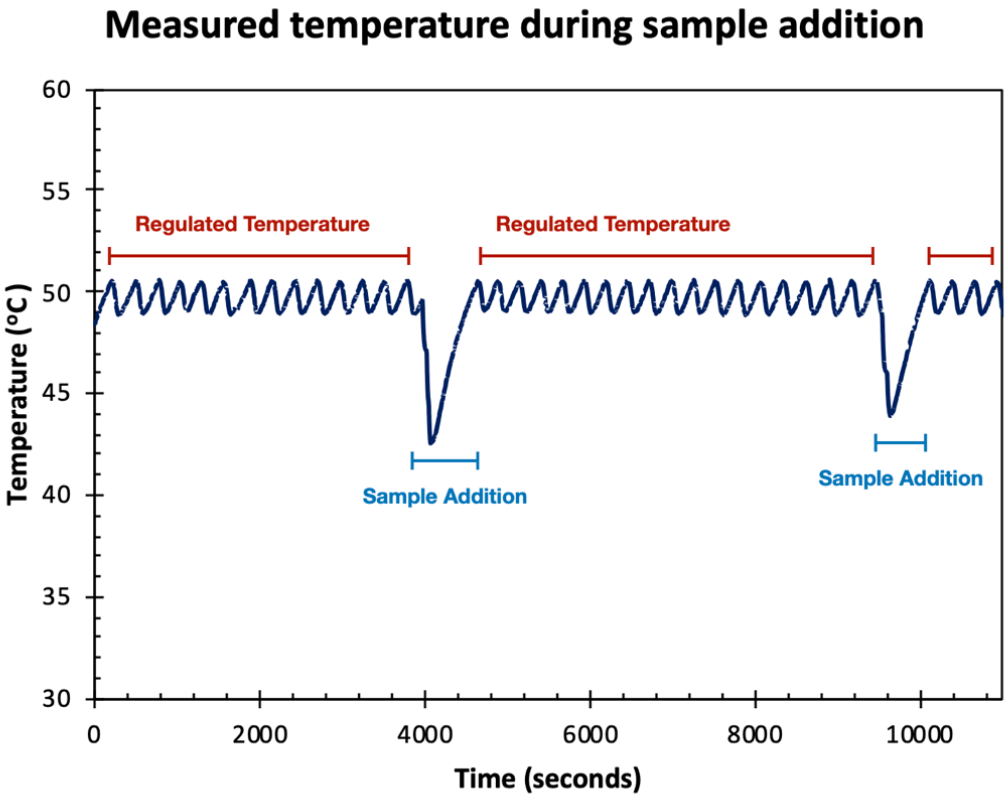

Figure SI.3.7. *Introduction of room temperature solution (5 mL) to the heated fluidic cell showing a reduction in temperature upon sample addition before returning to regulated values.*

Figure SI.3.8. shows the results of higher reaction temperatures where bubble generation was observed within the fluidic channels. These microbubbles can become problematic as they can affect the optical measurement within the channel. Several methods are available to negate the effects of these bubbles such as the introduction of bubble traps or degassers to the system or through careful design of the microfluidic channels.

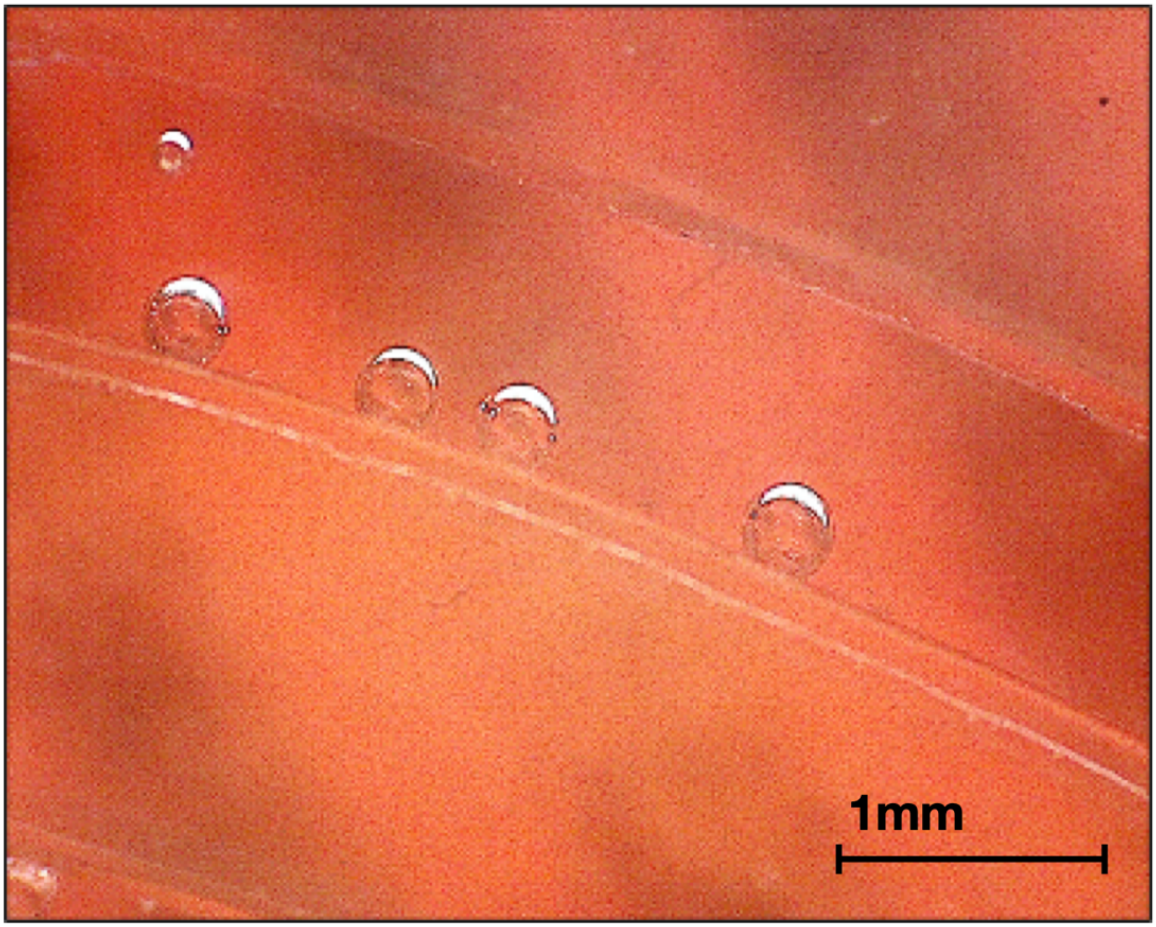

Figure SI.3.8. *Bubble generation within the microfluidic channels when heated reaction is occurring at higher temperatures.*

Figure SI.3.9. shows the calibration curves used to demonstrate the linear dynamic range on the benchtop sensing platform in chapter 3 section 3.3.3.1. A dynamic linear range for the benchtop platform of 0-15 μM for nitrate was measured. 15 μM was shown to be the upper limit as at concentrations above this point the detectable difference in colour and absorbance values decreased.

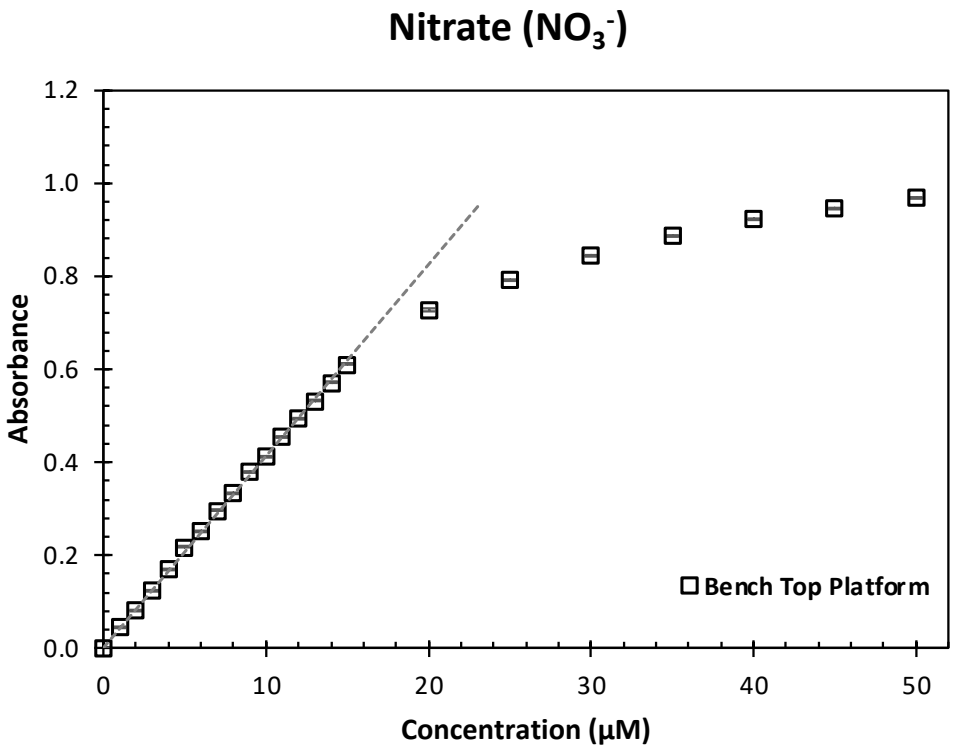

Figure SI.3.9. *Calibration curve of nitrate standards ranging from 0-50 μM carried out on Benchtop sensing platform. The error bars represent the standard deviations for n=3.*

Six environmental samples of unknown concentration were collected from the river Boyne across a 7 km transect starting at Stackallen Weir, Stackallen, Co. Meath and finishing at Slane Bridge, N2, Fennor, Co. Meath, Ireland. Figure SI.3.10. shows a scaled version of the sampling map to give context to the site's location across the greater Boyne catchment.

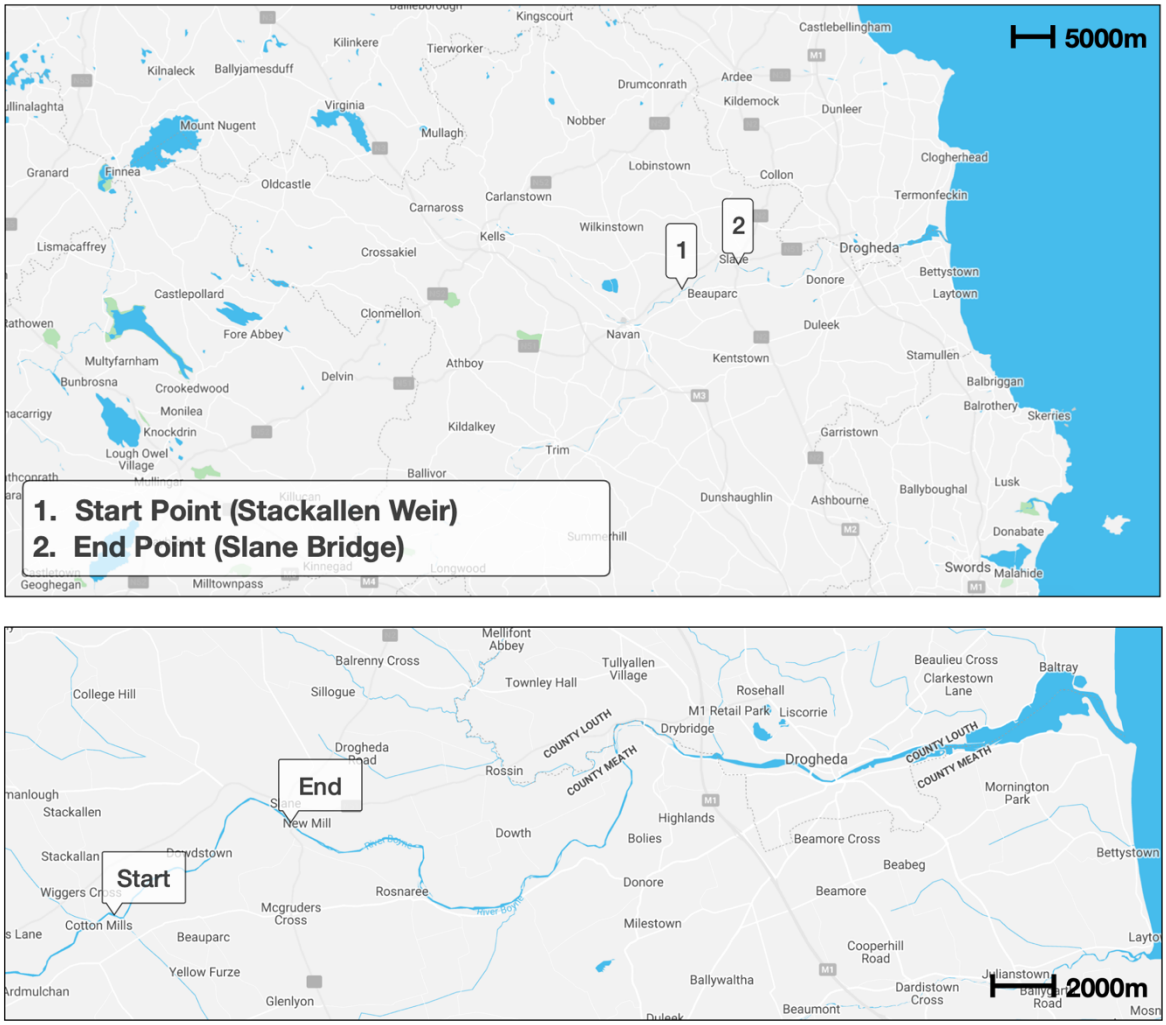

Figure SI.3.10. *Environmental sampling map showing the start and end point of the samples collected across the 7 km transect of the river Boyne catchment.*

Figure SI.3.11. shows the combined results for the six samples measured across the river Boyne for nitrite and nitrate measured using Griess reagent and Vanadium Chloride III before the results generated were converted to individual nitrite and nitrate concentrations.

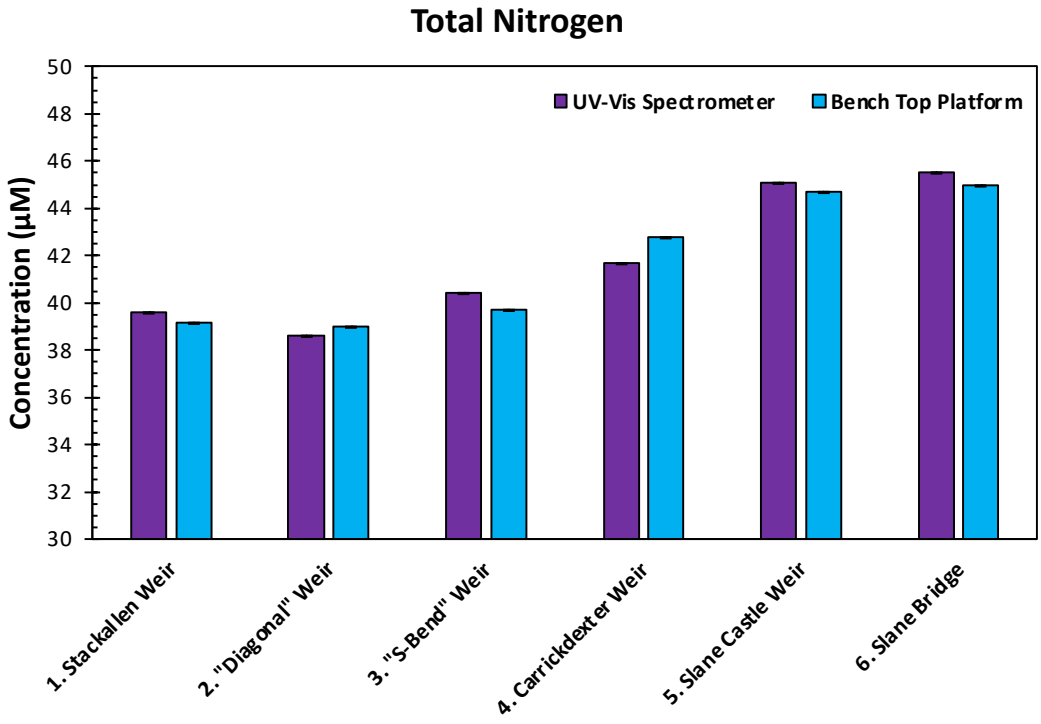

Figure SI.3.11. *Combined nitrite and nitrate concentrations measured across the six sampling points along the river Boyne.*

Chapter 5

Fabrication of Rugged and Reliable Fluidic Chips for Autonomous Environmental Analysers using combined thermal and pressure bonding of PMMA layers.

Thermal bonding was carried out as shown in figure SI.5.1. with the aligned two-layer fluidic chip positioned between two glass compression plates with a 220g weight positioned on top of the compression plates.

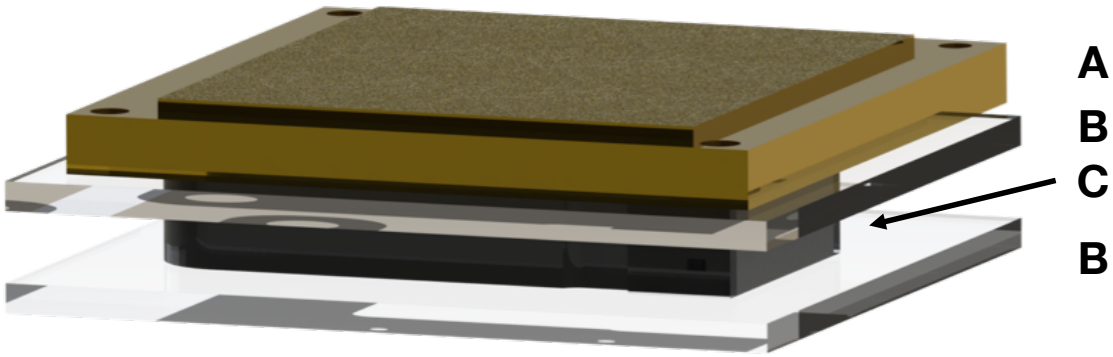

Figure SI.5.1. *Experimental setup for thermal bonding of two-layer PMMA fluidic chip. (A) brass weight (220 g), (B) glass compression plates (200 x 100 mm) with (C) Aligned two-layer fluidic chip.*

The conditions used for thermal and pressure bonding of the two-layer PMMA fluidic chips were assessed and optimised. Varying experimental conditions were assessed as initial bonding using just heat resulted in a sealed chip with a weak bond that could be pried apart by hand. Bonding conditions tested included temperature and time with a set vacuum before altering vacuum pressure once the optimum temperature and time had been assessed, results are summarised in table SI.5.1.

Following bonding at each condition the batches of chips were checked for leakage between the channel and capping layer and the optically clear windows. Leakage was assessed initially at 3 mL per minute before a higher flow rate of 12 mL per min was used over a one-hour period.

Table SI.5.*1*. *Assessment of optimum bonding conditions necessary for sealing of the two-layer fluidic chips.*

Batch Number (N=3)	Temperature (°C)	Time (Minutes)	Pressure (mBar)	Failure Rate (3ml/min)	Failure Rate (12ml/min)
1	145	10	200	3 of 3	3 of 3
2	145	20	200	3 of 3	3 of 3
3	145	40	200	3 of 3	3 of 3
4	145	60	200	3 of 3	3 of 3
5	155	10	200	3 of 3	3 of 3
6	155	20	200	2 of 3	3 of 3
7	155	40	200	2 of 3	2 of 3
8	155	60	200	2 of 3	2 of 3
9	165	10	200	1 of 3	1 of 3
10	165	20	200	0 of 3	0 of 3
11	165	40	200	0 of 3	0 of 3
12	165	60	200	0 of 3	0 of 3
13	165	20	100	1 of 3	1 of 3
14	165	20	400	0 of 3	0 of 3
15	165	20	600	0 of 3	0 of 3
16	165	20	800	0 of 3	0 of 3

The optimum temperature and time chosen was 165 °C for 20 minutes at the set pressure of 200 mBar. These conditions were selected as no leaks were recorded for the batch tested. The time of 20 minutes was chosen as this was the shortest time recorded without leakage occurring. No leakage was seen when chips were bonded for 40 and 60 minutes at 165 °C however the longer time lengthens the bonding process and there is more potential for channel deformation.

Once a set time and temperature had been chosen a number of batches were further tested with increasing vacuum at 100, 200, 400, 600 and 800 mBar. 200 mBar was

chosen as it was the lowest vacuum that sealed a chip without any failures. The lowest successful pressure was chosen as it was least likely to cause deformation of the channels once the PMMA reached transition temperatures.

Optical profilometry was used to generate 3D maps of the surfaces from which channel widths and depths could be measured before and after bonding. Optical profiles were taken at the target regions shown in figure SI.5.2. and results presented in figure SI.5.3. Figure SI.5.3. shows a high correlation at the target regions for channel depth and height. These results are presented in table 5.2. and 5.3. of the main text.

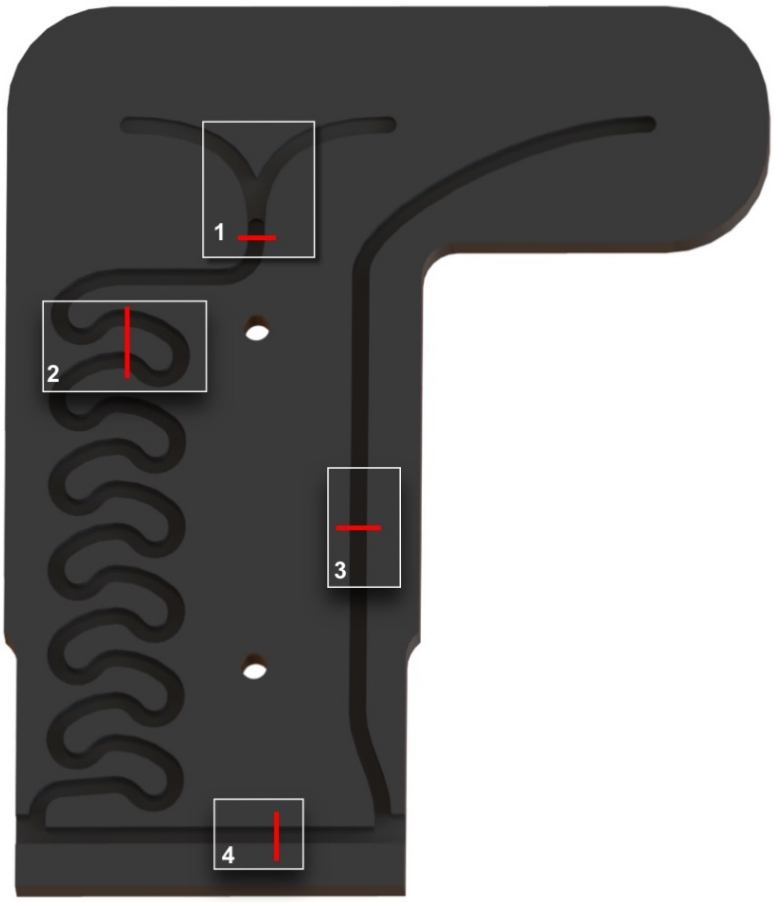

Figure SI.5.2. *Channel layout and the target areas used for characterisation of the channels in the channel layer of the Fluidic chip. 1) Sample and reagent inlet where sample and reagent merge after intake onto the chip, 2) initial portion of the serpentine mixing region where the sample and reagent mix on chip prior to measurement, 3) waste outlet channel through which sample and reagent are flushed after analysis and 4) optical channel for colorimetric detection of the sample/reagent mixture. These regions are imaged in figure S3 and transects shown in red are graphed alongside.*

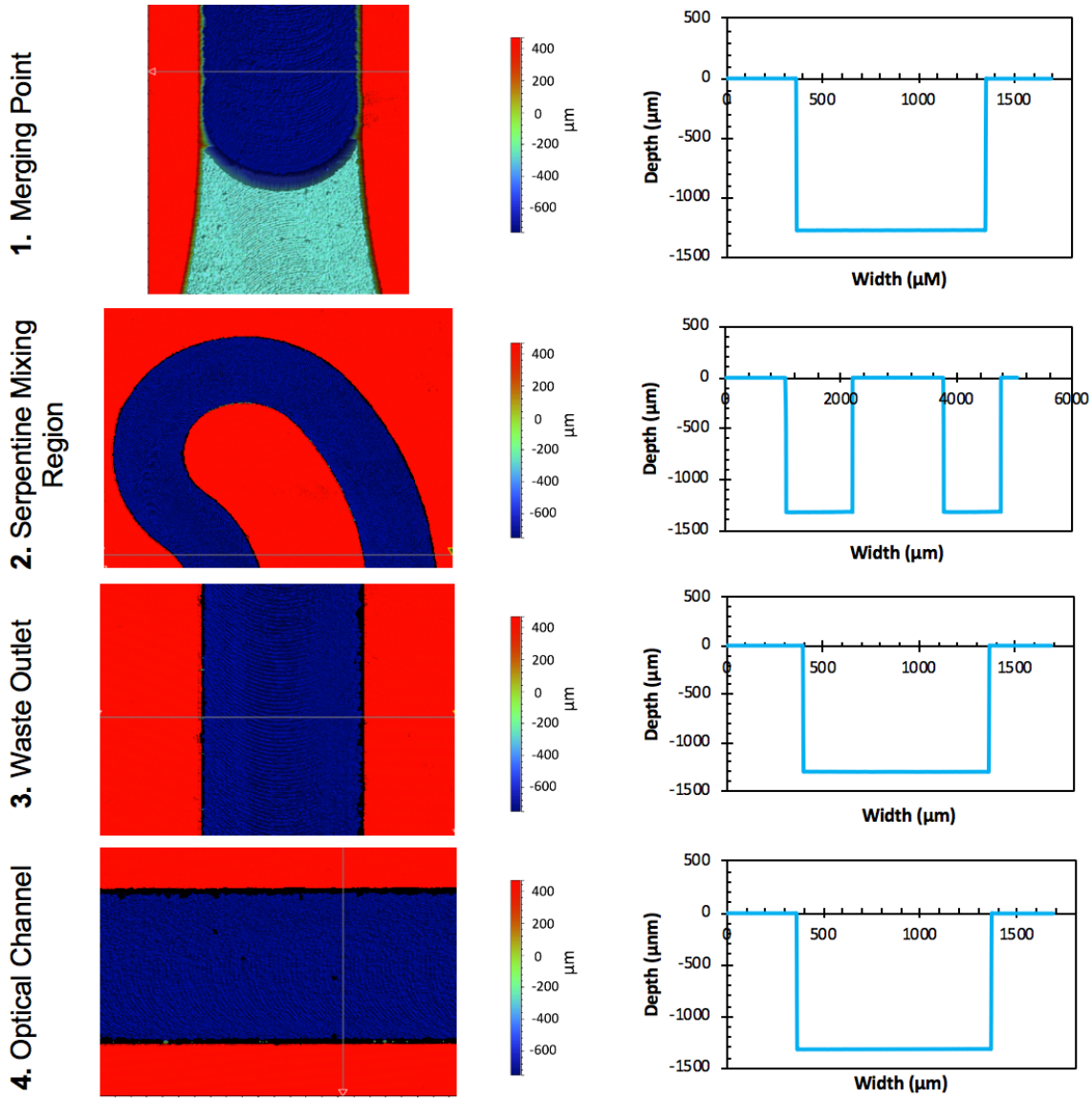

Figure SI.5.3. *Optical Profile images of channel layer target areas (see figure SI.5.2.) before bonding with transects showing channel width and depth of the (1) Merging Point, (2) Mixing Channel, (3) Waste Outlet, (4) Optical Channel.*

“Men wanted for hazardous journey. Small wages, bitter cold, long months of complete darkness, constant danger, safe return doubtful. Honour and recognition in case of success”

Ernest Shackleton